

# Experiments in Spectroscopy

Markus Lippitz

March 14, 2024

*cite as*

Lippitz, Markus, 2022.

Lecture Notes: Experiments in Spectroscopy (Winter 2022). Zenodo.

<https://doi.org/10.5281/zenodo.5377926>

# Contents

<b>I</b>	<b>Fundamentals</b>	<b>7</b>
1	Absorption	9
2	Fluorescence	17
3	Molecular Vibrations	23
4	Rayleigh and Mie Scattering	27
5	Molecular Aggregates – Coupled Two-Level Systems	33
<b>II</b>	<b>Two Level Systems</b>	<b>39</b>
6	Rabi Oscillations	41
7	(Perturbed) Free Induction Decay	49
8	Strong coupling of cavity and emitter	57
9	Weak coupling of cavity and emitter: Purcell Effect	63
<b>III</b>	<b>Nonlinear Spectroscopy</b>	<b>69</b>
10	Second Harmonic Generation	71
11	Four-Wave Mixing	79
12	Two-Photon Absorption	87
13	Two-Dimensional Spectroscopy	93
<b>IV</b>	<b>Plasmonics</b>	<b>103</b>
14	Plasmon hybridization	105
15	Surface plasmons as example of optics of layered media	115
16	Lattices of plasmonic particles	123



This work is licensed under a [Creative Commons "Attribution-ShareAlike 4.0 International"](https://creativecommons.org/licenses/by-sa/4.0/) license.

4 Experiments in Spectroscopy

17 Plasmonic Nano-Rods 129

V Nanooptics 137

18 Angular spectrum representation 139

19 Dipole emission at interfaces 145

Appendix 153

A Julia and Pluto 155

B Fourier transformation 159

# Preface

These are the lecture notes of my lecture on optical spectroscopy. The lecture aims at students in the first year of the master's program, but should be accessible also to students in the last year of the bachelor's program. You need some quantum mechanics and an introduction to the physics of molecules.

The idea of this lecture was to focus on *experiments*. Each chapter is build around an experiment and tries to explain everything that is needed to appreciate that experiment. As I am convinced that one only understands something if one really has worked with the concepts, each chapter has a *task*, which is in many cases to evaluate 'real' experimental data, or to simulate the experiment in a computer. The chapters are rather independent of each other, although the order has some sense. One thus can choose appealing chapters and skip others.

In the corona semester, I handed out these lecture notes to the students and prepared short (approx. 15 minutes) introductory videos to each chapter. I have the impression that it is easier for me to put things into context when talking then when writing, as I dare to be more sloppy. I did not enforce any timing, any rhythm during the semester. Everyone could select his or her pace and choice of chapters. During live video conferences, we discussed open questions and the results of the students work on the tasks<sup>1</sup>.

These notes are 'work in progress', and probably never really finished. If you find mistakes, please tell me. I am also always interested in other sources covering these topics. The most current version of the lecture notes can be found at github<sup>2</sup>. There you also find the material for the tasks. I have put everything under a CC-BY-SA license (see footer). In my words: feel free to do with it whatever you like. If you make your work available to the public, mention me and use a similar license.

The lecture notes are typeset using the LaTeX class 'tufte-book' by Bil Kleb, Bill Wood, and Kevin Godby<sup>3</sup>, which approximates the work of Edward Tufte<sup>4</sup>. I applied many of the modifications introduced by Dirk Eddebuettel in the 'tint' R package<sup>5</sup>. For the time being, the source is LaTeX, not markdown.

Markus Lippitz  
Bayreuth, July 28, 2021

<sup>1</sup> The tasks were also uploaded on the elearning platform and visible to all others who have completed a task.

<sup>2</sup> <https://github.com//Lippitz-Lab/Spectroscopy>

<sup>3</sup> [tufte-latex](#)

<sup>4</sup> [edwardtufte.com](http://edwardtufte.com)

<sup>5</sup> [tint](#): Tint is not Tufte





## **Part I**

# **Fundamentals**





# Chapter1

## Absorption

Markus Lippitz

March 15, 2024

### Tasks

- On the last page of Borri et al., 2002, the authors write 'From the measured 1-ns exciton radiative lifetime and with 3.5 refractive index we calculate  $\mu = 34$  Debye.' Convince yourself that this is true! My solution is [task\\_borri](#)<sup>1</sup>.
- Get a feel for typical absolute values and compare them to other relevant quantities such as geometric size, bond lengths, transition rates, etc. Sometimes it makes sense to factor out some constants and compare only then.
- Why are there so many different measures of absorption? Find use cases where it makes especially sense to use one measure and not the others.

In case you have doubts about the units of variables and equations, see [check\\_units](#)<sup>2</sup>.

<sup>1</sup>  [download](#) [run on binder](#)

<sup>2</sup>  [download](#) [run on binder](#)

### Experimental technique

A UV/VIS spectrometer measures the power  $P$  transmitted through a cuvette of optical path length  $L$  and compares it to the power  $P_0$  in a reference path. In most cases, also here, the reference path contains a cuvette with the pure solvent. The transmission  $T = P/P_0$  is converted into the absorbance  $A = -\log_{10} T = -\log_{10}(P/P_0)$ . The data set gives the absorbance as function of wavelength.

Grating spectrometers use an entrance slit to define the spectral resolution  $d\lambda$ , which is independent of the actual wavelength  $\lambda$ , as can be seen by inspecting the angular dispersion relation of a grating. Due to the reciprocal relationship between wavelength and frequency or energy, the spectral resolution in units of energy  $d\nu$  is no longer constant.

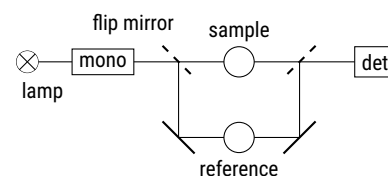


Figure 1.1: Sketch of a UV/VIS spectrometer



This work is licensed under a [Creative Commons "Attribution-ShareAlike 4.0 International"](#) license.

## Lambert-Beer law and the absorption coefficient

The transmitted power decreases exponentially with concentration  $C$  and path length  $L$ :

$$P = P_0 10^{-\alpha L} = P_0 10^{-\epsilon C L} \quad (1.1)$$

where  $\alpha$  is the absorption coefficient and  $\epsilon$  the (decadic) molar absorption coefficient<sup>3</sup>. We stick to a base of 10 here, so that the absorbance or optical density is equal to

$$A = \epsilon C L \quad (1.2)$$

However, similar definitions based on  $e$  are sometimes used. Our choice leads to the occasional appearance of factors of  $\ln(10)$ . The concentration is usually given in molarity (1 M = 1 mol/l), and for practical reasons, the lengths are given in centimeters. so that the molar absorption coefficient has the unit 1/(M cm). Of course, since we are dealing with spectroscopy, the molar absorption coefficient  $\epsilon$  depends on the wavelength or frequency of the light.

<sup>3</sup> The difference between absorption and extinction will be discussed elsewhere.

## Absorption cross section

The interaction cross section  $\sigma$  of a process is an imagined area around the particle which, when hit by a photon, triggers the considered process. If a photon hits the absorption cross section  $\sigma_{\text{abs}}$  of a molecule, it will be absorbed. If it does not hit it will pass unchanged. All the details of the physics are summarized in this area, which makes it easy to relate the absorption cross section to the absorbance.

We consider randomly arranged molecules of molar concentration  $C$  in a thin slab of thickness  $dx$ . The probability of a photon being absorbed in this slab is

$$1 - T = 1 - 10^{-\epsilon C dx} \approx \ln(10) \epsilon C dx \quad (1.3)$$

By comparison, if each molecule has an absorption cross section  $\sigma_{\text{abs}}$ , we get an absorption probability

$$1 - T = \sigma_{\text{abs}} C N_A dx \quad (1.4)$$

where  $N_A = 6.022 \cdot 10^{23}$  1/mol is the Avogadro number. We also made the Born approximation, i.e. that multiple interactions can be neglected, or that the absorption cross sections do not overlap, which is equivalent to the approximation made above to remove the exponential function. Thus we find

$$\sigma_{\text{abs}}(\omega) = \frac{\ln(10)}{N_A} \epsilon(\omega) \quad (1.5)$$

which has the unit of an area. Like the molar absorption coefficient  $\epsilon$ , the absorption cross section  $\sigma_{\text{abs}}$  depends on the wavelength of the light. If no wavelength is given, the value at the peak of the spectrum is meant.

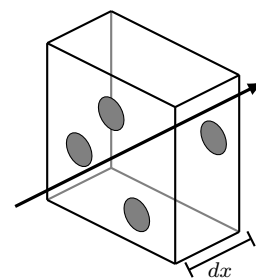


Figure 1.2: Sketch of disks hit by rays for the derivation of the absorption cross section.

## Questions

1. Define what one means by a 'cross section' and find other uses of the concept 'cross sections'.

2. Convince yourself that eq. 1.4 is correct!
3. Many things will have a Gaussian shape. Convince yourself that one can approximate a Gaussian of amplitude  $a$  and FWHM  $dx$  by a rectangle of the same width and height, i.e., that both have approximately the same integral.
4. Borri et al., 2002 investigate InGaAs quantum dots in a waveguide (see sketch). Each of the 3 QD layers has a dot areal density of  $2 \times 10^{10} \text{ cm}^{-2}$ . The size of the waveguide mode in the direction perpendicular to the QD planes is  $0.37 \mu\text{m}$  intensity FWHM. Calculate the absorption cross section from the measured absorption coefficient  $\alpha = 30 \text{ cm}^{-1}$ . You should find a value similar to  $2 \text{ nm}^2$ . See [example\\_ingaas](#)<sup>4</sup> for a solution.


 [download](#) [run on binder](#)

Figure 1.3: Sketch of the waveguide used by Borri et al., 2002.

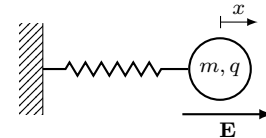


Figure 1.4: A Lorentz oscillator

## Lorentz oscillator and oscillator strength

The Lorentz oscillator is a simple classical model to describe the interaction of light and matter. A mass  $m$  of charge  $+e$  is connected to a spring. The oscillator has an angular eigenfrequency  $\omega_0$  and a damping  $\gamma$ . It is driven by an external electric field  $E(t) = E_0 \exp(i\omega t)$ . The differential equation for the position  $x$  is

$$\ddot{x} + 2\gamma\dot{x} + \omega_0^2 x = \frac{e}{m} E_0 e^{i\omega t} . \quad (1.6)$$

This results in a steady state solution of

$$x(t) = \frac{e}{m} \frac{1}{\omega_0^2 - \omega^2 + 2i\gamma\omega} E_0 e^{i\omega t} . \quad (1.7)$$

In the case of small damping ( $\gamma \ll \omega_0$ ) this simplifies near the resonance ( $\omega \approx \omega_0$ ) to

$$x(t) \approx \frac{e}{2m\omega_0} \frac{1}{\omega_0 - \omega + i\gamma} E_0 e^{i\omega t} . \quad (1.8)$$

In this approximation, the time-averaged power extracted by the damped oscillator from the driving force  $F(t) = eE(t)$  can be calculated as

$$P_{\text{abs}} = -\frac{1}{T} \int_0^T F \frac{ds}{dt} dt = -\frac{1}{T} \int_0^T \text{Re}\{eE(t)\} \text{Re}\{\dot{x}(t)\} dt \quad (1.9)$$

$$= -\text{Re} \left\{ i\omega \frac{e^2 E_0^2}{2m\omega_0} \frac{1}{\omega_0 - \omega + i\gamma} \right\} \frac{1}{T} \int_0^T (\cos \omega t)^2 dt \quad (1.10)$$

$$= \frac{e^2 E_0^2}{4m} \frac{\gamma}{(\omega_0 - \omega)^2 + \gamma^2} \quad (1.11)$$

$$= \frac{e^2}{2\epsilon_0 m c} \frac{\gamma}{(\omega_0 - \omega)^2 + \gamma^2} |S| . \quad (1.12)$$

The time average has produced a factor of  $1/2$  and in the last step we have used the definition of the amplitude of the Poynting vector  $|S| = \frac{1}{2} \epsilon_0 c |E_0|^2$ . We thus find an absorption cross section  $\sigma_{\text{abs,Lorentz}}$  of the classical Lorentz oscillator

$$\sigma_{\text{abs,Lorentz}}(\omega) = \frac{P_{\text{abs}}}{|S|} = \frac{e^2}{2\epsilon_0 m c} \frac{\gamma}{(\omega_0 - \omega)^2 + \gamma^2} . \quad (1.13)$$

While many optical transitions show a Lorentzian line shape as predicted by the Lorentz oscillator, the peak height of the absorption line deviates. This deviation is cast into an oscillator strength  $f$ , so that

$$\sigma_{\text{abs}}(\omega) = \frac{e^2}{2\epsilon_0 m c} \frac{\gamma}{(\omega_0 - \omega)^2 + \gamma^2} f . \quad (1.14)$$

The spectral integral of the absorption cross section is independent of its width  $\gamma$  as

$$\int \sigma_{\text{abs}}(\omega) d\omega = \frac{\pi e^2}{2\epsilon_0 m c} f \quad . \quad (1.15)$$

### Questions

5. Why does it make sense that the integral over a Lorentz absorption line is independent of its width?

### Transition dipole moment

Fermi's Golden Rule gives the transition rate from the initial state  $|i\rangle$  to the final state  $|f\rangle$  caused by the time-dependent perturbation  $H'$  to the stationary Hamilton operator  $H_0$  as

$$\Gamma_{i \rightarrow f} = \frac{2\pi}{\hbar} |\langle f | H' | i \rangle|^2 \rho(E) \quad , \quad (1.16)$$

where  $\rho(E) = dn/dE = \rho(\omega)/\hbar$  is the density of final states. The idea is that the initial state  $|i\rangle$  is well known, but the outcome of the interaction  $|f\rangle$  may have free parameters, for example the direction of the emitted electron or the mode of the absorbed photon. The density of states  $\rho(E)$  can thus describe either electronic or photonic states, or both.

In general, the interaction of a charged particle with an electromagnetic vector potential  $\mathbf{A}$  is described by the perturbation

$$H' = -\frac{i\hbar e}{m} \mathbf{A} \cdot \nabla \quad . \quad (1.17)$$

Since the spatial extent of our wavefunctions is small compared to the wavelength of light, we employ the dipole approximation and assume  $\exp(i\mathbf{k} \cdot \mathbf{r}) \approx 1$  in the plane-wave description of the vector potential. In this way, the perturbation operator  $H'$  simplifies to<sup>5</sup>

$$H' = e \mathbf{E}(t) \cdot \mathbf{r} = e E_0 \hat{\mathbf{x}} \cdot \mathbf{r} \cos(\omega t) \quad , \quad (1.18)$$

where  $\hat{\mathbf{x}}$  is a unit vector defining the polarization direction of the light field. We simplify further by using the rotating wave approximation and keeping only the co-rotating parts<sup>6</sup>

$$\cos(\omega t) = \frac{1}{2} (e^{i\omega t} + e^{-i\omega t}) \approx \frac{1}{2} e^{i\omega t} \quad (1.19)$$

so that

$$H' = \frac{e E_0}{2} \hat{\mathbf{x}} \cdot \mathbf{r} e^{i\omega t} \quad . \quad (1.20)$$

We introduce the transition dipole matrix element  $\mu_{if}$  as

$$\mu_{if} = -e \langle f | \mathbf{r} | i \rangle \quad . \quad (1.21)$$

It has the units of an electric dipole moment, i.e., charge times distance, and is the central element of an optical transition in quantum mechanics. For practical reasons, one uses the unit of 1 Debye = 1 electron displaced by 0.208 Å. With this the matrix element becomes

$$|\langle f | H' | i \rangle|^2 = \frac{1}{4} E_0^2 |\hat{\mathbf{x}} \cdot \mu_{if}|^2 \quad . \quad (1.22)$$

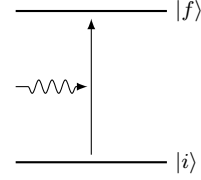


Figure 1.5: A light beam induces a transition from  $|i\rangle$  to the  $|f\rangle$ .

<sup>5</sup> see Bransden and Joachain (1996) for details

<sup>6</sup> More on this in the chapter on Rabi oscillations and the Bloch sphere.

Plugging everything into Fermi's Golden Rule, we get

$$\Gamma_{i \rightarrow f} = \frac{\pi}{2\hbar^2} E_0^2 |\hat{\mathbf{x}} \cdot \boldsymbol{\mu}_{if}|^2 \rho(\omega) \quad . \quad (1.23)$$

Now we have to take into account that we use an incoherent multimode light source.<sup>7</sup> The electric field  $E$  is here an incoherent superposition of modes with the spectral energy density  $u(\omega)$ .<sup>8</sup> The total power is thus

$$\frac{1}{2} \epsilon_0 E_0^2 = \int u(\omega) d\omega \quad . \quad (1.24)$$

The transition rate is thus

$$\Gamma_{i \rightarrow f} = \frac{\pi}{\hbar^2 \epsilon_0} |\hat{\mathbf{x}} \cdot \boldsymbol{\mu}_{if}|^2 \int u(\omega) \rho(\omega) d\omega \quad . \quad (1.25)$$

As the atomic transition is narrow compared with the light spectrum, the density of states  $\rho(\omega)$  selects the transition frequency  $\omega_{if}$

$$\Gamma_{i \rightarrow f} = \frac{\pi}{\hbar^2 \epsilon_0} |\hat{\mathbf{x}} \cdot \boldsymbol{\mu}_{if}|^2 u(\omega_{if}) \quad . \quad (1.26)$$

As each absorption event takes out a photon of energy  $\hbar\omega_{if}$ , and the energy density moves with the speed of light  $c$  we get an integrated absorption cross section  $\sigma_{||}$

$$\int \sigma_{||}(\omega) d\omega = \frac{\hbar\omega_{if} \bar{\Gamma}_{i \rightarrow f}}{c u(\omega_{if})} = \frac{\pi\omega_{if}}{\hbar c \epsilon_0} |\mu_{if}|^2 \quad . \quad (1.27)$$

The index  $||$  is necessary, as we dropped the dot product between the direction of the transition dipole moment  $\mu_{if}$  and the polarization direction  $\hat{\mathbf{x}}$ , assuming optimal parallel orientation. In case of random orientation, i.e., averaging over all possible orientation directions, one finds a reduction by one third, i.e.  $\sigma = 1/3 \sigma_{||}$ .

We can recover the spectral resolved absorption cross section  $\sigma_{||}(\omega)$  by assuming a line-shape function  $L(\omega - \omega_0)$  so that

$$\sigma_{||}(\omega) = \frac{\pi\omega_{if}}{\hbar c \epsilon_0} |\mu_{if}|^2 L(\omega - \omega_{if}) \quad (1.28)$$

where the integral over  $L$  equals one. Assuming a Lorentzian line shape, the peak value of  $L$  equals  $1/(\pi\gamma)$  so that the peak value of the absorption cross section equals

$$\sigma_{||}(\omega_{if}) = \frac{\omega_{if}}{\hbar c \epsilon_0 \gamma} |\mu_{if}|^2 \quad . \quad (1.29)$$

## Questions

6. The thing  $\langle f | \mathbf{r} | i \rangle$  is called a transition dipole moment. Why? What is similar and different to a plain dipole moment?
7. Do you find the Lorentz oscillator in  $\langle f | \mathbf{r} | i \rangle$  ? What is oscillating there?
8. What is the difference between  $\Gamma$  and  $\gamma$  ?

<sup>7</sup> The effect of a coherent single mode source will be investigated in the context of Rabi oscillations.

<sup>8</sup> see Cohen-Tannoudji, Diu, and Laloë (1977) and Fox (2007) for details

## Some remarks

Thomas-Reiche-Kuhn sum rule For single-electron transitions starting from the same quantum mechanical level  $i$ , one finds<sup>9</sup>

$$\sum_f (E_f - E_i) |\langle f | \hat{x} | i \rangle|^2 = \sum_f (E_f - E_i) |\mu_{if}|^2 = \frac{\hbar^2}{2m_0} \quad (1.30)$$

<sup>9</sup> see, for example, wikipedia

This is the Thomas-Reiche-Kuhn sum rule. The (weighted) sum over all transition dipole moments is constant. As consequence, the sum over all oscillator strengths  $f$  is equal to one. For this reason one can interpret the oscillator strength  $f$  to some extent as the number of electrons involved in the transition, but one has to be careful, as Z. Hens<sup>10</sup> points out.

<sup>10</sup> Hens, 2008.

Fluorescence emission as the only damping mechanism Several mechanisms can contribute to the damping  $\gamma$  of the Lorentz oscillator. One that is always present is fluorescence emission, which we will discuss in more detail in the next chapter. When fluorescence emission is the only damping term, the absorption cross section takes a very simple form, which is also its largest value. We have defined the differential equation of the oscillator (eq. 1.6) so that the amplitude of an undamped oscillator decays as  $\exp(-\gamma t)$ . The energy stored in the oscillator is proportional to the square of the amplitude, so the energy decays as  $\exp(-2\gamma t)$ . This decay rate  $2\gamma$  is the fluorescence emission rate, or the Einstein coefficient  $A_{21}$  when fluorescence emission is the only damping mechanism. With the following chapter (eqs. 2.10 and 2.12) we get

$$2\gamma = A_{21} = \frac{\omega^3}{3\pi\hbar c^3 \epsilon_0} |\mu_{if}|^2 \quad (1.31)$$

so that in this case the absorption cross section reduces to

$$\sigma_{\parallel}(\omega_{if}) = \frac{3}{2\pi} \lambda^2 \quad (1.32)$$

The absorption cross section of an atom, molecule or nanocrystal is therefore limited to about one square of the wavelength. The damping term  $\gamma$  also defines the width of the absorption line in the spectrum. A line width determined only by fluorescence decay is called lifetime-limited or Fourier-limited. In most cases, a spectral line is broader, the damping  $\gamma$  is stronger, and an absorption cross section is smaller. The reduction is given by the ratio of the Fourier-limited line width to the observed transition width.

Spectrally broad absorbers When relating to the (decadic) molar absorption coefficient  $\epsilon(\omega)$ , we have to realize that in the more 'atomic' contexts of transition dipole moments and Einstein coefficients, we have integrated over the spectral width of the absorption line. We have assumed that the incoming light beam is spectrally much broader than the optical transition. This is not the case for molecular spectra at room temperature. Therefore, we must also integrate the absorption spectrum over  $\omega$  and take into account that  $\omega_{if}$  varies even though we assign everything to the same electronic transition and thus use only one transition dipole moment  $\mu_{if}$ . We get

$$\int_{\text{transition}} \frac{\epsilon(\omega)}{\omega} d\omega = \frac{\pi N_A}{3 \ln(10) \hbar c \epsilon_0} |\mu_{if}|^2 = \frac{\hbar N_A}{\ln(10) c} B_{12} \quad (1.33)$$

where the last part again uses an Einstein coefficient, which will be introduced in the next chapter.

**Effect of a medium** All equations in this chapter have assumed a vacuum as the environment of the absorber. Except for atoms in a dilute gas, this is not the case in most cases. We can account for the effect of the dielectric function  $\epsilon$  or the index of refraction  $n = \sqrt{\epsilon}$  by replacing all occurrences of  $\epsilon_0$  by  $\epsilon\epsilon_0$  and all occurrences of  $c$  by  $c_0/n$ . The effect of the polarizability of the medium can be taken into account by the local field correction, see Parson, 2015 (chapter 3.1.6).

## Questions

9. Convince yourself that the first equal sign in eq. 1.33 is correct.
10. Continuing on question 4, calculate the transition dipole moment from the absorption coefficient. My solution [exmaple\\_ingaaas](#)<sup>11</sup> seems to deviate from the authors'.
11. CdSe nanocrystals (Jasieniak et al., 2009) in a chloroform ( $n \approx 1.4$ ) have a molar extinction coefficient  $\epsilon = 4 \cdot 10^5 \text{ (M cm)}^{-1}$  at a wavelength of 600 nm. The peak width is about 120 meV. This corresponds to nanocrystals of about 5 nm diameter. Calculate the absorption cross section  $\sigma$  and the transition dipole moment  $\mu$ . My solution is [example\\_cdse](#)<sup>12</sup>.
12. The xanthene dye JA26 been investigated in Kastrup and Hell, 2004. Take the relevant data from the paper and calculate the molar extinction coefficient  $\epsilon$  and the transition dipole moment  $\mu$ . You should find values of about  $10^4 \text{ (M cm)}^{-1}$  and 1 D, respectively.

<sup>11</sup>  [download](#) [run on binder](#)

<sup>12</sup>  [download](#) [run on binder](#)

## References

- Borri, Paola et al. (2002). "Rabi oscillations in the excitonic ground-state transition of InGaAs quantum dots". In: *Physical Review B* 66.8, p. 81306. [↗](#).
- Bransden, B. H. and C. J. Joachain (1996). *Physics of atoms and molecules*. Longman.
- Cohen-Tannoudji, Claude, Bernard Diu, and Franck Laloë (1977). *Quantum Mechanics*. Wiley.
- Fox, Mark (2007). *Quantum optics*. Oxford University Press.
- Hens, Z. (2008). "Can the oscillator strength of the quantum dot bandgap transition exceed unity?" In: *Chemical Physics Letters* 463.4-6, pp. 391–395. [↗](#).
- Jasieniak, Jacek et al. (2009). "Re-examination of the Size-Dependent Absorption Properties of CdSe Quantum Dots". In: *The Journal of Physical Chemistry C* 113.45, pp. 19468–19474. [↗](#).
- Kastrup, Lars and Stefan W Hell (2004). "Absolute Optical Cross Section of Individual Fluorescent Molecules". In: *Angewandte Chemie International Edition* 43.48, pp. 6646–6649. [↗](#).
- Parson, William W. (2015). *Modern optical spectroscopy*. Springer. [↗](#).





# Chapter2

## Fluorescence

Markus Lippitz  
May 4, 2021

### Tasks

- On the server, you find experimental data of the TDI dye. Compare the fluorescence emission rate obtained from the emission spectrum with the fluorescence lifetime from time-correlated single photon counting. Discuss differences.
- Find absolute values for other transition rates in atoms, molecules and solid state and compare to fluorescence rates.

### Experimental techniques

#### Measuring the spectrum of light

It is helpful to consider how the spectrum of light is really measured. A light beam is dispersed, typically on a grating. As function of the dispersion angle one measures light intensity by converting photons into electrons, either in a CCD camera or a photodiode. The signal amplitude is thus proportional to the photon rate, not the power, or the energy per photon.

The resolution of a grating spectrometer is determined by the width of the CCD pixels, the size of the diode or of the entrance slit, by the size of a monochromatic focus, or a combination of all. But in all cases, it is constant over the spectrum when measured in wavelength. The natural unit of a grating spectrometer is wavelength, not frequency. The reciprocal relation between wavelength and frequency leads to

$$\Delta\nu = \nu_2 - \nu_1 = \frac{c}{\lambda_2} - \frac{c}{\lambda_1} = c \frac{\lambda_1 - \lambda_2}{\lambda_1 \lambda_2} \approx \frac{c}{\lambda^2} \Delta\lambda \quad (2.1)$$

In the frequency domain, the spectral resolution is thus not constant, but proportional to  $\nu^2$ . As consequence, converting a data set from wavelength domain to frequency domain does not only entail converting the  $x$ -values, but also the  $y$ -values. The integral or total number of photons has to stay the same.

$$(\lambda; F(\lambda)) \rightarrow \left( \nu = \frac{c}{\lambda}; F(\nu) = \frac{\lambda^2}{c} F(\lambda) \right) \quad (2.2)$$

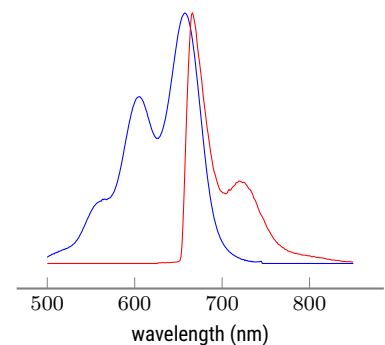


Figure 2.1: Absorption and emission spectrum of a dye molecule (TDI).



This work is licensed under a [Creative Commons "Attribution-ShareAlike 4.0 International"](https://creativecommons.org/licenses/by-sa/4.0/) license.

This problem only occurs for spectra of light. Absorption spectra are the ratio of two spectra of light, of the signal and reference beam. In this case, the prefactors cancel out and only the  $x$ -values need to be converted. The spectrally integrated absorption does not have any meaning, in contrast to the spectrally integrated photon flux.

### Time correlated single photon counting

This technique measures the arrival time of single photons relative to the laser pulse that excites the sample. It requires that each laser pulse leads to on average much less than one detected photon. This can be achieved using weak laser pulses or diluted samples. A high repetition rate (MHz) reduces the overall acquisition time. The probability to detect a photon at a time lag  $\tau$  after the laser pulse is directly connected to the probability, that the emitting system is still in the excited state. This statement does not require that each emitted photon is detected or that the excited state is depopulated only by fluorescence emission.



Figure 2.2: Sketch of a TCSPC setup

### Einstein coefficients

The Einstein coefficients for emission  $A_{21}$ , absorption  $B_{12}$  and stimulated emission  $B_{21}$  relate the populations  $N_1$  and  $N_2$  of a lower and upper state to the spectral energy density  $u(\omega)$  of the optical field (units of energy per volume and angular frequency interval). They define transition rates in units of Hz

$$k_{\text{spontaneous emission}} = A_{21} \quad (2.3)$$

$$k_{\text{absorption}} = B_{12} u(\omega) \quad (2.4)$$

$$k_{\text{stimulated emission}} = B_{21} u(\omega) \quad (2.5)$$

In steady state we get

$$\frac{dN_1}{dt} = A_{21}N_2 - B_{12}N_1 u(\omega) + B_{21}N_2 u(\omega) = 0 \quad (2.6)$$

At the same time, the ratio of the populations is given by Boltzmann's law as

$$\frac{N_2}{N_1} = \frac{g_2}{g_1} \exp\left(-\frac{\hbar\omega}{kT}\right) \quad (2.7)$$

where the  $g_i$  are the degeneracy of the respective state. The spectral energy density is given by the black-body spectrum, as we are in thermal equilibrium

$$u(\omega) = \frac{\omega^2}{\pi^2 c^3} \hbar\omega \frac{1}{\exp(\hbar\omega/kT) - 1} \quad (2.8)$$

Altogether this leads to

$$g_1 B_{12} = g_2 B_{21} \quad (2.9)$$

$$A_{21} = \frac{\hbar\omega^3}{\pi^2 c^3} B_{21} \quad (2.10)$$

Different prefactors can be found in literature for these equations, depending on the exact definition of  $u$ .<sup>1</sup> As each absorption event takes out the energy



Figure 2.3: Einstein coefficients

<sup>1</sup> Hilborn, 2002.

$\hbar\omega$  and the energy density  $u(\omega)$  moves with the velocity of light  $c$ , we get for the absorption cross section

$$\int \sigma(\omega) d\omega = \frac{\hbar\omega_{12} B_{12} u(\omega_{12})}{c u(\omega_{12})} = \frac{\hbar\omega_{12}}{c} B_{12} \quad (2.11)$$

assuming that almost all atoms are in the ground state ( $N_2 \ll N_1$ ). Using 1.27 and taking rotational averaging into account, we get

$$B_{12} = \frac{\pi}{3 \hbar^2 \epsilon_0} |\mu_{if}|^2 \quad (2.12)$$

## Relation between absorption and emission spectra for atoms

As we have seen in the last chapter, the extinction spectrum  $A(\omega)$  of an atomic gas is.

$$A(\omega) = \epsilon(\omega) C d = \frac{N_A C d}{\ln(10)} \sigma(\omega) = \frac{N_A C d}{\ln(10)} \frac{\pi \omega_{if}}{\hbar c \epsilon_0} L(\omega - \omega_{if}) |\mu_{if}|^2 \quad (2.13)$$

where  $C$  is the concentration of the atoms in the gas cell of thickness  $d$ . We used again the line-shape function  $L(\Delta\omega)$ .

The spectrum<sup>2</sup> of the spontaneous fluorescence emission  $F(\omega)$  is proportional to the spectral dependence of the radiative decay rate and thus to the Einstein  $A_{21}$  coefficient. Combining eq. 2.12 and 2.10 we get

$$A_{21} = \frac{\hbar \omega_{if}^3}{\pi^2 c^3} B_{21} = \frac{\omega_{if}^3}{3 \pi \hbar \epsilon_0 c^3} |\mu_{if}|^2 \quad (2.14)$$

or, with the line-shape function  $L$  and a concentration  $C$

$$F(\omega) \propto C \frac{\omega_{if}^3}{3 \pi \hbar \epsilon_0 c^3} L(\omega - \omega_{if}) |\mu_{if}|^2 \quad (2.15)$$

Note that both the absorption and the emission spectrum are proportional to the square of the transition dipole moment  $|\mu_{if}|^2$ , but the first is obtained by multiplying with  $\omega_{if}$ , the second by multiplying with  $\omega_{if}^3$

<sup>2</sup> Note that the spectrum is in units of photons per wavelength or frequency interval, and not power per interval.

## Molecules

Molecules are a bit more complicated than atoms. The Born-Oppenheimer approximation allows to separate the wave functions of electrons  $\phi(\mathbf{r}, \mathbf{R})$  and nucleus  $\chi(\mathbf{R})$ :

$$\Psi = \chi(\mathbf{R}) \phi(\mathbf{r}, \mathbf{R}) \quad (2.16)$$

where the nuclear ( $\mathbf{R}$ ) and electron ( $\mathbf{r}$ ) coordinates include the coordinate of *all* electrons and nuclei, respectively, and the nuclear coordinates  $\mathbf{R}$  are only fixed parameters in the electronic wave function. The matrix element of the dipole transition operator  $\hat{\mu}$  then reads

$$\mu_{if} = \iint \chi_f(\mathbf{R}) \phi_f(\mathbf{r}, \mathbf{R}) \hat{\mu} \chi_i(\mathbf{R}) \phi_i(\mathbf{r}, \mathbf{R}) d\mathbf{r} d\mathbf{R} \quad (2.17)$$

We now divide the dipole operator  $\hat{\mu}$  into a part acting only on the position of the negative charges, i.e., the electrons, and a part acting only on the position of the positive charges, i.e., the nuclei

$$\hat{\mu} = \hat{\mu}_e + \hat{\mu}_k = q_e \mathbf{r} + q_k \mathbf{R} \quad (2.18)$$

Thus we obtain

$$\mu_{if} = \langle \chi_f, \phi_f | \hat{\mu}_e | \chi_i \phi_i \rangle + \langle \chi_f, \phi_f | \hat{\mu}_k | \chi_i \phi_i \rangle \quad (2.19)$$

$$= \langle \chi_f | \chi_i \rangle \langle \phi_f | \hat{\mu}_e | \phi_i \rangle + \langle \phi_f | \phi_i \rangle \langle \chi_f | \hat{\mu}_k | \chi_i \rangle \quad (2.20)$$

In the second step, we assumed that the electron wavefunction  $\phi(\mathbf{r}, \mathbf{R})$  depends only weakly on  $\mathbf{R}$ . The electron wavefunctions  $\phi_i$  are orthogonal to each other. Thus, the second summand vanishes. The prefactor in front of the first one is not zero because the nuclear wavefunctions belong to different equilibrium distances. This factor

$$F = \langle \chi_f | \chi_i \rangle = \int \chi_f(\mathbf{R}) \chi_i(\mathbf{R}) d\mathbf{R} \quad (2.21)$$

is called *Franck-Condon factor*. It describes the spatial overlap of the oscillatory wave function of the initial and target states. We will investigate this more in detail in the next chapter. In essence, we need to decorate all equations stemming from atomic transitions with  $|F|^2$  to take the nuclear vibration into account.

## Strickler-Berg-Equation

In condensed matter at room temperature, optical transitions are spectrally broad and not at all delta-like. One still finds a relation similar to the relation between the Einstein  $A$  and  $B$  coefficient between absorption and emission, when integrating over the spectral width. This relation is the Strickler-Berg equation.<sup>3,4</sup>

A molecule has the electronic ground state  $g$  and the first excited state  $e$ , and each electronic state has a progression of vibrational states  $m$  and  $n$ . We first look at the spontaneous emission rate  $k_{sp} = A_{21}$  from the state  $e, n$  into any vibrational state of  $g$ ,

$$k_{e,n \rightarrow g} = \sum_m k_{e,n \rightarrow g,m} = \frac{\hbar}{\pi^2 c^3} \sum_m \omega_{e,n \rightarrow g,m}^3 |\langle \chi_m | \chi_n \rangle|^2 B_{ge} \quad (2.22)$$

where we have used the relation between the Einstein  $A$  and  $B$  coefficients and taken into account the Frank-Condon factors  $|\langle \chi_m | \chi_n \rangle|^2$  for the overlap of the vibrational wave functions  $\chi$  of the nuclei. The Einstein coefficient for absorption  $B_{ge}$  is related to the molar extinction coefficient  $\epsilon(\omega)$ , as we have seen in the chapter on absorption

$$k_{e,n \rightarrow g} = \frac{\ln(10)}{\pi^2 c^2 N_A} \sum_m \omega_{e,n \rightarrow g,m}^3 |\langle \chi_m | \chi_n \rangle|^2 \int \frac{\epsilon(\omega)}{\omega} d\omega \quad (2.23)$$

As the  $\chi_m$  form a full basis set  $\sum_m |\langle \chi_m | \chi_n \rangle|^2 = 1$ , we can write

$$k_{e,n \rightarrow g} = \frac{\ln(10)}{\pi^2 c^2 N_A} \frac{\sum_m \omega_{e,n \rightarrow g,m}^3 |\langle \chi_m | \chi_n \rangle|^2}{\sum_m |\langle \chi_m | \chi_n \rangle|^2} \int \frac{\epsilon(\omega)}{\omega} d\omega \quad (2.24)$$

The fluorescence emission spectrum  $F(\omega)$  is determined<sup>5</sup> up to spectrally constant factors by the  $\omega^3$  term and the Franck-Condon factors, i.e.

$$F(\omega = \omega_{e,n \rightarrow g,m}) \propto \omega_{e,n \rightarrow g,m}^3 |\langle \chi_m | \chi_n \rangle|^2 |\mu_{eg}|^2 \quad (2.25)$$

<sup>3</sup> chapter 5.3 Parson, 2015; S. J. Strickler and Berg, 1962.

<sup>4</sup> Köhler and Bässler, 2015, chapter 1.4.3.2.

<sup>5</sup> see also next chapter

so that we can write by replacing the sums over  $m$  by spectral integrals

$$k_{e,n \rightarrow g} = \frac{\ln(10)}{\pi^2 c^2 N_A} \frac{\int F(\omega) d\omega}{\int \omega^{-3} F(\omega) d\omega} \int \frac{\epsilon(\omega)}{\omega} d\omega \quad (2.26)$$

This is the Strickler-Berg equation. Conveniently, all prefactors connected to  $F(\omega)$  drop out, especially also experimentally difficult to access absolute emission intensities. Absolute absorption is much easier to measure. The Strickler-Berg equation conveniently connects these spectra such that we can calculate the rate of spontaneous fluorescence emission. For molecules in a solvent, one should take into account that the refractive index  $n$  of the solvent enters via  $c = c_0/n$ .

In the literature, different prefactors can be found, related to integrals over frequency  $\nu$  or wave numbers  $\bar{\nu}$ . Sometimes also an additional factor of 1000 appears, stemming from assumptions on the units of the molar extinction.

## Fluorescence quantum yield and fluorescence lifetime

In contrast to an atom in vacuum, a molecule in condensed matter has other options beyond light emission to lower its total energy. These non-radiative processes include vibrational relaxation, inter-system crossing, internal conversion and other energy transfer mechanism. The total rate  $k_{tot}$  by which the population of an excited state changes is thus the sum of several rates, a radiative (as given by the Strickler-Berg equation) and several non-radiative rates

$$k_{tot} = k_{rad} + k_{nonrad} \quad (2.27)$$

The population of an excited state is thus, neglecting other processes that potentially re-excite this state,

$$N(t) = N(0) \exp(-k_{tot} t) \quad (2.28)$$

The fluorescence intensity  $F(t)$  is given by the population and the radiative rate

$$F(t) = k_{rad} N(t) = k_{rad} N(0) \exp(-k_{tot} t) \quad (2.29)$$

After switching off the excitation laser, the fluorescence intensity drops thus exponentially with the total rate, not the radiative rate. When measuring the arrival time of a fluorescence photon after impulsive laser excitation, one can find this exponential decay in the arrival time histogram. This technique is called time-correlated single-photon counting (TCSPC). The total rate is thus much easier to measure than the radiative rate.

The fluorescence lifetime is the reciprocal of the total decay rate  $k_{tot}$  and determines the TCSPC trace. The reciprocal of the radiative rate is sometimes called radiative lifetime.

The fluorescence quantum yield  $\eta$  gives the probability that a decay out of the excited state results in a photon, i.e.

$$\eta = \frac{k_{rad}}{k_{tot}} = \frac{k_{rad}}{k_{rad} + k_{nonrad}} \quad (2.30)$$



Figure 2.4: A fluorescence decay trace gives the total rate.

## References

- Hilborn, Robert C. (2002). *Einstein coefficients, cross sections,  $f$  values, dipole moments, and all that*. arXiv: [physics/0202029](https://arxiv.org/abs/physics/0202029).
- Köhler, Anna and Heinz Bässler (2015). *Electronic processes in organic semiconductors*. Weinheim: Wiley-VCH. [↗](#).
- Parson, William W. (2015). *Modern optical spectroscopy*. Springer. [↗](#).
- Strickler, S J and Robert A Berg (1962). "Relationship between Absorption Intensity and Fluorescence Lifetime of Molecules". In: *The Journal of Chemical Physics* 37.4, p. 814. [↗](#).

# Chapter3

## Molecular Vibrations

Markus Lippitz  
May 6, 2021

### Tasks

- Get the raw data of the absorption and emission spectra of the dye BODIPY 650/665 from [thermofischer.com](http://thermofischer.com). Convince yourself that the mirror-law holds.
- Make an as accurate as possible sketch of the potentials of ground and excited state of BODIPY 650/665, assuming that only one vibrational mode contributes.

### Franck-Condon and Huang-Rhys

A molecule with an electronic ground state  $g$  and electronic excited state  $e$  can undergo periodic oscillations of the nuclei positions along a coordinate  $R$ . We assume<sup>1</sup> that the potential of these oscillations is harmonic, i.e.

$$U_g(R) = \frac{1}{2} K R^2 = \frac{1}{2} M \Omega^2 R^2 \quad (3.1)$$

$$U_e(R) = U_g(R) + E_{eg} - A R = E_{eg} - A R + \frac{1}{2} M \Omega^2 R^2 \quad (3.2)$$

where  $E_{eg}$  is the electronic contribution to the energy difference. We assumed that both potentials have the same shape, i.e., the same vibrational frequency. The term  $AR$  couples the electronic state and the nuclear oscillator. It shifts the excited state potential along the  $R$  coordinate. We introduce a reduced space coordinate  $\tilde{R}$  with

$$\tilde{R} = \frac{R}{x} \quad \text{with} \quad x = \sqrt{\frac{\hbar}{M\Omega}} \quad (3.3)$$

The new space coordinate  $\tilde{R}$  is scaled such that the parabola of the potential crosses the energy of the vibrational ground state  $\hbar\Omega/2$  at  $\tilde{R} = 1$ . In these coordinates, the minimum of the excited state parabola is at  $\tilde{R} = \tilde{R}_e$  with

$$\tilde{R}_e = \frac{Ax}{\hbar\Omega} \quad (3.4)$$

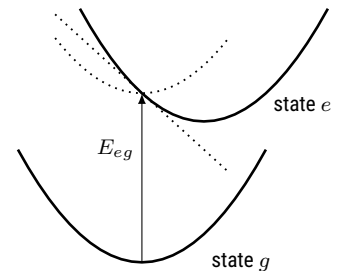


Figure 3.1: The coupling term  $-AR$  in the potential of the excited state  $e$  shifts the minimum of the parabola to larger values of  $R$  and lower values of the potential.

<sup>1</sup> Kuzmany, 2009.



The equations then become

$$U_g(\tilde{R}) = \frac{1}{2} \hbar \Omega \tilde{R}^2 \quad (3.5)$$

$$U_e(\tilde{R}) = E_{eg} + \frac{1}{2} \hbar \Omega \left[ (\tilde{R} - \tilde{R}_e)^2 - \tilde{R}_e^2 \right] \quad (3.6)$$

The energies of the quantum mechanical eigenstates are

$$E_{g,n} = (n + 1/2) \hbar \Omega \quad (3.7)$$

$$E_{e,m} = E_{eg} + (m + 1/2 - \tilde{R}_e^2/2) \hbar \Omega = E_{eg} + (m + 1/2 - S) \hbar \Omega$$

where we have introduced the Huang-Rhys factor  $S$  as dimensionless coupling constant

$$S = \frac{1}{2} \tilde{R}_e^2 = \frac{A^2}{\hbar \Omega} \frac{1}{2M\Omega^2} \quad (3.8)$$

The eigenfunctions  $\chi_n$  of the nuclear vibrations are Hermite polynomials. The Franck-Condon factor describes the overlap integral of the vibrational wavefunction of ground and excited state. As the electronic transition is fast compared to nuclear motion, the nuclear coordinate cannot change during the transition (Born-Oppenheimer approximation), and both ground and excited state need a non-vanishing probability to be at the same coordinate  $R$ . When one of the states is in a vibrational ground state, i.e.,  $n$  or  $m$  equals zero, the Franck-Condon factor takes the form<sup>2</sup>

$$|\langle \chi_0 | \chi_m \rangle|^2 = |\langle \chi_m | \chi_0 \rangle|^2 = \frac{S^m \exp(-S)}{m!} \quad (3.9)$$

which is a Poisson distribution of mean value  $S$ . The strongest transition is thus the transition into  $m \approx S$ , which for large coupling between electronic and nuclear system, i.e. large  $S$ , will deviate from the 0-0 transition.

<sup>2</sup> This notation is sloppy in the sense that the bra wavefunction is an electronic excited state, the ket function an electronic ground state!



Figure 3.2: Poisson distributions

The Debye-Waller factor  $D$  gives the ratio of the coherently scattered wave to all scattering processes. For molecules, this corresponds to the amplitude of the 0-0 line to the integral over the whole band. As the sum over all Franck-Condon factors to the same final state is one, we get

$$D = |\langle \chi_0 | \chi_0 \rangle|^2 = \exp(-S) \quad (3.10)$$

## Mirror rule

When we keep the assumptions of the last section, that the vibrational frequency of ground and excited state is the same, both potentials are harmonic, and of course the Born-Oppenheimer approximation hold, then absorption and emission spectrum are closely related. The 0-0 transition at energy  $E_{00}$  from the vibrational ground state of the electronic ground state



to the vibrational ground state of the electronic excited state appears both in absorption and emission. As the thermal energy  $kT$  is in most cases small compared to the vibrational energy  $\hbar\Omega$ , almost all molecules are in the vibrational ground state. Absorption then only occurs at energies larger than  $E_{00}$  into higher vibrational state of the electronic excited state. These energies are

$$E_{abs,n} = E_{00} + n \hbar\Omega \quad (3.11)$$

Fluorescence emission also occurs out of a vibrational ground state, but due to different reasons than absorption. In molecules, vibrational relaxation (some ps) is much faster<sup>3</sup> than fluorescence emission (some ns). The emission occurs thus into different vibrational levels of the electronic ground state at

$$E_{em,n} = E_{00} - n \hbar\Omega \quad (3.12)$$

The spectral position of the absorption and emission peaks are thus mirrored<sup>4</sup> around the 0–0 transition energy  $E_{00}$ .

Not only the spectral positions, but also the amplitude of the peaks in absorption spectrum  $\epsilon(\omega)$  and fluorescence spectrum  $F(\omega)$  are related. The reason is that the Einstein  $A$  and  $B$  coefficients are related, or that there is only one transition dipole moment  $\mu$  which governs both absorption and emission. The only caveat is the relation between the transition dipole moment and the spectra<sup>5</sup>

$$\epsilon(\omega = \omega_{g,m \rightarrow e,n}) \propto \omega_{g,m \rightarrow e,n} |\langle \chi_n | \chi_m \rangle|^2 B_{eg} \quad (3.13)$$

$$F(\omega = \omega_{e,n \rightarrow g,m}) \propto \omega_{e,n \rightarrow g,m}^3 |\langle \chi_m | \chi_n \rangle|^2 B_{ge} \quad (3.14)$$

This is the same as in eq.2.13 and 2.15. The spectral integral over a line in  $A(\omega)$  or  $F(\omega)$  is associated with a transition and thus a Franck-Condon factor. The integral has been solved assuming a line shape. Thereby a factor  $\omega$  remains on the right side of both equations. The fluorescence spectrum gets an additional factor of  $\omega^2$  due to the optical mode density in three-dimensional space, as it appears in the blackbody spectrum and in the relation between the Einstein coefficients  $A_{12}$  and  $B_{12}$ . All together, therefore, one should compare  $A/\omega$  and  $F/\omega^3$ .

## Stokes shift

When comparing absorption and emission spectra as above, one realizes that the 0–0 transition energies do not fully agree. This is the Stokes shift. Its amplitude depends on the molecule and the environment of the molecule. When a molecule is transferred into an electronic excited state, the spacial distribution of electron density changes. This influences the environment, for example the solvent molecules, in position and orientation. Directly after excitation, the solvent molecules are still in the position that gives lowest energy when the dye molecule is in the ground state. With the excited state, they will shift and reorient to reduce the overall energy. The fluorescence emission takes thus place from a different electric environment than the absorption, which leads to a shift in transition energy, the Stokes shift.

In a more general way, not only the difference between then 0–0 transition, but the difference between the peaks of absorption and emission

<sup>3</sup> 'Faster' means here that the rates are larger. The event itself can be assumed to be instantaneous.

<sup>4</sup> Lakowicz, 2010, chapter 1.3.2 and 1.3.3.

<sup>5</sup> Parson, 2015, Chapter 5.2.

spectra is sometimes called Stokes shift. This then includes also vibrational relaxation of the dye molecule itself.

## References

Kuzmany, Hans (2009). *Solid-state spectroscopy. An introduction*. Second edition. Heidelberg: Springer.

Lakowicz, Joseph R. (2010). *Principles of fluorescence spectroscopy*. New York, NY: Springer. [↗](#).

Parson, William W. (2015). *Modern optical spectroscopy*. Springer. [↗](#).

# Chapter4

## Rayleigh and Mie Scattering

Markus Lippitz  
May 6, 2021

### Tasks

- Determine the size and the concentration of the gold particles from their extinction spectrum (data by Patrick Knödler, Bayreuth). Are they spherical? On the server you find an Matlab / Octave implementation of the Mie  $a_n$  and  $b_n$  coefficients. The dielectric functions can be found at [refractiveindex.info](http://refractiveindex.info).
- Assign transitions to the peaks in the spectrum. For which spectra does the Rayleigh approximation hold?

### Rayleigh scattering of small spheres

In this chapter, we change our point of view a little bit. We consider small, mostly spherical, inclusion of material with one dielectric function in an environment with another dielectric function. At the end, we will make the connection to molecules and nanocrystals, but for the moment we stay with classical electrodynamics.

A sphere of radius  $R$  and dielectric constant  $\epsilon_{in}$  is embedded in a medium of dielectric constant  $\epsilon_{out}$ . We assume that the radius  $R$  is much smaller than the wavelength  $\lambda$  of the electromagnetic light field. This means that the phase is constant across the sphere and that we can employ the quasi-static approximation. One solves the Laplace equation taking boundary conditions and symmetry into account.<sup>1,2,3</sup> The sphere responds to the light field with a polarization of

$$\mathbf{p}(t) = \epsilon_0 \epsilon_{out} \alpha \mathbf{E}(t) \quad (4.1)$$

with the polarizability

$$\alpha = 4\pi R^3 \frac{\epsilon_{in} - \epsilon_{out}}{\epsilon_{in} + 2\epsilon_{out}} \quad (4.2)$$

We find a resonance when  $\epsilon_{in}(\omega) + 2\epsilon_{out}(\omega) = 0$ , which requires one dielectric function to be negative, as it is the case in metals. Small metal particles show thus exceptional strong interaction with light in a certain spectral range.

<sup>1</sup> Jackson, 1999.

<sup>2</sup> Nolting, 2016, exercise 2.4.2.

<sup>3</sup> Bohren and Huffman, 2007, chapter 5.2.



As the electric field oscillates  $E(t) = E_0 e^{-i\omega t}$ , also the polarization  $p$  oscillates and radiates a secondary, scattered electromagnetic field

$$\mathbf{E}_S = \frac{e^{ikr}}{4\pi\epsilon_0\epsilon_{out}} \frac{1}{r^3} \left\{ (kr)^2 (\hat{\mathbf{r}} \times \mathbf{p}) \times \hat{\mathbf{r}} + (1 - ikr) (3\hat{\mathbf{r}} [\hat{\mathbf{r}} \cdot \mathbf{p}] - \mathbf{p}) \right\} , \quad (4.3)$$

where  $k = 2\pi/\lambda$  is the length of the wave vector in the medium. In the optical far-field, i.e. for  $r \gg \lambda$  or  $kr \gg 1$  this simplifies to

$$\mathbf{E}_S = \frac{e^{ikr}}{4\pi\epsilon_0\epsilon_{out}} \frac{(kr)^2}{r^3} (\hat{\mathbf{r}} \times \mathbf{p}) \times \hat{\mathbf{r}} . \quad (4.4)$$

The total, space-integrated and time-averaged power of this scattered wave is<sup>4</sup>

$$P_{scat} = \frac{c}{12\pi\epsilon_0\epsilon_{out}} k^4 |p|^2 = \frac{c\epsilon_0\epsilon_{out}}{12\pi} k^4 |\alpha|^2 |E_0|^2 . \quad (4.5)$$

The power density of the incoming plane wave is given by the absolute value of the Poynting vector to<sup>5</sup>

$$|S| = \frac{1}{2} c \epsilon_0 \epsilon_{out} |E_0|^2 \quad (4.6)$$

and we thus can define a scattering cross section

$$\sigma_{scat} = \frac{P_{scat}}{|S|} = \frac{k^4}{6\pi} |\alpha|^2 . \quad (4.7)$$

We find the  $\omega^4$  frequency dependence typical for Rayleigh scattering.

## Optical Theorem and Extinction Cross Section

The scatted wave is not only responsible for light propagation in direction different from the incoming beam, but also for a reduction of the transmitted beam. Both effects are two sides of the same coin. This relation runs under the name of Optical Theorem<sup>6,7</sup>.

Far away from the scattering object, the scattered wave will be spherical, only the amplitude<sup>8</sup>  $f$  could depend on scattering direction  $\theta$ . Taking the incoming and the scatted wave together, and restricting us to a scalar discussion, we get<sup>9</sup>

$$E_{tot} = e^{ikz} E_{in} + \frac{e^{ikr}}{r} f(\theta) E_{in} , \quad (4.8)$$

where  $E_{in}$  is the incoming field at the position at which we place the particle. In almost forward direction ( $\theta \ll 1$ ) we get

$$r = \sqrt{x^2 + y^2 + z^2} \approx z + \frac{x^2 + y^2}{2z} . \quad (4.9)$$

The field in forward direction is thus

$$E_{tot} \approx E_{in} e^{ikz} \left[ 1 + \frac{1}{z} f(\theta) e^{ik(x^2+y^2)/2z} \right] , \quad (4.10)$$

where we once even took  $r \approx z$ . When dropping terms quadratic in the scattering amplitude  $f$  and assuming  $f(\theta) \approx f(0)$  we get for the intensity<sup>10</sup>

$$I \approx \frac{1}{2} c \epsilon_0 |E_{in}|^2 \left[ 1 + \frac{1}{2z} \Re \left( f(0) e^{ik(x^2+y^2)/2z} \right) \right] . \quad (4.11)$$



Figure 4.1: Scattered field of a sphere

<sup>4</sup> Nolting, 2016, chapter 4.5.2.

<sup>5</sup> Nolting, 2016, chapter 4.3.8.



Figure 4.2: Scattering in forward direction interferes with the exciting beam.

<sup>6</sup> Jackson

<sup>7</sup> Newton, 1976.

<sup>8</sup>  $f$  has the unit of a length

<sup>9</sup> Newton, 1976.

<sup>10</sup> units W/m<sup>2</sup>

We now integrate<sup>11</sup> over a screen that is so large that the argument of the exponential function oscillates rapidly ( $kR^2/z \gg 2\pi$ ), but that is still concentrated along the forward direction ( $R/z \ll 1$ ):

<sup>11</sup> Newton, 1976.

$$P_{\text{screen}} = \int_{\text{screen}} I dR^2 \approx \frac{1}{2} c \epsilon_0 |E_{in}|^2 \left[ A - \frac{4\pi}{k} \Im(f(0)) \right] \quad , \quad (4.12)$$

where  $A$  is the size of the screen. The second term in the brackets is the extinction cross section

$$\sigma_{ext} = \sigma_{scat} + \sigma_{abs} = \frac{4\pi}{k} \Im(f(0)) \quad . \quad (4.13)$$

Extinction looks at missing power in a transmitted beam. It does not distinguish between power that remains in the object, e.g. in form of heat, and power that is scattered into a different direction.

## Absorption and Scattering of a Small Sphere

Let us apply the Optical Theorem to the case of a small sphere, described by an ideal dipole. The scattering amplitude in forward direction of a dipolar scatterer is related to its polarizability  $\alpha$  by

$$f(0) = \frac{k^2}{4\pi} \alpha \quad . \quad (4.14)$$

We then get the extinction coefficient from the optical theorem

$$\sigma_{ext} = k \Im(\alpha) \quad . \quad (4.15)$$

We can also calculate the power that is absorbed by the dipole<sup>12</sup>

<sup>12</sup> Novotny and Hecht, 2012, Chapter 8.

$$P_{abs} = \frac{\omega}{c} \Im(\mathbf{p} \mathbf{E}^*) \quad , \quad (4.16)$$

so that we get

$$\sigma_{abs} = k \Im(\alpha) \quad . \quad (4.17)$$

If both  $\sigma_{abs}$  and  $\sigma_{ext}$  would equal  $k \Im(\alpha)$ , then now power would be left for scattering. But we calculated a non-zero scattering cross section. This puzzle is solved by taking radiation reaction into account, as discussed in chapter 8.4.2 of Novotny and Hecht, 2012. Starting from a quasi-static polarizability  $\alpha$  was a too much of a simplification to calculate propagating and oscillating fields for the optical theorem. An effective polarizability  $\alpha_{\text{eff}}$  can be constructed<sup>13</sup>

<sup>13</sup> Our definition of  $\alpha$  does not include an  $\epsilon_0$  as in exercise 8.5 in Novotny and Hecht, 2012

$$\alpha_{\text{eff}} = \frac{\alpha}{1 - \frac{ik^3}{6\pi}\alpha} \approx \alpha - \frac{ik^3}{6\pi}\alpha^2 \quad (4.18)$$

and then we get

$$\sigma_{ext} = k \Im(\alpha_{\text{eff}}) \approx k \Im(\alpha) + \frac{k^4}{6\pi} (\Im(\alpha)^2 - \Re(\alpha)^2) \quad (4.19)$$

$$\sigma_{scat} = \frac{k^4}{6\pi} |\alpha_{\text{eff}}|^2 \approx \frac{k^4}{6\pi} |\alpha|^2 \quad (4.20)$$

$$\sigma_{abs} = \sigma_{ext} - \sigma_{scat} \approx k \Im(\alpha) \quad (4.21)$$

## Mie Scattering

Above we have discussed the optical properties of a small particle, small compared to the wavelength of light in the medium. The reason for this restriction was that in this case we could use the quasi-static approximation to obtain a solution for the polarization  $\mathbf{p}$  and continue from there. In the special case of spherical particles in a homogeneous environment, we also can find analytical solutions, first published by Gustav Mie.<sup>14</sup> The idea is to develop the scattered field in vector spherical harmonics.

<sup>14</sup> Bohren and Huffman, 2007, chapter 4.

For the cross sections one gets

$$\sigma_{scat} = \frac{2\pi}{k^2} \sum_{n=1}^{\infty} (2n+1) (|a_n|^2 + |b_n|^2) \quad (4.22)$$

$$\sigma_{ext} = \frac{2\pi}{k^2} \sum_{n=1}^{\infty} (2n+1) \Re(a_n + b_n) \quad (4.23)$$

with the coefficients

$$a_n = \frac{m S_n(mx) S'_n(x) - S_n(x) S'_n(mx)}{m S_n(mx) C'_n(x) - C_n(x) S'_n(mx)} \quad (4.24)$$

$$b_n = \frac{S_n(mx) S'_n(x) - m S_n(x) S'_n(mx)}{S_n(mx) C'_n(x) - m C_n(x) S'_n(mx)} \quad (4.25)$$

where  $x = ka$  is the dimensionless size of the sphere with radius  $a$  and  $m = n_{particle}/n_{medium}$  is the relative refractive index. The prime indicates a differentiation with respect to the argument. The  $S_n$  and  $C_n$  are Ricatti-Bessel functions, which can be expressed in terms of spherical Bessel functions:

$$S_n(\rho) = \rho j_n(\rho) \quad (4.26)$$

$$C_n(\rho) = \rho h_n^{(1)}(\rho) = \rho (j_n(\rho) + i y_n(\rho)) \quad (4.27)$$

The index  $n$  gives the order of the spherical harmonics and thus the order of the multipole.  $n = 1$  corresponds to dipole fields,  $n = 2$  to quadrupole fields,  $n = 3$  to octupole fields etc.<sup>15</sup> The  $a$  coefficients describe electric modes, the  $b$  coefficients magnetic modes.<sup>16</sup>

<sup>15</sup> Kreibig and Vollmer, 1995.

We can recover the physics of a small sphere from the full Mie theorie.<sup>17</sup> A Taylor-expansion of the coefficients  $a_n$  and  $b_n$  for small size parameter  $x$  gives

<sup>16</sup> Bohren and Huffman, 2007; Kreibig and Vollmer, 1995.

<sup>17</sup> Bohren and Huffman, 2007, chapter 5.

$$a_1 = -i \frac{2x^3}{3} \frac{m^2 - 1}{m^2 + 2} - i \frac{2x^5}{5} \frac{(m^2 - 2)(m^2 - 1)}{(m^2 + 2)^2} + \mathcal{O}(x^6) + \mathcal{O}(x^7) \quad (4.28)$$

$$b_1 = -i \frac{2x^5}{45} (m^2 - 1)^2 + \mathcal{O}(x^7) \quad (4.29)$$

$$a_2 = -i \frac{2x^5}{15} \frac{m^2 - 1}{2m^2 + 3} + \mathcal{O}(x^7) \quad (4.30)$$

$$b_2 = + \mathcal{O}(x^7) \quad (4.31)$$

We note that the magnetic dipolar  $b_1$  mode appears to the same order as the electric quadrupolar  $a_2$  mode. The distinction between them is dependent on the gauge used.<sup>18</sup>

<sup>18</sup> Needs reference !

When we restrict us to third order in  $x$ , we recover the Rayleigh limit

$$\sigma_{scat} = \frac{2\pi}{k^2} 3 |a_1|^2 = \frac{k^4}{6\pi} \left| 4\pi a^3 \frac{\epsilon_{in} - \epsilon_{out}}{\epsilon_{in} + 2\epsilon_{out}} \right|^2 \quad (4.32)$$

$$\sigma_{ext} = \frac{2\pi}{k^2} 3 \Re(a_1) = k \Im \left( 4\pi a^3 \frac{\epsilon_{in} - \epsilon_{out}}{\epsilon_{in} + 2\epsilon_{out}} \right) \quad (4.33)$$

## More questions

- Sketch the field amplitude close to and far from the particle at these resonances, either by hand based on analytic solutions or numerically.

## References

- Bohren, Craig F. and Donald R. Huffman (2007). *Absorption and Scattering of Light by Small Particles*. John Wiley & Sons, Ltd. [↗](#).
- Jackson, John David (1999). *Classical electrodynamics*. 3. ed. New York [u.a.]: Wiley.
- Kreibig, Uwe and Michael Vollmer (1995). *Optical properties of metal clusters*. Berlin u.a.: Springer.
- Newton, Roger G (1976). "Optical theorem and beyond". In: *American Journal of Physics* 44.7, p. 639. [↗](#).
- Nolting, Wolfgang (2016). *Theoretical Physics 3 Electrodynamics*. Springer. [↗](#).
- Novotny, Lukas and Bert Hecht (2012). *Principles of nano-optics*. 2. ed. Cambridge Univ. Press. [↗](#).





# Chapter5

## Molecular Aggregates – Coupled Two-Level Systems

Markus Lippitz

May 20, 2021

### Tasks

- The data contains absorption spectra of the molecule TDBC in solution at different concentrations. Determine the number of chromophores that contribute to the delocalized state. Data by Tobias Kroh, Bayreuth.
- The second data set contains emission spectra of TDBC in solution at different concentrations. Plot the normalized emission spectrum and discuss. Data by Tobias Kroh, Bayreuth.

### Coupled Pendulum

A mathematical pendulum of point mass  $m$  and rod length  $L$  is governed by the differential equation of its angular displacement  $\phi$

$$\ddot{\phi} + \frac{g}{L} \phi = 0 \quad \text{with} \quad \omega^2 = \frac{g}{L}, \quad (5.1)$$

where  $g$  is the acceleration due to gravity and  $\omega$  its angular eigen-frequency. When two of such pendula are coupled by a spring between the two masses, we get a coupled system of differential equations

$$\ddot{\phi}_1 + \frac{g}{L_1} \phi_1 + \frac{k}{m_1} (\phi_1 - \phi_2) = 0 \quad (5.2)$$

$$\ddot{\phi}_2 + \frac{g}{L_2} \phi_2 - \frac{k}{m_2} (\phi_1 - \phi_2) = 0 \quad (5.3)$$

with the spring constant  $k$ . For the moment, we assume that the pendula are identical, i.e.,  $L = L_1 = L_2$  and  $m = m_1 = m_2$ . The eigen-frequencies are then

$$\omega_+^2 = \frac{g}{L} \quad \text{and} \quad \omega_-^2 = \frac{g}{L} + 2\frac{k}{m}, \quad (5.4)$$

where in the mode with frequency  $\omega_+$  both masses move to the same direction, in the  $\omega_-$  in opposite directions. Only in the latter case the coupling spring comes into play.



This work is licensed under a [Creative Commons "Attribution-ShareAlike 4.0 International"](https://creativecommons.org/licenses/by-sa/4.0/) license.

To investigate the general case, we assume harmonic oscillations, i.e.  $\phi(t) = \phi_0 \exp(i\omega t)$  and write the differential equation as matrix

$$\mathbf{M} \phi = \begin{pmatrix} \frac{g}{L_1} + \frac{k}{m_1} & -\frac{k}{m_1} \\ -\frac{k}{m_2} & \frac{g}{L_2} + \frac{k}{m_2} \end{pmatrix} \phi = \omega^2 \phi \quad (5.5)$$

We thus search eigen-values and eigen-vectors of  $\mathbf{M}$ . Assuming individual lengths, but identical masses, we get

$$\omega_{\pm}^2 = \left( \frac{\omega_1^2 + \omega_2^2}{2} + \frac{k}{m} \right) \pm \sqrt{\left( \frac{\omega_1^2 - \omega_2^2}{2} \right)^2 + \left( \frac{k}{m} \right)^2} \quad (5.6)$$

For identical lengths, i.e., identical eigen-frequencies  $\omega_1 = \omega_2$ , this recovers the results from above.

## Quantum Mechanics of Coupled States

A quantum mechanical state is described by its eigen-functions  $\psi_i$  and the corresponding eigen-energies  $E_i$  so that

$$\hat{H} \psi_i = E_i \psi_i \quad (5.7)$$

The eigen-functions  $\psi_j$  form a basis. We can describe all wave functions  $\phi$  as

$$\phi = \sum_n c_n \psi_n \quad (5.8)$$

In the same way, all operators  $\hat{A}$  are fully described by their matrix element

$$A_{ij} = \langle \psi_i | \hat{A} | \psi_j \rangle \quad (5.9)$$

where the brackets describe the integral over all relevant coordinates. We can then<sup>1</sup> represent the wave function  $\phi$  by a vector of the complex entries  $c_n$  and the operator by a matrix of the elements  $A_{ij}$ .

With two states  $\psi_a$  and  $\psi_b$  we have

$$\hat{H}_0 = \begin{pmatrix} E_a & 0 \\ 0 & E_b \end{pmatrix} \quad (5.10)$$

The Hamilton operator  $\hat{H}_0$  is thus described by a  $2 \times 2$  matrix. When the two states  $a$  and  $b$  are coupled, then the energy of one state depends somehow on the other. In the matrix we include a coupling energy  $J$  in the off-diagonal elements

$$\hat{H}_{coupled} = \begin{pmatrix} E_a & J \\ J & E_b \end{pmatrix} \quad (5.11)$$

As a consequence, the original eigen-functions  $\psi_0$  are no longer eigen-functions of this coupled Hamilton operator. We find new eigen-functions and eigen-values by diagonalizing  $\hat{H}_{coupled}$ , so that the diagonal elements become

$$E_{\pm} = \frac{E_a + E_b}{2} \pm \sqrt{\left( \frac{E_a - E_b}{2} \right)^2 + J^2} \quad (5.12)$$

and the new eigen-functions are<sup>2</sup>

<sup>1</sup> For details see a book on quantum mechanics, for example Schwabl, 2002, chapter 8.

<sup>2</sup> Parson, 2015, eq. 8.10.

$$\psi_{\pm} = \sqrt{\frac{1 \pm s}{2}} \psi_a \pm \sqrt{\frac{1 \mp s}{2}} \psi_b, \quad (5.13)$$

with

$$s = \frac{E_a - E_b}{\sqrt{(E_a - E_b)^2 + (2J)^2}}. \quad (5.14)$$

We can distinguish two limiting cases. The coupling energy  $J$  can be larger than the energy difference between the two states, i.e.  $|J| \gg |E_a - E_b|/2$ . Then the new eigen-energies are split up by  $\pm J$  around the average of the old eigen-energies  $(E_a + E_b)/2$ . The eigen-functions in this situation are symmetric and anti-symmetric combinations of the old eigen-function, i.e.  $\psi_{\pm} = \pm \psi_a + \psi_b$ . When the coupling energy is small, i.e.  $|J| \ll |E_a - E_b|/2$ , then the new eigen-energies and eigen-functions are close to the old.



Figure 5.1: Eigen-Energies and weights of the eigen-functions as function of the unperturbed energies ( $E_b = 1$ ).

A few side remarks and things that are left open for future versions of this text:

- When the coupling interaction is the electromagnetic wave, then this formalism describes the AC Stark effect, i.e., the shift of atomic transitions in the presence of strong optical fields.
- The coupling constant  $\beta$  can be complex-valued, i.e., can include a phase lag.
- Preparation and temporal evolution of coupled states could be interesting to discuss.

## Coupling of two transition dipole moments

We consider two molecules,  $a$  and  $b$ , each with a ground (0) and excited (1) state. We write the wave function on the form  $|ab\rangle$ , i.e.  $|01\rangle$  is molecule  $a$  in ground state, molecule  $b$  in excited state. In each molecule, an optical transition dipole moment couples ground and excited state, i.e.  $\langle 10|\hat{\mu}_a|00\rangle$  and  $\langle 01|\hat{\mu}_b|00\rangle$  are different from zero and describe an excitation of the molecule  $a$  and  $b$ , respectively. Additionally, the two transition dipole moments interact and lead to a resonant coupling of the  $|01\rangle$  and  $|10\rangle$  state<sup>3</sup>

$$\hat{H}_{coupling} = J(|10\rangle\langle 01| + |01\rangle\langle 10|). \quad (5.15)$$

The coupling energy  $J$  depends on distance  $r_{ab}$  and relative orientation of the transition dipoles  $\mu_{a,b}$ . It can be seen as the energy of one dipole in the field of another<sup>4</sup>

<sup>3</sup> Knoester, 2002.

<sup>4</sup> does this need more details? See Parson

$$J = \frac{\boldsymbol{\mu}_a \cdot \boldsymbol{\mu}_b}{|\mathbf{r}_{ab}|^3} + 3 \frac{(\boldsymbol{\mu}_a \cdot \mathbf{r}_{ab})(\boldsymbol{\mu}_b \cdot \mathbf{r}_{ab})}{|\mathbf{r}_{ab}|^5} \quad (5.16)$$

$$= \frac{\mu_a \mu_b}{r_{ab}^3} (\cos \theta - 3 \cos \alpha \cos \beta) = \frac{\mu_a \mu_b}{r_{ab}^3} \kappa \quad (5.17)$$

where the angles are defined in the sketch.

A similar coupling term also exist for the non-resonant coupling<sup>5</sup>

$$\hat{H}_{non-res} = J (|11\rangle \langle 00| + |00\rangle \langle 11|) \quad (5.18)$$

but this can be ignored, as it is non-resonant. Altogether, the Hamilton operator reads in matrix form

$$\hat{H} = \begin{pmatrix} 0 & \mu_a & \mu_b & J \\ \mu_a^* & \hbar\omega_a & J & \mu_b \\ \mu_b^* & J^* & \hbar\omega_b & \mu_a \\ J^* & \mu_b^* & \mu_a^* & \hbar(\omega_a + \omega_b) \end{pmatrix}. \quad (5.19)$$

When we ignore the double-excited state  $\langle 11|$ , the essence is contained in the center  $2 \times 2$  matrix which we discussed already in the preceding section.

When  $|\psi\rangle$  is a linear combination of  $|01\rangle$  and  $|10\rangle$ , then also the transition dipole moment from  $|00\rangle$  to  $|\psi\rangle$  is a linear combination of  $\mu_a$  and  $\mu_b$  with the same weights. When  $J \gg |E_a - E_b|/2$  then we get

$$\boldsymbol{\mu}_{\pm} = \sqrt{1/2} (\boldsymbol{\mu}_a \pm \boldsymbol{\mu}_b) \quad (5.20)$$

The brightness of the absorption line is for identical molecules, i.e.  $\mu_a = \mu_b$

$$I \propto |\boldsymbol{\mu}_{\pm}|^2 = (1/2) |\boldsymbol{\mu}_a \pm \boldsymbol{\mu}_b|^2 = (1 \pm \cos \theta) |\boldsymbol{\mu}|^2, \quad (5.21)$$

where  $\theta$  is as above the angle between the transition dipole moments. The same relation hold for the radiative rate.

The spectroscopic signature of coherent coupling between two molecules is thus a splitting of the absorption line into two lines, separated by twice the coupling energy  $J$ . The sum of the line amplitudes remains unchanged, but in some cases (H- and J-aggregates, see below) one transition will take the whole amplitude and the other remains dark. In these cases, no splitting but a shift of the absorption line is observed. The coupling vanishes when both dipoles are oriented perpendicular to each other ( $\theta = 90^\circ$ )

## H- and J-aggregates

Two important limiting cases are the H- and J-aggregates<sup>6</sup> In a J-aggregate, the dipoles are oriented parallel and head-to-tail, i.e.  $\alpha = \beta = \theta = 0$  and therefore  $\kappa = -2$ . A negative  $\kappa$  implies that the coupling constant  $J$  is negative. The state  $\Psi_+$ , which carries all the oscillator strength, has the energy  $E_+ = (E_a + E_b)/2 + J$ , which is lower than the average energy of the uncoupled states. The absorption line thus shifts to the red. The same hold for the fluorescence emission spectrum.

In an H-aggregate, the dipoles orient also parallel, but side-to-side, i.e.  $\alpha = \beta = 90^\circ$  and  $\theta = 0$ . In this case is  $\kappa = 1$  and  $J$  positive. The absorption line shifts to the blue upon formation of aggregates, as again the

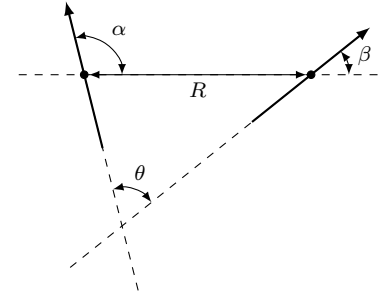


Figure 5.2: Sketch showing the angles used to calculate the coupling factor  $\kappa$

<sup>5</sup> Knoester, 2002.

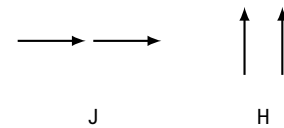


Figure 5.3: J- and H aggregates.

<sup>6</sup> Köhler and Bässler, 2015, chapters 2.1.4.3, 2.2.5.3.

$\Psi_+$  state gets all the oscillator strength. However, as fluorescence emission is slow compared to other relaxation processes, this high energy state does not emit light. In emission, H-aggregates appear dark.

The width of the absorption line of a dye at room temperature is determined by dephasing, i.e., fluctuations in the environment that are fast compared to the lifetime of the excited state, and by static differences in the environment of different chromophores. The spectral position of the absorption line in a molecular aggregate is the average of two single chromophore transitions. As in the propagation of uncertainties in an experiment, the width of the new distribution, generated as the average over two values from the old distribution, is reduced by a factor of  $\sqrt{2}$ . This holds more generally<sup>7</sup>, so that an aggregate of  $N$  chromophores is expected to have a spectral line width reduced<sup>8</sup> by  $\sqrt{N}$ .

<sup>7</sup> Knapp, 1984.

<sup>8</sup> This is the same physics as motional narrowing in NMR.

## References

- Knapp, E.W. (1984). "Lineshapes of molecular aggregates, exchange narrowing and intersite correlation". In: *Chemical Physics* 85.1, pp. 73–82. [↗](#).
- Knoester, J. (2002). "Optical properties of molecular aggregates". In: *Proceedings of the International School of Physics 'Enrico Fermi'*. Volume 149: Organic Nanostructures: Science and Applications. IOS Press, pp. 149–186. [↗](#).
- Köhler, Anna and Heinz Bässler (2015). *Electronic processes in organic semiconductors*. Weinheim: Wiley-VCH. [↗](#).
- Parson, William W. (2015). *Modern optical spectroscopy*. Springer. [↗](#).
- Schwabl, Franz (2002). *Quantenmechanik*. 6. Auflage. Springer. [↗](#).



## **Part II**

# **Two Level Systems**





# Chapter6

## Rabi Oscillations

Markus Lippitz  
May 20, 2021

### Tasks

- Visualize the path of the Bloch vector and its components when a laser pulse shines on a two-level system. Use a numerical method to integrate the differential equation. Investigate both resonant and non-resonant cases.

### Experiment

Many experimental realizations show Rabi oscillations. We will discuss them in terms of a two-level system interacting with an optical field, for example an atom in vacuum or a molecule or quantum dot in solid state at low temperature. But the same description holds also for many other systems. In fact, a two-level system is equivalent to a spin  $1/2$  system, as an electron spin or nuclear spin. The same concepts are thus applied in electron spin resonance or nuclear magnetic resonance experiments (ESR and NMR).

We shine a laser beam on an atom, molecule, quantum dot. The laser frequency is close to the optical transition. We measure the populations of the excited state by, e.g. fluorescence emission or tunneling of the electron out of this state. We switch on the laser for a given time duration  $t$  and measure the signal amplitude as function of  $t$ . This a little bit indirect experiment is necessary, as  $t$  is in many cases short compared to the emission or tunneling rate. Only in theory we can measure the population of the state while it is evolving. We find periodic oscillations of the signal amplitude, the Rabi oscillations.<sup>1</sup>

<sup>1</sup> needs papers!

### Density Matrix

We start by introducing the density matrix.<sup>2</sup> It is a tool in quantum mechanics to describe not only purely coherent states, but also statistical mixtures, as we will see below. The density matrix is a bit at the edge of the classical canon of quantum mechanics lectures.

<sup>2</sup> Hamm, 2005; Parson, 2015; Rand, 2016.



This work is licensed under a [Creative Commons "Attribution-ShareAlike 4.0 International"](https://creativecommons.org/licenses/by-sa/4.0/) license.

When writing our wave function  $|\psi\rangle$  in a basis  $|n\rangle$  as

$$|\psi\rangle = \sum_n c_n |n\rangle \quad (6.1)$$

then we can define a density operator  $\hat{\rho}$  as

$$\hat{\rho} = |\psi\rangle \langle\psi| = \sum_{m,n} c_n c_m^* |n\rangle \langle m| \quad (6.2)$$

and the matrix elements of  $\hat{\rho}$  are  $\rho_{n,m} = c_n c_m^*$  or

$$\rho = \begin{pmatrix} \rho_{00} & \rho_{01} \\ \rho_{10} & \rho_{11} \end{pmatrix} \quad (6.3)$$

The density matrix allows to calculate the expectation value of any operator  $\hat{A}$  as

$$\langle\hat{A}\rangle = \langle\psi|\hat{A}|\psi\rangle = \sum_{m,n} c_n c_m^* A_{m,n} = \sum_{m,n} \rho_{n,m} A_{m,n} = \text{Tr}(A\rho) \quad , \quad (6.4)$$

where the trace sums over the diagonal elements

$$\text{Tr}(U) = \sum_n U_{n,n} \quad . \quad (6.5)$$

The trace of the density matrix is one for normalized states

$$\text{Tr}(\rho) = \sum_n \rho_{n,n} = \sum_n c_n c_n^* = 1 \quad \text{if normalized} \quad . \quad (6.6)$$

The interesting thing comes when looking at pure and mixed states. Pure states are the 'conventional' states discussed in quantum mechanics, for example this superposition of states

$$|\psi\rangle = \sqrt{\frac{1}{2}} (|1\rangle + |2\rangle) \quad . \quad (6.7)$$

In this example, the density matrix reads

$$\rho = \frac{1}{2} \begin{pmatrix} 1 & 1 \\ 1 & 1 \end{pmatrix} \quad (6.8)$$

and its trace is one. But the density matrix also allows to describe new things, beyond pure states, namely statistical mixtures of states. We can describe an ensemble of two-level systems, of which half the ensemble is in state  $|1\rangle$ , the other half in state  $|2\rangle$ . This can *not* be written as  $|1\rangle + |2\rangle$ , but a density matrix description is possible. If the statistical probability of each pure state with density matrix  $\rho_i$  is  $p_i$ , then the density matrix of the mixed state is given by

$$\rho_{\text{mixed}} = \sum_i p_i \rho_i \quad . \quad (6.9)$$

For a 50 : 50 mixture of  $|1\rangle$  and  $|2\rangle$  we get

$$\rho = \frac{1}{2} \begin{pmatrix} 1 & 0 \\ 0 & 1 \end{pmatrix} \quad . \quad (6.10)$$

We can distinguish between pure and mixed states by looking at the trace of the squared density matrix

$$\text{Tr}(\rho^2) = 1 \quad \text{pure state} \quad (6.11)$$

$$< 1 \quad \text{mixed state.} \quad (6.12)$$

Mixed states can be used not only to describe an ensemble of systems in different states, but also to describe a single system that at different times is in different states. Even if we can do an experiment on a single quantum system, we have to repeat it very often to reduce noise by averaging. But the experiment does not always run along the same path: either a photon is absorbed or not, but it will most likely not *always* be absorbed. The time-average of such an experiment will thus need an statistical mixture for its description.

The diagonal elements of the density matrix describe the populations of the states, i.e.  $|c_n|^2$ . The off-diagonal elements describe coherence between states. 'Coherence' means 'constant phase relation' or 'possibility to interfere', as with coherent (laser) or incoherent (candle) light. When writing  $|1\rangle + |2\rangle$  we have defined the phase between the states to be zero, as

$$r e^{i\phi} = \frac{c_1}{c_2} \quad \text{gives here} \quad \phi = 0 \quad . \quad (6.13)$$

In a statistical mixture there is no<sup>3</sup> coherence between the states, as one sub-ensemble is in one state, another in another state, and they don't know anything of each other.

<sup>3</sup> better: not enough

## Questions

1. For which values of  $b$  is the following density matrix describing a pure state ?

$$\rho = \frac{1}{2} \begin{pmatrix} 1+a & b^* \\ b & 1-a \end{pmatrix}$$

where  $a$  is real and  $b$  could be complex.

2. Assume a normalized wave function  $|\psi\rangle = c_1 |1\rangle + c_2 |2\rangle$ . Calculate its density matrix and convince yourself that it describes a pure state.
3. Investigate the off-diagonal elements of a density matrix describing a 50 : 50 mixture of  $|1\rangle$  and  $\sqrt{1/2}(|1\rangle + |2\rangle)$ .

## Liouville-von Neumann equation

We can construct a differential equation for the time evolution of the density matrix that is a direct analogue of the Schrödinger equation, just that is also takes mixed states into account.

The time-derivative of the density operator  $\hat{\rho}$  is

$$\frac{d}{dt} \hat{\rho} = \frac{d}{dt} (|\psi\rangle \langle\psi|) = \left( \frac{d}{dt} |\psi\rangle \right) \langle\psi| + |\psi\rangle \left( \frac{d}{dt} \langle\psi| \right) \quad . \quad (6.14)$$

Making use of the Schrödinger equation

$$\frac{d}{dt} |\psi\rangle = -\frac{i}{\hbar} \hat{H} |\psi\rangle \quad (6.15)$$

we get the Liouville–von Neumann equation

$$\frac{d}{dt}\hat{\rho} = -\frac{i}{\hbar} [\hat{H}, \hat{\rho}] \quad . \quad (6.16)$$

As an example, let us look at a two-level system with the eigen-energies  $E_0 = 0$  and  $E_1 = \hbar\omega_0$ . The Hamilton operator is thus

$$H = \begin{pmatrix} 0 & 0 \\ 0 & \hbar\omega_0 \end{pmatrix} \quad . \quad (6.17)$$

The commutator becomes

$$[\hat{H}, \hat{\rho}] = \begin{pmatrix} 0 & -\hbar\omega_0 \rho_{01} \\ \hbar\omega_0 \rho_{10} & 0 \end{pmatrix} \quad . \quad (6.18)$$

The diagonal elements of the density matrix  $\rho$ , i.e., the populations, remain thus constant in time, as expected for this Hamiltonian. The off-diagonal elements, the coherences acquire a phase-factor proportional to the energy difference, i.e.

$$\rho_{01}(t) = \rho_{01}(0) \exp(i\omega_0 t) \quad . \quad (6.19)$$

## Questions

4. Derive eqs. 6.18 and 6.19.

## Optical Bloch Equations

Now we switch on light and add an interaction Hamiltonian  $\hat{H}_I = -\boldsymbol{\mu} \cdot \mathbf{E}$  with the dipole operator  $\boldsymbol{\mu}$  and the optical field  $\mathbf{E}$ . In total, the Hamilton operator reads<sup>4</sup>

$$\hat{H} = \begin{pmatrix} 0 & -\boldsymbol{\mu} \cdot \mathbf{E} \\ -\boldsymbol{\mu}^* \cdot \mathbf{E}^* & \hbar\omega_0 \end{pmatrix} \quad . \quad (6.20)$$

<sup>4</sup> Rand, 2016, chap. 3.8.

The differential equations for the density matrix become the Bloch equations

$$\dot{\rho}_{00} = -\frac{i}{\hbar} (\rho_{01} \boldsymbol{\mu}^* \cdot \mathbf{E}^* - \rho_{10} \boldsymbol{\mu} \cdot \mathbf{E}) \quad (6.21)$$

$$\dot{\rho}_{11} = -\frac{i}{\hbar} (\rho_{10} \boldsymbol{\mu} \cdot \mathbf{E} - \rho_{01} \boldsymbol{\mu}^* \cdot \mathbf{E}^*) \quad (6.22)$$

$$\dot{\rho}_{01} = -\frac{i}{\hbar} (-\rho_{01} \hbar\omega_0 + (\rho_{00} - \rho_{11}) \boldsymbol{\mu} \cdot \mathbf{E}) \quad (6.23)$$

$$\dot{\rho}_{10} = -\frac{i}{\hbar} (+\rho_{10} \hbar\omega_0 + (\rho_{11} - \rho_{00}) \boldsymbol{\mu}^* \cdot \mathbf{E}^*) \quad (6.24)$$

These are effectively only 3 differential equations, as the wave function has to stay normalized, i.e.,  $\rho_{00} + \rho_{11} = 1$ . We can simplify things by skipping some algebraic transformations and introducing the Bloch vector  $\mathbf{S}$  with

$$\mathbf{S} = \begin{pmatrix} u \\ v \\ w \end{pmatrix} = \begin{pmatrix} \rho_{01} + \rho_{10} \\ i(\rho_{01} - \rho_{10}) \\ \rho_{00} - \rho_{11} \end{pmatrix} = \begin{pmatrix} 2\Re(\rho_{01}) \\ 2\Im(\rho_{01}) \\ \rho_{00} - \rho_{11} \end{pmatrix} \quad . \quad (6.25)$$

The density matrix elements are recovered by

$$\rho = \frac{1}{2} \begin{pmatrix} 1+w & u-iv \\ u+iv & 1-w \end{pmatrix} \quad (6.26)$$

With this we can write the system of differential equation as

$$\dot{\mathbf{S}} = \mathbf{M} \times \mathbf{S} \quad \text{with} \quad \mathbf{M} = \begin{pmatrix} -\frac{2}{\hbar} \Re(\boldsymbol{\mu} \mathbf{E}) \\ -\frac{2}{\hbar} \Im(\boldsymbol{\mu} \mathbf{E}) \\ \omega_0 \end{pmatrix}. \quad (6.27)$$

The time evolution of the Bloch vector, and by this of the density matrix, can be described by the action of a torque vector  $\mathbf{M}$ .

These equations have been derived by Felix Bloch for the magnetization of an ensemble of atomic nuclei in an NMR experiment. With nuclear or electronic (ESR) magnetic moments, the vector corresponds to the direction of the ensemble average of the magnetization, i.e., it is a real-space vector in the laboratory frame. In our case,  $\mathbf{S}$  is a vector in an abstract 3d vector space that describes the density matrix of an ensemble of two-level systems. Therefore, I use the variables  $uvw$  instead of  $xyz$ , but the physics is the always the same. Also spin-1/2 systems like electron spins or nuclear spins in ESR and NMR experiments form a two-level system.

Without optical field, the Bloch vector rotates around its  $w$  axis, as seen in the phase oscillation of the coherences in the last chapter. With optical field, also the populations changes, and things become complicated. To simplify things, we assume that our optical field is a single mode with a slowly varying amplitude only, i.e.

$$\mathbf{E}(t) = \mathbf{x} E_0(t) (e^{i\omega_L t} + e^{-i\omega_L t}) \quad (6.28)$$

The time-dependence of  $E_0(t)$  should be slow compared to  $\omega_L$ . This is the slowly varying amplitude approximation (SVEA). We do the same with the off-diagonal elements of the density matrix

$$\rho'_{01} = \rho_{01} e^{-i\omega_L t} \quad \text{and} \quad \rho'_{10} = \rho_{10} e^{+i\omega_L t} = \rho'_{01}^* \quad (6.29)$$

We thus factor out a phase oscillation with the laser frequency and keep only the slowly varying rest.<sup>5</sup> Inspecting the differential equations for the density matrix, this leads together with our definition of  $\mathbf{E}$  to the following modifications

$$\omega_0 \rightarrow \omega_0 - \omega_L \quad \text{and} \quad \boldsymbol{\mu} \mathbf{E} \rightarrow \boldsymbol{\mu} E_0 (1 + e^{i2\omega_L t}) \approx \boldsymbol{\mu} E_0 \quad (6.30)$$

As we assumed the elements of  $\rho'$  to vary slowly, we neglect the term  $\exp(i2\omega_L t)$ , as it will average out. This is the rotating wave approximation (RWA). Effectively, we are going into a rotating frame. Our new coordinate system rotates around the  $w$  axis with the angular frequency of the laser  $\omega_L$ . The optical frequency of the transition  $\omega_0$  is close to this laser frequency. We neglect terms of  $\omega_0 + \omega_L$  and only keep terms of  $\omega_0 - \omega_L$ . In total we get<sup>6</sup>

$$\dot{\mathbf{S}}' = \mathbf{M}' \times \mathbf{S}' \quad \text{with} \quad \mathbf{M}' = \begin{pmatrix} -\mu E_0(t)/\hbar \\ 0 \\ \omega_0 - \omega_L \end{pmatrix} = \begin{pmatrix} -\Omega \\ 0 \\ \omega_0 - \omega_L \end{pmatrix} \quad (6.31)$$

with the (angular) Rabi frequency<sup>7</sup>  $\hbar\Omega = \mu E_0(t)$  and  $\mu = \boldsymbol{\mu} \mathbf{x}$  the projection of the transition dipole moment on the polarization direction of the light field. In the following, we stay in the rotating frame and leave out the prime symbols.

<sup>5</sup> The diagonal elements do not phase-rotate and remain unchanged.

<sup>6</sup> someone should check this!

<sup>7</sup> Some definitions include a factor of 2 here.

## Questions

5. Derive the Bloch equations 6.21 to 6.24 from the Hamilton operator eq. 6.20 and the Liouville-von Neumann equation.

## Rabi Oscillations

Let us discuss the time evolution of the Bloch vector in the rotating frame. Applying only a torque  $\mathbf{M}$ , the length of the Bloch vector does not change. It moves along the surface of a sphere, the Bloch sphere. The sphere has a diameter of one when the density matrix describes a normalized pure state. For mixed states, the Bloch vector is shorter. Below we will see how dephasing and relaxation processes reduce the length of the Bloch vector.

A two-level system in the ground state is on the north pole of the sphere. The state  $|0\rangle + |1\rangle$  is on the equator, pointing along the  $u$  axis. All points except the poles contain a coherence between the two levels.

The torque  $\mathbf{M}$  rotates the Bloch vector around  $\mathbf{M}$  with an angular frequency  $|\mathbf{M}|$ . A resonant laser field, i.e.,  $\omega_L = \omega_0$  rotates the Bloch vector around the  $u$  axis. When this field acts continuously, the Bloch vector moves from the north pole via the equator to the south pole and back to the north pole and so on. The population of the state changes periodically from zero to one:

$$\rho_{00} = \cos(\Omega t/2)^2 \quad . \quad (6.32)$$

These are the Rabi oscillations. In a laser pulse, the amplitude  $E_0(t)$  of the optical field varies, for example like a Gaussian. In this case, the instantaneous Rabi frequency  $\Omega$  also varies and it is convenient to quantify the total effect of a single pulse by the pulse area  $\theta$

$$\theta = \int_{pulse} \Omega(t) dt \quad . \quad (6.33)$$

A  $\pi$  pulse, acting on a system in the ground state, will thus lead to a system in the excited state. A  $2\pi$  pulse leaves the populations unchanged.<sup>8</sup>

When the laser is not fully resonant, the Bloch vector is rotated around an axis in the  $u$ - $w$  plane. Starting from the ground state at the north pole, it thus does not reach the south pole anymore. The population of the excited state will not reach one. At the same time, the phase oscillations of the two-level system are not fully taken care of by the rotating frame anymore. A little bit of rotation remains. In combination, this gives a complicated precession of the Bloch vector  $\mathbf{S}$  around the torque  $\mathbf{M}$  with an effective Rabi frequency

$$\Omega_{eff} = \sqrt{\Omega^2 + (\omega_0 - \omega_L)^2} \quad . \quad (6.34)$$

We can observe these oscillations by any method that can determine the population of the excited state, for example fluorescence emission, electron emission or (transient) absorption.

## Questions

6. Re-visit questions 1–3 from above and discuss the density matrix on the Bloch sphere.



Figure 6.1: Some Bloch vectors and their positions on the Bloch sphere.

<sup>8</sup> but has an effect on the phase

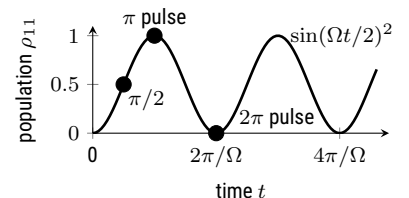


Figure 6.2: Rabi oscillations

7. Write a computer program to calculate the trajectory of the Bloch vector in the rotating wave approximation, eq. 6.31. Use

$$\mathbf{S}'(t + \Delta t) \approx \mathbf{S}'(t) + \Delta t \mathbf{M}' \times \mathbf{S}'(t)$$

with a small enough  $\Delta t$ . The approximation holds when  $|\mathbf{S}'(t)|$  remains close to one. Plot  $\mathbf{S}'(t)$  in 3D on the Bloch sphere (Fig. 6.1) and in 2D as function of time.

## Damping and dephasing

In reality, both a coherence as well as the population of an excited state decays in the course of time. Without going into further detail, we can add these processes phenomenologically as operator  $\mathbf{L}$  to the Liouville-von Neumann equation

$$i\hbar\dot{\hat{\rho}} = [\hat{H}, \hat{\rho}] - \mathbf{L}\hat{\rho} \quad . \quad (6.35)$$

Excited state populations decay exponentially with a lifetime  $T_1$ . The coherence between two states decays with a time constant  $T_2$  with

$$\frac{1}{T_2} = \frac{1}{T_2^*} + \frac{1}{2T_1} \quad , \quad (6.36)$$

where  $T_2^*$  is called pure dephasing time. The  $T_1$  time enters, as a decaying population also removes coherence. The prefactor of 2 is a consequence of effective spin-1/2-system. On the Bloch sphere, these processes let the Bloch vector move back to the north pole, but not along the surface of the sphere but with varying length of the vector.<sup>9</sup>

<sup>9</sup> In the original work of Bloch this scheme was applied to the magnetization of a spin-1/2 system which decays towards the center of the sphere, as thermal energy leads to almost equal population of both states.

## References

- Hamm, Peter (2005). *Principles of Nonlinear Optical Spectroscopy: A Practical Approach or: Mukamel for Dummies*. [↗](#).
- Parson, William W. (2015). *Modern optical spectroscopy*. Springer. [↗](#).
- Rand, Stephen C. (2016). *Lectures on light. nonlinear and quantum optics using the density matrix*. Second edition. Oxford University Press. [↗](#).





# Chapter7

## (Perturbed) Free Induction Decay

Markus Lippitz  
June 18, 2021

### Tasks

- Reproduce Fig. 4b of Wolpert et al., 2012 to model the data in Fig. 4a. As the quantum dot is buried beneath the surface, the reflected reference field  $E_0$  is in its phase earlier than the signal field  $E_S$  of the dot. In this sample, the lag is  $\Delta\phi = 0.4\pi$ .



Figure 7.1: Perturbed free induction decay (at negative delay  $\tau$ ) of a single GaAs quantum dot measured by pump-probe spectroscopy (Wolpert et al., 2012). At negative delay, the pump comes after the probe pulse.

### Experiment

In the experiment, one measures the change in the spectrum of a probe pulse due to the presence of a pump pulse. The probe pulse is reflected at a sample surface under which a quantum dot is buried. The vertical slices of the figure contain the spectrum. The energy axis is relative to the quantum dot transition energy. The pulse is temporally short ( $\approx 1$  ps) and thus spectrally broad. The pump pulse is also short, and comes at a variable delay before or after the probe pulse (positive delay means pump before probe). The pump pulse is switched on and off, and the figure contains only the difference in reflected probe spectrum (grey means no difference). As only the quantum dot is influenced by the pump pulse, this makes visible the small contribution of the quantum dot reflectivity. At positive pump-probe delays, the pump comes before the probe and the spectrum is just the expected absorption spectrum. At negative delays, the probe comes before the pump pulse, and the spectrum shows fringes that increase in spacing with decreasing pump-probe delay. This is the perturbed free induction decay. The diagonal element



This work is licensed under a [Creative Commons "Attribution-ShareAlike 4.0 International"](https://creativecommons.org/licenses/by-sa/4.0/) license.

of the density matrix is created by the probe pulse and removed by the pump. In between, it radiates a field that we see in the spectrum.

To understand the influence of the pump pulse, we need to look more in detail at the levels of an epitaxial quantum dot, which can be approximated by a V-shaped level system: depending on the polarization direction of the light, two different excited states  $|h\rangle$  and  $|v\rangle$  can be populated. The excited states differ in the spin of the electron, so that an interchange is slow on the relevant timescales. Such a V-system allows to use one transition as 'normal' two-level system, and the other transition to switch off the first: when the system is in  $|v\rangle$ , the transition  $\langle h|\mu|g\rangle$  is not possible anymore. This does not change much the physics, but makes experiments much simpler, as the influence of the  $\langle h|\mu|g\rangle$  transition can be modulated in a pump-probe scheme and is such much easier to detect.



Figure 7.2: Sketch of a V-level system. The energy difference is the fine structure splitting (FSS).

## Pump-Probe Experiments

The timescale of the experiment is set by the decay of the coherence and the populations. In many cases, this is faster than the temporal resolution of photodetectors. One method to investigate the dynamics of a system under these conditions is pump-probe spectroscopy. A pump-pulse starts a process and some (short) time later, a probe-pulse interrogates the system. The detector does not need a time resolution and can average over many pump-probe pulse pairs. The time resolution comes by the pulse length and their temporal separation. In many cases, the effect of the pump pulse on the system is weak, i.e. the probe pulse would measure almost the same, independent whether the pump was present or not. To increase the signal to noise ratio in these cases, one investigates the relative change of the signal

$$\frac{\Delta I}{I} = \frac{I_{\text{with pump}} - I_{\text{without pump}}}{I_{\text{without pump}}} . \quad (7.1)$$

The pump-pulse is switched using a mechanical chopper or an acousto-optical modulator at as high as possible frequencies to avoid  $1/f$ -noise. The detector should only detect the probe pulse (and the field radiated by the coherence), otherwise  $\Delta I$  is overwhelmed by leaking pump pulse. A convenient way to discriminate pump and probe is the polarization direction of the light field, setting the orientation of the transition dipole moment at  $45^\circ$  between pump and probe.

### Questions

1. Estimate the fraction of probe power that is absorbed by the quantum dot, i.e., that is then missing in the reflected beam. The numerical aperture of the microscope objective is about 0.5. The spectral width of a pixel of the CCD camera is about 100  $\mu\text{eV}$ .

## Coherence as a Source of Radiation

Let us look at methods to measure elements of the density matrix  $\rho$ . We can measure populations, i.e., diagonal elements of  $\rho$  by fluorescence emission

or electron tunneling. If an atom, molecule, quantum dot is in the excited state, it can emit a fluorescence photon and revert to the ground state. All coherence is lost in this process, neither the fluorescence photon nor the ground state carries any phase relation to the excited state. The excited state is also destroyed, as afterwards the system is in the ground state. But we can observe the fluorescence photon and from the fluorescence rate we can determine how many systems of an ensemble or how often a single system is (better: was) in the excited state. We thus measure population of the emitting state. In the same way, we can use electrons tunneling out of the excited state, for example in a diode structure which also supplies a new electron to the ground state. Also this tunneling signal is incoherent.

We can also measure coherences, i.e., off-diagonal elements in the density matrix  $\rho$ , as these coherences are the source of radiation. To see this, we need to connect the microscopic description by the density matrix to the macroscopic world of Maxwell's equations, resulting in the Maxwell-Bloch equations<sup>1,2,3</sup>. This is what the expectation value does. The polarization  $p$  of a single two-level system at position  $z$  in the laser beam is given by the expectation value of the polarization operator  $\hat{\mu}$

$$p(t, z) = \langle \hat{\mu} \rangle = \text{Tr}(\mu \rho) = \mu_{01} \rho'_{10} e^{-i(\omega_L t - kz)} \quad , \quad (7.2)$$

where the polarization operator has only off-diagonal entries in the matrix representation.<sup>4</sup> The prime signals denote once more the density matrix in the rotating frame. The macroscopic polarization  $P = N p$  of a volume of identical atoms is a source term in the one-dimensional wave equation

$$\frac{\partial^2}{\partial z^2} E_S - \frac{1}{c^2} \frac{\partial^2}{\partial t^2} E_S = \frac{1}{c^2 \epsilon_0} \frac{\partial^2}{\partial t^2} P \quad . \quad (7.3)$$

$E_S$  is the generated field:

$$E_S = E_S(z, t) e^{-i(\omega_L t - kz)} \quad . \quad (7.4)$$

We assume that its amplitude  $E_S(z, t)$  varies slowly in time and space, i.e., we use the slowly-varying envelope approximation and get (with  $\rho'_{10} = u - iv$ )

$$\frac{\partial}{\partial z} E_S - \frac{1}{c} \frac{\partial}{\partial t} E_S = N \frac{ik}{2\epsilon_0} \mu_{01} (u - iv) \quad . \quad (7.5)$$

This forms together with the Bloch equations from last chapter the Maxwell-Bloch equations of a coupled light-matter system. As solution we find

$$E_S = NL \frac{ik}{2\epsilon_0} \mu_{01} (u - iv) = NL \frac{k}{2\epsilon_0} \mu_{01} (v + iu) \propto \mu_{01} \Im(\rho'_{01}) \quad . \quad (7.6)$$

It is thus the  $v$  component of the Bloch vector (or  $\Im(\rho'_{01})$ ) that produces the optical field<sup>5</sup>.

<sup>1</sup> Milonni and Eberly, 1988, chapter 8.3.

<sup>2</sup> Rand, 2016, chapter 3.9.

<sup>3</sup> Meschede, 2017.

<sup>4</sup> Only the real part has physical significance, or, we leave out the complex-conjugate part here.

<sup>5</sup> Cohen-Tannoudji, Dupont-Roc, and Grynberg, 2004, chapter V.B.1.

## Questions

2. Read in a textbook of your choice on the wave equation with a source term. Usually this is discussed in 3d for dipole radiation and in 1d for lasers.
3. Which requirements on  $E_S(z, t)$  does the slowly-varying envelope approximation have to transform second to first order derivatives along space and time?
4. Think about Fermi's Golden Rule (chapter 1) and how the transition matrix element  $\langle 2|\hat{\mu}|1 \rangle$  is necessary for absorption. Compare the temporal evolution of  $\langle 2|\hat{\mathbf{r}}|1 \rangle$  with that of a system at the equator of the Bloch sphere.

## Absorption of a single photon

Let us discuss as example the absorption of a single photon, which transfers the system from the ground state to the excited state, or equivalently is the action of a  $\pi$ -pulse. We start by a two-level system in den ground state. The Bloch vector points to the north pole. We shine in an optical field on resonance with the system ( $\omega_0 = \omega_L$ ). The duration of the light pulse  $\Delta t$  should be such that is a  $\pi$ -pulse, i.e.

$$\theta = \pi = \int_0^{\Delta t} \Omega(t) dt = \int_0^{\Delta t} \frac{\mu E(t)}{\hbar} dt \quad (7.7)$$

When the light pulse has the amplitude  $E_0$  during  $t = 0 \cdots \Delta t$  we get

$$\Delta t = \pi \frac{\hbar}{\mu E_0} = \pi \frac{1}{\Omega} \quad (7.8)$$

The  $w$  component of the Bloch vector follows the Rabi oscillation, i.e.

$$w(t) = \cos(\Omega t) = \cos\left(\pi \frac{t}{\Delta t}\right) \quad (7.9)$$

and the excited state population accordingly

$$\rho'_{11}(t) = \frac{1-w}{2} = \sin^2(\Omega t/2) \quad (7.10)$$

The imaginary part of the coherence, related to the  $v$  component of the Bloch vector, is

$$\Im(\rho'_{01}) = \frac{1}{2}v = -\frac{1}{2}\sin\left(\pi \frac{t}{\Delta t}\right) \quad (7.11)$$

The radiated field is

$$E_S = NL \frac{k}{\epsilon_0} \mu_{01} \Im(\rho'_{01}) = -NL \frac{k}{2\epsilon_0} \mu_{01} \sin\left(\pi \frac{t}{\Delta t}\right) \quad (7.12)$$

On the detector, the pumping field  $E_0$  and the radiated field  $E_S$  interfere. We measure the power  $P$  of a single pulse per area of the beam

$$P = \frac{1}{2} \epsilon_0 c \int_{\text{pulse}} |E_0 + E_S|^2 dt \quad (7.13)$$

The presence of the absorbing two-level system leads to a change in detected power density, assuming real-valued amplitudes with  $E_S \ll E_0$

$$\Delta P = \frac{1}{2} \epsilon_0 c \int_{\text{pulse}} 2E_0 E_S dt = -\sigma \frac{kc}{2} E_0 \mu_{01} \int_0^{\Delta t} \sin\left(\pi \frac{t}{\Delta t}\right) dt \quad (7.14)$$

where  $\sigma = NL$  is the projected area density of the two-level systems. The integral gives  $2\Delta t/\pi$  so that

$$\Delta P = -\sigma \frac{kc}{2} E_0 \mu_{01} \frac{2\Delta t}{\pi} = -\sigma kc E_0 \mu_{01} \frac{\hbar}{\mu E_0} = -\sigma \hbar \omega \quad (7.15)$$

Each atom removes the energy of one photon!

## Questions

- Using your code to integrate the Bloch equations from last chapter, reproduce fig. 7.4. Calculate  $\Delta P$  with eqs. 7.13 and 7.14 for arbitrary detuning between laser and quantum dot and for arbitrary pulse length. Plot an absorption spectrum by scanning the laser frequency. What determines the spectral width?

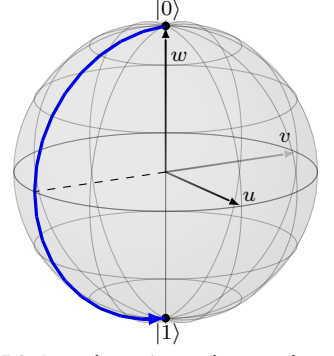


Figure 7.3: A  $\pi$  pulse acting on the ground state.

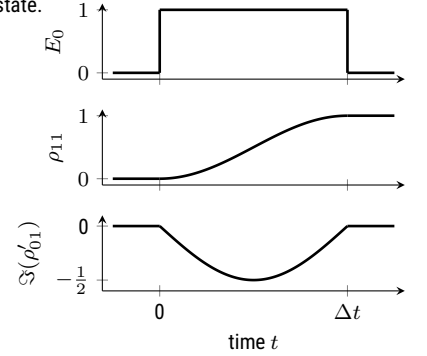


Figure 7.4: Absorption of a photon as seen in the density matrix

## Absorption of half of a photon

We keep the amplitude of the laser field the same but reduce the pulse length to  $\Delta t/2$ , i.e. a  $\pi/2$  pulse. This does only change the upper limit in the integral, so that

$$\Delta P = -\frac{1}{2}\sigma\hbar\omega \quad (7.16)$$

Each atom removes half the energy of a photon. How is that possible? Here the power of the density matrix comes into play. It describes a statistical ensemble. Half of the atoms absorb a photon, half of them don't. But all atoms undergo the  $\pi/2$  Rabi cycle, moving the Bloch vector into the equatorial plane, and describing a state  $|\psi\rangle$

$$|\psi\rangle = \sqrt{\frac{1}{2}}(|0\rangle - i|1\rangle) \quad (7.17)$$

However, at this point our experiment is not finished yet. We still have coherence in the system, it is not decided yet if Schrödinger's cat is dead or alive. The experiment is finished only when all coherence has decayed, into

$$|\psi\rangle = |0\rangle \quad \text{or} \quad |\psi\rangle = |1\rangle \quad (7.18)$$

When the decay of coherence is much faster than population decay, both final states will be reached with equal probability. On average, each atom absorbs half the energy of a photon.

## Spectra

Even after applying the slowly-varying envelop approximation, the amplitude  $E(t)$  of the electric field is varying so fast that we can not measure it. Even the fastest photo detectors have a response time of only picoseconds. We can measure time-integrated properties, such as  $P$  in eq. 7.13. Or we can measure properties related to the Fourier transform of  $E(t)$ . This is what a spectrometer does. Diffraction at the grating performs the Fourier transform. The CCD chip then measures

$$P(\omega)d\omega = \frac{1}{2}\epsilon_0 c |E(\omega)|^2 d\omega = \frac{1}{2}\epsilon_0 c |\mathcal{FT}(E(t))|^2 d\omega \quad (7.19)$$

When interpreting the frequency  $\omega$  in this equation, we have to pay attention to the definition of  $E(t)$ . If it contains a part  $e^{i\omega_0 t}$  oscillating with the frequency of the optical field, then also  $\omega$  is an optical frequency of some 100 THz. If the carrier frequency is split off, as in eq. 7.4, the frequency of the Fourier transform is only additive to the carrier frequency, can thus be much lower than THz. This comes from the convolution property of Fourier transforms

$$\mathcal{FT}(E(t)e^{i\omega_0 t}) = \mathcal{FT}(E(t)) \otimes \mathcal{FT}(e^{i\omega_0 t}) \quad (7.20)$$

$$= E(\omega) \otimes \delta(\omega - \omega_0) = E(\omega - \omega_0) \quad (7.21)$$

where  $\otimes$  is the convolution operator.

We Fourier transform the fields with and without pump pulse and subtract the resulting intensities. Using  $E_S \ll E_0$  we get

$$|E_0(\omega) + E_S(\omega)|^2 - |E_0(\omega)|^2 \approx 2\Re[E_0(\omega)^* E_S(\omega)] \quad (7.22)$$

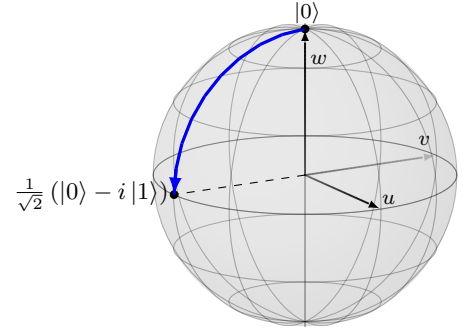


Figure 7.5: A  $\pi/2$  pulse acting on the ground state.

or

$$\Delta P(\omega) = \epsilon_0 c \Re [E_0(\omega)^* E_S(\omega)] \quad (7.23)$$

## Questions

6. Derive eqs. 7.22 and 7.23.

## Free induction decay

We discussed how a coherence in a two-level system is generated, but not so much how it decays. At the end of last chapter we mentioned the Lindblad  $\mathcal{L}$  operator that decays entries of the density matrix. But it is this decay that defines the spectral shape of an absorption line.

We assume a short laser pulse, shorter than any characteristic decay time of a coherence population in our system. Such a pulse will generate a coherence, move the Bloch vector away from the north pole. A  $\pi/2$  pulse would generate the maximum possible coherence, but any other pulse (except an exact  $\pi$  pulse) will also create a coherence. After the pulse, coherence and population decay like

$$\rho_{11}(t) \propto \rho_{11}(0) e^{-t/T_1} \quad (7.24)$$

$$\rho_{01}(t) \propto \rho_{01}(0) e^{-t/T_2} \quad (7.25)$$

Excited state populations decay exponentially with a lifetime  $T_1$ . The coherence between two states decays with a time constant  $T_2$  with

$$\frac{1}{T_2} = \frac{1}{T_2^*} + \frac{1}{2T_1} \quad , \quad (7.26)$$

where  $T_2^*$  is called pure dephasing time. The  $T_1$  time enters, as a decaying population also removes coherence. The prefactor of 2 is a consequence of effective spin-1/2-system.

This decay of the coherence is called 'free induction decay' (dt: 'freier Induktionszerfall') in NMR experiments. In these experiments, the Bloch vector corresponds to a magnetization vector that rotates with the eigenfrequency of the system. This rotation induces a current in a pickup coil that is detected. The induction decays freely after switching off the exciting fields. This term is taken for the same effect in all equivalent spin-1/2 systems, so also for the decay of the coherence in our two-level system.

The coherence, the off-diagonal entry of the density matrix  $\rho_{01}(t)$  is source of the radiated field  $E_S$ . The time-dependence of the decay thus determines via Fourier transformation the spectral shape of the radiated field<sup>6</sup>

<sup>6</sup> see also appendix in Fourier pairs

$$f(t) = \begin{cases} e^{-\gamma t} & \text{for } t > 0 \\ 0 & \text{else} \end{cases} \quad \leftrightarrow \quad F(\omega) = \frac{1}{\gamma + i\omega} \quad (7.27)$$

The absorption spectrum is thus

$$\Delta P(\omega) \propto \Re \left[ \frac{e^{i\phi}}{\gamma + i\omega} \right] \stackrel{\phi=0}{=} \frac{\gamma}{\omega^2 + \gamma^2} \quad (7.28)$$

where we have assumed that the driving probe pulse  $E_0(\omega)$  is spectrally much broader than the absorption line and thus assumed to be constant.

The factor  $e^{i\phi}$  allows a phase lag between incoming and radiated field, as needed for buried quantum dots. For  $\phi = 0$  we recover the expected Lorentz function. For other values the spectral shape changes

### Questions

- Using a computer program of your choice, calculate the numerical Fourier transform of an exponential decay and compare to the Lorentz function. Take care the get the frequency axis right.

## Perturbed free induction decay

A second laser pulse can perturb the decay of the coherence. In the experiment described at the beginning of this chapter, a pump-pulse acts on the other transition in the V-shaped level scheme. A full model, as used in (Wolpert et al., 2012), would need a  $3 \times 3$  density matrix and 9 coupled differential equations for its entries. We can simplify things when we do not care so much what happens during the laser pulses, but only how the relevant entry of the density matrix evolves between the pulses.

The relevant entry is the coherence  $\rho_{hg} = c_h c_g^*$  that is generated by the probe pulse and observed by measuring the reflected spectrum of the probe pulse. Without the pump pulse, it follows an exponential decay as described above. If the pump pulse comes before the probe pulse (positive delays in the figure), the pump has moved population to  $|v\rangle$ , i.e.,  $\rho_{vv} = |c_v|^2 \neq 0$ . This reduces the population of the ground state and therefore also the coherence  $\rho_{hg}$  that the probe pulse can generate. The radiated field will be lower, but have the same spectral shape.

Things change when the pump pulse comes after the probe pulse. The action of  $\langle v|\mu|g\rangle$  increases  $c_v$ , but also decreases  $c_g$  which decreased the probe coherence  $\rho_{hg} = c_h c_g^*$ . The pump pulse leads to an abrupt drop in the coherence that is observed by the probe pulse. One can approximate

$$\rho_{hg}(t) = \rho_{hg}(0) e^{-t/T_2} [1 - \beta \Theta(t - t_{\text{pump}})] \quad (7.29)$$

where  $\Theta$  is the Heaviside step function and  $\beta$  describes the effect of the pump pulse on the coherence. The two laser pulses define a rectangle of the coherence. Its Fourier transform, a sinc, causes the fringes at negative delay in the figure.

### Questions

- Calculate numerically the Fourier transform of 7.29 and adjust the parameters to obtain Fig. 7.1

## References

- Cohen-Tannoudji, Claude, Jacques Dupont-Roc, and Gilbert Grynberg (2004). *Atom photon interactions*. Weinheim: Wiley-VCH. [↗](#).
- Meschede, Dieter (2017). *Optics, light, and lasers*. Weinheim, Germany: Wiley-VCH. [↗](#).

- Milonni, Peter W. and Joseph H. Eberly (1988). *Lasers*. New York [u.a.]: Wiley.
- Rand, Stephen C. (2016). *Lectures on light. nonlinear and quantum optics using the density matrix*. Second edition. Oxford University Press. [↗](#).
- Wolpert, Christian et al. (2012). "Transient Reflection: A Versatile Technique for Ultrafast Spectroscopy of a Single Quantum Dot in Complex Environments". In: *Nano Letters* 12.1, pp. 453–457. [↗](#).



# Chapter8

## Strong coupling of cavity and emitter

Markus Lippitz

June 18, 2021

### Tasks

- Assume a single quantum dot with dipole moment  $\mu$  in the center of a planar  $\lambda/2$  cavity of index of refraction  $n = 3.5$  (diameter 800 nm). Calculate the effective volume of this cavity. Which dipole moment is required so that a coupling strength of  $\hbar g = 80 \mu\text{eV}$  is reached, as in Reithmaier et al., 2004.
- Build a model function for the data in the top left panel of Fig. 4 in Reithmaier et al., 2004.

### Experiment

Reithmaier et al., 2004, observed strong coupling between a single emitter in solid state (an InGaAs quantum dot) and a micro-cavity. This is again an analogue of a coupled pendulum. One cannot say anymore if the excitation is in the dot or in the cavity. On resonance, both cease to exist and new coupled states emerge. The new states are in all properties mixtures of the old ones, for example in line width or intensity, see Fig. 4 in the manuscript.

### Quantization of the light field

The Rabi model assumed a classical electrical field in which the particle nature of light is not relevant. But now we need to take the quantized nature of light into account. In quantum mechanics this is often called 'second quantization' and we will briefly have a look at the main results.

The principle idea is very similar to a quantum mechanical harmonic oscillator, i.e. a series of equidistant states that has a bottom boundary. We describe the states by a quantum number  $n$ , starting from  $n = 0$ . The Hamiltonian reads

$$\hat{H} |n\rangle = E_n |n\rangle = \left(n + \frac{1}{2}\right) \hbar\omega |n\rangle \quad , \quad (8.1)$$

where  $\hbar\omega$  is the energy distance between the states.



This work is licensed under a [Creative Commons "Attribution-ShareAlike 4.0 International"](https://creativecommons.org/licenses/by-sa/4.0/) license.

It is convenient to use ladder operators for the creation ( $\hat{a}^\dagger$ ) and annihilation ( $\hat{a}$ ) of a quantum of energy, i.e.

$$\hat{a}^\dagger |n\rangle = \sqrt{n+1} |n+1\rangle \quad \text{and} \quad \hat{a} |n\rangle = \sqrt{n} |n-1\rangle \quad . \quad (8.2)$$

Useful properties are

$$\hat{a} |0\rangle = |0\rangle \quad \text{and} \quad \hat{a}^\dagger \hat{a} |n\rangle = n |n\rangle \quad . \quad (8.3)$$

Now this needs to be connected to classical electrodynamics. We assume a single optical mode in a small optical resonator, similar to a laser cavity. In the dark, i.e. in the state  $|0\rangle$ , quantum mechanics gives an eigen-energy  $E_0 = 1/2 \hbar\omega$ . This is what we require also from classical electrodynamics<sup>1</sup>

$$E_0 = \int_{\text{cavity}} \frac{1}{2} (\mathbf{H} \cdot \mathbf{B} + \mathbf{E} \cdot \mathbf{D}) d\mathbf{r} = \int_{\text{cavity}} \epsilon_0 \mathbf{E}^2 d\mathbf{r} = \frac{1}{2} \hbar\omega \quad (8.4)$$

so that

$$E_{vac} = \sqrt{\frac{\hbar\omega}{2\epsilon_0 V}} \quad (8.5)$$

is the amplitude of the field in the dark vacuum, with  $V$  being the volume of the cavity.<sup>2</sup> One obtains the volume by integrating over full space, weighted by the local intensity

$$V = \frac{1}{\max(\mathbf{E}_c)^2} \int_{\text{cavity}} \mathbf{E}_c^2 d\mathbf{r} \quad , \quad (8.6)$$

where  $\mathbf{E}_c$  can be a field of any amplitude inside the cavity. It just defines the spatial distribution of the optical mode. The vacuum field in total is thus

$$\mathbf{E}(\mathbf{r}) = \frac{E_{vac}}{\max(\mathbf{E}_c)} \mathbf{E}_c(\mathbf{r}) \quad (8.7)$$

The electrical field of a single optical mode in a cavity then becomes<sup>3,4</sup>

$$\hat{\mathbf{E}}(z, t) = \mathbf{x} E_{vac} \left( \hat{a} e^{i(kz - \omega t)} + \hat{a}^\dagger e^{-i(kz - \omega t)} \right) \quad , \quad (8.8)$$

where  $\mathbf{x}$  is a unit vector defining the direction of polarization.

## Questions

1. Two flat perfect mirrors of diameter  $d$  and distance  $L$  form a resonator. Calculate its mode volume at an eigenfrequency, assuming that no field leaks out of the cylinder formed by the mirrors. How would the index of refraction of a medium between the mirrors enter?
2. In an elevator cabin, two opposing walls are covered by mirrors. Calculate the amplitude of the electric field in the cabin.

## Pauli matrices for atoms

The two-level system representing our atom is a spin 1/2 system, i.e., a Fermion, not a Boson as the photons in the cavity. We can use operators similar to the ladder operators to excite ( $\hat{\sigma}_+$ ) or relax ( $\hat{\sigma}_-$ ) the two-level system

$$\hat{\sigma}_+ = |e\rangle \langle g| \quad \text{and} \quad \hat{\sigma}_- = |g\rangle \langle e| \quad . \quad (8.9)$$

The third operator to complete the Pauli spin algebra is the inversion operator, i.e. the third component of the Bloch vector

$$\hat{\sigma}_3 = |e\rangle \langle e| - |g\rangle \langle g| \quad . \quad (8.10)$$

<sup>1</sup> Fox, 2007, chap. 7.5.

<sup>2</sup> This is the reason we require a cavity. Otherwise the integral would diverge.

<sup>3</sup> Gerry and Knight, 2005, chap. 2.1 and 2.4.

<sup>4</sup> Rand, 2016, chap. 6.1.

### Questions

3. Write the operators  $\hat{\sigma}_+$ ,  $\hat{\sigma}_-$  and  $\hat{\sigma}_3$  in matrix form.

### Jaynes-Cummings-Model

Now we put everything together to the Jaynes-Cummings-model. Sometimes this model is also called 'dressed atom' model.<sup>5,6,7,8</sup>

We construct an Hamiltonian of three parts: atom, optical field, and light-matter interaction. The atom part is, using  $\hbar\omega_0 = E_e - E_g$

$$\hat{H}_A = \frac{1}{2} \hbar\omega_0 \hat{\sigma}_3, \quad (8.11)$$

where we have set the zero of the energy scale half way between ground and excited state. The optical field part is

$$\hat{H}_F = \hbar\omega \hat{a}^\dagger \hat{a}, \quad (8.12)$$

with the optical frequency  $\omega$  and the zero of the energy scale set to the vacuum energy. Light-matter interaction is given in the dipole approximation and neglecting terms that violate energy conservation by<sup>9</sup>

$$\hat{H}_I = -\boldsymbol{\mu} \cdot \mathbf{E} = \hbar g (\hat{\sigma}_+ \hat{a} + \hat{\sigma}_- \hat{a}^\dagger). \quad (8.13)$$

Absorption of a photon ( $\hat{a}$ ) excites the atom ( $\hat{\sigma}_+$ ) and the other way round. The coupling constant  $g$  is given by

$$g = \frac{\mu_{eg} E_{vac}}{\hbar} = \mu_{eg} \sqrt{\frac{\omega}{2\hbar\epsilon_0 V}}, \quad (8.14)$$

where  $\mu_{eg}$  is the projection of the transition dipole moment on the polarization direction of the light field. In total we have thus

$$\hat{H} = \frac{1}{2} \hbar\omega_0 \hat{\sigma}_3 + \hbar\omega \hat{a}^\dagger \hat{a} + \hbar g (\hat{\sigma}_+ \hat{a} + \hat{\sigma}_- \hat{a}^\dagger). \quad (8.15)$$

The idea of the Jaynes-Cummings-Model is to find eigen-states of this Hamiltonian. This is the same idea as in a coupled pendulum: the atom is one pendulum, the light field another, and the spring connecting the pendula is the coupling constant  $g$ . The uncoupled eigen-states are  $|g, n\rangle$  and  $|e, n-1\rangle$ , i.e. atom in ground or excited state, and either  $n$  or  $n-1$  photons in the cavity. For these two states, the Hamilton operator reads in matrix form

$$\hat{H} = \hbar \begin{pmatrix} n\omega - \frac{1}{2}\omega_0 & g\sqrt{n} \\ g\sqrt{n} & (n-1)\omega + \frac{1}{2}\omega_0 \end{pmatrix}. \quad (8.16)$$

The new eigen-states are linear combinations of the old, obtained by diagonalizing the Hamilton operator in matrix form. For the eigen-energy we get

$$E_{\pm} = \left(n - \frac{1}{2}\right) \hbar\omega \pm \frac{1}{2} \hbar \sqrt{\Delta^2 + 4|g|^2 n}, \quad (8.17)$$

where  $\Delta = \omega_0 - \omega$  is energy difference between the uncoupled eigen-states, or the detuning between atom and field. The square-root is called generalized

<sup>5</sup> Rand, 2016, chap. 6.8.

<sup>6</sup> Gerry and Knight, 2005, chap. 4.5.

<sup>7</sup> Fox, 2007, chap. 10.4.

<sup>8</sup> Haroche, 2006, chap. 3.4.

<sup>9</sup> Rand, 2016, chap. 6.7.1.

Rabi frequency  $\Omega_R = \sqrt{\Delta^2 + 4|g|^2 n}$ . The new eigen-states are called dressed states  $|D_{\pm}\rangle$  as the photons are 'dressing' the atom

$$|D_+\rangle = \sin \theta |g, n\rangle + \cos \theta |e, n-1\rangle \quad (8.18)$$

$$|D_-\rangle = \cos \theta |g, n\rangle - \sin \theta |e, n-1\rangle \quad (8.19)$$

with  $\cos 2\theta = \Delta/\Omega_R$ . On resonance, i.e.  $\Delta = 0$ , the two dressed states are the symmetric and anti-symmetric combinations of the uncoupled states.

### Questions

4. Convince yourself that the Hamilton operators  $\hat{H}_A$  and  $\hat{H}_F$  indeed give the energy of atom and field.
5. Derive the matrix form of the total Hamilton operator, eq. 8.16, especially that the two off-diagonal element are the same.
6. Why and how is the interaction part of the Hamiltonian  $\hat{H}_I$  coupling the two states? What is rotating with the angular frequency  $g$ ? Compare to the spring between two pendula.
7. Play with <https://demonstrations.wolfram.com/CavityQuantumElectrodynamicsWithBosonsEmissionSpectrumInTheSt>

### Mollow Triplet

We now label the above dressed states by their characteristic photon number  $n$  as  $|D_+^{(n)}\rangle$  and  $|D_-^{(n)}\rangle$ . This allows us to take into account also the two states  $|D_+^{(n+1)}\rangle$  and  $|D_-^{(n+1)}\rangle$ . When  $n \gg 1$  as in a laser field, we can assume that the Rabi frequency  $\Omega_R = \sqrt{\Delta^2 + 4|g|^2 n}$  does not differ between these states. In this case, the four optical transitions that take out energy will lead to only three different lines in the spectrum. This is called the Mollow Triplet. The (degenerate) center line is at the laser frequency, the outer two separated by the Rabi frequency.

### Questions

8. Draw a level scheme containing the uncoupled and the coupled states involved in the Mollow Triplet and the resulting spectrum. Which transition leads to which peak?
9. Play with <https://demonstrations.wolfram.com/MollowTriplet>

### Vacuum Rabi Splitting

The splitting into dressed states  $|D_+^{(n)}\rangle$  and  $|D_-^{(n)}\rangle$  does only exist for a photon number  $n \geq 1$ . The uncoupled state  $|g, n=0\rangle$  cannot couple with the non-existing state  $|e, n=-1\rangle$ . The lowest state in the ladder does thus not split. From there we can reach two states,  $|D_+^{(1)}\rangle$  and  $|D_-^{(1)}\rangle$ , by absorbing a single photon in the system. These two states are at  $\omega_0 \pm \hbar g$ . (as  $\omega_{cav} = \omega_{atom}$ ). This effect is called Vacuum Rabi Splitting, as it exists in the dark. The photon is only needed to detect its presence.

A consequence of this effect is the photon blockade. The first photon can be absorbed at  $\omega_0 \pm \hbar g$ , but not a second one! In this regime, we cannot neglect that the Rabi frequency depends on the photon number  $n$ . The second pair of states is at  $2\omega_0 \pm \sqrt{2}\hbar g$ , i.e., not at twice the energy of the first pair. Absorbing the first photon blocks this transition for any further absorption.

### Questions

10. Draw a level scheme containing the uncoupled and the coupled states involved in Vacuum Rabi Splitting. Draw the absorption spectrum as seen by the first and by the second photon in the system.

### References

- Fox, Mark (2007). *Quantum optics*. Oxford University Press.
- Gerry, Christopher C. and Peter L. Knight (2005). *Introductory quantum optics*. Cambridge Univ. Press. [↗](#).
- Haroche, Serge (2006). *Exploring the quantum. atoms, cavities and photons*. Oxford Univ. Press. [↗](#).
- Rand, Stephen C. (2016). *Lectures on light. nonlinear and quantum optics using the density matrix*. Second edition. Oxford University Press. [↗](#).
- Reithmaier, JP et al. (2004). "Strong coupling in a single quantum dot-semiconductor microcavity system". In: *Nature* 432.7014, pp. 197–200.



# Chapter9

## Weak coupling of cavity and emitter: Purcell Effect

Markus Lippitz  
June 18, 2021

### Tasks

- This is an experiment you can do at home: test the Purcell effect in acoustics<sup>1</sup>! You need a suspended gong (or metal plate) and a small spherical object which you let roll down a slide to excite the gong as controlled as possible. Acquire with your smartphone<sup>2</sup> or a computer the emitted sound as function of distance to a hard wall. Plot the width of the peaks in the Fourier spectrum and compare with theory.  
NB: in this text the optical equations are given. You need the acoustical variants from the paper to compare to your data.

<sup>1</sup> Langguth et al., 2016.

<sup>2</sup> [phyphox.org](http://phyphox.org)

### Weak and strong coupling

Already in the last chapter we discussed the properties of an optical cavity that contains a two-level system such as an atom or molecule. Atom and cavity couple because the transition dipole operator interacts with the field of the cavity. In the last chapter we assumed that this coupling is 'strong'. This means that the effect of the coupling dominates other effects. We have seen that atom and cavity lose their identity. We found new eigenstates as a symmetric and antisymmetric combination of 'photon in the atom and not in the cavity' and 'photon in the cavity and not in the atom'. In this chapter, we continue to discuss atoms in cavities, but we relax the condition on the coupling strength. 'Weak' coupling is enough. Atom and cavity will no longer lose their identity. The excitation is either in the atom or in the cavity.

Let us without going much into the details<sup>3</sup> look at the parameters that decide whether a system is in the weak or strong coupling limit. Already in the chapter on molecular aggregates we have required that the coupling energy  $J$  is larger than the difference in eigen-energies of the systems to be coupled, i.e.

<sup>3</sup> Khitrova et al., 2006; Pelton, Storm, and Leng, 2019; Thomas et al., 2020.

$$J \gg |E_a - E_b| \quad \text{or} \quad g \gg |\Delta| = |\omega_0 - \omega| \quad . \quad (9.1)$$

While this is still required, it is not sufficient. In many cases, the atom is resonant with the cavity, i.e.  $\Delta = 0$ . This does not automatically lead to



strong coupling. We require that the energy can make one round trip from cavity to atom and back to cavity without being dissipated. Then one can not say any more if the excitation is in atom or cavity and we are in the regime of strong coupling. In this way, the decay rates of atom  $\gamma_A$  and cavity  $\gamma_C$  come into play. We require for strong coupling

$$4g > \gamma_A + \gamma_C \quad . \quad (9.2)$$

This is similar, but not in all cases identical to requiring that a dip should be seen between the two split states, i.e., their separation should be larger than their width.

## Spontaneous Emission

Spontaneous emission like fluorescence is a tricky problem from the point of view of quantum mechanics, which we tried to avoid up to now. The reason is that the electronic excited state is an eigen-state of the Hamilton operator and should be stable in time. As fluorescence also happens in the dark, an electric field that couples states in a perturbation operator does not help here. We circumvented this point by either discussing absorption (bright fields that couple states) or by using Einstein coefficients (no quantum mechanics). The quantization of the electrical field introduced in the last chapter now in principle allows to investigate spontaneous emission with the tools of quantum mechanics.

We again couple two states of the type  $|g, n\rangle$  and  $|e, n-1\rangle$ , i.e.  $n$  photons in the cavity and the atom in either ground or excited state. Let us look at the case  $n = 1$ , i.e.  $|g, 1\rangle$  and  $|e, 0\rangle$ . This is what we need to describe spontaneous emission: an excited atom in a dark cavity coupled to the atom in the ground state with a single photon in the cavity. The coupling constant is again  $g$ , as defined in the last chapter, without any prefactors.

The first thing to note is that a dark cavity without any photons ( $n = 0$ ) is not dark in all senses. The expectation value of the electric field is zero in this case

$$\langle 0 | \hat{E} | 0 \rangle = E_{vac} \langle 0 | \hat{a} + \hat{a}^\dagger | 0 \rangle = 0 \quad , \quad (9.3)$$

while the intensity does not vanish

$$\langle 0 | \hat{E}^2 | 0 \rangle = E_{vac}^2 \langle 0 | (\hat{a} + \hat{a}^\dagger)^2 | 0 \rangle = E_{vac}^2 \quad . \quad (9.4)$$

We required the vacuum to contain the ground state energy of  $\frac{1}{2}\hbar\omega$  which results in a non-zero intensity. While the average value of the field is zero, its fluctuations lead to an average non-zero intensity. These vacuum fluctuations cause spontaneous emission. Spontaneous emission is stimulated emission by vacuum fluctuations.

Second, spontaneous emission depends on the position of the atom in the cavity. The coupling constant  $g$  is defined by

$$\hbar g = \mu_{eg} E_{vac} \quad , \quad (9.5)$$

but the field amplitude  $E_{vac}$  inside the cavity is not constant, but a standing wave. At the nodes of the field the coupling constant  $g$  is zero, for example



when the two mirrors are separated by exactly a wavelength and the atom is positioned in the exactly the middle. In such a situation, the states  $|g, 1\rangle$  and  $|e, 0\rangle$  are *not coupled* and the excited atom will not decay by spontaneous emission.<sup>4</sup>

At this level of description, the excited atom will be converted into an atom in the ground state plus a photon in the cavity, but also the other way round. The atom undergoes permanent, undamped vacuum Rabi oscillations between ground and excited state. Only taking an ensemble of optical modes into account, as done in the Weisskopf-Wigner theory<sup>5,6</sup>, leads to an exponential decay of the excited state population.

In contrast to the effects of strong coupling between atom and cavity, the effects of weak coupling are also obtained from a classical theory of an emitting classical dipole.<sup>7</sup>

<sup>4</sup> Better: will not decay into this cavity mode. If other modes are available, for example of the free space, then the atom can decay by emission into these modes.

<sup>5</sup> Novotny and Hecht, 2012, chapter 8.4.

<sup>6</sup> Meystre and Sargent, 2007, chapter 14.3.

<sup>7</sup> Loudon, 2001, chapter 4.10.

## Questions

1. Derive eqs. 9.3 and 9.4
2. How long would it take that an emitted fluorescence photon would be absorbed back into the atom when only a single optical mode would exist?

## Purcell Effect

Let us ignore the problem of the semi-classical description of spontaneous emission and just use Fermi's Golden Rule<sup>8</sup>

$$\Gamma_{\text{spontaneous}} = \frac{2\pi}{\hbar} |\langle g | H' | e \rangle|^2 \rho(E) \quad , \quad (9.6)$$

where we use as perturbation operator  $H'$

$$H' = \frac{1}{\sqrt{3}} \mu_{ge} E_{vac} \quad (9.7)$$

the orientation-averaged interaction of the transition dipole moment with the vacuum field. We thus plug a result from the quantized field in a semi-classical theory. The density of final states  $\rho(E)$  is defined by the states for the photon, as the atom will always be in its ground state. For free space, i.e., a very large 3D cavity of volume  $V$ , we have the free-space density of states<sup>9</sup> times the cavity volume

$$\rho(E) = \frac{\rho(\omega)}{\hbar} = \frac{1}{\hbar} \frac{\omega^2}{\pi^2 c^3} V \quad . \quad (9.8)$$

Plugging everything together we get

$$\Gamma_{\text{spontaneous, free space}} = \frac{\omega^3 |\mu_{ge}|^2}{3 \pi \epsilon_0 \hbar c^3} \quad , \quad (9.9)$$

which is identical to the Einstein  $A_{21}$  coefficient.

This formalism allows us now to change the environment of the emitter. The simplest is a cavity with only a single optical mode. In this case

$$\int_0^\infty \rho(\omega) d\omega = 1 \quad (9.10)$$

<sup>8</sup> Fox, 2007, chapter 10.3.

<sup>9</sup> this is  $d\omega dV$  but we need only a  $d\omega$  density

and

$$\rho(\omega) = \frac{1}{2\pi} \frac{Q}{\omega_c} \frac{(\omega_c/Q)^2}{(\omega - \omega_c)^2 + \frac{1}{4}(\omega_c/Q)^2} \quad , \quad (9.11)$$

where  $\omega_c$  is the center frequency of the mode and  $Q$  is the quality factor of the cavity. On resonance, this becomes

$$\rho(\omega_c) = \frac{2Q}{\pi \omega_c} \quad . \quad (9.12)$$

Plugging again everything together, assuming  $\omega = \omega_c$  we get

$$\Gamma_{\text{spontaneous, single mode}} = |\mu_{ge}|^2 \frac{2Q}{3\epsilon_0 \hbar V} \quad . \quad (9.13)$$

The Purcell Factor is the ratio of emission rate into the cavity compared to that of free space, i.e.

$$F_{\text{Purcell}} = \frac{\Gamma_{\text{cav}}}{\Gamma_{\text{free}}} = \frac{Q}{V} \frac{(\lambda/n)^3}{4\pi^2} \quad . \quad (9.14)$$

It is by a factor of 3 larger when the transition dipole moment is optimally aligned with the optical field of the cavity. A single-mode cavity of small mode volume and large quality factor thus drastically increases the spontaneous emission rate of an emitter<sup>10</sup>. The emission rate is not a property of the emitter alone, but also depends on the environment. The environment changes the density of optical modes in frequency space.

<sup>10</sup> when it is not placed in a node of the field

The Purcell effect can be observed in the fluorescence lifetime of emitters. An increased spontaneous emission rate reduces the excited state lifetime. The concept is derived having atoms in cavities in mind. Solid-state and nanophotonic realizations have been demonstrated. However, in such experimental realizations one has to take care that the environment does not also modifies non-radiative rates. Quenching of emission would lead to a similar reduction of excited state lifetime but is not a Purcell effect.

## Questions

3. Convince yourself that eq. 9.9 holds, i.e., was derived correctly.
4. Discuss potential solutions to the problem that also other effects of the nano-environment could change the excited state lifetime and make it thus challenging to demonstrate a Purcell effect.

## Classical description

To be able to describe more complicated environments than single-mode cavities, we now move to a purely classical description of spontaneous emission. A damped harmonic oscillation is triggered in an electric dipole. We do not care how this oscillation has started, but just follow its evolution afterwards. The dipole emits radiation that is reflected back by the environment and then acts as 'driving' term on the dipole<sup>11</sup>

<sup>11</sup> Novotny and Hecht, 2012, chapter 8.5.2.

$$\ddot{\mu} + \gamma_0 \dot{\mu} + \omega_0^2 \mu = \frac{q^2}{m} E_s(t) \quad . \quad (9.15)$$

Let us first discuss the dipole alone, without back-scattered field. It will oscillate with a frequency

$$\omega = \sqrt{\omega_0^2 - \frac{1}{4}\gamma_0^2} \quad (9.16)$$

and its oscillation amplitude will decay proportional to  $\exp(-\gamma_0 t/2)$  (the stored energy drops as  $\exp(-\gamma_0 t)$ ). We now require that all energy removed from the oscillator is converted into radiated power and no other sources of damping are present. This fixes the damping rate<sup>12</sup>

$$\gamma_0 = \frac{1}{4\pi\epsilon_0} \frac{2q^2\omega_0^2}{3mc^3} . \quad (9.17)$$

When we now include the back-scattered field, we find<sup>13</sup> that both the damping rate as well as the oscillation frequency change. Not even the emission frequency is the property of an emitter alone, but also it is influenced by the environment.

$$\frac{\gamma}{\gamma_0} = 1 + q_e \frac{6\pi\epsilon_0}{|\mu_0|^2} \frac{1}{k^3} \Im(\mu_0^* \cdot E_s(r_0)) \quad (9.18)$$

$$\frac{P}{P_0} = \left. \frac{\gamma}{\gamma_0} \right|_{q_e=1} \quad (9.19)$$

$$\frac{\Delta\omega}{\gamma_0} = q_e \frac{3\pi\epsilon_0}{|\mu_0|^2} \frac{1}{k^3} \Re(\mu_0^* \cdot E_s(r_0)) \quad (9.20)$$

where  $q_e$  is the quantum efficiency of the emitter. As the amplitude of  $E_s(r_0)$  at the position of the dipole depends on the dipole's oscillation amplitude  $|\mu_0|$ , the latter cancels out, as expected. The easiest way to calculate  $E_s(r_0)$ , the field of the source at the source, is to use the dyadic Green's function as shown in Novotny and Hecht, 2012 and Hohenester, 2020. At the end of chapter 15 we discuss the case of a dipole in a layered medium.

When we are only interested in the decay rate or the emitted power, then an alternative point of view comes to help. We now continuously drive the dipole oscillator and calculate the optical far-field as superposition of direction emission into the direction of the observer and emission into other directions, that is in the following reflected towards the observer. These fields interfere constructively or destructively, depending on their phase relation. The total emitted power is obtained by integration over a suitable surface.

## Drexhage's Experiment

The most famous experiment on this topic is that of Karl Drexhage<sup>14</sup> who studied the fluorescence of a layer of emitters near a silver mirror. The distance to the mirror was varied by stacking of multiple molecular spacer layers. He found an oscillation of both emission rate and emission frequency with the distance to the mirror, as  $\mu_0$  and  $E_s(r_0)$  change their phase relation with the distance to the mirror.

Following the notation of Langguth et al., 2016, the field at the observer in distance  $R$  can be written as

$$E(R) \propto \frac{e^{ikR}}{R} S(\theta, \phi) (e^{i\psi} + r e^{-i\psi}) , \quad (9.21)$$

<sup>12</sup> Novotny and Hecht, 2012.

<sup>13</sup> Novotny and Hecht, 2012, chapter 8.5.2.

<sup>14</sup> Drexhage, 1974.

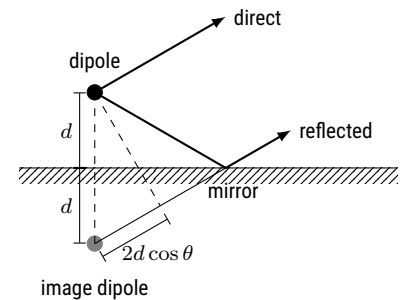


Figure 9.1: Two paths of emission interfere at the observer. This can be seen as additional emission of an image dipole.

where  $r$  is the (Fresnel) reflection coefficient of the surface and  $\pm\psi = \pm kd \cos \theta$  the phase difference between the two paths.  $S(\theta, \phi)$  describes the dipolar emission pattern. Now we assume a perfect reflection ( $r = 1$ ), abbreviate the phase difference by  $x = 2kd$  and integrate over the half space above the mirror. One gets

$$\frac{\gamma_{\perp}}{\gamma_0} = 1 + 3 \left( -\frac{\cos x}{x^2} + \frac{\sin x}{x^3} \right) \quad (9.22)$$

$$\frac{\gamma_{\parallel}}{\gamma_0} = 1 + \frac{3}{2} \left( -\frac{\sin x}{x} - \frac{\cos x}{x^2} + \frac{\sin x}{x^3} \right) . \quad (9.23)$$

For completeness, the relative shift of the eigen-frequencies in this case are

$$\frac{\Delta\omega_{\perp}}{\gamma_0} = -\frac{3}{2} \left( \frac{\sin x}{x^2} + \frac{\cos x}{x^3} \right) \quad (9.24)$$

$$\frac{\Delta\omega_{\parallel}}{\gamma_0} = \frac{3}{4} \left( \frac{\cos x}{x} - \frac{\sin x}{x^2} - \frac{\cos x}{x^3} \right) . \quad (9.25)$$

## References

- Drexhage, Karl H. (1974). “Interaction of Light with Monomolecular Dye Layers”. In: *Progress in Optics*. Ed. by E. Wolf. Vol. 12. Elsevier, pp. 163–232. [↗](#).
- Fox, Mark (2007). *Quantum optics*. Oxford University Press.
- Hohenester, Ulrich (2020). *Nano and Quantum Optics. An Introduction to Basic Principles and Theory*. Springer. [↗](#).
- Khitrova, G et al. (2006). “Vacuum Rabi splitting in semiconductors”. In: *Nature Physics* 2.2, pp. 81–90. [↗](#).
- Langguth, Lutz et al. (2016). “Drexhage’s Experiment for Sound”. In: *Physical Review Letters* 116.22, pp. 224301–224306. [↗](#).
- Loudon, Rodney (2001). *The quantum theory of light*. Oxford University Press.
- Meystre, Pierre and Murray Sargent (2007). *Elements of quantum optics*. 4. ed. Berlin [u.a.]: Springer, XII, 507 S. [↗](#).
- Novotny, Lukas and Bert Hecht (2012). *Principles of nano-optics*. 2. ed. Cambridge Univ. Press. [↗](#).
- Pelton, Matthew, S David Storm, and Haixu Leng (2019). “Strong coupling of emitters to single plasmonic nanoparticles: exciton-induced transparency and Rabi splitting”. In: *Nanoscale* 11.31, pp. 14540–14552. [↗](#).
- Thomas, Philip A et al. (2020). “A New Signature for Strong Light–Matter Coupling Using Spectroscopic Ellipsometry”. In: *Nano letters* 20.9, pp. 6412–6419. [↗](#).

## **Part III**

# **Nonlinear Spectroscopy**



# Chapter10

## Second Harmonic Generation

Markus Lippitz  
July 1, 2021

### Tasks

- The data set contains the electric field at the surface of two gold nanostructures for two different laser polarization directions at the same laser power. Compare the (relative) efficiency of second harmonic generation for these four cases.
- Assuming that the fundamental field distribution would not change (which is not true), estimate how large the nanorod would need to be so that opposing surfaces do not cancel out anymore. Calculate the angular emission pattern in this case.

### Experiment

Metal nanostructures of almost arbitrary (two-dimensional) shape can be fabricated by electron beam lithography (EBL). A resist is patterned by the electron beam, similar to how a photoresist is exposed by a light beam. During development, the resist is dissolved at the exposed positions. At these places, an evaporated metal film touches the glass substrate and sticks to the substrate. Dissolving now also the remaining resist (in another solvent than the developer), the metal film on top is lifted off and only the patterned surfaces remain as metal patterns.

In the experiment, rectangular and U-shaped structures are investigated. The rectangular ones are called 'rods', the U-shaped 'split rings', as one can imagine a ring that is cut open. The spectroscopic properties of these split rings go beyond the scope of this chapter<sup>1</sup>. We stick here to a single wavelength.

<sup>1</sup> Klein et al., 2006.

For second-harmonic generation, one focuses a laser beam of short pulses (about 100 fs) on the sample and detects in transmission or reflection the generated light at half the wavelength. Experiments on single nanostructures are possible using a microscope objective.



This work is licensed under a [Creative Commons "Attribution-ShareAlike 4.0 International"](https://creativecommons.org/licenses/by-sa/4.0/) license.

## Nonlinear Susceptibility

The interaction of light with a dielectric medium is described<sup>2</sup> by the susceptibility  $\chi$ . An electric field  $E$  moves the charge carriers and generates a polarization  $P$

$$P(E) = \epsilon_0 \chi E \quad . \quad (10.1)$$

This can be described by the classical Lorentz oscillator model, in which electrons are bound in a one-dimensional potential  $V(x)$ . In first approximation this potential is a harmonic potential so that the deflection  $x$  of the electrons is proportional to the incoming field  $E$ . If the field strength of the field  $E$  increases, the deflection  $x$  sometime is so large that the approximation of the potential by a parabola is no longer valid and higher-order terms in the potential need to be added. This then leads to the deflection  $x$  and thus also the polarization  $P$  depending also in higher order on the electric field  $E$ :

$$P(E) = \epsilon_0 \left( \chi^{(1)} E + \chi^{(2)} E^2 + \chi^{(3)} E^3 + \dots \right) \quad . \quad (10.2)$$

The higher-order terms in  $E$  put an end to the superposition principle of linear optics. Waves of different frequency  $\omega$  can no longer be treated independently. A  $n$ -th order process in  $E$  mixes  $n$  monochromatic waves  $E(\omega_i)$ . In addition, the individual waves  $E(\omega_i)$  do not have to have parallel wave vectors and also the polarization  $P$  not necessarily needs to be parallel to the electric field. The susceptibilities  $\chi^{(i)}$  are therefore tensors of  $(i+1)$ -th rung, so that the above equation should be written as

$$P_i = \epsilon_0 \left( \sum_j \chi_{ij}^{(1)} E_j(\omega_1) + \sum_{j,k} \chi_{ijk}^{(2)} E_j(\omega_1) E_k(\omega_2) + \sum_{j,k,l} \chi_{ijkl}^{(3)} E_j(\omega_1) E_k(\omega_2) E_l(\omega_3) + \dots \right) , \quad (10.3)$$

where  $E_i(\omega_j)$  is the  $i$ -th vector component of a monochromatic wave with frequency  $\omega_j$ . The polarization  $P$  in turn is the source of the electric field  $E$ :

$$\nabla^2 E - \epsilon_0 \mu_0 \ddot{E} = \mu_0 \ddot{P} \quad . \quad (10.4)$$

Due to the non-linear relationship between the field  $E$  and the polarization  $P$  new frequency components appear in  $E$ . This is shown in figure 10.1, where the series expansion was limited to the quadratic term. In the output field  $E$ , there is additional to the input frequency  $\omega$  a component with frequency zero and – based on the asymmetry of the positive and negative half-waves – one with the doubled frequency. The first causes a shifting the average value compared to the input field, the second an asymmetry of the oscillation around this mean value. The absolute value of the polarization  $P$  is not invariant under flipping of the sign of the electric field  $E$ , as can be seen in part A of the figure.

Let us investigate the mixing of waves more in detail. We assume the fields  $E(\omega)$  as plane waves

$$E(\omega) = \hat{E}(z) e^{-i(\omega t - k z)} \quad (10.5)$$

<sup>2</sup> Milonni and Eberly, 1988; Yariv, 1989.





Figure 10.1: Influence of a non-linear relationship between incident field  $E$  and polarization  $P$ . A: linear and non-linear relationship between  $E$  and  $P$ . B: in the linear case the polarization follows the field. C: in the nonlinear case, on the one hand the mean value shifted (DC part of the output field) and on the other hand the curve is deformed (additional component with doubled frequency).

with

$$k = n\omega/c = \omega \sqrt{\epsilon_0 \mu_0 [1 + \chi^{(1)}(\omega)]} . \quad (10.6)$$

The left side of the wave equation 10.4 is calculated using the slowly varying envelope approximation (SVEA), i.e., assuming that the amplitude  $\hat{E}(z)$  does not vary much on the wavelength scale. We get

$$\nabla^2 E \approx \left( 2ik \frac{d\hat{E}(z)}{dz} - k^2 \hat{E}(z) \right) e^{-i(\omega t - kz)} , \quad (10.7)$$

$$\epsilon_0 \mu_0 \frac{\partial^2 E}{\partial t^2} = -\epsilon_0 \mu_0 \omega^2 E(\omega) . \quad (10.8)$$

In the collinear case, the second time derivative  $\ddot{P}$  of the polarization on the right-hand side of the wave equation Eq. 10.4 becomes, again limiting us the quadratic terms,

$$\mu_0 \ddot{P} = -\mu_0 \epsilon_0 \left( \sum_j \chi_j^{(1)} \omega_j^2 E(\omega_j) + \sum_{j,k} \chi_{jk}^{(2)} (\omega_j + \omega_k)^2 E(\omega_j) E(\omega_k) \right) . \quad (10.9)$$

If the wave equation has to be fulfilled for three fixed but different frequencies  $\omega_i$  for all times  $t$ , it must be fulfilled independent of  $t$  for each  $\omega_i$ . To simplify things, we distinguish incoming waves from outgoing waves by the sign of the frequency  $\omega$  or the wave vector  $k$ : incoming waves are given a negative sign. Likewise, their amplitude  $\hat{E}$  will be inserted as complex conjugated. Conservation of energy can then be conveniently expressed as  $\sum \omega_i = 0$ . Finally, one obtains after some shuffling three equations

$$\frac{d\hat{E}_a(z)}{dz} = -\frac{i}{2} \sqrt{\frac{\mu_0}{\epsilon_a}} \epsilon_0 \omega_a \chi^{(2)} \hat{E}_b^* \hat{E}_c^* e^{-i\Delta k z} \quad \text{with} \quad \Delta k = \sum k_i \quad (10.10)$$

with cyclically swapped indices  $\{a, b, c\} = \{1, 2, 3\}$ .

## Questions

1. Derive eq. 10.9
2. Compare the generation of a new field  $\hat{E}_a(z)$  in eqs. 10.10 and 10.4 with the formalism we used to describe the wave emitted by a coherence in a two-level system in chapter 7.

## Frequency Doubling

The simplest case of non-linear generation of new frequencies is the one already shown in figure 10.1: frequency doubling or second harmonic genera-

tion. It results from the equation 10.10, if we set

$$\omega_1 = \omega_2 = -\omega \quad \text{and} \quad \omega_3 = 2\omega \quad (10.11)$$

This satisfies energy conservation. The conservation of momentum, in this context also called phase matching, is described by

$$\Delta k = 2k_\omega - k_{2\omega} = 2\omega\sqrt{\epsilon_0\mu_0} [n(\omega) - n(2\omega)] \quad (10.12)$$

We will consider only the case of non-depleted pump, i.e., that the amplitude of the incoming wave does not change although energy is transferred into the beam at the second harmonic, so that  $\hat{E}_1(z) = \hat{E}_2(z) = \text{const.}$  This allows simple integration of  $\hat{E}_3(z) = \hat{E}_{2\omega}(z)$  and we obtain

$$\hat{E}_{2\omega}(L) = -\frac{i}{2}\sqrt{\frac{\mu_0}{\epsilon_{2\omega}}}\epsilon_0(2\omega)\chi^{(2)}(\hat{E}_\omega)^2\int_0^L e^{i\Delta k z'} dz' \quad (10.13)$$

$$= -\sqrt{\frac{\mu_0}{\epsilon_{2\omega}}}\epsilon_0\omega\chi^{(2)}(\hat{E}_\omega)^2\frac{e^{i\Delta k L}-1}{\Delta k} \quad (10.14)$$

and

$$\left|\hat{E}_{2\omega}(L)\right|^2 = \frac{\mu_0}{\epsilon_{2\omega}}\left(\epsilon_0\omega\chi^{(2)}\right)^2(\hat{E}_\omega)^4 L^2 \text{sinc}^2(\Delta k L/2) \quad (10.15)$$

The intensity at the doubled frequency is proportional to the square of the intensity of the incident wave, since two photons of frequency  $\omega$  are converted into one photon of frequency  $2\omega$ . The conversion efficiency increases with the square of the crystal length  $L$ . At the same time with growing  $L$  the condition for phase matching becomes stricter, because we need  $\Delta k L/2 \ll 1$ . To obtain a high conversion efficiency, phase matching should therefore be optimal. This also holds if the above restriction to constant intensity of the excitation wave is dropped.

The idea of phase matching is qualitatively shown in figure 10.2. The upper part shows the nonlinear polarization  $P \propto E_\omega^2$ . It oscillates at twice the frequency of the incident field. At the instances indicated by the circles, a partial wave should be generated with the doubled frequency (half wavelength). If the refractive index  $n$  at both wavelengths  $\lambda_1$  and  $\lambda_2$  is equal, then both partial waves overlap constructively, and the initial intensity of the second harmonic is rising. However, if the refractive index  $n(\lambda_2)$  is higher, the two partial waves are partially extinguished, and the output intensity is lower. Equation 10.15 also shows that phase matching (i.e. momentum conservation) does not need to be fulfilled exactly. The Heisenberg uncertainty relation gives some freedom<sup>3</sup>: The conversion of the two fundamental photons into one second-harmonic photon must occur somewhere in the crystal. This gives an upper limit for the position uncertainty and thus a lower limit for the momentum uncertainty. Within this range of momentum mismatch frequency doubling is possible, which is described by  $\text{sinc}(\Delta k L/2)$ .<sup>4</sup>

<sup>3</sup> Demtröder, 2014; Saleh and Teich, 1991.

<sup>4</sup> This is the same Fourier transform that also connects a slit and its diffraction pattern.

## Questions

3. Explain the phase matching condition  $\text{sinc}(\Delta k L/2)$  using the space-momentum uncertainty relation.
4. Explain the need of phase matching by requiring energy and momentum conservation.

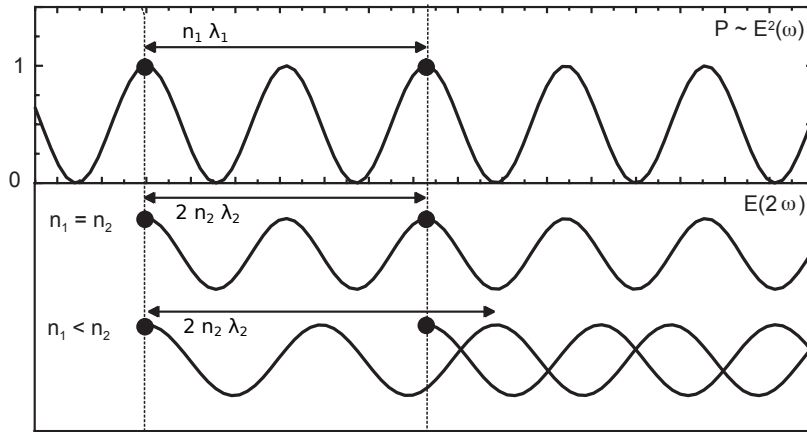


Figure 10.2: Schematic representation of phase matching. In the instances marked by circles a partial wave with doubled frequency is launched. When the refractive indices  $n(\omega)$  and  $n(2\omega)$  do not match, the partial waves cancel out each other and the intensity of the second harmonic does not increase.

### Phase matching by birefringent crystals

For optimum phase matching, the refractive index of excitation wave and second harmonic need to coincide. Since the refractive index depends on the frequency of the field, this match is usually not given. Birefringent crystals provide a way out. In such crystals, the refractive index differs between ordinary and extraordinary polarized waves as long as the propagation direction is not along the optical crystal axis. Figure 10.3 shows the relationship between the axes. For the refractive index  $n_{eo}(\omega, \theta)$  of a extraordinary wave holds

$$\frac{1}{n_{eo}^2(\omega, \theta)} = \frac{\cos^2 \theta}{n_o^2(\omega)} + \frac{\sin^2 \theta}{n_{eo}^2(\omega)}, \quad (10.16)$$

where  $n_{eo}(\omega) = n_{eo}(\omega, \theta = \pi/2)$ . By choosing the angle  $\theta$  between the direction of propagation and of the optical crystal axis, the refractive index can now be tuned so that (in case of a negative uniaxial crystal with  $n_{eo} < n_o$ )

$$n_{eo}(2\omega, \theta) = n_o(\omega) \quad (10.17)$$

This is illustrated by the example of  $\beta$ -bariumborate (BBO,  $\beta\text{-BaB}_2\text{O}_4$ ) in figure 10.3. Fundamental and second harmonic wave are polarized perpendicular to each other. With this method it is therefore possible to achieve optimum phase matching for a pair of frequencies  $\omega, 2\omega$ . But it has several disadvantages: The crystal must be rotated to achieve phase matching. This results in a variable beam offset when tuning the fundamental frequency, so that this method can only be used with great effort in a laser resonator. Moreover, to achieve a high intensity of the incident field, the laser beam needs to be focused tightly. However, this changes the angle of incidence over the beam cross section and thus the quality of the phase matching, so that not the whole beam is frequency doubled. Finally, birefringence means that the propagation direction of ordinary and extraordinary ray is different, so that they do not overlap optimally over the whole crystal length. The beams walk off. All these disadvantages are compensated by the so-called *non-critical phase matching*<sup>5</sup>: the angle  $\theta$  is chosen to be 90 degrees. Thus the refractive index  $n_{eo}(\omega, \theta)$  depends only very weakly (not critical) on the angle of incidence  $\theta$ , so that the phase adjustment is equally good even with strong

<sup>5</sup> Demtröder, 2014; Hopf and Stegeman, 1986.

focusing. In this case the direction of propagation does not differ between ordinary and extraordinary beam, so that the entire crystal length can be exploited. To use non-critical phase matching, the different temperature dependence of the two refractive indices is exploited and the crystal is either cooled or heated. This process does not require a change of the beam path with variation the wavelength anymore, making it suitable for use in a laser resonator.

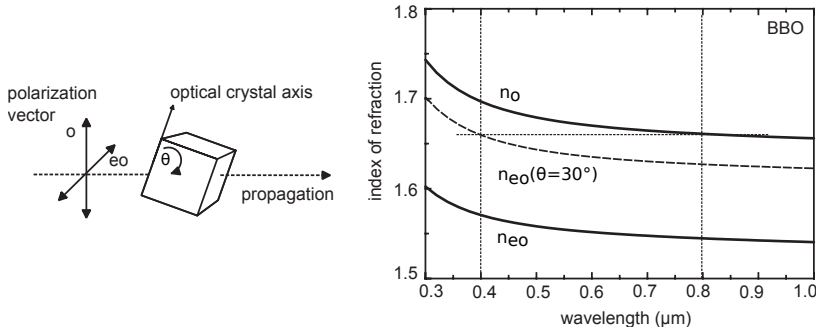


Figure 10.3: Phase matching by birefringence using the example of  $\beta$ -barium borate (BBO). By suitable choice of the angle  $\theta$  of the optical crystal axis to the direction of propagation of beams, the refractive index for the extraordinary wave is adjusted so that  $n_{eo}(2\omega, \theta) = n_o(\omega)$ .

## Questions

- Read in an optics textbook of your choice on birefringence and eq. 10.16.
- Calculate the phase-matching angle for frequency doubling of 700 nm light using BBO. You will need the Sellmeier coefficients of BBO, which can be found online.

## Symmetry

Second harmonic generation cannot take place in all media. It requires that the medium does not have a center of inversion, i.e., is not centrosymmetric. The medium needs to be able to distinguish an electric field pointing to the left from one pointing to the right. Not many materials fulfill this requirement.

Centrosymmetry means that we mirror all points at a center of inversion, i.e.,  $(x, y, z) \rightarrow (-x, -y, -z)$ , assuming the origin to be the center of inversion. If a material possesses this symmetry, it will *not* show SHG. To see this, let's assume an electric field  $E(t)$  that produces a nonlinear polarization

$$P^{(2)}(t) = \chi^{(2)} E(t)^2 \quad . \quad (10.18)$$

With inversion symmetry, we can just mirror all vectors, i.e., it should hold

$$-P^{(2)}(t) = \chi^{(2)} (-E(t))^2 = \chi^{(2)} E(t)^2 \quad . \quad (10.19)$$

Both equations can only be fulfilled if  $\chi^{(2)} = 0$ .

We have seen this effect already in Fig 10.1. An electric field pointing into the positive direction has a different effect, produces a different polarization than the same amplitude of electric field pointing in negative direction. Only if this is the case, then second harmonic can be generated.

Typical materials used for second harmonic generation such as BBO or LBO have a crystal structure that lacks centrosymmetry.

### Questions

7. Convince yourself that BBO is not centrosymmetric.
8. Draw a sketch similar to Fig. 10.1, but for a centrosymmetric material, which does not allow  $\chi^{(2)}$  but only  $\chi^{(3)}$  processes.

### SHG at surfaces

A surface by definition violates centrosymmetry. Inside has to be different from outside, or there would be no interface. This means that second harmonic generation is possible at the interface of two centrosymmetric media. Interface-SHG or -SFG (sum frequency generation) is a spectroscopic method to investigate molecules at interfaces of, e.g., droplets. The signal stems from the molecules at the interface and is thus able to discriminate against molecules in bulk solution.

Let us discuss interface SHG at the example of a metal surface, that is responsible for the signal in the experiment of this chapter. Which elements of the nonlinear susceptibility tensor  $\chi^{(2)}$  do contribute? As the interface is responsible, we describe everything in a local coordinate system where  $n$  is the surface normal and  $t$  and  $s$  are parallel to the surface and perpendicular to each other. The tensor components are  $\chi_{ijk}^{(2)}$  where  $i, j, k \in \{n, t, s\}$ . The value of these tensor components was determined experimentally<sup>6</sup>, but we can estimate some things.

<sup>6</sup> Mäkitalo, Suuriniemi, and Kauranen, 2011; Wang et al., 2009.

At least one vector component needs to be along the surface normal  $n$ , as otherwise the surface would not contribute. It is not surprising that

$$\chi_{nnn}^{(2)} = 250\chi_0^{(2)} \quad (10.20)$$

is the largest component, where both incoming fields and the generated polarization is perpendicular to the surface. A much weaker effect is observed when only one of the vectors is oriented along the surface normal

$$\chi_{nts}^{(2)} = \chi_{nst}^{(2)} = 1\chi_0^{(2)} \quad \text{and} \quad \chi_{tsn}^{(2)} = \chi_{tns}^{(2)} = \chi_{stn}^{(2)} = \chi_{snt}^{(2)} = 3.6\chi_0^{(2)} \quad (10.21)$$

All other tensor components are zero up to experimental accuracy.

### Questions

9. Assume that the optical field at the equator (coordinates  $x^2 + y^2 = 1$ ) of a gold sphere (coordinates  $x^2 + y^2 + z^2 = 1$ ) is constant in amplitude and points everywhere in the  $+x$  direction. Calculate the nonlinear polarisation  $P^{(2)}$  along the equator.

### SHG at nanostructures

A nanostructure is on the size of the wavelength of light or smaller. At all surface elements a second order nonlinear polarization can be generated. However, in the optical far field, the contributions of all surface elements interfere with each other. At this point, the symmetry of the nanostructure enters, while the symmetry of the material is broken by the surface.

In case the nanostructure is centrosymmetric, we find for each surface element an identical but mirrored element with opposing direction of the surface normal. As the direction of the surface normal enters in the direction of the nonlinear polarization and thus the direction of the generated second harmonic field, the contributions of opposing surface elements cancel out in the optical far field. This breaks down as soon as the size of the structure is not small anymore. Then the field emitted at one surface element can acquire a phase difference relative to the field generated at the opposing surface so that the interference is not fully destructive anymore.

If the nanostructure is not centrosymmetric, the fundamental field at two opposing surface elements will not be the same. Then the nonlinear polarization differs, and the two partial fields do not cancel. Second harmonic generation at nanostructure is thus a sensitive measure for the symmetry of the particle. In reality, nominally symmetric structures such as spheres are never ideally symmetric. Small protrusions and facets break the symmetry. Gold 'spheres' produce a stronger second harmonic signal than third harmonic, although the latter is symmetry-allowed (but a higher order of nonlinearity and therefore weaker).

### Questions

10. What is the minimum distance of the grooves in a grating (at a given wavelength) so that the structure works as dispersive grating?
11. How could one design a grating that does not have a zeroth order in transmission?

### References

- Demtröder, Wolfgang (2014). *Laser spectroscopy 1*. Berlin [u.a.]: Springer. [↗](#).
- Hopf, Frederic A. and George I. Stegeman (1986). *Applied classical electrodynamics: Nonlinear optics*. New York: Wiley.
- Klein, Matthias W et al. (2006). "Second-harmonic generation from magnetic metamaterials". In: *Science* 313.5786, pp. 502–504. [↗](#).
- Mäkitalo, J, S Suuriniemi, and M Kauranen (2011). "Boundary element method for surface nonlinear optics of nanoparticles". In: *Optics Express* 19.23, p. 23386. [↗](#).
- Milonni, Peter W. and Joseph H. Eberly (1988). *Lasers*. New York [u.a.]: Wiley.
- Saleh, Bahaa E. A. and Malvin C. Teich (1991). *Fundamentals of photonics*. New York, NY [u.a.]: Wiley. [↗](#).
- Wang, Fu Xiang et al. (2009). "Surface and bulk contributions to the second-order nonlinear optical response of a gold film". In: *Physical Review B* 80.23, pp. 233402–233404. [↗](#).
- Yariv, Amnon (1989). *Quantum electronics*. 3. ed. New York: Wiley.

# Chapter11

## Four-Wave Mixing

Markus Lippitz  
July 1, 2021

### Tasks

- A laser shines on a gold film which generates almost degenerate four-wave mixing signal, i.e., close in frequency but not identical. Predict the FWM spectrum and compare with the experiment (Data by Christoph Schnupfhagn, Bayreuth). You can assume a spectrally constant nonlinear susceptibility.
- In a similar experiment, the relative phase between two parts of the laser spectrum is modified by a pulse shaper. Predict the resulting FWM spectrum and compare with the experiment.

### Experiment

The laser creates pulses that are shorter than 10 fs, or about 250 nm wide. Such pulses are very delicate, as almost all reflecting and transmitting optical elements change the phase differently for the red and the blue part of the laser pulse spectrum. For longer, i.e. spectrally narrower pulses, this does not pose a relevant problem, but for wide pulses, this has to be taken into account. A 'pulse shaper' is a device to compensate these effects and will be discussed in a separate chapter.

Such a pulse shaper allows to generate laser pulses of almost arbitrary amplitude and phase spectrum. Here, we use it to demonstrate four-wave mixing. The data gives the laser intensity spectrum. The phase is either made to be constant or varies linear in time. We separate excitation and detection spectrally by a dichroic beam splitter and detect all light below a certain corner wavelength.

### Generation of short pulses

All non-linear effects require high intensities of at least one wave. This is relatively easy to achieve, if one does not require a permanently high laser intensity, but periodic intensity peaks are sufficient. During these pulses



This work is licensed under a [Creative Commons "Attribution-ShareAlike 4.0 International"](https://creativecommons.org/licenses/by-sa/4.0/) license.

the intensity is sufficiently high for nonlinear optics. Between the pulses the intensity is so low that no other processes take place. The averaged power of such a laser can therefore be in the range of about one Watt and still peak values of about 100 kW are reached when a pulse duration of 100 fs is compared to a pulse spacing of 13 ns. In this section we will discuss how such short laser pulses can be generated.

The starting point is the wide gain spectrum of a titanium-sapphire laser. The coupling of the atomic titanium levels to vibrational states of the sapphire crystal cause a strong homogeneous broadening of the transitions<sup>1</sup>, so that this type of laser can operate in the wavelength range 700–1000 nm. This allows many longitudinal modes  $E_n$  of electric field in the cavity to reach the laser threshold. The resonator length  $L$  defines the frequency spacing of the modes. Mode  $n$  has the frequency

$$\omega_n = n \pi c / L \quad . \quad (11.1)$$

The field of a multi-mode laser is the sum of its modes:

$$E(t) = \sum_n E_n(t) = \sum_n \hat{E}_n e^{i\phi_n} e^{i(c/L)\pi n t} \quad . \quad (11.2)$$

The temporal evolution of the initial field is thus the Fourier transform of the spectral amplitudes  $\hat{E}_n$  multiplied by a phase factor  $e^{i\phi_n}$ . The pulse period  $T = 2L/c$  corresponds to the round-trip time in the resonator. If no further precautions are taken, the phase  $\phi_n$  of each mode take a random and fluctuating value. This results<sup>2</sup> in a pattern of incoherent light, repeating in time with the period  $T$ . However, if the individual modes are coupled, i.e., if they have a fixed phase relationship to each other,

$$\delta\phi = \phi_{n+1} - \phi_n = \text{const.} \quad , \quad (11.3)$$

then the temporal evolution of the electric field corresponds to the Fourier transforms the amplitude distribution. The constant  $\delta\phi$  leads to a shift in time. A typical resonator length is  $L = 2$  m. At a center wavelength of  $\lambda_0 = 800$  nm and a spectral width of the gain region (limited through wavelength-selective (Lyot) filters) of  $\Delta\lambda = 4$  nm, about

$$N \approx \frac{\delta\lambda}{\lambda^2} \frac{L}{\pi} = 3980 \quad (11.4)$$

modes are above the gain threshold. It is thus justified to assume a continuous amplitude distribution  $\hat{E}(\omega)$ .

As an example, we discuss a Gaussian distribution, others are found in the literature.<sup>3</sup> We write the spectral amplitude distribution  $\hat{E}(\omega)$  as

$$\hat{E}(\omega) = \hat{E}_0 \sqrt{\pi} \tau_G e^{-\frac{1}{4}(\omega - \omega_0)^2 \tau_G^2} \quad . \quad (11.5)$$

The temporal evolution of the electric field follows from this by Fourier transformation

$$\hat{E}(t) = \hat{E}_0 e^{-(t/\tau_G)^2} \quad \text{and} \quad E(t) = \hat{E}(t) e^{i\omega_0 t} \quad . \quad (11.6)$$

The pulse width  $\tau_p$  is the full width at half maximum (FWHM) of the electric field envelop

$$\tau_p = \sqrt{2 \ln 2} \tau_G \quad . \quad (11.7)$$

<sup>1</sup> Rullière, 2005, chapter 4.

<sup>2</sup> Diels and Rudolph, 1996.

<sup>3</sup> Diels and Rudolph, 1996; Rullière, 2005.



The spectral width of the laser is expressed as FWHM  $\Delta\nu$  of the laser spectrum  $S(\omega) = |\hat{E}(\omega)|^2$  and

$$\delta\nu = \frac{\delta\omega}{2\pi} = \frac{\sqrt{8 \ln 2}}{2\pi \tau_G} . \quad (11.8)$$

The Fourier transform relates these two quantities and leads to the so-called *time-bandwidth product*

$$\delta\nu \tau_p = \frac{2 \ln 2}{\pi} \approx 0.441 . \quad (11.9)$$

Laser pulses whose time-bandwidth product reach this value are called *Fourier-limited*. If the available spectral bandwidth  $\Delta\nu$  is not used to get the shortest possible pulses, i.e. the smallest  $\tau_p$ , then the measured time-bandwidth product exceeds the value of 0.441. Provided that pulse shape is Gaussian, the time-bandwidth product tells whether the laser system is adjusted optimally.

### Questions

1. All the prefactors in the time-bandwidth product of a Gaussian pulse stem from the use of the FWHM as measure of the spectral and temporal pulse width. Use a  $1/e$  width and derive a 'cleaner' form.
2. Assume a few (2 to 20) spectrally equi-distant modes, their amplitudes and phases, and calculate numerically the output field of such a laser. When do you get nice pulses in time? Diels and Rudolph, 1996, have a picture of this.

### Dispersion

How does it come that the time-bandwidth product is increased? Let us investigate the influence of a time-dependent phase  $\phi(t)$  of the electric field. For simplification we assume that  $\phi(t)$  is a polynomial in  $t$ . This means that

$$E(t) = \hat{E}(t) e^{i(\omega_0 t + \phi(t))} = \hat{E}(t) e^{i(\omega_0 + d\phi(t)/dt)t} e^{i\phi_0} . \quad (11.10)$$

As long as  $\phi(t)$  is only linearly dependent on the time  $t$ , the effect is only a shift the central frequency  $\omega_0$  to  $\omega'_0 = \omega_0 + d\phi(t)/dt$ . In frequency space – through Fourier transform of the above equation – this means that the phase  $\phi$  depends only linearly on the frequency  $\omega$ . This is what we required already above by  $\delta\phi = \text{const.}$ . For a square dependence of the phase on the time a temporal variation occurs in the central frequency  $\omega_0$  of the pulse. One speaks of *chirp*, because in the acoustic analogy of a rising or falling tone sequence. Square (and higher) dependence of the phase on time (and thus on the frequency) is determined by the group velocity dispersion (GVD) in optical elements, e.g. glasses, but also mirrors. This is associated with the first and second derivative of the refractive index with wavelength. Assuming  $\phi = -a t^2 / \tau_G^2$  we then get

$$\hat{E}(t) = \hat{E}_0 e^{-(1+i a) (t/\tau_G)^2} \quad (11.11)$$

and for the time-bandwidth product

$$\delta\nu \tau_p = \frac{2 \ln 2}{\pi} \sqrt{1 + a^2} \approx 0.441 \sqrt{1 + a^2} , \quad (11.12)$$

as the spectral bandwidth  $\Delta\nu$  is just increased by a factor of  $\sqrt{1+a^2}$ . Higher order polynomial terms in the time-dependence of the phase  $\phi$  are discussed in the chapter on pulse shaping.

Group velocity dispersion (GVD) cannot be avoided in an optical resonator. How transmitting and also reflective elements change the phase of the electromagnetic wave depends strongly on the wavelength. In order to still achieve an optimal, i.e. Fourier limited pulse the entire GVD must be as wavelength independent as possible. The influence of the individual elements should therefore compensate each other. In glasses, the positive second derivative of the refractive index is dominating the GVD. To compensate for this, a section with negative GVD is needed in the resonator. This can be achieved by two prisms as shown in figure 11.1. Two equal prisms are placed in front of a mirror such that all spectral components hit the mirror perpendicularly and the resonator is closed.

Detailed calculations<sup>4</sup> show that the pure geometric path length difference causes negative GVD. The path inside the prisms contributes positive GVD. By varying the position  $z$  one can obtain almost arbitrary values of net GVD of this prism system.

### Questions

3. Draw / calculate the laser pulse given by eq. 11.11 and its properties so that one can understand why this is called a 'chirp'.

### Autocorrelation

A pulse width  $\tau_P$  in the range of a few pico- or femto-seconds cannot be measured electronically, as the involved frequencies would be too high. The idea is to measure the pulse length optically, using the laser pulse to sample itself. The beam is divided into two parts, one of which is delayed with respect to the other before they are overlaid again. Times in the range of femtoseconds correspond to lengths in the range of micrometers, which can be easily controlled. A detector that responds quadratically in intensity (not field!) is able to measure overlap of two halves  $a$  and  $b$  as

$$\text{after each other} \quad a^2 + b^2 \neq (a + b)^2 \quad \text{simultaneously.} \quad (11.13)$$

Often frequency doubling is used for this purpose by focusing the recombined beam onto a frequency doubling crystal. The detector is sensitive only for light at half the wavelength. With variable delay  $\tau$  the time-integrated signal is sufficient, and the temporal resolution of the detector is irrelevant. One thus measures

$$G(\tau) = \langle I(t) \times I(t - \tau) \rangle \quad (11.14)$$

The function  $G(\tau)$  is called as intensity autocorrelation function. It is always symmetrical ( $G(\tau) = G(-\tau)$ ) and is relatively insensitive to the actual pulse shape. One has to assume a pulse as Gaussian or  $\text{sec}^2$ -shaped to calculate<sup>5</sup> the pulse length  $\tau_P$  from the FWHM of the autocorrelation  $\tau_{AC}$

$$\tau_P = \tau_{AC} / \sqrt{2} \quad \text{for Gauss pulses,} \quad (11.15)$$

$$= \tau_{AC} / 1.543 \quad \text{for sec}^2\text{-shaped pulses.} \quad (11.16)$$

<sup>4</sup> Diels and Rudolph, 1996.



Figure 11.1: This prism sequence allows to adjust the group velocity dispersion by the prism position along  $z$ .

<sup>5</sup> Diels and Rudolph, 1996.

## Questions

4. Why is the intensity autocorrelation symmetric in delay  $\tau$ ?

## Four-wave mixing

Let us now turn to the spectroscopic consequences of the phase dispersion over the spectral width of a laser pulse. We use the example of four-wave mixing. In general, a third-order nonlinearity can be written as

$$P_i^{(3)} = \epsilon_0 \sum_{j,k,l} \chi_{ijkl}^{(3)} E_j(\omega_1) E_k(\omega_2) E_l(\omega_3) \quad (11.17)$$

where three optical waves produce a nonlinear polarization, which radiates a new optical field<sup>6</sup>. This field is sometimes detected directly, sometimes interfered with a fourth field acting as local oscillator. A *third-order* nonlinearity describes thus the mixing of *four* waves.

Several different processes are summarized as four-wave mixing (FWM) effects and depicted in figure 11.2. The generated nonlinear polarization oscillates at the sum of the three input frequencies. Complex conjugate input fields are again counted as negative frequencies and depicted as downward arrows in Fig. 11.2.

<sup>6</sup> Similar to the chapter on the free induction decay



Figure 11.2: Sketches of  $\chi^{(3)}$  processes: third-harmonic generation (THG), pump-probe spectroscopy (PP), coherent anti-Stokes Raman scattering (CARS), and non-degenerate four-wave mixing (FWM). All processes start and end at a real state that can be populated (solid horizontal line). Intermediate states can be virtual states (dashed horizontal line). The interaction between light and matter occurs in time from left to right within each diagram. The last downward arrow symbolizes the emission process. Other downward arrows symbolize incoming complex-conjugate fields that count negative when calculating the emission frequency.

In third-harmonic generation, one optical wave at frequency  $\omega$  generates a new optical field at frequency  $3\omega$ :

$$P^{(THG)}(3\omega) = \epsilon_0 \chi^{(3)} E(\omega)^3 \quad (11.18)$$

This is a coherent process, i.e., the phase of the new field is related to the phase of the fundamental wave, but homodyne interference is in contrast to linear absorption not possible. The detected signal intensity  $I^{(THG)}$  is thus proportional to the third power of the fundamental intensity  $I(\omega)$

$$I^{(THG)} \propto |P^{(THG)}(3\omega)|^2 = |\epsilon_0 \chi^{(3)} E(\omega)^3|^2 \propto I(\omega)^3 \quad (11.19)$$

In pump-probe spectroscopy, a pump-beam is absorbed and its influence on the absorption of a second, probe beam is monitored. Here it is the intensity of the pump beam, not the field amplitude that enters. The probe beam appears only linear in field amplitude as in linear absorption spectroscopy. All together pump-probe spectroscopy can be written as

$$\begin{aligned} P^{(pp)}(\omega_{\text{probe}}) &= \epsilon_0 \chi^{(3)} E(\omega_{\text{pump}}) E^*(\omega_{\text{pump}}) E(\omega_{\text{probe}}) \\ &= \epsilon_0 \chi^{(3)} |E(\omega_{\text{pump}})|^2 E(\omega_{\text{probe}}) \end{aligned} \quad (11.20)$$

From this notation, it is obvious that pump-probe spectroscopy does not depend on the phase relation between pump- and probe-beam. The generated nonlinear polarization oscillates at the frequency of the incoming probe beam which again allows homodyne detection. The observed signal is thus proportional to the amplitude of the interference between nonlinear polarization and probe field and not to the square of the nonlinear polarization itself as in third-harmonic generation. The signal scales linearly both in pump and in probe power.

In coherent anti-Stokes Raman scattering (CARS) the pump field also enters twice, as in pump-probe spectroscopy, but here it enters twice with the same phase. Both pump arrows point up in Figure 11.2. The nonlinear polarization is given by

$$P^{(CARS)}(\omega_{\text{CARS}}) = \epsilon_0 \chi^{(3)} E(\omega_{\text{pump}}) E(\omega_{\text{pump}}) E^*(\omega_{\text{Stokes}}) \quad (11.21)$$

and oscillates at a new frequency  $\omega_{\text{CARS}} = 2\omega_{\text{pump}} - \omega_{\text{Stokes}}$ . Either one detects its square (similar to third-harmonic generation) or one supplies an additional field acting as local oscillator to produce a signal that is linear in the generated polarization. The intermediate state of lowest energy in Fig. 11.2 is a vibrational state of a molecule. It enhances the efficiency of this process which can also take place without a real state at this energy.

In the most general case of four-wave mixing all three input waves differ in frequency. The examples above are cases of degenerate four-wave mixing (DFWM) where some frequencies coincide. Here, I use the term 'four-wave mixing' only for the non-degenerate case and stick to the more specialized terms otherwise. An experimentally accessible variant of four-wave mixing is depicted in Fig. 11.2 where three similar but not identical waves produce a fourth wave which again is spectrally close to the input waves. This process scales linearly in all three input powers and also the phase relation between all waves is relevant.

Note that for a given material the value of  $\chi^{(3)}$  depends on all three incoming frequencies  $\omega_1, \omega_2, \omega_3$  and the outgoing frequency  $\omega_4$ , which is written as  $\chi^{(3)}(\omega_4; \omega_1, \omega_2, \omega_3)$ .

## Questions

5. Convince yourself that the direction of the arrows in Fig. 11.2 fits to the equations given in this chapter.
6. Draw a level scheme for a hypothetical  $\chi^{(5)}$  process and give the equation to calculate its intensity.

## Spectral interference

How does now the spectral phase enter? With the broad spectrum of a laser pulse, many different combinations of  $\omega_1, \omega_2, \omega_3$  lead to the same outgoing frequency  $\omega_4$ . All these paths interfere with each other so that with each frequency  $\omega_i$  also its phase  $\phi_i$  enters.

Neglecting the tensorial nature of  $\chi$  we can write

$$P^{(3)}(\omega_4) = \epsilon_0 \int_{\omega_1, \omega_2} \chi^{(3)}(\omega_4; \omega_1, \omega_2, \omega_3) E(\omega_1) E(\omega_2) E(\omega_3) d\omega_1 d\omega_2 \quad (11.22)$$

where  $\omega_3$  is calculated at each point of the integral such that energy conservation is fulfilled, e.g.  $\omega_3 = \omega_4 - \omega_1 - \omega_2$ . Again, the above rule for negative frequencies, complex conjugates, and downward arrows applies.

The spectral dependence of  $\chi^{(3)}(\omega_4; \omega_1, \omega_2, \omega_3)$  is determined by the process that causes the nonlinearity. As in linear spectroscopy, the spectral shape of  $\chi^{(3)}$  is related to the response of the system in time domain, its pulse response<sup>7</sup>. A fast system has thus a spectrally flat susceptibility. In the limit of instantaneous response, the nonlinear susceptibility is spectrally constant.

When assuming a flat nonlinear susceptibility is too much of an approximation, one can make use of Miller's rule<sup>8</sup>, which connects linear and nonlinear optical properties

$$\chi^{(3)}(\omega_4; \omega_1, \omega_2, \omega_3) \propto \chi^{(1)}(\omega_1) \chi^{(1)}(\omega_2) \chi^{(1)}(\omega_3) \chi^{(1)}(\omega_4) \quad . \quad (11.23)$$

<sup>7</sup> Multiplication in frequency domain becomes by Fourier transform a convolution in time domain.

<sup>8</sup> Boyd, 2008; Miller, 1964; Obermeier, Schumacher, and Lippitz, 2018.

## Questions

7. A laser pulse has a spectral width of 10 nm. How broad is the spectrum of the second- and third-harmonic that is created by this laser, assuming nonlinear susceptibilities that are spectrally flat in the relevant spectral range?

## References

- Boyd, Robert W. (2008). *Nonlinear Optics*. 3. ed. Amsterdam [u.a.]: Elsevier, Acad. Press.
- Diels, Jean-Claude and Wolfgang Rudolph (1996). *Ultrashort laser pulse phenomena. fundamentals, techniques, and applications on a femtosecond time scale*. San Diego [u.a.]: Academic Press. [↗](#)
- Miller, Robert C. (1964). "Optical second harmonic generation in piezoelectric crystals". In: *Applied Physics Letters* 5.1, pp. 17–19. [↗](#)
- Obermeier, Julian, Thorsten Schumacher, and Markus Lippitz (2018). "Nonlinear spectroscopy of plasmonic nanoparticles". In: *Advances in Physics: X* 3.1, p. 1454341. [↗](#)
- Rullière, Claude, ed. (2005). *Femtosecond laser pulses. principles and experiments*. 2. ed. New York, NY: Springer, XVI, 426 S. [↗](#)



# Chapter12

## Two-Photon Absorption

Markus Lippitz  
July 1, 2021

### Tasks

- Derive eq. 12.21 which is the same as the result of section 2.3.(i) in Winterhalder et al., 2011 and plug in some typical values. The paper investigates the possibility of single molecule vibrational spectroscopy by stimulated Raman scattering followed by a 'normal' electronic excitation. The interesting part is the first half of the process, a two-photon excitation of a vibrational state. The technique to 'read' the formula from the interaction diagram will be discussed in the chapter on 2d spectroscopy.

### History of Two-Photon Absorption

The possibility of simultaneous absorption of two photons in a quantum process was described already in 1931 by Maria Göppert-Mayer in of her dissertation<sup>1</sup> 'Über Elementarakte mit zwei Quantensprüngen'. One year after the realization of the ruby laser by Maiman<sup>2</sup> succeeded in 1961 the first experimental proof of two-photon excitation of  $\text{CaF}_2:\text{Eu}^{2+}$  by Kaiser and Garrett<sup>3</sup>. Two years later, fluorescence of organic crystals (pyrene, anthracene) was observed after two-photon excitation<sup>4</sup>. Important fields of application of two-photon absorption are Doppler-free spectroscopy of atoms and molecules in the molecular beam (introduction in Demtröder, 2014) and the optical spectroscopy of transitions which are forbidden for a single-photon process<sup>5</sup>. The development of two-photon microscopy with the aim of detecting individual molecules began with the work of Denk, J. H. Strickler, and Webb, 1990. Nowadays, two-photon absorption is widely used in live science for imaging in tissues.

### Second-order perturbation theory

In this section, we derive an expression for the absorption rate of a two-photon transition using time-dependent perturbation theory<sup>6</sup>. Figure 12.1 outlines the involved states. We only consider the case that both absorbed photons come from the same monochromatic wave of the frequency  $\omega$ . The

<sup>1</sup> Göppert-Mayer, 1931, About elementary acts with two quantum jumps.

<sup>2</sup> Maiman, 1960.

<sup>3</sup> Kaiser and Garrett, 1961.

<sup>4</sup> Petricolas, Goldsborough, and Rieckhoff, 1963.

<sup>5</sup> Birge, 1986.

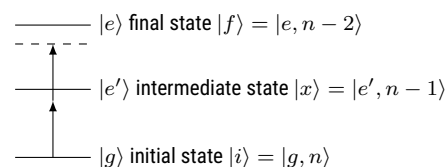


Figure 12.1: We distinguish between the states of the absorbing system ( $|g\rangle$ ,  $|e'\rangle$ ,  $|e\rangle$ ) and the states of the whole system, which also includes the light field with initially  $n$  photons:  $|i\rangle$ ,  $|x\rangle$ ,  $|f\rangle$ .

<sup>6</sup> Haken and H. Wolf, 2004; Meystre and Sargent III, 2007.



intermediate state  $|e'\rangle$  does not necessarily have to be energetically below the final state  $|e\rangle$ . The wave function  $\psi$  of the entire system is

$$\psi = \sum_{\mu \in \{i, x, f\}} c_\mu \psi_\mu \quad (12.1)$$

At the beginning the system is in the ground state, so  $c_i(0) = 1$  and all others  $c_\mu(0) = 0$ . We are looking for the population of the final state  $|f\rangle$  depending on the time  $t$ , i.e.,  $|c_f(t)|^2$ . The Hamilton operator  $H$  is split in a fixed and a perturbing part as  $H = H^0 + H^S$ . The matrix elements of the perturbing part evolve in time as

$$H_{\mu\nu}^S(t) = H_{\mu\nu}^S(0) e^{i\omega_{\mu\nu}t} \quad (12.2)$$

where  $\hbar\omega_{\mu\nu} = E_\mu - E_\nu$ . We now only consider processes that require the absorption of two photons at times  $t_1$  and  $t_2$ . We get<sup>7</sup>

<sup>7</sup> Haken and H. Wolf, 2004.

$$c_f(t) = -\frac{1}{\hbar^2} \sum_{\mu} H_{f\mu}^S(0) H_{\mu i}^S(0) \int_0^t e^{i\omega_{f\mu}t_1} dt_1 \int_0^{t_1} e^{i\omega_{\mu i}t_2} dt_2 \quad (12.3)$$

The inner integral gives

$$\int_0^{t_1} e^{i\omega_{\mu i}t_2} dt_2 = \frac{1}{i\omega_{\mu i}} (e^{i\omega_{\mu i}t_1} - 1) \quad (12.4)$$

and the outer integral

$$\int_0^t e^{i\omega_{f\mu}t_1} \frac{1}{i\omega_{\mu i}} (e^{i\omega_{\mu i}t_1} - 1) dt_1 = \int_0^t \frac{e^{i(\omega_{f\mu} + \omega_{\mu i})t_1}}{i\omega_{\mu i}} - \frac{e^{i\omega_{f\mu}t_1}}{i\omega_{\mu i}} dt_1 \quad (12.5)$$

$$= \left[ \frac{e^{i\omega_{f\mu}t_1}}{(-1)\omega_{\mu i}\omega_{f\mu}} + \frac{e^{i\omega_{f\mu}t_1}}{\omega_{f\mu}\omega_{\mu i}} \right]_0^t = -\frac{e^{i\omega_{f\mu}t} - 1}{\omega_{\mu i}\omega_{f\mu}} + \frac{e^{i\omega_{f\mu}t} - 1}{\omega_{f\mu}\omega_{\mu i}} \quad (12.6)$$

While  $\omega_{f\mu} + \omega_{\mu i} = (E_e - E_g)/\hbar - 2\omega = \Delta\omega \approx 0$  guarantees energy conservation, terms with  $\omega_{f\mu} \gg 1$  oscillate so fast that they average out and can be neglected. This is again the rotating wave approximation. This results in

$$c_f(t) = \frac{1}{\hbar} \frac{e^{i\Delta\omega t} - 1}{\Delta\omega} \sum_{\mu} \frac{H_{f\mu}^S(0) H_{\mu i}^S(0)}{E_\mu - E_i} = \frac{1}{\hbar} \frac{e^{i\Delta\omega t} - 1}{\Delta\omega} X_{fi} \quad (12.7)$$

and

$$|c_f(t)|^2 = \frac{|X_{fi}|^2}{\hbar^2} \cdot t^2 \cdot \text{sinc}^2(\Delta\omega t/2) \quad (12.8)$$

This is the most interesting point, the definition of an effective transition matrix element  $X_{fi}$

$$X_{fi} = \sum_{\mu} \frac{H_{f\mu}^S(0) H_{\mu i}^S(0)}{E_\mu - E_i} \quad (12.9)$$

From now on, we follow the normal route also used when deriving Fermi's Golden Rule. The effect of the second order in the perturbation theory is collapsed into  $X_{fi}$ . Again we realize that with infinitesimally sharp optical



transitions the transition rate  $w_{fi}$  at resonance ( $\Delta\omega = 0$ ) increases linearly with time  $t$ :

$$w_{fi} = \frac{d|c_f(t)|^2}{dt} = 2 \frac{|X_{fi}|^2}{\hbar^2} \cdot t \cdot \text{sinc}^2(\Delta\omega t/2) \quad . \quad (12.10)$$

By assuming a Lorentz-shaped line of width  $\Gamma$ , whose form is described by the function  $D(\Delta\omega)$ ,

$$D(\Delta\omega) = \frac{\Gamma/\pi}{(\Delta\omega)^2 + \Gamma^2} \quad (12.11)$$

the population  $P_e$  of  $|e\rangle$  can be calculated<sup>8</sup>:

<sup>8</sup> Meystre and Sargent III, 2007.

$$P_e = \int D(\Delta\omega) \frac{|X_{fi}|^2}{\hbar^2} t^2 \text{sinc}^2[\Delta\omega t/2] d(\Delta\omega) \quad . \quad (12.12)$$

For times  $t \gg 1/\Gamma$  we find that  $\text{sinc}^2[\Delta\omega t/2]$  is different from zero only for  $\Delta\omega = 0$  so that

$$P_e = \frac{2}{\Gamma} \frac{|X_{fi}|^2}{\hbar^2} t \quad \text{and} \quad w_{fi} = \frac{2}{\Gamma} \frac{|X_{fi}|^2}{\hbar^2} \quad . \quad (12.13)$$

Let us examine the term  $|X_{fi}|^2$  more closely. The matrix elements of the perturbation operator  $H^S$  are the product of the complex dipole matrix element  $\mu_{\mu\nu}$  and the amplitude of the electric field

$$H_{\mu\nu}^S = \hat{E}(\omega) \mu_{\mu\nu} \quad . \quad (12.14)$$

The energy difference  $E_\mu - E_i$  can also be expressed as  $E_u - \hbar\omega$  ( $u \in \{g, e', e\}$ ) so that

$$|X_{fi}|^2 = \left| \sum_\mu \frac{H_{f\mu}^S(0) H_{\mu i}^S(0)}{E_\mu - E_i} \right|^2 = |\hat{E}(\omega)|^4 \left| \sum_u \frac{\mu_{eu} \mu_{ug}}{E_u - \hbar\omega} \right|^2 \quad . \quad (12.15)$$

All in all, this results in the following transition rate  $w_{fi}$

$$w_{fi} = \frac{2}{\hbar^2 \Gamma} |\hat{E}(\omega)|^4 \left| \sum_u \frac{\mu_{eu} \mu_{ug}}{E_u - \hbar\omega} \right|^2 = \frac{1}{2} \sigma_{TPE} \left( \frac{I(\omega)}{\hbar \omega} \right)^2 \quad , \quad (12.16)$$

where  $\sigma_{TPE}$  is the two-photon absorption cross section<sup>9</sup> and the factor  $1/2$  takes into account<sup>10</sup> that two photons must be absorbed. The excitation intensity  $I$  is usually not temporally constant, because it is advantageous to use a pulsed laser. This leads to an average excitation rate  $\alpha$

<sup>9</sup> Note that  $\sigma_{TPE}$  does *not* have the units of an area! See below.

<sup>10</sup> Xu and Webb, 1997.

$$\alpha = \langle w_{fi} \rangle = \frac{1}{2} \sigma_{TPE} \frac{\langle I^2 \rangle}{(\hbar \omega)^2} = \frac{1}{2} \sigma_{TPE} g^{(2)}(\tau = 0) \left( \frac{\langle I \rangle}{\hbar \omega} \right)^2 \quad . \quad (12.17)$$

Here  $g^{(2)}(\tau = 0)$  denotes the intensity autocorrelation function, evaluated at time zero. Knowing the pulse shape we can calculate  $g^{(2)}(\tau = 0)$  so that

$$\alpha = \frac{1}{2} \sigma_{TPE} \frac{g_P}{f \tau_P} \left( \frac{\langle I \rangle}{\hbar \omega} \right)^2 \quad . \quad (12.18)$$

For Gaussian pulses the pulse shape factor  $g_P$  has the value  $g_P = 0.66$ , for sec<sup>2</sup>-shaped pulses  $g_P = 0.59$  applies<sup>11</sup>.  $f$  denotes the repetition rate of the laser and  $\tau_P$  the temporal FWHM of the pulse.

<sup>11</sup> Xu and Webb, 1997.

## Questions

1. How does it come that  $|X_{fi}|^2$  can be used in the same way independent whether it stems from a first or second order perturbation theory? Why are its units independent of the order?
2. The requirement  $\omega_{f\mu} \gg 1$  after eq.12.6 is formulated a bit sloppy. How can this be improved?
3. What is the difference between  $w_{fi}$  and  $\alpha$ ? Why does this distinction become necessary?

## Selection rules and cross sections

For two-photon absorption to take place, the final state  $|e\rangle$  has to be reached over two successive electrical dipole transitions from the ground state  $|g\rangle$ . All intermediate states  $|x\rangle$  of the molecule contribute, weighted with their energetic distance to the photon energy. Since the summation occurs before taking the absolute value squared, interference between individual terms may arise.

An estimation of the order of magnitude of typical two-photon absorption cross sections can be obtained by assuming only one intermediate state  $|x\rangle$ , which is also close to the final state  $|e\rangle$ . The two-photon absorption cross section is then related to the product of two one-photon absorption cross sections<sup>12</sup>:

$$\sigma_{TPE} \approx \frac{\sigma_{OPE} \sigma_{OPE}}{\omega} = \frac{(10^{-17} \text{ cm}^2)^2}{10^{15} \text{ sec}^{-1}} = 10^{-49} \text{ cm}^4 \text{ sec}^{-1} = 10 \text{ GM} \quad (12.19)$$

In a first approximation, the TPE absorption cross section is therefore proportional to the square of the OPE absorption cross section. The two-photon absorption cross section  $\sigma_{TPE}$  is often given in of the unit Göppert-Meier ( $1 \text{ GM} = 10^{-50} \text{ cm}^4 \text{ sec}^{-1}$ ) and typical values are between 1 and 500 GM. Some values are given in table 12.1.

Things get even simpler if *no* intermediate state  $x$  is assumed, e.g. because all states in question are energetically too far away. Then the sum runs only over the states  $e$  and  $g$ , so that

$$\sigma_{TPE} \propto \left| \frac{\mu_{eg}}{\omega} \right|^2 |\mu_{ee} - \mu_{gg}|^2 \quad (12.20)$$

The absorption cross section is therefore proportional to the change in static dipole moment  $\mu_{ii}$  from ground to excited state. The change of the dipole moment then becomes particularly large, if charges in the molecule are shifted during excitation. Efforts to find molecules with particularly large two-photon absorption cross section, concentrate on this effect and find values of  $\sigma_{TPE}$  of more than 1000 GM<sup>13</sup>.

With two-photon excitation states in atoms and molecules can be reached that are not accessible for one-photon absorption (OPA). In the case of TPE the parity of the initial state is equal to the final state, whereas it must be different for OPE. However, even for large atoms the selection rules are relaxed, so that the distinction between different classes of molecular states is not always possible.

<sup>12</sup> Xu and Webb, 1997.

Dye	$\lambda_{\text{ex}}$ (nm)	$\sigma_{TPE}$ (GM)
Rhodamin B	840	$210 \pm 55$
Dil	700	$95 \pm 28$
Fluorescein	782	$38 \pm 9.7$
Coumarin 307	776	$19 \pm 5.5$
Indo-1	700	$12 \pm 4$
Bis-MSB	691	$6.3 \pm 1.8$
Lucifer Yellow	860	$0.95 \pm 0.3$

Table 12.1: Two photon absorption cross sections  $\sigma_{TPE}$  for dyes at different excitation wavelengths  $\lambda_{\text{ex}}$  (from Xu and Webb, 1996).

<sup>13</sup> Albota, Beljonne, Brédas, et al., 1998.

## Stimulated Raman Scattering

As an example, we discuss stimulated Raman scattering to populate a vibrational excited state of the electronic ground state. This follows the same formalism as two-photon absorption, although the second photon is a stimulated emission. The two interactions with a light field lead in both cases to second-order perturbation theory. As intermediate states, we take the electronic excited state and its first vibrational excitation into account. We find interference between these two paths, i.e., the amplitudes have to be added to a common  $X_{fi}$  before we take the absolute square of  $X_{if}$ . In contrast to two-photon absorption, the two interactions happen with different fields, defined by the frequencies  $\omega_1, \omega_2$  and amplitudes  $E_1, E_2$ . The table summarizes the variables used.

state	atom	elec.	vibr.	light $\omega_1$	light $\omega_2$
initial $ i\rangle$	ground $ g\rangle$	0	0	a	b
intermediate $ x\rangle$	excited $ e\rangle$	1	0	a-1	b
intermediate' $ x'\rangle$	excited' $ w\rangle$	1	1	a-1	b
final $ f\rangle$	vibronic $ v\rangle$	0	1	a-1	b+1

The vibrational energy is denoted as  $\Omega_v$ . The detuning of the first light field from the electronic resonance is very large compared to the vibrational frequency, i.e.,  $\delta_1 = \omega_{eg} - \omega_1 \gg \Omega_v$ . We write the Frank-Condon-Integral from vibronic level  $a$  in the electronic ground state to  $b$  in the electronic excited state as  $F_a^b$ . We assume  $F_0^0 = F_1^1 \approx 1$  and  $F_0^1 = -F_1^0$ . The only transition dipole moment that we need is that for the transition  $g \rightarrow e$ , i.e.

$\mu_{eg}$ .

With this, eq. 12.13 from above becomes

$$P_v(t) = \frac{2t}{\Gamma_v} \left| \frac{|\mu_{eg}|^2 E_1 E_2 F_0^1}{\hbar^2} \frac{\Omega_v}{(\delta_1)^2} \right|^2 \quad (12.21)$$

which agrees<sup>14</sup> with the outcome of section 2.3(i) in Winterhalder et al., 2011.

parameter	value
wavelength $\lambda$	570 nm
fluorescence lifetime $\tau_{fl}$	4 ns
laser power $P_1 = P_2$	100 mW
laser repetition rate $f$	76 MHz
laser pulse width $\tau$	1 ps
laser spot radius $r$	3 $\mu\text{m}$
Franck-Condon factor $F_0^1$	0.5
vibrational frequency $\Omega_v$	1500 $\text{cm}^{-1}$
vibrational width $\Gamma_v$	10 $\text{cm}^{-1}$
detuning $\delta_1$	8000 $\text{cm}^{-1}$

## Questions

- Derive eq. 12.21 from eq. 12.13.
- Calculate the transition dipole moment  $\mu_{eg}$  from the fluorescence lifetime  $\tau_{fl}$ , assuming a quantum efficiency of one.



Figure 12.2: Level scheme

Table 12.2: States of the quantum mechanical system

<sup>14</sup> The paper makes the distinction between  $\omega_{eg}$  and  $\omega_{wg}$  which is dropped here.

Table 12.3: Numerical values which are more optimistic than those in Winterhalder et al., 2011.

6. Calculate the field amplitude  $E_1$  assuming a rectangular pulse shape and focus profile.
7. Calculate the population of the vibrational state at the end of a laser pulse.

## References

- Albota, M., D. Beljonne, J.-L. Brédas, et al. (1998). "Design of Organic Molecules with Large Two-Photon Absorption Cross Section". In: *Science* 281, pp. 1653–1656. [↗](#)
- Birge, R. R. (1986). "Two-Photon Spectroscopy of Protein-Bound Chromophores". In: *Acc. Chem. Res.* 19, pp. 138–146. [↗](#)
- Demtröder, Wolfgang (2014). *Laser spectroscopy 1*. Berlin [u.a.]: Springer. [↗](#)
- Denk, W., J. H. Strickler, and W. W. Webb (1990). "Two-Photon Laser Scanning Fluorescence Microscopy". In: *Science* 248, pp. 73–76. [↗](#)
- Göppert-Mayer, M. (1931). "Über Elementarakte mit zwei Quantensprüngen". In: *Ann. Phys.* 9, pp. 273–295. [↗](#)
- Haken, H. and H.C. Wolf (2004). *Molecular Physics and Elements of Quantum Chemistry*. Springer.
- Kaiser, W. and C. G. B. Garrett (1961). "Two-Photon excitation in  $\text{CaF}_2:\text{Eu}^{2+}$ ". In: *Phys. Rev. Lett.* 7.6, pp. 229–231. [↗](#)
- Maiman, T. H. (1960). "Stimulated Optical Radiation in Ruby". In: *Nature* 187.4736, pp. 493–494. [↗](#)
- Meystre, Pierre and Murray Sargent III (2007). *Elements of Quantum Optics*. 4. Springer. [↗](#)
- Peticolas, W. L., J. P. Goldsborough, and K. E. Rieckhoff (1963). "Double photon excitation in organic crystals". In: *Phys. Rev. Lett.* 10.2, pp. 43–45. [↗](#)
- Winterhalder, M J et al. (2011). "Toward Far-field Vibrational Spectroscopy of Single Molecules at Room Temperature". In: *The Journal of Physical Chemistry B* 115.18, pp. 5425–5430. [↗](#)
- Xu, C. and W. W. Webb (1996). "Measurement of two-photon excitation cross sections of molecular fluorophores with data from 690 to 1050 nm". In: *J. Opt. Soc. Am. B* 13.3, pp. 481–491. [↗](#)
- (1997). "Multiphoton Excitation of Molecular Fluorophores and Nonlinear Laser Microscopy". In: *Topics in Fluorescence Spectroscopy, Vol. 5: nonlinear and two-photon induced fluorescence*. Ed. by J. R. Lakowicz. Plenum Press, New York, pp. 471–540.

# Chapter13

## Two-Dimensional Spectroscopy

Markus Lippitz  
July 28, 2021

### Tasks

- Find all possible Feynman diagrams for a 3-level V-system, by hand or using a computer. Group them by their phase-matching condition. Assume some parameters and plot 2D spectra. The elearning course has some useful Matlab routines.
- Investigate the possibility of 2D spectroscopy to find coupling between systems with the example of a 'diamond' level system. A ground state  $|0\rangle$  is connected to a top-most excited state  $|3\rangle$  via two 'paths' passing state  $|1\rangle$  or  $|2\rangle$ . The energetic position of state  $|3\rangle$  is  $E_3 = E_1 + E_2 + \delta$  ( $E_0 = 0$ ). Discuss why  $\delta = 0$  corresponds to two uncoupled systems. Plot the rephased and non-rephased spectra and their sum for zero and non-zero values of  $\delta$ .

### Interaction Picture

A more complete introduction into 2D-spectroscopy and double-sided Feynman Diagrams can be found in Hamm, 2005 which is a short version of Hamm and Zanni, 2011 which is a short version of Mukamel, 1995.

In the Schrödinger picture, all the time-dependence sits in the wave function

$$\hat{H} = \text{const.} \quad (13.1)$$

$$\frac{d}{dt} |\psi(t)\rangle = -\frac{i}{\hbar} \hat{H} |\psi(t)\rangle \quad (13.2)$$

$$\langle \hat{A} \rangle = \langle \psi(t) | \hat{A} | \psi(t) \rangle \quad (13.3)$$

The solution to the differential equation for  $|\psi(t)\rangle$  is

$$|\psi(t)\rangle = \exp\left(-\frac{i}{\hbar} \hat{H} t\right) |\psi(0)\rangle \quad (13.4)$$



This work is licensed under a [Creative Commons "Attribution-ShareAlike 4.0 International"](https://creativecommons.org/licenses/by-sa/4.0/) license.

In the Heisenberg picture, all the time-dependence sits in the operator

$$|\psi_H\rangle = \text{const.} \quad (13.5)$$

$$\frac{d}{dt} \hat{A}_H(t) = -\frac{i}{\hbar} [\hat{H}, \hat{A}_H(t)] \quad (13.6)$$

$$\langle \hat{A}_H \rangle = \langle \psi | \hat{A}_H(t) | \psi \rangle \quad (13.7)$$

The solution to the differential equation for  $\hat{A}_H(t)$  is

$$\hat{A}_H(t) = \exp\left(+\frac{i}{\hbar} \hat{H} t\right) \hat{A}(0) \exp\left(-\frac{i}{\hbar} \hat{H} t\right) \quad (13.8)$$

At time  $t = 0$  both pictures come together, i.e.,  $\hat{A}_H(0) = \hat{A}$  and  $\psi_H = \psi(0)$  and of course both pictures give the same result for the expectation value of an operator.

In this chapter, we use the interaction picture, which is in a sense half-way between Schrödinger and Heisenberg: We assume a small perturbation  $\hat{H}'(t)$  addition to an unperturbed  $\hat{H}_0$

$$\hat{H}(t) = \hat{H}_0 + \hat{H}'(t) \quad (13.9)$$

The effect of  $\hat{H}_0$  is to modify the operators, while  $\hat{H}'(t)$  modifies the wave functions

$$\frac{d}{dt} |\psi(t)\rangle = -\frac{i}{\hbar} \hat{H}' |\psi(t)\rangle \quad (13.10)$$

$$\frac{d}{dt} \hat{A}(t) = -\frac{i}{\hbar} [\hat{H}_0, \hat{A}(t)] \quad (13.11)$$

$$\langle \hat{A} \rangle = \langle \psi(t) | \hat{A}(t) | \psi(t) \rangle \quad (13.12)$$

In the interaction picture, we now can integrate up the Schrödinger equation 13.10 and transform back into the Schrödinger picture. To keep things simple, I only show the results when transformed back. Intermediate steps are given in Hamm, 2005.

We assume that the system experiences a perturbation by the operator  $\hat{H}'$  at time  $\tau$ , but evolves unperturbed in the remaining parts of the time interval from  $t_0$  to  $t$ . We made the approximation that only one interaction takes place in that interval, which is only the first element of a power series. With that we get

$$|\psi(t)\rangle \approx |\psi(t_0)\rangle - \frac{i}{\hbar} \int_{t_0}^t d\tau U_0(t, \tau) \hat{H}'(\tau) U_0(\tau, t_0) |\psi(t_0)\rangle \quad (13.13)$$

with the operator for free (= unperturbed) time evolution  $U_0$  from time  $t_1$  to  $t_2$

$$U_0(t_2, t_1) = \exp\left(-\frac{i}{\hbar} \hat{H}_0 (t_2 - t_1)\right) \quad (13.14)$$

We are especially interested in the time evolution of the density matrix according to the Liouville-von Neumann equation. Starting from  $\tau = t_0$ , we take more and more interactions into account.  $\rho^{(n)}$  describes the change of the density matrix assuming  $n$  interactions between  $\tau = t_0$  and  $\tau = t$

$$\rho(t) = \rho_0 + \sum_n \rho^{(n)}(t) \quad (13.15)$$

where  $\rho_0$  is the equilibrium density matrix which does not evolve in time. The term for  $n = 1$  reads, equivalent to eq. 13.13 above,

$$\rho^{(1)}(t) = -\frac{i}{\hbar} \int_{t_0}^t d\tau U_0(t, \tau) [\hat{H}'_I(\tau), \rho_0] U_0^\star(t, \tau) \quad (13.16)$$

where  $\hat{H}'_I(\tau)$  is the perturbation operator in the interaction picture

$$\hat{H}'_I(\tau) = U_0^\star(\tau, t_0) \hat{H}'(\tau) U_0(\tau, t_0) \quad (13.17)$$

Multiple interactions now lead to cascaded commutators, i.e.

$$\rho^{(2)}(t) = \left(-\frac{i}{\hbar}\right)^2 \int_{t_0}^t d\tau_2 \int_{t_0}^{\tau_2} d\tau_1 U_0(t, \tau_2) [\hat{H}'_I(\tau_2), [\hat{H}'_I(\tau_1), \rho_0]] U_0^\star(t, \tau_2) \quad (13.18)$$

In spectroscopy, we are interested in a perturbation operator  $\hat{H}'$  that contains an  $\mu \cdot E$  term for the incoming, exciting field. We see that  $\rho^{(n)}$  depends on  $n$  optical fields, so that we identify these processes with the  $n$ -th order nonlinear processes described by the nonlinear susceptibility  $\chi^{(n)}$ . This nonlinear susceptibility creates a nonlinear polarization  $P^{(n)}$ . In quantum mechanics, this is the expectation value of the dipole operator

$$P^{(n)}(t) = \langle \mu \rho^{(n)}(t) \rangle \quad (13.19)$$

For third-order nonlinear effects, we thus get

$$\left(-\frac{i}{\hbar}\right)^3 \iiint E(\tau_3) E(\tau_2) E(\tau_1) \langle \mu [\mu_3, [\mu_2, [\mu_1, \rho_0]]] \rangle \quad (13.20)$$

The cascaded commutator expands to  $2^3 = 8$  terms, where one half is the complex-conjugate of the other, effectively giving 4 terms.

In the experiment, the electric fields for a third-order nonlinearity would be created by three different laser pulses. Generally, each electric field  $E(\tau_i)$  at time  $\tau_i$  could be a superposition of the three pulses. We make the approximation, that the pulses do not overlap in time (time ordering). We also assume that the pulses are shorter than the time scale of the system<sup>1</sup>, but much longer than the oscillation period of the light wave. Each electric field can thus be described by two terms of the form  $\exp(\pm i(\omega t - kr))$ . In total, this makes  $2^3 = 8$  terms for the field, multiplied by the 4 terms from the commutator gives 32 terms. In the remaining, we try to keep track of all these terms.

<sup>1</sup> and thus shorter than the delay between the pulses

## Double-Sided Feynman Diagrams

The idea is to describe the evolution of the density matrix when interacting with multiple optical fields. Time runs from bottom to top. The two vertical lines represent the ket (left) and bra (right) part of the density matrix element. The quantum numbers are written between the lines and we start from the ground state  $|0\rangle \langle 0|$ . Diagonal arrows represent the light fields interacting with the system. Inwards pointing arrows increase the quantum number, outwards pointing fields are the complex-conjugate with negative frequency that decrease the quantum number. The last, top-most arrow is drawn with a



Figure 13.1: Example of a Double-Sided Feynman Diagram.

dashed or wavy line and represents the dipole operator  $\mu$  outside the commutator in eq. 13.20. This is the radiating nonlinear polarization. By convention, it is on the left side and points to the top left. This convention fixes the mirror symmetry that all schemes would exist also in a complex-conjugate form. At the end, after the nonlinear polarization is emitted, all coherences have to have vanished and the system has to be in a population state, i.e., both quantum number have to be identical<sup>2</sup>.

We still have the choice of the sign in  $E \propto \exp(\pm i(\omega t - kr))$ . We write this as  $\exp(-i(\omega t - kr))$  and chose the sign of  $\omega$  and  $k$ . A positive sign is represented by an arrow pointing to the right, a negative sign pointing to the left. The positive frequency is thus absorption at the left vertical line, or emission at the right, and the vice versa. Phase matching, i.e.  $\Delta k = 0$  and the rotating wave approximation come together here. The number of left and right going arrows have to agree when including the special radiation polarization arrow.

Each diagram has an overall sign, stemming from the minus sign in the commutators in eq. 13.20. The sign is  $(-1)^m$  where  $m$  is the number of interactions on the right side of the diagram.

The diagram represents a path between elements of the density matrix. As we have seen in the chapter on Rabi Oscillations when introducing the density matrix, a light field causes as first step a non-zero value of the corresponding off-diagonal element. A field acting from the left generates  $|1\rangle\langle 0|$ , while a field acting from the right generates  $|0\rangle\langle 1|$ . Figure 13.2 shows possible paths in Liouville space.

At the end, we are interested in  $P^{(3)}(t)$  or  $P^{(3)}(\omega)$ . We can easily obtain it by multiplying the elements along the path. In time domain<sup>3</sup>, each interaction with an optical field contributes

$$-\frac{i}{\hbar} \mu_{ba} E_i(t) e^{-i\omega_i t} \quad (13.21)$$

where  $a$  ( $b$ ) is the quantum number before (after) the interaction. When the arrow points to the left, the field is taken complex-conjugate (and thus with negative frequency, see below). The time interval  $t_i$  between two interactions contributes

$$e^{-i\omega_{ab} t_i - \Gamma_{ab} t_i} \quad (13.22)$$

where we have assumed the state to be  $|a\rangle\langle b|$ , and  $\hbar\omega_{ab} = E_a - E_b$  so that  $\omega_{ab} = -\omega_{ba}$ . The last outgoing arrow of the radiating polarization only contributes a dipole moment, as this is the dipole moment multiplied to the left of the cascaded commutators.

In frequency domain<sup>4</sup>, we get for the interactions

$$-\frac{i}{\hbar} \mu_{ba} E_i(\omega_i) \quad (13.23)$$

The phase evolution during the time interval  $t_j$  needs a Fourier transform. The Fourier-conjugate variable<sup>5</sup> to  $t_j$  is  $\Omega_j$ , which is the sum of all laser frequencies up to interaction  $j$ , i.e.,

$$\Omega_j = \sum_{k=1}^j \pm \omega_k \quad (13.24)$$

<sup>2</sup> but not necessarily zero



Figure 13.2: Two different paths through the density matrix by applying four times the dipole operator. The red path corresponds to Fig. 13.1.

<sup>3</sup> Hamm, 2005; Hamm and Zanni, 2011; Mukamel, 1995.

<sup>4</sup> Boyd, 2008; Shen, 2003.

<sup>5</sup> Tokmakoff, 2009.



The sign is again taken from the direction of the arrow (positive to the right). We thus get by a Fourier transform<sup>6</sup> along  $t_j$

$$e^{(-i\omega_{ab}-\Gamma_{ab})t_j} \rightarrow \frac{i}{\Omega_j - \omega_{ab} + i\Gamma_{ab}} \quad (13.25)$$

<sup>6</sup> Note that  $P = 0$  for  $t_j < 0$

### Example: Pump-Probe Spectroscopy

Let us discuss pump-probe spectroscopy as an example. As we have seen on the chapter in four-wave mixing, pump-probe spectroscopy is a third-order nonlinear optical process of the form

$$P^{(3)} = \chi^{(3)} E_{\text{pump}} E_{\text{pump}}^* E_{\text{probe}} \quad (13.26)$$

We assume for simplicity that the probe pulse comes after the pump pulse. The nonlinear emission has to be in the direction of the probe pulse so that it can serve as local oscillator. As the emitting arrow points to the left, the probe arrow has to point to the right. The sub-schemes A and B fulfil this requirement.



Figure 13.3: Building blocks for the interaction of the probe pulse (panels A and B) and the pump-pulse (panels 1 to 4) in a pump-probe experiment.

The direction of the pump beam has to cancel out,  $E_{\text{pump}}$  enters only as absolute-squared. This means that the two pump arrows have to point in different directions. The sub-schemes 1 to 4 fulfill this requirement.

Of the eight combinations two are not allowed. The variants A3 and A4 would describe emission from ground state  $|0\rangle \langle 0|$  which is of course forbidden. Variants A2 and A2 describe stimulated emission, B1 and B2 excited state absorption and B3 and B4 ground state bleaching.

From the diagrams we can now read the nonlinear polarization, multiplying together the contribution of each interaction and the times  $t_i$  between them. For the diagram A1 and A2 we get

$$P_{A1}^{(3)} = \frac{i}{\hbar^3} E_1 E_2^* E_3 \mu_{10}^4 e^{(-i\omega_{10}-\Gamma_{10})t_1} e^{-\Gamma_{11}t_2} e^{(-i\omega_{10}-\Gamma_{10})t_3} \quad (13.27)$$

$$P_{A2}^{(3)} = \frac{i}{\hbar^3} E_1^* E_2 E_3 \mu_{10}^4 e^{(+i\omega_{10}-\Gamma_{10})t_1} e^{-\Gamma_{11}t_2} e^{(-i\omega_{10}-\Gamma_{10})t_3} \quad (13.28)$$

where only the direction of the phase rotation during time interval  $t_1$  between the first and second interaction changes (and the field that enters started). In pump-probe spectroscopy we assume that both  $E_1$  and  $E_2$  stem from the same laser pulse, the pump pulse, and that we can neglect  $t_1$  as the pulse is



Figure 13.4: Six double-sided Feynman diagrams describe pump-probe spectroscopy.

short. We thus get for stimulated emission (SE)

$$P_{SE}^{(3)} = 2 \frac{i}{\hbar^3} |E_{\text{pump}}|^2 E_{\text{probe}} \mu_{10}^4 e^{-\Gamma_{11}t_2} e^{(-i\omega_{10}-\Gamma_{10})t_3} \quad (13.29)$$

In a similar way we get for excited state absorption (ESA) and ground state bleaching (GSB)

$$P_{ESA}^{(3)} = -2 \frac{i}{\hbar^3} |E_{\text{pump}}|^2 E_{\text{probe}} \mu_{10}^2 \mu_{21}^2 e^{-\Gamma_{11}t_2} e^{(-i\omega_{21}-\Gamma_{21})t_3} \quad (13.30)$$

$$P_{GSB}^{(3)} = 2 \frac{i}{\hbar^3} |E_{\text{pump}}|^2 E_{\text{probe}} \mu_{10}^4 e^{(-i\omega_{10}-\Gamma_{10})t_3} \quad (13.31)$$

The minus sign in the ESA term stems from the global sign of the diagram, as the ESA diagrams have only one interaction from the right side. The GSB term does not contain a decay of the population during time interval  $t_2$ , as the ground state does not decay. When we neglect the decay of the population during  $t_2$ , the terms for GSB and SE are identical. The nonlinear polarization is the sum of these three terms.

As discussed in the chapter on the free induction decay, a polarization (or coherence) is source of a radiated field that interference with a local oscillator, if present. In pump-probe spectroscopy, the probe field acts as local oscillator. The pump-induced variation in the probe power is caused by the cross term of local oscillator and signal field

$$\Delta P = \frac{1}{2} \epsilon_0 \int_{\text{pulse}} 2E_{\text{probe}} \Im(E_{\text{signal}}) dt = NL \frac{k}{2} \int_{\text{pulse}} E_{\text{probe}} \Im(P^{(3)}) dt \quad (13.32)$$

For pump-probe spectroscopy we get for the differential spectrum, assuming a spectrally flat probe pulse with  $\omega_3 = \omega_{\text{probe}}$

$$\frac{\Delta P(\omega_3)}{P_{\text{probe}}(\omega_3)} \propto -\frac{4\mu_{10}^4 \Gamma_{10}}{(\omega_3 - \omega_{10})^2 + \Gamma_{10}^2} + \frac{2\mu_{10}^2 \mu_{21}^2 \Gamma_{21}}{(\omega_3 - \omega_{21})^2 + \Gamma_{21}^2} \quad (13.33)$$

### Example: Two-Photon Absorption

The formalism of double-sided Feynman diagrams allows us to obtain results from perturbation theory by just reading the diagram. For comparison, we turn back to the example of Winterhalder et al., 2011, discussed in the last chapter. We read the  $\nu g$ -coherence as

$$\rho_{\nu g}(t_1, t_2) = \frac{(-i)^2}{\hbar^2} \mu_{eg} \mu_{\nu e} E_1 E_2 e^{-i\omega_{eg}t_1 - \Gamma_{eg}t_1} e^{-i\omega_{\nu g}t_2 - \Gamma_{\nu g}t_2} \quad (13.34)$$

Fourier transformation leads to

$$\begin{aligned} \rho_{\nu g}(\omega_1, \omega_2) &= \frac{(-i)^2}{\hbar^2} \mu_{eg} \mu_{\nu e} E_1 E_2 \frac{i}{\Omega_1 - \omega_{eg} + i\Gamma_{eg}} \frac{i}{\Omega_2 - \omega_{\nu g} + i\Gamma_{\nu g}} \quad (13.35) \\ &= \frac{\mu_{eg} \mu_{\nu e} E_1 E_2}{\hbar^2} \frac{1}{\omega_1 - \omega_{eg} + i\Gamma_{eg}} \frac{1}{\omega_1 - \omega_2 - \omega_{\nu g} + i\Gamma_{\nu g}} \quad (13.36) \end{aligned}$$

which is eq. 1b in Winterhalder et al., 2011.

## 2D spectroscopy

In contrast to pump-probe spectroscopy, we now assume that all three interactions happen at three different times so that we do not neglect any time interval  $t_i$  anymore. However, all three pulses stem from the same laser, have the same spectrum, but individual propagation directions  $k_i$ . In 2D spectroscopy, in most cases one detects the generated nonlinear polarization by interfering it with a fourth laser pulse acting as local oscillator<sup>7</sup>. In some variants, one uses the fourth pulse to generate a population that is then detected via electron or fluorescence emission. Also in some cases, not the propagation direction  $k_i$  but an individual phase  $\phi_i$  is used to distinguish the pulses. In the following discussion, we stick with the most common or 'traditional' approach.

How can we do spectroscopy when all laser pulses have the same spectrum? The approach is the same as in Fourier transform (infrared) spectroscopy. Two laser pulses separated by a short time interval interfere with each other and lead to a sinusoidal modulation of the combined spectrum. Fourier transform from the delay time interval to frequency space then gives the frequency axis for spectroscopy. In 2D spectroscopy, we Fourier-transform along the first and third time interval. During these times, the system is in a coherent superposition between two states, described by the density matrix element  $|a\rangle\langle b|$  with  $a \neq b$ . The second, not Fourier-transformed time interval is called population time, as here the system is (typically) in a population state  $|a\rangle\langle a|$ . Note that the third time interval needs an end. It ends via the radiation of the nonlinear polarization. This is not controlled by a laser pulse on the system. However, when we use the fourth laser pulse as local oscillator, we can decide at which time we want to amplify and then detected the emitting polarization. Or we let physics do the Fourier transform and detected the emitted radiation without further interference by a spectrometer, which does not need time resolution.<sup>8</sup>

We obtain 2D spectra, along an excitation and a detection frequency, for a fixed population time interval  $t_2$ . One can imagine getting similar spectra

<sup>7</sup> Brańczyk, Turner, and Scholes, 2013; Fuller and Ogilvie, 2015.

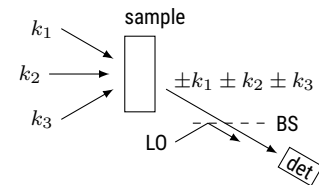


Figure 13.5: The phase-matching direction selects the observed process. Interference with a local oscillator (LO) after reflection at a beam splitter (BS) allows detection (det) of a complex-valued polarization.

<sup>8</sup> We detect  $|P|^2$  in this way, not the complex valued  $P$ .

by scanning both pump and probe wavelength in a pump-probe experiment. One big difference is that the pulses in such a pump-probe experiment would need to be rather long, as they need to be spectrally rather narrow. This limits the time resolution in  $t_2$ . With the four-pulse experiment, we get both high time resolution and spectral information.

Which features do we find in a 2D spectrum? Along the diagonal, it contains the linear absorption spectrum. We pump and probe the same molecules. If our ensemble of molecules is inhomogeneously broadened, i.e., the molecules differ in absorption wavelength much more than the width of their individual absorption spectrum, then the peak in the 2D spectrum will be elongated along the diagonal and narrow along the anti-diagonal. We pump one sub-ensemble of molecules, and only these will not be able to absorb the probe pulse. 2D spectroscopy thus can distinguish between homogeneous and inhomogeneous broadening, similar to spectral hole burning.

2D spectroscopy can also find coupled (or interacting) systems. With linear spectroscopy, we only find the energy difference between initial and final state. When we have two peaks in an absorption spectrum, we cannot say if there are three or four states involved. We could have two different molecules (4 states) or a V level system in one molecule (3 states). 2D spectroscopy can decide this question: In the coupled case, we find cross-peaks at the other two corners of the square which is formed by the two transition frequencies. At these points, we pump one transition and find an influence on the other transition. This is only possible if these transitions are somehow coupled. Molecule A would not care if molecule B would be excited.



Figure 13.6: An inhomogeneous ensemble of molecules leads to an elongated peak in the 2D spectrum. Along the anti-diagonal direction it has the *homogeneous* linewidth.



Figure 13.7: Cross-peaks outside the diagonal (blue circles) signal coupling between systems. This information is not present in the linear absorption spectrum.

## Rephasing

The set of all allowed double-sided Feynman diagrams for a given quantum-mechanical system can be grouped by their phase-matching condition, i.e., the signs on front of the  $\pm k_i$ . An important property of these groups of diagrams is whether rephasing occurs or not. The question is how the coherences during interval one and three are related. When the system is during interval one in state  $|a\rangle \langle b|$  and then during interval three in state  $|b\rangle \langle a|$ , this

is called rephasing. Both intervals cancel their phase contribution to  $P^{(3)}$ , as

$$e^{-i\omega_{ba} t_1} e^{-i\omega_{ab} t_3} = e^{-i\omega_{ba} (t_1 - t_3)} \quad (13.37)$$

This is important as the transition energy  $\hbar\omega_{ba}$  varies between different molecules in an ensemble and fluctuates for a single molecule during time. In rephasing diagrams the influence of this inhomogeneity is canceled out. This is very similar to the echo formation in pulsed NMR, as the sign of the phase factor represents the rotation direction. Rephasing diagrams let the phase rotate first in one direction, then in the opposite direction, so that all 'runners' arrive together again.<sup>9</sup> When adding rephasing and non-rephasing 2D spectra, one obtains a purely absorptive spectrum which has narrow peaks and no side-effects from Fourier transform.

<sup>9</sup> See the 'runner' example for NMR echos is this sounds strange to you.

## References

- Boyd, Robert W. (2008). *Nonlinear Optics*. 3. ed. Amsterdam [u.a.]: Elsevier, Acad. Press.
- Brańczyk, Agata M, Daniel B Turner, and Gregory D Scholes (2013). "Crossing disciplines – A view on two-dimensional optical spectroscopy". In: *Annalen der Physik* 526.1-2, pp. 31–49. [↗](#)
- Fuller, Franklin D and Jennifer P Ogilvie (2015). "Experimental Implementations of Two-Dimensional Fourier Transform Electronic Spectroscopy". In: *Annual Review of Physical Chemistry* 66.1, pp. 667–690. [↗](#)
- Hamm, Peter (2005). *Principles of Nonlinear Optical Spectroscopy: A Practical Approach or: Mukamel for Dummies*. [↗](#)
- Hamm, Peter and Martin T. Zanni (2011). *Concepts and methods of 2D infrared spectroscopy*. Cambridge University Press.
- Mukamel, Shaul (1995). *Principles of nonlinear optical spectroscopy*. Oxford University Press.
- Shen, Yuen R. (2003). *The principles of nonlinear optics*. Wiley.
- Tokmakoff, Andrei (2009). "10.2 Diagrammatic Perturbation Theory". In: 5.74 *Introductory Quantum Mechanics II*. MIT OpenCourseWare. [↗](#)
- Winterhalder, M J et al. (2011). "Toward Far-field Vibrational Spectroscopy of Single Molecules at Room Temperature". In: *The Journal of Physical Chemistry B* 115.18, pp. 5425–5430. [↗](#)



## **Part IV**

# **Plasmonics**





# Chapter14

## Plasmon hybridization

Markus Lippitz

October 29, 2021

### Tasks

- Investigate the field at the positions of the dipoles when two particles hybridize. Explain why we observe no absorption at the anti-symmetric resonance of two equal particles although the field is not zero.
- Reconstruct the absorption spectrum of the single particle alone and when hybridized with the antenna in Fig. 14.1 below. Use the hybridization model to explain the antenna effect that is used to amplify the transient transmission signal of a small gold particle in Schumacher, Kratzer, et al., 2011

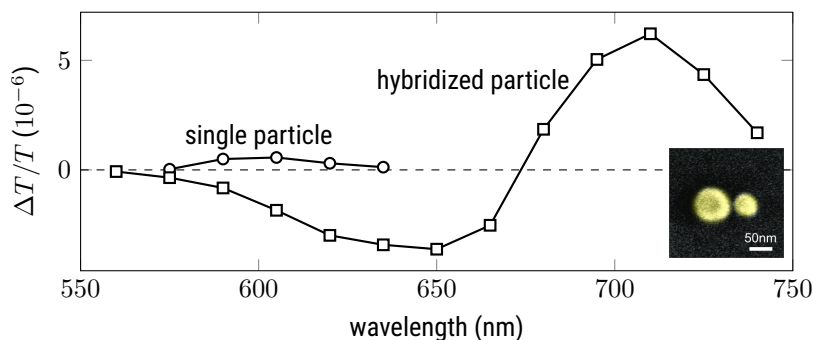


Figure 14.1: Enhancement of a transient absorption signal by plasmon hybridization Schumacher, Kratzer, et al., 2011. The inset shows a SEM micrograph of the gold nanodiscs.

### Overview

Plasmon hybridization<sup>1</sup> is another incarnation of a coupled oscillator, i.e., two pendula coupled by a spring. The coupled system has new eigen-functions and eigen-energies that can be derived from the old eigen-functions and the strength of the coupling. The term is borrowed from the hybridization of atom orbitals, for example in carbon atoms forming the famous  $sp^3$  orbitals.

The concept of plasmon hybridization helps to get a more intuitive understanding of the absorption spectra of arrangements of plasmonic nanoparticles. In this chapter, we discuss an experiment in which a larger plasmonic

<sup>1</sup> Prodan et al., 2003.



particle was used as antenna to enhance the optical response of a small particle. The antenna-effect can be understood in terms of hybridised particles. The optical response of the small particle is in this experiment dominated by acoustical breathing oscillations of the particle at frequencies of a few 10 GHz.

### Questions

1. Review the hybridization of atomic orbitals in carbon atoms, the coupled pendulum and molecular aggregates. How do these system couple? How does one obtain the response of the coupled system?

## Rayleigh scattering of small spheres

Let us start by going back to Rayleigh scattering of nanoparticles, as we discussed already in chapter 4. A sphere of radius  $R$  and dielectric constant  $\epsilon_{in}$  is embedded in a medium of dielectric constant  $\epsilon_{out}$ . We assume that the radius  $R$  is much smaller than the wavelength  $\lambda$  of the electromagnetic light field. This means that the phase is constant across the sphere and that we can employ the quasi-static approximation. One solves the Laplace equation taking boundary conditions and symmetry into account.<sup>2,3,4</sup> The sphere responds to the light field with a polarization of

$$\mathbf{p}(t) = \epsilon_0 \epsilon_{out} \alpha \mathbf{E}(t) \quad (14.1)$$

with the polarizability

$$\alpha = 4\pi R^3 \frac{\epsilon_{in} - \epsilon_{out}}{\epsilon_{in} + 2\epsilon_{out}} \quad (14.2)$$

We find a resonance when  $\epsilon_{in}(\omega) + 2\epsilon_{out}(\omega) = 0$ , which requires one dielectric function to be negative, as it is the case in metals. Small metal particles show thus exceptional strong interaction with light in a certain spectral range.

As the electric field oscillates  $E(t) = E_0 e^{-i\omega t}$ , also the polarization  $p$  oscillates and radiates a secondary, scattered electromagnetic field

$$\mathbf{E}_S = \frac{e^{i k r}}{4\pi\epsilon_0 \epsilon_{out}} \frac{1}{r^3} \left\{ (kr)^2 (\hat{\mathbf{r}} \times \mathbf{p}) \times \hat{\mathbf{r}} + (1 - ikr) (3\hat{\mathbf{r}} [\hat{\mathbf{r}} \cdot \mathbf{p}] - \mathbf{p}) \right\} \quad (14.3)$$

where  $k = 2\pi/\lambda$  is the length of the wave vector in the medium. The power that is absorbed by the dipole<sup>5</sup> is

$$P_{abs} = \frac{\omega}{c} \Im(\mathbf{p} \mathbf{E}^*) \quad (14.4)$$

so that we get the absorption cross section

$$\sigma_{abs} = k \Im(\alpha) = 4\pi k R^3 \Im\left(\frac{\epsilon_{in} - \epsilon_{out}}{\epsilon_{in} + 2\epsilon_{out}}\right) \quad (14.5)$$

We are in the Rayleigh limit of a very small particle so that we can neglect the scattered power. In this way, the absorption cross section  $\sigma_{abs}$  equals the extinction cross section  $\sigma_{ext}$

We assume that the surrounding medium is a transparent dielectric, i.e.,  $\epsilon_{out}$  is real-valued. The material of the nanosphere should be described by

<sup>2</sup> Jackson, 1999.

<sup>3</sup> Nolting, 2016, exercise 2.4.2.

<sup>4</sup> Bohren and Huffman, 2007, chapter 5.2.

<sup>5</sup> Novotny and Hecht, 2012, Chapter 8.

the Drude model of metals. This is often the case when one is far enough away from inter-band transitions that lead to the color of metals, i.e., when one is far enough in the infrared. The dielectric function then reads

$$\epsilon_{in}(\omega) = \epsilon_{\infty} - \frac{\omega_P^2}{\omega(\omega + i\gamma)} \quad , \quad (14.6)$$

where  $\epsilon_{\infty}$  is the high-frequency limit,  $\gamma = 1/\tau_{\text{coll}}$  the damping parameter of the plasma oscillation, and  $\omega_P$  the plasma frequency

$$\omega_P = \sqrt{\frac{n e^2}{m^* \epsilon_0}} \quad . \quad (14.7)$$

The plasma frequency depends on the effective electron mass  $m^*$  and number density  $n$ .

The polarizability  $\alpha$  has a resonance when its denominator equals zero, i.e., at  $\epsilon_{in}(\omega_{res}) = -2\epsilon_{out}$ . For a Drude metal with low damping this happens at

$$\omega_{res} = \frac{\omega_P}{\sqrt{2\epsilon_{out} + \epsilon_{\infty}}} \quad (14.8)$$

The resonance wavelength in the absorption spectrum thus depends on the plasma frequency of the metal and the dielectric function of the environment.

## Questions

- Review Rayleigh and Mie scattering (Chapter 4). At which particle size does the Rayleigh model stop to be valid?

## Plasmon hybridization

Now we hybridize two particle plasmons. We investigate the optical properties of two small Rayleigh particles which are brought close to each other. The optical response of each particle is described by a dipole  $\mathbf{p}_i(t)$ , where  $i = 1, 2$ . Each dipole experiences the incident field  $\mathbf{E}^{\text{inc}}(\mathbf{r}_i)$  and the field scattered from the other dipole. The sum of these two fields multiplied by the dipole's polarizability  $\alpha_i$  has to give in a self-consistent way the dipole moment (see, for example, Myroshnychenko et al., 2008)

$$\mathbf{p}_1 = \epsilon_0 \epsilon_{out} \alpha_1 [\mathbf{E}^{\text{inc}}(\mathbf{r}_1) + \mathbf{E}_2^{\text{scat}}(\mathbf{r}_1)] \quad , \quad (14.9)$$

and vice versa.<sup>6</sup> The scattered electrical near field  $\mathbf{E}^{\text{scat}}$  of the dipole  $i$  at position of the dipole  $j$  is given by eq. 14.3 above. As we aim for a large influence of this scattered field, we will need short distances between the dipoles and thus can focus on the near-field contribution of the scattered field

$$\mathbf{E}_i^{\text{scat, nf}}(\mathbf{r}_j) = \frac{1}{4\pi\epsilon_0 \epsilon_{out}} \frac{1}{d^3} (3\hat{\mathbf{r}}_{ij} [\hat{\mathbf{r}}_{ij} \cdot \mathbf{p}_i] - \mathbf{p}_i) \quad , \quad (14.10)$$

where  $\hat{\mathbf{r}}_{ij} = \mathbf{r}_j - \mathbf{r}_i$  is a vector of length one pointing from the dipole to the point where the field is evaluated, and  $d$  is the distance between the particles

For simplicity, we assume that both particles have the same dielectric function and are of course embedded in the same medium. We can chose the polarization direction of the incoming electric field  $\mathbf{E}^{\text{inc}}$ . Things become



Figure 14.2: Sketch of the light field shining on two small particles

<sup>6</sup> Note that this is a system of two equations.

simple when we chose it to be either parallel or perpendicular to the connecting axis of the particles. In both cases, the scattered near-field at particle  $j$  has the direction of the dipole  $i$ , which is not the case for other polarization directions. This allows us to use scalar dipole amplitudes  $p_i$  and a simplified scattered field amplitude

$$E_i^{\text{scat, nf}}(\mathbf{r}_j) = \frac{1}{4\pi\epsilon_0 \epsilon_{out}} \frac{v}{d^3} p_i \quad , \quad (14.11)$$

where the factor  $v$  is  $-1$  for perpendicular and  $+2$  for parallel polarization.

We solve the equation system for  $p_{1,2}$ , which we write as effective polarizabilities  $\alpha_{1,2}^{\text{eff}}$

$$\alpha_1^{\text{eff}} = \frac{p_1}{\epsilon_0 \epsilon_{out} E^{\text{inc}}} = \frac{\alpha_1 - v \frac{\alpha_1 \alpha_2}{4\pi d^3}}{1 - v^2 \frac{\alpha_1 \alpha_2}{16\pi^2 d^6}} \quad (14.12)$$

and vice versa. The total polarizability<sup>7</sup> is then the sum of  $\alpha_1^{\text{eff}}$  and  $\alpha_2^{\text{eff}}$

$$\alpha^{\text{eff}} = \frac{\alpha_1 + \alpha_2 - v \frac{\alpha_1 \alpha_2}{2\pi d^3}}{1 - v^2 \frac{\alpha_1 \alpha_2}{16\pi^2 d^6}} \quad . \quad (14.13)$$

We are interested in resonance frequencies of  $\alpha^{\text{eff}}$ . As both particles are of the same material, the individual polarizability  $\alpha_i$  only differ in amplitude due to the factor  $R_i^3$ . The spectral shape is the same. The effective polarizability comes to resonance when the denominator vanishes, i.e.

$$R_1^3 R_2^3 \left( \frac{\epsilon_{in} - \epsilon_{out}}{\epsilon_{in} + 2\epsilon_{out}} \right)^2 v^2 = d^6 \quad (14.14)$$

or,

$$\frac{\epsilon_{in} - \epsilon_{out}}{\epsilon_{in} + 2\epsilon_{out}} v = \pm \left( \frac{d}{\sqrt{R_1 R_2}} \right)^3 \quad (14.15)$$

In total, we obtain the resonance frequency  $\omega_{\text{res}}$  of the coupled two-particle system<sup>8</sup>

$$\omega_{\text{res}} = \frac{\omega_P}{\sqrt{2\epsilon_{out} + \epsilon_{\infty}}} \sqrt{\frac{1+g}{1+\eta g}} \quad (14.16)$$

with

$$\eta = \frac{\epsilon_{\infty} - \epsilon_{out}}{\epsilon_{\infty} + 2\epsilon_{out}} \quad \text{and} \quad g = m \left( \frac{\sqrt{R_1 R_2}}{d} \right)^3 \quad . \quad (14.17)$$

In the case of gold particles in vacuum, the factor  $\eta$  takes a value of about  $8/11 \approx 0.73$ . For the electric field being parallel to the pair axis, the index  $m$  assumes the value  $-2$  for parallel dipoles (head to tail) and  $2$  for anti-parallel dipoles (head-to-head). When the electric field is perpendicular to the pair-axis,  $m$  is  $+1$  for the parallel configuration and  $-1$  for the anti-parallel configuration. This is the classical electrodynamics analogon of H and J aggregates in coupled dye molecules, discussed in chapter 5.

Finally, lets have a look at the amplitudes of the resonance. We evaluate the numerator of eq. 14.13 at the resonance condition (eq. 14.14).<sup>9</sup> It becomes

$$\alpha^{\text{eff, peak}} \propto \alpha_1 + \alpha_2 \pm 2\sqrt{\alpha_1 \alpha_2} = (\sqrt{\alpha_1} \pm \sqrt{\alpha_2})^2 \quad (14.18)$$

As in the case of molecular aggregates, the combined oscillator strength of both particles is re-distributed over the two new peaks in the absorption spectrum. For two equal particles ( $R_1 = R_2$ ), the symmetric mode carries twice the oscillator strength of a single particle and the antisymmetric mode is dark.

<sup>7</sup> see Aizpurua and Hillenbrand, 2012, Eq. 5.14

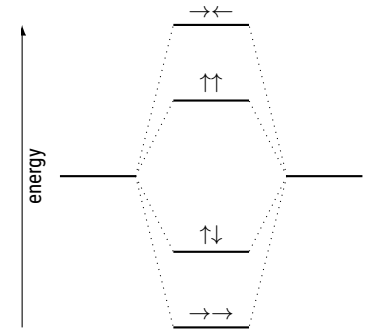


Figure 14.3: Level scheme

<sup>8</sup> Myroshnychenko et al., 2008.

<sup>9</sup> Without damping, the peaks would diverge, but in real material we have a non-zero  $\gamma$  in the Drude model.

## Questions

3. In which aspects is this calculation different from the approach that was chosen when describing molecular aggregates (chapter 5) ?
4. Use the Pluto script [hybridization](#)<sup>10</sup> to investigate the mode splitting in small Rayleigh particles. Compare the absorption spectrum with the analytic equations for resonance position and amplitude. Discuss differences.

<sup>10</sup> [download](#) [run on binder](#)

## Real metals

In the last section, we assumed a Drude metal for both particles. This allowed us to give analytical expressions for peak positions and width. But of course plasmon hybridization also exists for real metals. In stead of the Drude formula (eq. 14.6) we use measured dielectric functions  $\epsilon_{in}$ , for example from Johnson and Christy<sup>11</sup>. We assume an incoming polarization direction  $\mathbf{E}^{\text{inc}}$  and wavelength  $\lambda$ . Then we solve the equation system given by eq 14.9 (and the same with swapped indices) to obtain the dipole amplitudes and directions  $\mathbf{p}_i$ . With this we can calculate the absorption cross section. To get the full absorption spectrum we iterate over the wavelength  $\lambda$ .

<sup>11</sup> Johnson and Christy, 1972.

The effect of a real metal is additional damping due to interband absorption. For gold this happens at wavelengths below about 520 nm, leading to the color of gold. With  $\omega_P = 9\text{eV}$ ,  $\epsilon_\infty = 9$  and vacuum as medium ( $\epsilon_{out} = 1$ ), the plasmon resonance would appear in the Drude model at  $\omega_{res} \approx 2.7\text{ eV}$  or  $\lambda = 460\text{ nm}$ . The interband absorption shifts the resonance position to about 530 nm wavelength, just at the rim of the absorption band. Plasmon hybridization splits the peak. The lower wavelength / higher frequency peak overlaps more with interband absorption and will be damped out. Splitting of peaks is thus difficult to observe for small gold nanoparticles.

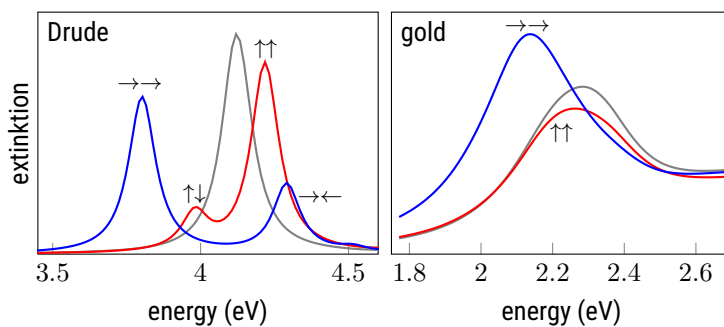


Figure 14.4: Comparison of plasmon hybridization in a Drude metal and n gold. The d-band absorption shifts the resonance and suppresses half of the modes. The simulations assume two spheres of 50 and 90 nm diameter with a gap of 10 nm. They go beyond the Rayleigh approximation and use Doicu, Wriedt, and Eremin, 2006.

## Questions

5. Use the Pluto script [jc\\_gold](#)<sup>12</sup> to investigate difference between the Drude model and the measured dielectric function of gold.
6. Plot the hybridized absorption spectrum in the Rayleigh approximation using the measured dielectric function of gold and silver.

<sup>12</sup> [download](#) [run on binder](#)

## Beyond the Rayleigh approximation

We used the Rayleigh approximation, i.e. assumed that each particle is much smaller than the wavelength of light. Such small particles have only very small polarizabilities  $\alpha$ , as these scale as the volume of the particle. To obtain sizeable effects, one thus uses particles that are a bit larger, i.e. smaller but not much smaller than the wavelength.

We discussed the Mie formalism (chapter 4) as method to model the optical response of spheres of arbitrary size. It should be in principle possible to model two neighbouring spheres using Mie scattering for each sphere, but this get a bit tedious as the scattered field is not homogeneous over the receiving sphere. More general numerical method such as the finite element method (FEM) or discrete dipole approximation (DDA) are better suited.

The effect of plasmon hybridization exists also for larger and also for non-spherical particles. Especially when the distance between the particles is not large anymore to their size, simple models relying on a few dipoles break down. As beyond the Rayleigh approximation, the resonance wavelength of a single particle depends on size and shape, one has to consider spectral differences between two particles which should hybridize. Hybridization requires that both particles scatter conceivable amount of light at the same wavelength, so the resonance of both particles needs to partially overlap. This again is similar to all coupled-pendula models that require the uncoupled eigen-energies to be similar.

## Ultrafast optical response of metals

To understand the experiment of Schumacher, Kratzer, et al., 2011, we need to make an excursion to the variation of the optical properties of metals and metal nanoparticles shortly after a laser pulse was absorbed. This could be a chapter on its own. More details can be found for example in Block et al., 2019 and Crut et al., 2017.

For simplicity, we again assume a Drude metal. The free electrons follow a Fermi-Dirac distribution. Most states are either filled or empty. Only in a energy range of (a few)  $k_B T$  around the Fermi energy the states are partially filled. A near infrared laser pulse of about 100 fs length is absorbed and some electrons are transferred to higher energy states. For a short time, the distribution is not a Fermi-Dirac distribution anymore. It has additional peaks and holes and thus can not be described by a temperature. But after a few 10 fs the electrons scatter and reach again a Fermi-Dirac distribution, now with a higher temperature  $T$ . We have to distinguish here the temperature  $T_e$  of the electrons and that of the lattice  $T_l$ , as it takes about 1 ps until the energy of the absorbed photons is transferred from the electrons to the lattice. On this time scale, the electrons cool and the lattice heats up, until both are in equilibrium with each other again. On a much larger timescale of about 100 ps the lattice cools down again by heat conduction to the environment.

We can observe all steps in this process. The hot electron gas has a Fermi-Dirac distribution that is smeared out much more than in the cold state. In this way, many more states are neither completely filled nor completely empty, and thus accessible to electron-electron scattering. This in-

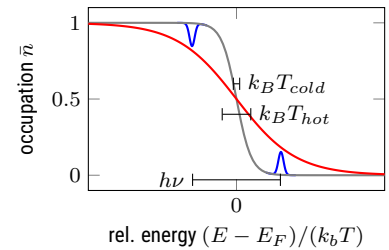


Figure 14.5: The electrons deviate from a Fermi-Dirac distribution for a very short time after absorption of a laser pulse. At all other times, a temperature of the electron gas  $T_e$  describes everything.

creases the damping parameter  $\gamma$  in the Drude model. The impulsive heating of the lattice within about 1 ps leads to thermal expansion of the lattice and acoustical oscillations of the particle. Both influence the electron density, as the number of electrons remains constant but the volume increases. This influences the plasma frequency  $\omega_P$  in the Drude model.



Figure 14.6: The influence of a pump pulse on the absorption spectrum of a plasmonic particle: via reduction of  $n$  (left) or increase of  $\gamma$  (right). In transient absorption spectroscopy, one detects the difference of the read and the green curve. The simulations assume a gold sphere. The influence of the pump is exaggerated.

A metal particle has acoustic eigenmodes, like a bell. In a first approximation, one can calculate from the velocity of sound of  $c_{\text{sound}} = 3240$  m/s an eigen-frequency of  $\nu_{\text{bell}} = c_{\text{sound}}/(4R)$ . One can just use the macroscopic continuum-mechanics models of vibrating spheres. The periodic variation in particle size leads to a periodic variation in electron density  $n$  and thus in the plasma frequency  $\omega_P$ . In a first approximation we can assume that the plasma frequency  $\omega_P$  is shifted by the particle expansion to  $\omega'_P = \omega_P(1 + \delta)$  with  $\delta \ll 1$ .

In a pump-probe or transient absorption experiment, a pump pulse modifies the dielectric properties of the particle. A probe pulse interrogates these properties after some time delay  $\tau$ . As the influence of the pump pulse is typically small, one plots the pump-induced change in probed transmission. An examples of such traces is given in Fig 14.7. The hot electron gas leads to a broader plasmon resonance due to increased damping. The expanded lattice and the periodic oscillation of the particle size lead to a shift in the plasmon resonance. Depending on probe wavelength, the signs of the individual contributions thus change.

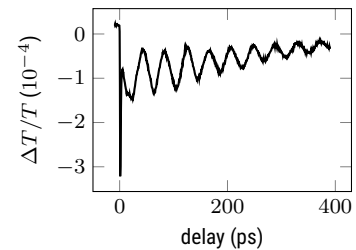


Figure 14.7: Transient transmission of a gold nanodisc probed near the plasmon resonance. Around a pump-probe delay of zero, the hot electron gas produces a spike. At longer delay, the acoustic oscillations dominate the signal.

## Questions

- Try to reproduce Fig. 14.6 in the Rayleigh approximation by applying (not too small) changes to the Drude damping  $\gamma$  (right) and the Drude plasma frequency (left).

## Pump-probe spectroscopy of hybridized particles

Now we combine transient absorption pump-probe spectroscopy and plasmon hybridization, as in Schumacher, Kratzer, et al., 2011. The pump-pulse launches acoustic oscillations which modulate the electron density  $n$  in the particle. This should then be amplified by plasmon hybridization.

First we need to take care of one subtle point: the pump pulse acts on both particles. The distribution of the roles 'antenna' and 'particle under investigation' is not fixed. But when using particles of different size, the

acoustic frequencies differ. In the transient absorption trace one thus observes a superposition of two different oscillations. Fourier-filtering allows to separate these and to determine the observed amplitude stemming from a single particle identified by its size. Fig 14.1 thus shows the Fourier-amplitude of the smaller particle.

When we vary the plasma frequency of only one particle on an hybridized pair by the factor  $\delta \ll 1$  we get for the new resonance positions

$$\omega_{\text{res}}' = \frac{\omega_P(1 + \delta/2)}{\sqrt{2\epsilon_{\text{out}} + \epsilon_{\infty}}} \sqrt{\frac{1+g}{1+\eta g}} \quad (14.19)$$

Plasmon hybridization does not increase the amount by which the resonance is shifted upon changing the plasma frequency of one sphere only. The shift is reduced by a factor of 2. This can be understood as we modify only part of the system, in most cases even less than half of the system's total volume.

However, the shift of the resonance position is only part of the answer to signal enhancement, as we detect changes in transmission. The signal is proportional to the product of resonance shift and peak height of the extinction resonance. A stronger extinction peak can overcompensate the reduced shift.

Already this twice as strong peak would compensate for the reduction in peak shift calculated above. However, the antenna would not enhance the signal. As soon as the second sphere becomes larger ( $R_2 > R_1$ ), the symmetric mode continuously increases in amplitude and the antenna starts to enhance the signal. In the dipole approximation we find no upper bound for the antenna enhancement. More detailed calculations show that the shift of the plasmon resonance with particle size, as seen in Mie theory, limits the available enhancement<sup>13</sup>.

<sup>13</sup> Schumacher, Brandstetter, et al., 2016.

## References

- Aizpurua, Javier and Rainer Hillenbrand (2012). "Localized Surface Plasmons: Basics and Applications in Field-Enhanced Spectroscopy". In: *Plasmonics*. Ed. by Stefan Enoch and Nicolas Bonod. Vol. 167. Springer series in optical sciences. [↗](#)
- Block, A et al. (2019). "Tracking ultrafast hot-electron diffusion in space and time by ultrafast thermomodulation microscopy". In: *Science Advances* 5.5, eaav8965. [↗](#)
- Bohren, Craig F. and Donald R. Huffman (2007). *Absorption and Scattering of Light by Small Particles*. John Wiley & Sons, Ltd. [↗](#)
- Crut, Aurélien et al. (2017). "Linear and ultrafast nonlinear plasmonics of single nano-objects". In: *Journal of Physics: Condensed Matter* 29.12, pp. 123002–123023. [↗](#)
- Doicu, Adrian, Thomas Wriedt, and Yuri Eremin (2006). *Light Scattering by Systems of Particles-Null-Field Method with Discrete Sources-Theory and Programs*. Vol. 124. Springer series in optical sciences. Springer. [↗](#)
- Jackson, John David (1999). *Classical electrodynamics*. 3. ed. New York [u.a.]: Wiley.
- Johnson, Peter B and R.W. Christy (1972). "Optical constants of the noble metals". In: *Physical review B* 6.12, p. 4370. [↗](#)



- Myroshnychenko, V et al. (2008). "Modelling the Optical Response of Gold Nanoparticles". In: *Chem. Soc. Rev.* 39.49. [↗](#).
- Nolting, Wolfgang (2016). *Theoretical Physics 3 Electrodynamics*. Springer. [↗](#).
- Novotny, Lukas and Bert Hecht (2012). *Principles of nano-optics*. 2. ed. Cambridge Univ. Press. [↗](#).
- Prodan, E et al. (2003). "A hybridization model for the plasmon response of complex nanostructures". In: *Science* 302.5644, p. 419. [↗](#).
- Schumacher, Thorsten, Matthias Brandstetter, et al. (2016). "The optimal antenna for nonlinear spectroscopy of weakly and strongly scattering nanoobjects". In: *Applied Physics B* 122, p. 91. [↗](#).
- Schumacher, Thorsten, Kai Kratzer, et al. (2011). "Nanoantenna-enhanced ultrafast nonlinear spectroscopy of a single gold nanoparticle". In: *Nature Communications* 2.1, p. 333. [↗](#).



# Chapter15

## Surface plasmons as example of optics of layered media

Markus Lippitz

November 11, 2021

### Tasks

- Model the angle-dependent reflectivity of a silver surface in the geometry used by Otto, 1968, i.e. reproduce Fig. 5 or 7.
- Calculate the dispersion relation of the surface plasmon modes of a thin metal film, as measured by Pettit, Silcox, and Vincent, 1975, i.e., reproduce Fig. 5.

The Pluto notebook [tmatrix\\_template](#)<sup>1</sup> can serve as starting point.

 [download](#) [run on binder](#)

### Plasmons

A plasmon is the quasi-particle of the plasma oscillation, i.e., the collective oscillation of the free electrons in a bulk material. In solid state physics, one calculates the restoring force when extending all electrons by  $\Delta x$  from their equilibrium position. One finds the characteristic bulk plasma frequency for Drude metal of

$$\omega_P = \sqrt{\frac{n e^2}{m \epsilon_0}} \quad (15.1)$$

with the electron density  $n$  and the effective mass  $m$  of the electrons in the material.

Such a collective oscillation of the electrons can also happen at a metal-dielectric interface. The eigen-frequency of the surface plasmon then depends on the dielectric properties of the second half space, as we will see below

$$\omega_{SP} = \frac{\omega_p}{\sqrt{1 + \epsilon_{\text{medium}}}} \quad (15.2)$$

The oscillation of the electrons is connected with an electromagnetic wave. If the interaction is strong in the quantum-optical sense, i.e., leading to an anti-crossing in the dispersion relation, one calls the new hybrid quasi-particle surface plasmon polariton (SPP). In the following, we will omit the term 'polariton' for simplicity, although the interaction is always 'strong'.



This work is licensed under a [Creative Commons "Attribution-ShareAlike 4.0 International"](#) license.

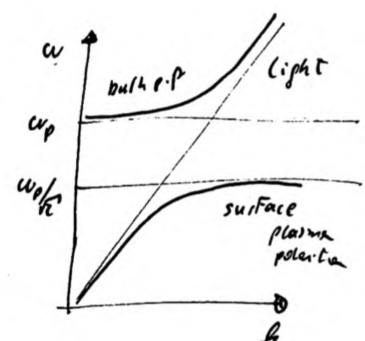


Figure 15.1: Sketch of the plasmon and surface plasmon and both polariton dispersion.

## Optics of layered media

We do a detour here, by introducing the T-matrix method, which is much more versatile than needed to investigate surface plasmons at a simple metal-dielectric interface. The method present here allows to investigate the optical properties of layered media, i.e., stacks of unstructured films of material with different dielectric functions. These could be dielectric materials, leading to, e.g., Bragg reflections and dielectric filters, or metal films, leading to surface plasmons. We discuss transmission and reflection of these stacks, which we then apply to surface plasmons.

In another chapter, we model – based on this T-matrix method – the absorption and emission of quantum emitters as dipoles that are situated in a plane within the layered medium. This leads to the emission pattern of a molecule near a metal or dielectric interface and the coupling of emitters to propagating surface plasmons.

This text assumes a time-dependence of the form  $e^{-i\omega t}$ , as usual in physics and used in Novotny and Hecht, 2012 or Born and E. Wolf, 2002. Note, however, that this is complex-conjugate to the convention in engineering, as used in Saleh and Teich, 1991 and Yeh, 2005.

## Transmission and scattering matrix

In a layered medium, a wave travelling through the stack of layers is partially reflected and partially transmitted at every interface. The multiple reflections interfere with each other. To keep track of this, we use in each layer one combined wave travelling in  $+z$  direction, and one travelling in  $-z$  direction. At interfaces, these waves mix. This formalism is described in chapter 7 of Saleh and Teich, 1991 and Yeh, 2005. A similar formalism with a  $E$  and  $B$  field travelling in the same direction is described in Pedrotti et al., 2008 and Macleod, 2001.

Let us assume that we have left of the interface a wave travelling to the right ( $+z$  direction) of amplitude  $U_1^+$ , and one wave travelling to the left of amplitude  $U_1^-$ . On the right side of the interface, we get the amplitudes  $U_2^\pm$  by multiplication with a *transmission* or *transfer* matrix  $\mathbf{M}$

$$\begin{pmatrix} U_2^+ \\ U_2^- \end{pmatrix} = \begin{pmatrix} A & B \\ C & D \end{pmatrix} \cdot \begin{pmatrix} U_1^+ \\ U_1^- \end{pmatrix} = \mathbf{M} \begin{pmatrix} U_1^+ \\ U_1^- \end{pmatrix} \quad (15.3)$$

Below we will derive transmission matrices  $\mathbf{M}_i$  for every interface and the homogeneous space in between. The full stack can then be described by a product matrix, multiplying together all partial matrices  $\mathbf{M}_i$  along the stack

$$\mathbf{M}_{\text{total}} = \mathbf{M}_n \cdot \mathbf{M}_{n-1} \cdots \mathbf{M}_2 \cdot \mathbf{M}_1 \quad (15.4)$$

This is a very convenient feature of the transmission matrix. Note that we label the interactions from left to right with 1 to  $n$ , but the matrices are multiplied from right to left, as mathematics has it origin in Arabic culture.

An inconvenient feature of the transmission matrix is that its matrix element have no direct physical meaning. The problem is that we multiply on the matrix a vector that is half an input, half an output of this interface. We



Figure 15.2: The operation of the transmission matrix

know what comes out (travels to the left), and the matrix should tell us what comes in from the other side. In this sense, the related *scattering matrix*  $\mathbf{S}$  is closer to physical meaning:

$$\begin{pmatrix} U_2^+ \\ U_1^- \end{pmatrix} = \begin{pmatrix} t_{12} & r_{21} \\ r_{12} & t_{21} \end{pmatrix} \cdot \begin{pmatrix} U_1^+ \\ U_2^- \end{pmatrix} = \mathbf{S} \begin{pmatrix} U_1^+ \\ U_2^- \end{pmatrix} . \quad (15.5)$$

The scattering matrix connects waves travelling towards the interface with those travelling away from the interface. The entries  $t_{ij}$  and  $r_{ij}$  are the transmission and reflection coefficients for the amplitudes of the waves travelling from  $i$  to  $j$  (i.e. 12 is travelling towards the right,  $+z$  direction). However, for the scattering matrix  $\mathbf{S}$ , the full stack can not be calculated by multiplying together all partial matrices.

It is therefore convenient to switch between both representations, derive the scattering matrix  $\mathbf{S}$  for each situation, and then convert into a transmission matrix  $\mathbf{M}$ . The relations are<sup>2</sup>

$$\mathbf{M} = \begin{pmatrix} A & B \\ C & D \end{pmatrix} = \frac{1}{t_{21}} \begin{pmatrix} t_{12}t_{21} - r_{12}r_{21} & r_{21} \\ -r_{12} & 1 \end{pmatrix} \quad (15.6)$$

$$\mathbf{S} = \begin{pmatrix} t_{12} & r_{21} \\ r_{12} & t_{21} \end{pmatrix} = \frac{1}{D} \begin{pmatrix} AD - BC & B \\ -C & 1 \end{pmatrix} \quad (15.7)$$

as long as  $D$  or  $t_{21}$  are not zero.

The transmission in backward direction  $t_{21}$  is thus the reciprocal of the  $D$ -element of  $\mathbf{M}_{\text{total}}$ . The transmission in forward direction is

$$t_{12} = \frac{\det \mathbf{M}_{\text{total}}}{D} \quad (15.8)$$

and similar for the reflection from the front side

$$r_{12} = -\frac{C}{D} . \quad (15.9)$$

## Electrical fields

We need to define the physical meaning of the amplitudes  $U_i^\pm$  to be able to calculate the reflection ( $r_{ij}$ ) and transmission ( $t_{ij}$ ) coefficients. We assume plane waves

$$\mathbf{E} e^{i(\mathbf{k} \cdot \mathbf{r} - \omega t)} = \hat{\mathbf{E}} U e^{i k_z z} e^{i k_x x} e^{-i \omega t} \quad (15.10)$$

where the wave vector  $\mathbf{k}$  lies in the  $xz$ -plane,  $U$  defines the amplitude of the wave and  $\hat{\mathbf{E}}$  the polarization direction. With the full length of the wave vector in vacuum  $k_0 = 2\pi/\lambda$  and the refractive index  $n$  of the medium we get

$$k_z^2 + k_x^2 = n^2 k_0^2 . \quad (15.11)$$

The polarization directions are

$$\hat{\mathbf{E}}^{(s)} = \begin{pmatrix} 0 \\ 1 \\ 0 \end{pmatrix} \quad \text{and} \quad \hat{\mathbf{E}}^{(p)} = \frac{1}{n k_0} \begin{pmatrix} \pm k_z \\ 0 \\ k_x \end{pmatrix} . \quad (15.12)$$

The  $\pm$ -sign takes the sign of the direction of travel, see Fig. 2.2 in Novotny and Hecht, 2012. Note that with this definition we have  $|\hat{\mathbf{E}}| = 1$ , which differs from problem 12.4 in Novotny and Hecht, 2012.



Figure 15.3: The operation of the scattering matrix

<sup>2</sup> Saleh and Teich, 1991 eq. 7.7

The left and right travelling waves are thus

$$\mathbf{E}^+ = \hat{\mathbf{E}} U^+ e^{+i k_z z} \quad \text{and} \quad \mathbf{E}^- = \hat{\mathbf{E}} U^- e^{-i k_z z} \quad (15.13)$$

where we have split off the global term  $e^{i(k_x x - \omega t)}$ .

## Propagation matrix

Before we come to interfaces, let us discuss the transmission matrix of a homogeneous material layer  $j$  of thickness  $d_j$  and (complex) refractive index  $n_j$ . Relevant is the  $z$ -component of the (complex) wave vector  $k_{z,j}$ . Note that we do *not* use the sign of  $k_{z,j}$  to describe the direction of travel. Independent of the propagation direction, each wave sees a reflection coefficient  $r = 0$  and a (complex) transmission coefficient  $t$

$$t = t_{12} = t_{21} = e^{+i k_{z,j} d_j} . \quad (15.14)$$

The transmission matrix of a homogeneous medium is thus

$$\mathbf{M} = \begin{pmatrix} e^{+i k_{z,j} d_j} & 0 \\ 0 & e^{-i k_{z,j} d_j} \end{pmatrix} . \quad (15.15)$$

## Interface matrix

The transmission and reflection coefficients of an interface are the Fresnel coefficients. We follow here Novotny and Hecht, 2012, who follow Born and E. Wolf, 2002, especially in the direction of the field vectors, see Fig. 2.2 in Novotny and Hecht, 2012. In this definition,  $r^s$  and  $r^p$  differ at normal incidence by a factor of  $-1$ . We assume non-magnetic materials ( $\mu = 1$ ) and get for a wave travelling from medium 1 towards medium 2

$$r_{12}^s = \frac{k_{z,1} - k_{z,2}}{k_{z,1} + k_{z,2}} = -r_{21}^s \quad (15.16)$$

$$t_{12}^s = \frac{2 k_{z,1}}{k_{z,1} + k_{z,2}} = \frac{k_{z,1}}{k_{z,2}} t_{21}^s \quad (15.17)$$

$$r_{12}^p = \frac{\epsilon_2 k_{z,1} - \epsilon_1 k_{z,2}}{\epsilon_2 k_{z,1} + \epsilon_1 k_{z,2}} = -r_{21}^p \quad (15.18)$$

$$t_{12}^p = \frac{2 \sqrt{\epsilon_1 \epsilon_2} k_{z,1}}{\epsilon_2 k_{z,1} + \epsilon_1 k_{z,2}} = \frac{k_{z,1}}{k_{z,2}} t_{21}^p . \quad (15.19)$$

We could also write these coefficients in terms of angle of incidence  $\theta$  with

$$\theta = \arcsin \frac{k_x}{n k_0} = \arcsin \sqrt{1 - \left( \frac{k_z}{n k_0} \right)^2} . \quad (15.20)$$

This would also hold in the case of evanescent waves ( $k_x > n k_0$ ) when we allow complex angles  $\theta$ . We nowhere need that  $\theta$  is a geometrical angle. We only need that  $n \sin \theta$  is the same for all layers.

With eq. 15.6 we get for both polarization directions the transmission matrix

$$\mathbf{M}_{12} = \frac{1}{t_{21}} \begin{pmatrix} 1 & r_{21} \\ r_{21} & 1 \end{pmatrix} , \quad (15.21)$$

as

$$t_{12}t_{21} - r_{12}r_{21} = t_{21}^2 \frac{k_{z,1}}{k_{z,2}} + r_{21}^2 = 1 \quad . \quad (15.22)$$

Note that the transmission matrix from medium 1 to medium 2 uses the Fresnel coefficients of the backwards direction! We can abbreviate this to<sup>3</sup> (see also appendix at the end of this chapter)

<sup>3</sup> In problem 12.4 in Novotny and Hecht, 2012 the leading  $1/\eta$  seems to be missing!

$$\mathbf{M}_{12} = \frac{1}{2\eta} \begin{pmatrix} 1 + \kappa & 1 - \kappa \\ 1 - \kappa & 1 + \kappa \end{pmatrix} \quad (15.23)$$

with

$$\kappa = \eta^2 \frac{k_{z,1}}{k_{z,2}} \quad \text{and} \quad \eta^s = 1 \quad \text{or} \quad \eta^p = \sqrt{\frac{\epsilon_2}{\epsilon_1}} \quad . \quad (15.24)$$

The factors  $\eta$  in front of the transmission matrix  $\mathbf{M}_{12}$  can be collected in front of the total transmission matrix  $\mathbf{M}_{\text{total}}$ , in case one is not interested in the distribution of the fields inside the stack. Then, all  $\eta^p$  collapse into  $\sqrt{\epsilon_{\text{first}}/\epsilon_{\text{last}}}$ , which is equal to one in case the terminating half-spaces of the layered medium have both the same dielectric constant.

## Bound modes and surface plasmons

Now we have all tools at hand and can calculate the properties of surfaces plasmons in layered media. These are bound modes. We are thus interested in field distributions that decay into both surrounding half-spaces. Another example is dielectric waveguide modes, when a material of higher index of refraction is embedded in a low-index environment.

We can find these modes by going back to our first equation 15.3 and requiring that both incoming field are zero, i.e.

$$U_1^+ = U_2^- = 0 \quad (15.25)$$

or

$$\begin{pmatrix} U_2^+ \\ 0 \end{pmatrix} = \begin{pmatrix} A & B \\ C & D \end{pmatrix} \cdot \begin{pmatrix} 0 \\ U_1^- \end{pmatrix} = \begin{pmatrix} B U_1^- \\ D U_1^- \end{pmatrix} \quad , \quad (15.26)$$

which means<sup>4</sup> that we search for  $D = 0$ .

<sup>4</sup> see also Yeh, 2005, eq. 11.3-5, but note the different 'direction' of the matrix.

Let us start with the most simple case, a surface plasmon at an interface between a Drude metal half-space and a dielectric half-space. The transmission matrix of the full 'stack' is then only one interface matrix

$$\mathbf{M}_{\text{total}} = \mathbf{M}_{12} = \frac{1}{2\eta} \begin{pmatrix} 1 + \kappa & 1 - \kappa \\ 1 - \kappa & 1 + \kappa \end{pmatrix} \quad . \quad (15.27)$$

We are interested in the conditions when  $D$  element is zero, i.e.,

$$D = \frac{1 + \kappa}{2\eta} = 0 \quad \text{or} \quad k_{z,2} = -\eta^2 k_{z,1} \quad . \quad (15.28)$$

The components of the wave vector in the different layers  $j$  have to fulfil

$$k_x^2 + k_{z,j}^2 = \epsilon_j k_0^2 \quad , \quad (15.29)$$

i.e.  $\eta = \eta^S = 1$  is not a solution. Surface plasmons are p-polarized. Setting  $\eta = \eta^P = \sqrt{\epsilon_2/\epsilon_1}$  leads to the condition

$$\epsilon_1 k_{z,2} = -\epsilon_2 k_{z,1} \quad . \quad (15.30)$$

Combining the last two equations, we get the dispersion relation of the surface plasmon

$$k_x = k_0 \sqrt{\frac{\epsilon_1 \epsilon_2}{\epsilon_1 + \epsilon_2}} . \quad (15.31)$$

propagating in  $x$ -direction along the interface. The  $z$  component of the wave vector in half-space  $j$  is

$$k_{z,j} = k_0 \sqrt{\frac{\epsilon_j^2}{\epsilon_1 + \epsilon_2}} . \quad (15.32)$$

For propagating surface plasmons, we need that  $k_x$  is real-valued, i.e., the propagation is not damped. At the same time,  $k_{z,j}$  should be purely imaginary, so that the field amplitudes decays exponentially when moving away from the interface. This is achieved when

$$\epsilon_1 \epsilon_2 < 0 \quad \text{and} \quad \epsilon_1 + \epsilon_2 < 0 , \quad (15.33)$$

i.e., one dielectric function needs to be more negative than the other is positive.

The interface between a Drude metal and a dielectric fulfills these requirements. We can assume a Drude model for the dielectric function of the metal in half-space  $j = 2$

$$\epsilon_2(\omega) = 1 - \frac{\omega_p^2}{\omega^2} . \quad (15.34)$$

Figure 15.1 shows the resulting dispersion relation eq. 15.31. For large values of  $k_x$ , the eigen-frequency  $\omega_{SP}$  of the surface plasmon is approached. We get

$$\omega_{SP} = \frac{\omega_p}{\sqrt{1 + \epsilon_1}} , \quad (15.35)$$

which is eq. 15.2.

### Example: slab waveguide

As a second example, let us look at a slab of material 2, thickness  $d_2$  embedded in two half-spaces of material 1 and 3. The transmission matrix is

$$\mathbf{M}_{\text{total}} = \mathbf{M}_{23} \cdot \mathbf{M}_{\text{prop}} \cdot \mathbf{M}_{12} \quad (15.36)$$

width  $\delta = d_2 k_{z,2}$  we get

$$\frac{1}{4\eta_{12}\eta_{23}} \begin{pmatrix} 1 + \kappa_{23} & 1 - \kappa_{23} \\ 1 - \kappa_{23} & 1 + \kappa_{23} \end{pmatrix} \begin{pmatrix} e^{+i\delta} & 0 \\ 0 & e^{-i\delta} \end{pmatrix} \begin{pmatrix} 1 + \kappa_{12} & 1 - \kappa_{12} \\ 1 - \kappa_{12} & 1 + \kappa_{12} \end{pmatrix} . \quad (15.37)$$

The  $D$  element is

$$D \propto (1 + \kappa_{12})(1 + \kappa_{23})e^{-i\delta} + (1 - \kappa_{12})(1 - \kappa_{23})e^{+i\delta} . \quad (15.38)$$

$D$  becomes zero if

$$\frac{(1 + \kappa_{12})(1 + \kappa_{23})}{(1 - \kappa_{12})(1 - \kappa_{23})} = -e^{+i2\delta} \quad (15.39)$$

or, using  $\kappa_{12} = (k_{z,1}/\epsilon_1)/(k_{z,2}/\epsilon_2)$ , for p-polarization<sup>5</sup>

<sup>5</sup> remove  $\epsilon_i$  for s-polarization



$$\frac{k_{z,2}/\epsilon_2 + k_{z,1}/\epsilon_1}{k_{z,2}/\epsilon_2 - k_{z,1}/\epsilon_1} \frac{k_{z,2}/\epsilon_2 + k_{z,3}/\epsilon_3}{k_{z,2}/\epsilon_2 - k_{z,3}/\epsilon_3} = e^{+i2\delta} \quad , \quad (15.40)$$

which agrees with Maier, 2007, eq. 2.28.<sup>6</sup> When assuming both half-spaces are equal, i.e.  $\epsilon_1 = \epsilon_3$  and  $k_{z,1} = k_{z,3}$ , we can simplify further<sup>7</sup>

$$\left( \tanh \frac{-i d k_{z,2}}{2} \right)^{\pm 1} = -\frac{\epsilon_1 k_{z,2}}{\epsilon_2 k_{z,1}} \quad . \quad (15.41)$$

One can understand these two solutions as symmetric and anti-symmetric linear combination of modes that reside at the left (12) and right (23) interface. They decouple when we let  $d \rightarrow \infty$ , so that the left side of the equation is always 1. We then recover the eq. 15.30 of the last section.

<sup>6</sup> Note that not only the layers are labelled differently here, but also  $k_z$  is defined differently. We assume  $e^{ik_{z,j}z}$ , in Maier, 2007 it is  $e^{k_j z}$ , i.e. our  $k_{z,j} = -ik_j$ .

<sup>7</sup> Maier, 2007, eq. 2.29. Here the  $-i$  difference to Maier, 2007 becomes relevant.

## Further ideas

- Model and discuss the dispersion relation of the surface plasmons in two thin metals films separated by a thin spacer.
- Model and discuss the reflection spectrum of a distributed Bragg reflector (DBR) used, e.g., in integrated semiconductor lasers.

## Appendix: derivation of eq. 15.23

We start from

$$\mathbf{M}_{12} = \frac{1}{t_{21}} \begin{pmatrix} 1 & r_{21} \\ r_{21} & 1 \end{pmatrix} \quad (15.42)$$

and abbreviate the Fresnel coefficients as

$$r_{21}^s = \frac{k_{z,2} - k_{z,1}}{k_{z,1} + k_{z,2}} = \frac{b - a}{a + b} \quad (15.43)$$

$$t_{21}^s = \frac{2k_{z,2}}{k_{z,1} + k_{z,2}} = \frac{2b\eta}{a + b} \quad (15.44)$$

$$r_{21}^p = \frac{\epsilon_1 k_{z,2} - \epsilon_2 k_{z,1}}{\epsilon_2 k_{z,1} + \epsilon_1 k_{z,2}} = \frac{b - a}{a + b} \quad (15.45)$$

$$t_{21}^p = \frac{2\sqrt{\epsilon_1 \epsilon_2} k_{z,2}}{\epsilon_2 k_{z,1} + \epsilon_1 k_{z,2}} = \frac{2b\eta}{a + b} \quad (15.46)$$

with  $a = \epsilon_2 k_{z,1}$ ,  $b = \epsilon_1 k_{z,2}$  and  $\eta = \sqrt{\epsilon_2/\epsilon_1}$ . In the case of s-polarization, the  $\epsilon_i$  are ignored / set to one. With this we get

$$\mathbf{M}_{12} = \frac{a + b}{2b\eta} \begin{pmatrix} 1 & (b - a)/(a + b) \\ (b - a)/(a + b) & 1 \end{pmatrix} = \frac{1}{2b\eta} \begin{pmatrix} b + a & b - a \\ b - a & b + a \end{pmatrix} \quad (15.47)$$

$$= \frac{1}{2\eta} \begin{pmatrix} 1 + \frac{a}{b} & 1 - \frac{a}{b} \\ 1 - \frac{a}{b} & 1 + \frac{a}{b} \end{pmatrix} = \frac{1}{2\eta} \begin{pmatrix} 1 + \kappa & 1 - \kappa \\ 1 - \kappa & 1 + \kappa \end{pmatrix} \quad (15.48)$$

with

$$\kappa = \frac{a}{b} = \eta^2 \frac{k_{z,1}}{k_{z,2}} \quad \text{and} \quad \eta^s = 1 \quad \text{or} \quad \eta^p = \sqrt{\frac{\epsilon_2}{\epsilon_1}} \quad . \quad (15.49)$$

## References

- Born, Max and Emil Wolf (2002). *Principles of optics*. 7. (expanded) ed., reprinted with corr. Cambridge [u.a.]: Cambridge Univ. Press.
- Macleod, H. Angus (2001). *Thin film optical filters*. 3. ed. Bristol [u.a.]: Inst. of Physics Publ. [↗](#).
- Maier, Stefan A. (2007). *Plasmonics*. Norwell: Springer Science+Business Media, LLC. [↗](#).
- Novotny, Lukas and Bert Hecht (2012). *Principles of nano-optics*. 2. ed. Cambridge Univ. Press. [↗](#).
- Otto, Andreas (1968). "Excitation of nonradiative surface plasma waves in silver by the method of frustrated total reflection". In: *Zeitschrift für Physik A* 216.4, pp. 398–410. [↗](#).
- Pedrotti, Frank L. et al. (2008). *Optik für Ingenieure*. 4., bearb. Aufl. Berlin [u.a.]: Springer. [↗](#).
- Pettit, RB, J Silcox, and R Vincent (1975). "Measurement of surface-plasmon dispersion in oxidized aluminum films". In: *Physical Review B* 11.8, p. 3116. [↗](#).
- Saleh, Bahaa E. A. and Malvin C. Teich (1991). *Fundamentals of photonics*. New York, NY [u.a.]: Wiley. [↗](#).
- Yeh, Pochi (2005). *Optical waves in layered media*. Hoboken, NJ: Wiley-Interscience.

# Chapter16

## Lattices of plasmonic particles

Markus Lippitz

November 18, 2021

### Tasks

- Model the angle-dependent extinction spectrum of an array of plasmonic particles, as measured by Simon Durst (Bayreuth) and shown below. Discuss the observed phenomena.
- Assume that the embedding medium contains a dye with a narrow Lorentzian absorption line. Model and discuss the dispersion relation.

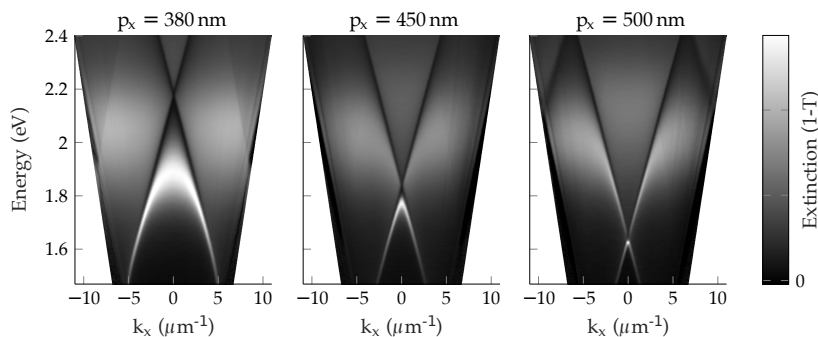


Figure 16.1: Angle-dependent extinction spectrum of an array of plasmonic particles (Figure by S. Durst).

### How this is measured

The samples consist of a rectangular lattice of gold particles on a glass substrate. The lattice constant  $p_y$  is always 200 nm,  $p_x$  varies and is given in the data set. In our data set, the particles are squares with a size of  $80 \times 80$  nm. To simplify things, we assume them to be small spheres. The lattice is coated with immersion oil ( $n = 1.5$ ) and covered by a second glass substrate so that the particles are embedded in a homogeneous dielectric environment.

We measure transmission spectra for white light as function of angle of incidence. As for technical reasons the lattice has only a finite size of  $30 \times 30 \mu\text{m}$ , it is difficult to keep the sample in the beam when rotating

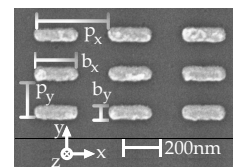


Figure 16.2: SEM micrograph of the gold nanorods in the lattice. Indicated are the dimensions of the rods and the lattice constants (Figure by S. Durst).



This work is licensed under a [Creative Commons "Attribution-ShareAlike 4.0 International"](https://creativecommons.org/licenses/by-sa/4.0/) license.

either the sample or the beam. We thus keep everything fixed and measure all angles at the same time. To this end, we illuminate the sample by a cone of light with large opening angle (NA = 0.9, max. angle =  $64^\circ$ ). The transmitted light is collected by a second microscope objective. In its back focal plane, i.e. at one focal length behind the lens, rays of equal angle of incidence cross at the same point at a height  $h$ , which is according to the Abbé sine condition

$$h = f \sin \theta \quad (16.1)$$

We image this back-focal plane (BFP) on the entrance slit of a spectrometer and thus get an image on the CCD camera which in one direction is angle of incidence, in the other wavelength of the light beam. This is converted into a energy- $k_x$  scale, where  $k_x$  is the component of the wave vector that is parallel to the sample surface along the x-coordinate. The light beam is polarized before the sample such that we image the s polarization on the entrance slit of the spectrometer, i.e. along the x-direction of the sample coordinate system.

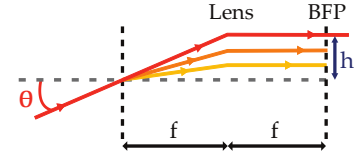
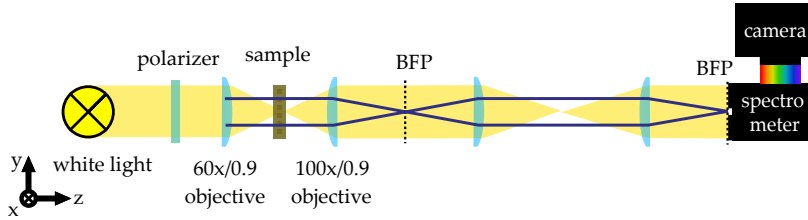


Figure 16.3: The back focal plane sorts rays by their angle in the front focal plane. (Figure by S. Durst).

Figure 16.4: Setup to measure angle-dependent transmission spectra without moving parts. (Figure by S. Durst).

## How to understand the dispersion relation

Each panel in Fig. 16.1 shows a dispersion relation, i.e., the relation between (in-plane) momentum and energy. Two features combine: the particle plasmon resonance and a lattice resonance. The particle resonance is at a given eigen-frequency (or energy), spectrally rather broad, and independent of the angle of incidence or  $k_x$ , as the particles are rather spherical. This gives the broad, medium gray band around an energy of 2 eV. The second feature is the lattice resonance. An optical wave travels parallel to the interface. Its dispersion relation is

$$E = \hbar (k_x + m \cdot G) \quad (16.2)$$

where  $G = 2\pi/p_x$  is the fundamental reciprocal lattice vector and  $m$  an integer. The lattice resonance is spatially extended over the whole lattice and spectrally narrow. The interaction of a broad and a narrow resonance leads to characteristic spectral features that are visible in Fig. 16.1 and could be described in a Fano model. But that is (currently) beyond the scope of this chapter.

Here we follow a more microscopic approach. We calculate the extinction spectrum of an arrangement of many small particles at positions  $\mathbf{r}_i$ . Each particle is modelled as sphere with a polarizability  $\alpha_i$  given by the material properties and the volume of the small particle. We want to calculate the absorption, scattering and extinction spectrum of this ensemble.

## Radiating electric dipole

Let us first look at a single electric dipole  $\boldsymbol{\mu}$  at the position  $\mathbf{r}_0$ . Its field at the position  $\mathbf{r}$  is given by<sup>1</sup>

$$\mathbf{E}(\mathbf{r}) = \frac{k^2}{\epsilon_0 \epsilon_{out}} \mathbf{G}(\mathbf{r}, \mathbf{r}_0) \boldsymbol{\mu} \quad (16.3)$$

with the length  $k$  of the wave vector in the medium of dielectric function  $\epsilon_{out}$ . The Greens function  $\mathbf{G}$  is given by<sup>2</sup>

$$\mathbf{G}(\mathbf{r}, \mathbf{r}_0) = \frac{e^{ikR}}{4\pi k^2 R^3} \left[ (k^2 R^2 + ikR - 1) \mathbf{1} + (3 - 3ikR - k^2 R^2) \frac{\mathbf{R}\mathbf{R}}{R^2} \right] \quad (16.4)$$

with  $\mathbf{R} = \mathbf{r} - \mathbf{r}_0$ ,  $R = |\mathbf{R}|$ ,  $\mathbf{1}$  the unity  $3 \times 3$ -tensor, and  $\mathbf{R}\mathbf{R}$  the outer product of  $\mathbf{R}$  with itself, i.e.

$$\mathbf{R}\mathbf{R} = \begin{pmatrix} R_x R_x & R_x R_y & R_x R_z \\ R_y R_x & R_y R_y & R_y R_z \\ R_z R_x & R_z R_y & R_z R_z \end{pmatrix} . \quad (16.5)$$

This is a convenient method to describe the full vectorial field emitted by a dipole at position  $\mathbf{r}_0$  everywhere in space, including both near- and far-field components.

### Questions

1. Convince yourself that eq. 16.4 agrees with the other commonly used form

$$\mathbf{E} = \frac{e^{ikr}}{4\pi\epsilon_0 \epsilon_{out}} \frac{1}{r^3} \left\{ (kr)^2 (\hat{\mathbf{r}} \times \boldsymbol{\mu}) \times \hat{\mathbf{r}} + (1 - ikr) (3\hat{\mathbf{r}} [\hat{\mathbf{r}} \cdot \boldsymbol{\mu}] - \boldsymbol{\mu}) \right\} . \quad (16.6)$$

## Scattering sphere

We need to know the oscillation amplitude of the emitting dipole  $\mathbf{p}$  to use eq. 16.4. It is related by the polarizability  $\alpha$  to the incoming optical field  $\mathbf{E}_{inc}$

$$\mathbf{p} = \epsilon_0 \epsilon_{out} \alpha \mathbf{E}_{inc} \quad (16.7)$$

with the dielectric function  $\epsilon_{out}$  of the embedding medium. When we assume that the scattering nanoobject is a sphere, we can calculate

$$\alpha = 3V \frac{\epsilon_{in} - \epsilon_{out}}{\epsilon_{in} + 2\epsilon_{out}} , \quad (16.8)$$

where  $V$  is the volume of the sphere and  $\epsilon_{in}$  the dielectric function of it. The sphere radiates a scattered field  $\mathbf{E}_S$

$$\mathbf{E}_S(\mathbf{r}) = \frac{k^2}{\epsilon_0 \epsilon_{out}} \mathbf{G}(\mathbf{r}, \mathbf{r}_0) \mathbf{p} \quad (16.9)$$

$$= \frac{1}{4\pi \epsilon_0 \epsilon_{out}} \frac{e^{ikR}}{R^3} [\dots] \mathbf{p} \quad (16.10)$$

where the contents of the square brackets is the same as in eq.16.4 above.  $k$  is again the length of the wave vector in a medium with dielectric function  $\epsilon_{out}$ .

<sup>1</sup> Novotny and Hecht, 2012, eq. 8.52.

<sup>2</sup> This follows Novotny and Hecht, 2012 eq. 8.55 and differs by  $4\pi k^2$  from eq. 2 in Yurkin and Hoekstra, 2007

## Multiple particles

When we have more than one particle, each particle  $i$  sees the incident field  $\mathbf{E}_{i,inc}$  at the position  $\mathbf{r}_i$  plus the sum over all scattered fields  $\mathbf{E}_{j,S}$  from all the other induced dipoles  $j$

$$\mathbf{E}_{i,loc} = \mathbf{E}_{i,inc} + \sum_{j \neq i} \mathbf{E}_{j,S} = \mathbf{E}_0 e^{i\mathbf{k} \cdot \mathbf{r}_i} + \sum_{j \neq i} \frac{k^2}{\epsilon_0 \epsilon_{out}} \mathbf{G}(\mathbf{r}_i, \mathbf{r}_j) \mathbf{p}_j \quad (16.11)$$

with the dipole moment  $\mathbf{p}_j$  of the particle at position  $\mathbf{r}_j$ . The position of the 'receiving' particle  $\mathbf{r}_i$  takes the role of  $\mathbf{r}$  in the Greens function; the position of the scattering particle  $\mathbf{r}_j$  takes the role of the dipole at position  $\mathbf{r}_0$  above.

The local field  $\mathbf{E}_{i,loc}$  then induces a dipole moment again

$$\mathbf{p}_i = \epsilon_0 \epsilon_{out} \alpha_i \mathbf{E}_{i,loc} \quad (16.12)$$

Both equations together form a coupled equation system for the dipole moments  $\mathbf{p}_i$

$$\mathbf{E}_0 e^{i\mathbf{k} \cdot \mathbf{r}_i} = \frac{1}{\epsilon_0 \epsilon_{out} \alpha_i} \mathbf{p}_i - \sum_{j \neq i} \frac{k^2}{\epsilon_0 \epsilon_{out}} \mathbf{G}(\mathbf{r}_i, \mathbf{r}_j) \mathbf{p}_j \quad (16.13)$$

which can be written as

$$\mathbf{E}_{inc} = \mathbf{A} \mathbf{p} \quad (16.14)$$

where  $\mathbf{p}$  and  $\mathbf{E}_{inc}$  are column vectors containing the induced dipole moment and the incident field of all dipoles and  $\mathbf{A}$  is an interaction matrix. Its elements are  $3 \times 3$ -sub-matrices given by<sup>3</sup>

$$\mathbf{A}_{ii} = \frac{1}{\epsilon_0 \epsilon_{out} \alpha_i} \mathbf{1} \quad (16.15)$$

$$\mathbf{A}_{ij} = - \frac{k^2}{\epsilon_0 \epsilon_{out}} \mathbf{G}(\mathbf{r}_i, \mathbf{r}_j) \quad (16.16)$$

<sup>3</sup> This assume an isotropic polarizability. Otherwise, the diagonal elements should be  $1/\alpha_{x,y,z}$  instead of  $1/\alpha$ .

Some publications put the minus sign of the last equation into the Greens function.

## Questions

2. Which size / dimension have  $\mathbf{A}$  and  $\mathbf{p}$  in eq. 16.14 ?
3. Sketch the interaction matrix  $\mathbf{A}$  and its components.

## Absorption, scattering and extinction

The extinction cross-section can be calculated by the optical theorem from the interference of the forward-scattered wave with the incident wave. We get<sup>4</sup>

$$\sigma_{ext} = \frac{k}{\epsilon_0 \epsilon_{out} |\mathbf{E}_{inc}|^2} \sum_i \Im(\mathbf{p}_i \cdot \mathbf{E}_{i,inc}^*) \quad (16.17)$$

<sup>4</sup> Draine, 1988; Yurkin and Hoekstra, 2007.

The absorption can be calculated from the field acting on each dipole<sup>5</sup>, i.e., replacing  $\mathbf{E}_{i,inc}$  by  $\mathbf{E}_{i,loc}$

$$\sigma_{abs} = \frac{k}{\epsilon_0 \epsilon_{out} |\mathbf{E}_0|^2} \sum_i \Im(\mathbf{p}_i \cdot \mathbf{E}_{i,loc}^*) \quad (16.18)$$

<sup>5</sup> Yurkin and Hoekstra, 2007.

The scattering cross section is the difference of both

$$\sigma_{scat} = \sigma_{ext} - \sigma_{abs} \quad . \quad (16.19)$$

With this we have now everything at hand to calculate the absorption, scattering and extinction cross-sections and spectra of arrangements of small scattering spheres or dipoles. We solve eq. 16.14 for  $\mathbf{p}$  and then calculate the cross-sections. Depending on the community (and the distance between the dipoles) this is called discrete dipole approximation (DDA) or coupled dipole approximate (CDA).

### Questions

4. Why do  $\sigma_{ext}$  and  $\sigma_{abs}$  differ only in the choice of the field that is multiplied on  $\mathbf{p}_i$ ? How can we understand this choice?

### Improvements: Radiation reaction

When we would have only a single dipole, then  $\sigma_{scat}$  as defined above would vanish. This problem finds its roots in our definition of the polarizability  $\alpha$ . We need to take the radiation reaction into account<sup>6</sup>. When we call the 'old' definition  $\alpha^{CM}$ , as Clausius-Mossotti, then we define<sup>7</sup>

$$\alpha^{RR} = \frac{\alpha^{CM}}{1 - \frac{ik^3}{6\pi}\alpha^{CM}} \approx \alpha^{CM} - \frac{ik^3}{6\pi}(\alpha^{CM})^2 \quad . \quad (16.20)$$

Along the same lines, an improved relation for the absorption cross-section should be used<sup>8</sup>

$$\sigma_{abs} = \frac{k}{\epsilon_0 \epsilon_{out} |\mathbf{E}_0|^2} \sum_i \Im \left( \mathbf{p}_i \cdot \left( \frac{\mathbf{p}_i}{\epsilon_0 \epsilon_{out} \alpha^{RR}} \right)^* \right) - \frac{2}{3} \frac{1}{4\pi \epsilon_0 \epsilon_{out}} k^3 |\mathbf{p}_i|^2 \quad . \quad (16.21)$$

<sup>6</sup> see chapter 8.4.2. in Novotny and Hecht, 2012

<sup>7</sup> here in SI, in contrast to Yurkin and Hoekstra, 2007

<sup>8</sup> see Draine, 1988 for a derivation, and Yurkin and Hoekstra, 2007 for a discussion

### Side note: Polarizability of a Lorentz oscillator

We started above with the polarizability  $\alpha$  of a sphere

$$\alpha = 3V \frac{\epsilon_{in} - \epsilon_{out}}{\epsilon_{in} + 2\epsilon_{out}} \quad . \quad (16.22)$$

We could also assume a Lorentz oscillator, taking into account our definition

$$\mathbf{p} = \epsilon_0 \epsilon_{out} \alpha_L \mathbf{E}_{inc} = e \mathbf{x} \quad . \quad (16.23)$$

With this we find

$$\alpha_L = \frac{e^2}{\epsilon_0 \epsilon_{out} m} \frac{1}{\omega_0^2 - \omega^2 + 2i\gamma\omega} \quad (16.24)$$

with the eigen-frequency  $\omega_0$ , the damping  $\gamma$  and the mass  $m$  of the oscillator.

## Lattice sum

Things become easier when we are interested in infinite lattices of identical scatterers. As we are on a lattice, all lattice points are equal, especially in the amplitude and vectorial direction  $\hat{\mathbf{n}}$  of the local field. It is then convenient to re-arrange eq. 16.11

$$\mathbf{E}_{i,loc} = \mathbf{E}_0 e^{i\mathbf{k}\cdot\mathbf{r}_i} + \sum_{j \neq i} k^2 \mathbf{G}(\mathbf{r}_i, \mathbf{r}_j) \alpha \mathbf{E}_{j,loc} \quad (16.25)$$

to

$$E_{i,loc} e^{-i\mathbf{k}\cdot\mathbf{r}_i} = \hat{\mathbf{n}} \cdot \mathbf{E}_0 + \sum_{j \neq i} k^2 \hat{\mathbf{n}} \mathbf{G}(\mathbf{r}_i, \mathbf{r}_j) \hat{\mathbf{n}} \alpha E_{j,loc} e^{-i\mathbf{k}\cdot\mathbf{r}_i} \quad (16.26)$$

so that we get

$$\hat{\mathbf{n}} \cdot \mathbf{E}_0 = E_{loc} \left( 1 - \alpha \sum_{j \neq i} k^2 \hat{\mathbf{n}} \mathbf{G}(\mathbf{r}_i, \mathbf{r}_j) \hat{\mathbf{n}} e^{i\mathbf{k}\cdot(\mathbf{r}_i - \mathbf{r}_j)} \right) = E_{loc} (1 - \alpha S) \quad (16.27)$$

with the retarded lattice sum  $S$ . The induced dipole moment becomes

$$\mathbf{p} = \epsilon_0 \epsilon_{out} \alpha \mathbf{E}_{loc} = \epsilon_0 \epsilon_{out} \frac{\alpha}{1 - \alpha S} \mathbf{E}_0 \quad (16.28)$$

or we define an effective (lattice) polarizability

$$\alpha_{lattice} = \frac{\alpha}{1 - \alpha S} \quad (16.29)$$

The extinction cross-section becomes then<sup>9</sup>

<sup>9</sup> somehow a  $4\pi$  is missing here....

$$\sigma_{ext} = k \Im(\alpha_{lattice}) \quad (16.30)$$

## References

- Draine, B T (1988). "The discrete-dipole approximation and its application to interstellar graphite grains". In: *The Astrophysical Journal* 333, p. 848. [↗](#).
- Novotny, Lukas and Bert Hecht (2012). *Principles of nano-optics*. 2. ed. Cambridge Univ. Press. [↗](#).
- Yurkin, Maxim A and Alfons G Hoekstra (2007). "The discrete dipole approximation: an overview and recent developments". In: *Journal Of Quantitative Spectroscopy & Radiative Transfer* 106.1-3, pp. 558–589. [↗](#).



# Chapter17

## Plasmonic Nano-Rods

Markus Lippitz

December 9, 2021

### Tasks

- Simulate the optical field above a plasmonic nano-rod and compare to the experimental data in Fig. 3 of Dorfmueller et al., 2010.
- Investigate how the spatial maximum amplitude of the field depends on rod length and illumination direction, and compare to Fig. 4 of Dorfmueller et al., 2010.

The first steps are implemented in Pluto**nanorods**<sup>1</sup>.

<sup>1</sup>  [download](#) [run on binder](#)

### How this is measured

Dorfmueller et al., 2010 measure the optical field in amplitude and phase about 20 nm above of gold nano-rods, using a near-field microscope. The operation of such device is topic of one of the following chapters.

The sample is a glass substrate on which gold nanostructures of rectangular shape were fabrication by electron-beam lithography. The structures can be understood as cut out a two-dimensional film. All have thus the same height. These gold nano-rods are illuminated by 911 nm laser light under a tilted angle from above. The polarization direction is along the long axis of the rods. The free electrons in the nano-rod come to a resonance, depending on the rod length. This resource leads to a locally increased field amplitude. Dorfmueller et al. measure the field component perpendicular to the sample surface by scattering it out with a sharp tip of an atomic force microscope. Phase-stable interference with a reference beam allows to obtain both amplitude and phase of the near-field. The spatial resolution is only limited by the sharpness of the AFM tip to about 20 nm. The near-field microscope operates thus outside the Abbé diffraction limit.

### Waveguides

Let us start by investigating the optical modes of a thin wire. We assume cylindrical symmetry and coordinates  $z$  and  $\rho$ . The wire has a radius  $a$  and is



This work is licensed under a [Creative Commons "Attribution-ShareAlike 4.0 International"](#) license.

made of a material (first dielectric, later metal) of dielectric function  $\epsilon_{in}$ . It is embedded in a dielectric matrix characterized by  $\epsilon_{out}$ . One solves Maxwell's equation with these boundary conditions.<sup>2</sup>

The electric field is described inside and outside the wire by cylindrical Bessel  $J$  and Hankel  $H^{(1)}$  functions of the first kind, respectively. The lowest order mode is<sup>3</sup>

$$\mathbf{E}_{in} = E_0 \left( J_0(\kappa_1 r) \hat{\mathbf{z}} + \frac{ik_z}{\kappa_1} J_1(\kappa_1 r) \hat{\mathbf{r}} \right) e^{i(k_z z - \omega t)} \quad (17.1)$$

$$\mathbf{E}_{out} = E_0 \left( H_0^{(1)}(\kappa_2 r) \hat{\mathbf{z}} - \frac{ik_z}{\kappa_2} H_1^{(1)}(\kappa_2 r) \hat{\mathbf{r}} \right) e^{i(k_z z - \omega t)} \quad (17.2)$$

where  $k_z$  is the component of the wave vector (length in vacuum  $k_0 = 2\pi/\lambda$ ) along the wire. The components perpendicular to the wire are defined as

$$\kappa_i = k_0 \sqrt{\epsilon_i - (k_z/k_0)^2} \quad (17.3)$$

with  $\epsilon_i = (\epsilon_{in}, \epsilon_{out})$ . The boundary condition at  $r = a$  leads to a condition for  $k_z$

$$\frac{\epsilon_{in}}{\kappa_1 a} \frac{J_1(\kappa_1 a)}{J_0(\kappa_1 a)} - \frac{\epsilon_{out}}{\kappa_2 a} \frac{H_1^{(1)}(\kappa_2 a)}{H_0^{(1)}(\kappa_2 a)} = 0 \quad (17.4)$$

Guiding of waves requires that the electric field is localized near the wire, i.e., the radial component of the wave vector outside the wire  $\kappa_2$  has to be imaginary, or  $k_z/k_0 > \sqrt{\epsilon_{out}}$ . At the same time, the wave should propagate inside the wire, i.e.,  $k_z$  should be (almost<sup>4</sup>) real, or  $\sqrt{\epsilon_{in}} > k_z/k_0$ .

For dielectric waveguides, the core has to have a higher index of refraction than the embedding medium. When the radius of the wire is decreased, the decay of the field outside the wire becomes slower and slower. By Fourier transformation from  $\kappa$  to  $\rho$  one finds a characteristic lower limit for radius  $R$  of the field distribution, independent of the wire diameter,

$$R > \frac{\lambda}{2\sqrt{\epsilon_{in}}} \quad (17.5)$$

Dielectric waveguides are thus limited in their size of the mode field to approximately the wavelength in the core medium.

Plasmonic waveguides in contrast can become very small. When the dielectric function  $\epsilon_{in}$  is negative, the mode field remains bound close to the wire even for a small wire radius. The downside is that losses increase. The wave vector in propagation direction becomes complex. The real part describes the effective index of refraction of the mode, the imaginary part the losses due to absorption in metal. These losses increase drastically when the wire becomes smaller, as shown in the Pluto script linked at the beginning of this chapter.

The large component of the wave vector in propagation direction  $k_z$  in a plasmonic waveguide corresponds to a short effective wavelength  $\lambda_{in} = 2\pi/k_z$ . The thinner the waveguide, the shorter the effective wavelength. Novotny shows that a linear relation to the vacuum wavelength exists<sup>5</sup>

$$\lambda_{in} = n_1 + n_2 \frac{\lambda}{\lambda_p} \quad (17.6)$$

where  $\lambda_p = 2\pi c/\omega_p$  is the plasma wavelength of the Drude metal and the  $n_i$  are constants depending on geometry and refractive indices.<sup>6</sup>

<sup>2</sup> Details see, e.g., Saleh and Teich, 1991 in the chapter on fiber optics

<sup>3</sup> Takahara et al., 1997.

see also Novotny and Hecht, 2012 eq. 12.53

<sup>4</sup> When the dielectric functions are complex-valued, also  $k_z$  becomes complex-valued

<sup>5</sup> Novotny, 2007.

<sup>6</sup> see eq. 14 in Novotny, 2007

### Side note: Leakage radiation

The component of the wave vector in propagation direction  $k_z$  is larger than the maximum possible length of a wave vector in the embedding medium  $k_0\sqrt{\epsilon_{out}}$ . This means that momentum conservation does not allow photons to leave the waveguide. Plane waves with such a value of  $k_z$  are evanescent (have an imaginary  $k_\perp$ ) in the embedding medium. In this way, a mode can propagate without losses to the environment. However, this also hinders observation of such a propagation. One only could detect the emission at the end of the waveguide or at defects.

One way around is leakage radiation. When the waveguide is placed on or near a medium with a higher index of refraction  $k_z/k_0 < \sqrt{\epsilon_{substrate}}$ , then this substrate supports suitable free-space modes. The distance between waveguide and substrate defines the coupling (as seen by the observer) or the losses (from the point of view of the waveguide). In such an experiment one can see bright emission along the whole waveguide.

### Fabry-Perot modes in nano-rods

We now cut out a piece of a thin plasmonic waveguide and call this object a nano-rod. The propagation of the plasmon mode along the waveguide is the same as in the preceding section, but now the wave is reflected back at the ends of the waveguide. The free space around the nano-rod does not support modes of sufficient high wave vector, so that the light can not just propagate out. The two ends thus form two mirrors of a Fabry-Perot cavity and the short piece of waveguide in between is similar to the medium in the cavity. We expect to find periodic resonances when varying the length of the rod. This is indeed what is observed. However, the apparent length of the rod is larger by some offset length  $L_o$

$$L_{res} = n \frac{\lambda_{in}}{2} + L_o \quad (17.7)$$

The exact value of the offset  $L_o$  depends on details of the waveguide end, for example how it is rounded or cut flat, and also how one defines the rod length  $L_{res}$  when the ends are rounded.

The physical origin of this apparent additional length  $L_o$  is that a propagating plasmon is a quasi-particle combined of free electrons and an electromagnetic field. The electrons have to stay inside the metal to within less than a lattice constant. The optical field however extends all around the nano-rod and thus also extends over the ends of the rod. This gives an additional length.

In some publications this additional length  $L_o$  is called a reflection phase  $\Delta\phi$ , as one could also describe the process in terms of phases as

$$\frac{2L_{res}}{\lambda_{in}} 2\pi = n 2\pi + 2\Delta\phi \quad (17.8)$$

This is in analogy to the phase acquired by an optical beam undergoing total internal reflection. In this case,  $k_{z,1}$  is real-valued, but  $k_{z,2}$  is complex, as it describes an evanescent wave. The reflection coefficient

$$r_{12}^s = \frac{k_{z,1} - k_{z,2}}{k_{z,1} + k_{z,2}} \quad (17.9)$$

becomes then also complex, so that the field acquires a phase shift

$$\Delta\phi = \arg(r_{12}^s) \quad (17.10)$$

### Excitation of resonances in nano-rods

We shine a plane wave on a nano-rod, i.e., a short piece of a thin plasmonic wire, and want to calculate the response of the particle in terms of scattered field and absorption. We follow here the analytical model by Dorfmueller et al., 2010, model the effect of the wire itself and assume an ad-hoc parameter for the effect of the wire ends. At the wire surface, the boundary condition for electric fields relates the  $z$  components of incident, scattered and internal fields

$$E_z^{inc}(r=a) + E_z^{scat}(r=a) = E_z^{inside}(r=a) \quad (17.11)$$

The plane wave is incident with an angle  $\theta$  to the symmetry axis of the wire

$$E_z^{inc}(r=a) = E_0 \sin(\theta) e^{i k_{\parallel} z} \quad \text{with} \quad \cos(\theta) = \frac{k_{\parallel}}{k_0} \quad (17.12)$$

where we omitted the time dependence  $e^{-i\omega t}$  and have put the phase factor of  $e^{i k_r a}$  into  $E_0$ .  $k_{\parallel}$  is the component of the plane wave's wave vector along the wire direction.

The scattered field is described by the current inside the wire. An oscillating current is source of radiation, as for example in an antenna. We assume that the current is spatially homogeneous and running only along  $z$  direction (not radially). One finds

$$E_z^{scat}(r=a) = \frac{i \tilde{Z}}{4\pi\epsilon_0\omega} \left( \frac{\partial^2}{\partial z^2} + k^2 \right) I_z(z) \quad (17.13)$$

where  $\tilde{Z}$  is the (antenna) impedance of the wire, which is unknown at this point.

Current and field inside the wire are connected by the conductivity  $\sigma$  or the imaginary part of the dielectric function of the wire  $\epsilon_{in}$

$$I_z(z) = \sigma E_z^{inside}(z) = \epsilon_0\omega \Im(\epsilon_{in}) E_z^{inside}(z) \quad (17.14)$$

Putting everything in eq. 17.11 we get a differential equation for  $I_z(z)$

$$E_0 \sin(\theta) e^{i k_z z} + \frac{i \tilde{Z}}{4\pi\epsilon_0\omega} \left( \frac{\partial^2}{\partial z^2} + k^2 \right) I_z(z) = \frac{1}{\epsilon_0\omega \Im(\epsilon_{in})} I_z(z) \quad (17.15)$$

We make the ansatz that the current either flows with the wave vector  $k_{\parallel}$  of the external field projected on the wire direction, or with the wave vector  $k_p$  of the plasmon mode calculated by eq. 17.4 (where it was called  $k_z$ ):

$$I_z(z) = I_{\parallel} e^{i k_{\parallel} z} + I_{+p} e^{i k_p z} + I_{-p} e^{-i k_p^* z} \quad (17.16)$$

Additionally we know that the current has to vanish at the ends of the wire, as the electrons can not flow out, i.e.,

$$I_z(z = \pm \tilde{L}/2) = 0 \quad (17.17)$$

where  $\tilde{L}$  is the effective length of the nano-rod, i.e., longer than the geometrical size to include the phase effect of the reflection at the wire end. All together one then finds<sup>7</sup>

<sup>7</sup> Dorfmueller et al., 2010.

$$\tilde{Z} = +i \frac{4\pi}{\Im(\epsilon_{in})} \frac{1}{k_p^2 - k^2} \quad (17.18)$$

$$I_{\parallel} = -i \frac{\omega \epsilon_0 \tilde{Z}}{4\pi} \frac{1}{k_p^2 - k_{\parallel}^2} E_0 \sin \theta \quad (17.19)$$

$$I_{\pm p} = -I_{\parallel} \frac{\sin([k_p \pm k_{\parallel}] \tilde{L}/2)}{\sin(k_p \tilde{L})} \quad (17.20)$$

The antenna impedance  $\tilde{Z}$  of the wire (eq. 17.18) has a resonance that goes with the momentum mismatch between free-space modes and plasmonic wire modes. For the excitation of the current in the wire (Eq. 17.19) only the momentum mismatch between the plasmon mode and the wave vector projected on the wire axis  $k_{\parallel}$  matters. As function of nano-rod length we find back the Fabry-Perot resonances at

$$k_p \tilde{L} = n \pi \quad (17.21)$$

where the index  $n$  enumerates the resonances.

## Dipole model of the modes in a nano-rod

Before we continue with the work of Dorfmueller, let us have a look at these resonances. We simplify the discussion by assuming that the incident plane wave propagates perpendicular to the wire axis, i.e.  $\theta = 90^\circ$  and  $k_{\parallel} = 0$ . The amplitudes of the plasmon currents  $I_{\pm p}$  become identical and come into resonance for

$$k_p \tilde{L} = n\pi \quad \text{for odd } n \quad (17.22)$$

By perpendicular incidence we can only excite odd resonances of the rod! In this case, the current distribution in the wire also simplify, as the term with  $I_{\parallel}$  is spatially constant, as  $k_{\parallel} = 0$ . We thus have

$$I_z(z) = I_{\parallel} + 2I_{\pm p} \cos(k_p z) \approx 2I_{\pm p} \cos(k_p z) \quad (17.23)$$

where the approximation certainly hold on resonance. We thus have current maxima at positions  $z$  along the nano-rod where  $|\cos(k_p z)|$  is maximal, or at

$$z_{\nu} = \pm \nu \frac{\tilde{L}}{n} \quad \text{where } \nu = 0, 1, \dots, \frac{n-1}{2} \quad (17.24)$$

As the current oscillates with  $e^{i\omega t}$ , we can replace  $I_z(z)$  by  $n$  dipoles placed at the positions  $z_{\nu}$ , when neighboring dipoles oscillate  $180^\circ$  out of phase.

This dipole model then also explains why we can not excite even Fabry-Perot orders. Here one half of the dipoles would require a field pointing into  $+z$  direction, the other one a field pointing in  $-z$  direction, which can not be fulfilled simultaneously. For odd-order modes, one of the two directions always has one dipole more than the other direction, so that some net excitation efficiency remains. But one also sees that the excitation efficiency drops with increasing order, as most dipoles cancel with each other. We will find this back in the data by Dorfmueller et al.

## Field distributions

Now that we know the current in the center of the nano-rod, we can go back to fields. We could start from the currents (eq. 17.16) and use Maxwell's equation, as done in Dorfmueller et al., 2010. Here, we take a shortcut as we have introduced the eigen-modes already with eqs. 17.1, 17.2, which we name here  $\mathbf{E}_m(k_z)$ , i.e. the argument is the component of the wave vector along the wire. The amplitudes of the currents  $I_{\pm p}$  and  $I_{\parallel}$  are also the amplitudes of the corresponding fields. Inside the wire we have

$$\mathbf{E}_{in} = I_{+p}\mathbf{E}_m(+k_{+p}) + I_{-p}\mathbf{E}_m(-k_{-p}^*) + I_{\parallel}\mathbf{E}_m(+k_{\parallel}) \quad (17.25)$$

Note that  $k_z = +k_{\parallel}$  does not fulfill the eigen-mode condition eq. 17.4. The fields with this value of  $k_z$  only match at the surface of the wire when the incident field is also taken into account. The fields outside the wire have thus one additional component

$$\mathbf{E}_{out} = I_{+p}\mathbf{E}_m(+k_{+p}) + I_{-p}\mathbf{E}_m(-k_{-p}^*) + I_{\parallel}\mathbf{E}_m(+k_{\parallel}) + \hat{\mathbf{n}}E_0e^{i\mathbf{k}\cdot\mathbf{r}} \quad (17.26)$$

where the vector  $\hat{\mathbf{n}}$  defines the p-polarization direction.

These fields are valid only along the wire, i.e. for  $|z| < \tilde{L}$ , but this is sufficient to explain the experiment. One could assume a flat wire end and calculate the fields near this end using the continuity conditions for fields parallel and perpendicular to a surface

$$E_{\parallel}^{in} = E_{\parallel}^{out} \quad \text{and} \quad \epsilon_{in}E_{\perp}^{in} = \epsilon_{out}E_{\perp}^{out} \quad (17.27)$$

The full field distribution would need near-field propagation of the fields on the wire surface, which is beyond the scope of this chapter.

To compare more systematically the model with the experiment, Jens Dorfmueller et al. vary the rod length and measure the  $r$  component of the near-fields. They compare then the maximum near-field amplitude under a certain illumination angle with the model. To this end, the exact calculation of the spatial dependence of the field can be skipped. If the wire is just long enough, at some point all three contributions will add up, so that the maximum field is approximately

$$|E_r|_{max} \approx |k_{\parallel} I_{\parallel}| + |k_{+p} I_{+p}| + |k_{-p} I_{-p}| \quad (17.28)$$

where the  $k_i$  are a consequence of the  $k_z$  in eq 17.2. This simplified model describes the dependence of the Fabry-Perot resonances on the effective rod-length  $\tilde{L}$ .

## Appendix: Far-field emission pattern

The Far-field emission pattern of a nano-rod is, according to Dorfmueller, 2010 appendix, eq. B.16,

$$\frac{dP}{d\Omega} = \frac{I_0^2}{8\pi^2 c\epsilon_0} \frac{k^2}{k_p^2} \sin^2 \theta \frac{f^2 (n \pi k_{\parallel} / (2k_p))}{\left(1 - k_{\parallel}^2 / k_p^2\right)^2} \quad (17.29)$$

where  $k_{\parallel} = k \cos \theta$  and

$$f(x) = \begin{cases} \sin(x) & \text{for } n \text{ even} \\ \cos(x) & \text{for } n \text{ odd} \end{cases}$$

with the order  $n$  of the Fabry-Perot resonance.

This has similarities and difference to the far-field diffraction pattern of  $n$  slits. The envelope function of a single slit is replaced by the  $\sin \theta$  angular dependence of dipolar emission. The biggest difference is that in contrast to slits, neighboring dipoles in the nano-rod emit  $180^\circ$  out of phase. This would correspond to a transmission grating where every second slit is covered by a thin glass plate to achieve the phase lag.

One should be able to obtain this equation by assuming two lattices of dipoles with doubled distance. Each would produce the familiar *amplitude* pattern. The two amplitude patterns are then added, taking care of the distance between the neighboring dipoles, and squared to get the intensity pattern shown above. But I did not try this yet ...

## References

- Dorfmüller, Jens (2010). "Optical Wire Antennas: Near-Field Imaging, Modeling and Emission Patterns". PhD thesis. École Polytechnique Fédérale de Lausanne. [↗](#).
- Dorfmüller, Jens et al. (2010). "Plasmonic nanowire antennas: experiment, simulation, and theory". In: *Nano Letters* 10.9, pp. 3506–3603. [↗](#).
- Novotny, Lukas (2007). "Effective Wavelength Scaling for Optical Antennas". In: *Physical Review Letters* 98.26, p. 266802. [↗](#).
- Novotny, Lukas and Bert Hecht (2012). *Principles of nano-optics*. 2. ed. Cambridge Univ. Press. [↗](#).
- Saleh, Bahaa E. A. and Malvin C. Teich (1991). *Fundamentals of photonics*. New York, NY [u.a.]: Wiley. [↗](#).
- Takahara, Junichi et al. (1997). "Guiding of a one-dimensional optical beam with nanometer diameter". In: *Optics Letters* 22.7, p. 475. [↗](#).





## **Part V**

# **Nanooptics**



# Chapter18

## Angular spectrum representation

Markus Lippitz

January 14, 2022

### Tasks

- A lens focuses a laser beam. Calculate the intensity distribution in the focal plane of a lens of finite aperture diameter. Compare a plane wave and a Gaussian beam as model for the laser beam.
- Find the optimum width of a Gaussian beam to maximize the absorption by a point-like object in the focus of an objective of given numerical aperture (NA).
- Simulate the image of a slit in a microscope, when reducing the slit width from above the wavelength to far below the wavelength, i.e., reproduce Fig. 18.1 or similar.

### Introduction

In this chapter, we assume a monochromatic optical field, i.e., a known single wavelength  $\lambda$ . We also use a time-dependence of the form  $e^{-i\omega t}$ , as usual in physics and used in Novotny and Hecht, 2012, or Goodman, 2005. Note, however, that this is complex-conjugate to the convention in engineering, as used in Saleh and Teich, 1991.

Let us first look at a single plane wave

$$u(x, y, z) = u_0 e^{i(k_x x + k_y y + k_z z)} e^{-i\omega t} . \quad (18.1)$$

In a plane of constant  $z$ -position, the field is periodic in  $x$  direction with a *spatial frequency*  $\nu_x = k_x/2\pi$ , and similar for the  $y$  direction. Knowing the spatial frequencies  $\nu_x$  and  $\nu_y$  is sufficient to know everything about this plane wave, everywhere in space, as the  $z$  component of the wave vector has to fulfil

$$k^2 = k_x^2 + k_y^2 + k_z^2 = \left(\frac{2\pi}{\lambda}\right)^2 . \quad (18.2)$$

We can extend<sup>1</sup> this to an arbitrary field in the plane  $z = z_0$ , i.e.  $u(x, y; z = z_0)$ . We decompose this field into its Fourier components<sup>2</sup>

<sup>1</sup> Novotny and Hecht, 2012, chapter 2.12.

<sup>2</sup> In this chapter, small letters refer to real-space quantities, capital letters to the corresponding Fourier space quantities.



$$U(k_x, k_y; z_0) = \iint u(x, y; z_0) e^{-i(k_x x + k_y y)} dx dy = \mathcal{FT}(u) \quad (18.3)$$

This is the *angular spectrum representation* of the field. Each Fourier component describes a plane wave with given spatial frequencies in  $x, y$  direction and a fixed  $k_z$  component and thus a given angular propagation direction. For each plane wave, we know thus the field everywhere in space. This allows us to write

$$u(x, y, z) = \frac{1}{(2\pi)^2} \iint U(k_x, k_y; z_0) e^{i(k_x x + k_y y + k_z z)} dk_x dk_y \quad (18.4)$$

where  $k_z$  has to fulfill eq. 18.2 and thus can have both signs. The prefactor differs from Goodman, 2005, as here we use  $k_x = 2\pi f_x$  as reciprocal variable.

## Transfer function of free space

It will be convenient to relate the angular spectrum  $U(k_x, k_y; z_0)$  at the position  $z_0$  to that at some other position  $z = z_0 + d$

$$U(k_x, k_y; z_0 + d) = U(k_x, k_y; z_0) \cdot H(k_x, k_y; d) \quad (18.5)$$

where  $H$  is the transfer function of free space<sup>3</sup>. Combining eq. 18.3 and 18.4 we get

<sup>3</sup> Saleh and Teich, 1991, chapter 4.1.B.

$$H(k_x, k_y; d) = e^{i d \sqrt{k^2 - k_x^2 - k_y^2}} = e^{i k d \sqrt{1 - k_{\parallel}^2/k^2}} \quad (18.6)$$

The transfer function  $H$  relates (complex) amplitudes of spatial frequencies at position  $z_0$  to those at some distance  $d$  apart. When  $k_{\parallel}^2 = k_x^2 + k_y^2 < k^2$ , i.e., the  $k_{x,y}$  are within a circle of radius  $k$ , then  $|H| = 1$  and only a phase-factor is introduced. This is the phase that the plane wave acquires when traveling the distance  $d$ . However, when  $k_{\parallel}^2 > k^2$ , the square root becomes imaginary and  $|H| < 1$ . The amplitude of these plane waves is exponentially decaying with distance  $d$ . These are called evanescent waves. For large distances  $d$  we can assume

$$H(k_x^2 + k_y^2 > k^2; d \gg \lambda) \approx 0 \quad (18.7)$$

Propagation in free space acts as low-pass filter for spatial frequencies. Plane waves corresponding to spatial frequencies larger than  $k$  can not propagate very far.

## Fresnel approximation

We can simplify the transfer function  $H$  by assuming that the spatial frequencies  $\nu_{x,y}$  are small compared to  $1/\lambda$ , or  $k_{\parallel} \ll k$ . In this case, we can neglect the third and higher terms in

$$\sqrt{1 - \frac{k_{\parallel}^2}{k^2}} \approx 1 - \frac{k_{\parallel}^2}{2k^2} + \frac{k_{\parallel}^4}{8k^4} - \dots \quad (18.8)$$

and the transfer function becomes

$$H(k_x, k_y; d) \approx e^{i k d} e^{-i d k_{\parallel}^2/(2k)} \quad (18.9)$$

## Impulse response of free space

Instead of multiplying the angular spectrum  $U(k_x, k_y; z_0)$  with the transfer function  $H(k_x, k_y; d)$ ,

$$U(k_x, k_y; z_0) \times H(k_x, k_y; d) \quad (18.10)$$

we could apply the Fourier transform to both, i.e., convolve the electrical field with the impulse response  $h(x, y; d)$ , i.e.,

$$u(x, y; z_0) \otimes \mathcal{FT}(H(k_x, k_y; d)) = u(x, y; z_0) \otimes h(x, y; d) \quad (18.11)$$

where  $\otimes$  denotes the convolution operation.

In the Fresnel approximation, the impulse response  $h$  of free space is

$$h(x, y; d) \approx \frac{e^{i k d}}{d} e^{i \frac{k}{2d} (x^2 + y^2)} \quad (18.12)$$

This is equivalent to the Huygens principle limited to the Fresnel approximation, i.e., small angles to the optical axis. Each point is source of a spherical wave, or

$$h(x, y; d) = \frac{1}{\sqrt{x^2 + y^2 + d^2}} e^{i k \sqrt{x^2 + y^2 + d^2}} \quad (18.13)$$

## A thin lens

The transfer function of a thin lens introduces a phase shift depending on the distance to the optical axis. When we assume that the lens is spherical (radius  $R$ ) and plano-convex, we get for  $x^2 + y^2 \ll R$

$$h(x, y) = h_0 e^{-i k \frac{x^2 + y^2}{2f}} \quad \text{with} \quad f = \frac{R}{n - 1} \quad (18.14)$$

where  $n$  is the index of refraction of the lens material (embedded in vacuum with  $n = 1$ ) and  $f$  is the usual focal length. The same hold for all other thin lenses with a given focal length  $f$  (but the different relation to the radius of curvature). The factor  $h_0$  takes a global phase factor into account, stemming from the optical thickness on the optical axis. In most cases, it can be neglected.

As a lens has only a finite size, one introduces an aperture function  $p(x, y)$  that describes the transmission of the lens as function of radial position  $(x, y)$ . For a circular aperture of radius  $r_L$  we have

$$p(x, y) = \Theta(r_L^2 - (x^2 + y^2)) \quad (18.15)$$

where  $\Theta$  is the Heaviside step function.

## Fourier transformation by a lens I

First we demonstrate that the field in the focal plane at the distance  $f$  after the lens is almost the Fourier transform of the field just in front of the lens.<sup>4</sup>

Let  $u_L(x, y)$  be the field just in front of the lens. Just after the lens, we thus have

$$u_{L'}(x, y) = u_L(x, y) \cdot e^{-i k \frac{x^2 + y^2}{2f}} \cdot p(x, y) \quad (18.16)$$

<sup>4</sup> Goodman, 2005, chapter 5.2.1.

where we neglected all constant phase factors.

In the focal plane at distance  $f$ , we call our coordinates  $(u, v)$  and get the field in the Fresnel approximation by convolution with the impulse response of free space

$$u_f(u, v) = \iint u_{L'}(x, y) f_{\text{free}}(u - x, v - y; d = f) dx dy \quad (18.17)$$

$$= \iint u_{L'}(x, y) e^{i \frac{k}{2f} ((u-x)^2 + (v-y)^2)} dx dy \quad (18.18)$$

again neglecting all constant phase factors. When multiplying out the phase term  $(u - x)^2$ , we get the terms  $u^2 + x^2 - 2ux$ . The term with  $u^2$  can be drawn in front of the integrals. The term with  $x^2$  cancels with that from eq. 18.16, and the cross-term remains, so that we get

$$u_f(u, v) = e^{i \frac{k}{2f} (u^2 + v^2)} \iint u_L(x, y) p(x, y) e^{-i \frac{k}{f} (xu + yv)} dx dy \quad (18.19)$$

$$= e^{i \frac{k}{2f} (u^2 + v^2)} U_{L,p} \left( u \frac{k}{f}, v \frac{k}{f} \right) \quad (18.20)$$

where  $U_{L,p} = \mathcal{FT}(p \cdot u_L)$ . The field in the focal plane  $u_f(u, v)$  is thus the Fourier transform of the field in front of the lens  $u_L(x, y)$  (times the aperture function  $p$ ), decorated by a phase factor squared in the radial distance. When one is interested in intensities, not fields, this phase factor can be neglected.

It makes sense that this relation exists. We can decompose the field in front of the lens into plane waves with wave vector components  $(k_x, k_y)$ . In the limit of small angles, each plane wave will be focused by the lens into a point in the focal plane at position  $u = f k_x / k$ . The amplitude of the field at this point is thus proportional to the Fourier component at  $k_x = uk/f$ .

## Fourier transformation by a lens II

The pre-factor in eq. 18.20 vanishes when we do not look at the field directly in front of the lens but at that one focal length earlier, more towards the source.

Let  $f_0(x, y) = u(x, y; z = -f)$  be the optical field in the first (front) focal plane of the lens. Its Fourier transform is  $F_0(k_x, k_y)$ . We propagate this field to the lens by applying the transfer function of free space, i.e.

$$U_L(k_x, k_y) = F_0(k_x, k_y) \cdot H(k_x, k_y; f) = F_0(k_x, k_y) e^{-i f k_{\parallel}^2 / (2k)} \quad (18.21)$$

We ignore<sup>5</sup> the aperture function  $p$  and get via eq. 18.20

$$u_f(u, v) = e^{i \frac{k}{2f} (u^2 + v^2)} U_L \left( u \frac{k}{f}, v \frac{k}{f} \right) \quad (18.22)$$

$$= e^{i \frac{k}{2f} (u^2 + v^2)} e^{-i f k_{\parallel}^2 / (2k)} F_0 \left( u \frac{k}{f}, v \frac{k}{f} \right) \quad (18.23)$$

$$= F_0 \left( u \frac{k}{f}, v \frac{k}{f} \right) \quad (18.24)$$

where we have used in the last step  $k_{\parallel}^2 = k_x^2 + k_y^2 = (k/f)^2 (u^2 + v^2)$ .

The fields in the first (front) and the second (back) focal plane of a lens are thus related by a Fourier transform, without the quadratic phase function

<sup>5</sup> Goodman also discusses the case with aperture

that comes into play when starting from a field directly at the lens. We will discuss an application of this effect as 'back focal plane imaging' to determine the emission pattern of a dipole in a structured environment in the next chapter.

## Nearfield microscopy

The angular spectrum representation and its transfer function of the free space allows to explain the limited resolution of a conventional optical microscope.<sup>6</sup> A small structure with fine details is equivalent to high spatial frequencies and thus large in-plane wave vectors  $k_{x,y}$ . These waves contain all information of the sample plane, but for  $k_{\parallel} > k$  they are exponentially damped. Far away from the sample, only wave vectors within the range of  $\pm k$  arrive at the detector. These contain only spatial frequencies of  $\lambda/2$  and larger. Smaller objects are blurred to this size.

<sup>6</sup> see chapter 4.6 of Novotny and Hecht, 2012 and Vigoureux and Courjon, 1992

Let us follow the example of Vigoureux and Courjon, 1992 and discuss imaging of a slit. We assume that the sample is a rectangular aperture in an opaque film. We ignore the  $y$  direction to simplify things. We thus have

$$f_0(x) = \Theta(|x| - a/2) = \text{rect}_a(x) \quad (18.25)$$

The Fourier transform is (see appendix B )

$$F_0(k_x) = a \frac{\sin k_x a/2}{k_x a/2} \quad (18.26)$$

The first zero crossing of the sinc-function is at  $k_x = 2\pi/a$ . So if  $a \gg \lambda$ , a very large fraction of the angular spectrum is within the propagation range. Clipping everything outside  $\pm k$  does not significantly change the image when doing the back transformation. The image of the sample is a good representation of the slit (see figure 18.1). Things change, when the size  $a$  decreases. At some point, the image does not become smaller anymore and different slit sizes lead to almost the same image. The size of the image is limited by diffraction.

Near-field microscopy allows to circumvent the diffraction limit. The idea is to keep some information from the wave vectors with  $k_{\parallel} > k$  and let this information propagate into the optical far-field.

Optical diffraction can be understood as adding in-plane momentum from the aperture to the optical wave. Assume we have an optical field of angular spectrum  $U_0(k_x)$  and transmit this field through a mask of transfer function  $m(x)$ , then the field on the other side of the mask would be

$$u_1(x) = m(x) \cdot \mathcal{FT}(U_0) = m(x) \cdot u_0(x) \quad (18.27)$$

or

$$U_1(k_x) = \mathcal{FT}(m) \otimes U_0(k_x) = M \otimes U_0 \quad (18.28)$$

We convolve the angular spectrum of the mask with that of the incoming field. If the mask itself has high enough frequency components, the convolution operation maps back high frequency component of the incoming field into the propagating wave-vector interval.

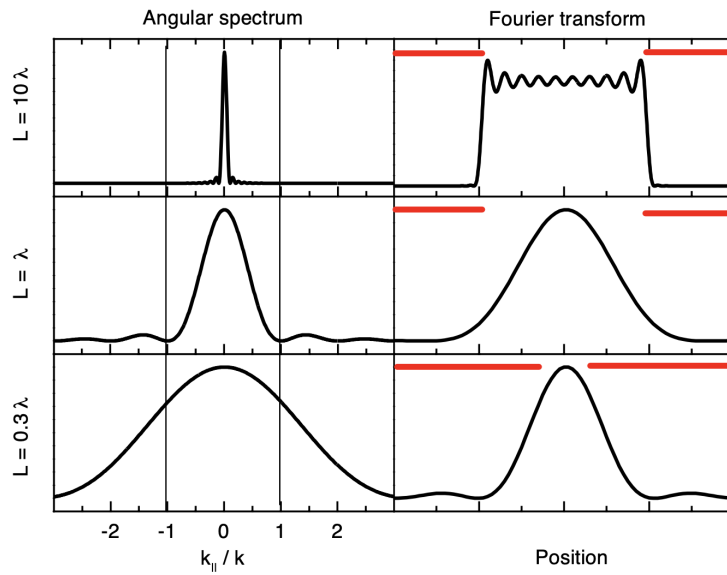


Figure 18.1: Angular spectrum and reconstructed image of the slit (width  $L$ ) after clipping to the propagating wave vector interval. The red bar depicts the size of the slit. The scale of the real-space panel changes.

This is sketched in fig. . The top panel shows the angular spectrum of our sample, again a slit. It contains frequency components  $k_{parallel}/k > 1$ . One of this component,  $K$ , is taken as example. This plane wave is diffracted at a second slit, which we call now probe. The slit / probe needs to be in the near-field of the sample, so that the plane wave with  $k_x = K > k$  still reaches the probe, i.e.  $\Delta z \ll \lambda$ . Diffraction at the slit / probe then leads to some waves in the  $\pm k$  range, which can propagate to the detector.

This procedure does not lead to an image. One can not use a CCD camera. One measures the total arriving power is function of the lateral position of the probe-slit, scans the probe and constructs an image pixel wise. However, the relation between the image generated in this way and the field distribution in the near field can be complicated and needs special attention. But thus example shows that there is the chance of information beyond the diffraction limit. It is also obvious that the size of the probe-slit ideally is (much) smaller than the features of the sample, as otherwise the back-mapping does not work out.

## References

- Goodman, Joseph W. (2005). *Introduction to Fourier optics*. 3. ed. Roberts.  
 Novotny, Lukas and Bert Hecht (2012). *Principles of nano-optics*. 2. ed. Cambridge Univ. Press. [↗](#)  
 Saleh, Bahaa E. A. and Malvin C. Teich (1991). *Fundamentals of photonics*. New York, NY [u.a.]: Wiley. [↗](#)  
 Vigoureux, J.M. and D. Courjon (1992). "Detection of nonradiative fields in light of the Heisenberg uncertainty principle and the Rayleigh criterion". In: *Applied Optics* 31.16, pp. 3170–3177. [↗](#)

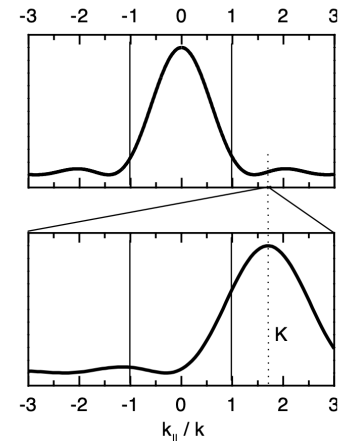


Figure 18.2: Diffraction at a slit maps back high frequency components.



# Chapter19

## Dipole emission at interfaces

Markus Lippitz

February 7, 2023

### Tasks

Reproduce Fig. 2 of Huang et al., 2021, i.e.,

- Calculate the collection efficiency for the dipole emission in the layered structure depending on wavelength and NA of the objective.
- Calculate the Purcell factor of the dipole in such a structure. Does the emitter launch surface plasmons on the metal layers?
- Calculate the angular emission pattern. Panel (d) shows as radial coordinate the emission angle  $\theta$  to the surface normal, or equivalently, the back focal plane of the microscope objective.

### Introduction

The angular emission pattern of a dipole follows in free space the typical  $\sin^2 \theta$  shape. In this chapter, we will investigate how this shape is influenced by the environment of the dipole, which we assume to consist of planar layers of dielectric and metals. We make use of the T-matrix method introduced in chapter 15 and the angular spectrum representation of chapter 18. As we have already seen in chapter 9, the environment can not only change the emission direction, but also the emission rate and center frequency of an oscillator. This Purcell effect comes back here.

### A planar optical antenna for a quantum dot

A quantum dot is an inclusion of a few nanometers size of a low bandgap semiconductor in an environment of larger bandgap. It forms a 3D particle-in-a-box, leading to discrete energy levels for the electron wave function. Its optical properties are thus dominated by discrete transition energies, similar to a single atom in vacuum. For the purpose of this chapter, we can model the quantum as point-like optical transition dipole.



This work is licensed under a [Creative Commons "Attribution-ShareAlike 4.0 International"](https://creativecommons.org/licenses/by-sa/4.0/) license.

The emission pattern of a dipole in free space assumes a  $\sin^2 \theta$  shape. When embedded in a semiconductor matrix with an index of refraction of about  $n = 3.5$ , reflection of the air-semiconductor interface can not be neglected. More than 90% of the emission ends up into the direction of the semiconductor half-space, but detection has to be outside the semiconductor, in the air side. Additionally, the collecting objective can not cover the whole solid angle of  $2\pi$ , as its numerical aperture is limited.

The idea of Huang et al., 2021 is to sandwich the quantum dot layer between two metal layers, acting similar to a Fabry-Perot resonator. The emission rate is enhanced due to the Purcell effect, but also the emission direction is modified to a smaller solid angle, so that more light can be collected by an objective. The authors compare the Purcell factor (Fig 5a) the collection efficiency (Fig 5b). The angular emission pattern (Fig. 4c) is measured in the back focal plane. The reflection spectrum of the cavity (Fig. 4a) allows to match the simulations (Fig. 2) to the experiment.

## A dipole in front of a dielectric half-space

As a first step, we discuss the excitation or emission properties of a single molecule, modelled as point dipole, in front of a dielectric half space. The dielectric should be glass ( $n = 1.5$ ), the distance of the dipole to the interface  $d = 20$  nm, and the other half-space air. We assume  $\lambda = 633$  nm. When light comes in from the air side, the dipole is excited directly and by reflection from the interface. When light comes in from the glass side, we can observe total internal reflection and the dipole is excited by evanescent waves. In emission, the same processes take place in reverse. The transmission matrix method is not strictly needed for this problem, but we get started and it helps to compare to direct analytical results in Novotny and Hecht, 2012, figure 10.9 of the first edition.

We want to calculate the field at the position of the molecule. In the T-matrix method, we take it as starting, left most point of our layered medium. Next to the right comes again air, so that we do not need an interface matrix, but only a propagation matrix  $\mathbf{M}_{\text{prop}}$  (eq. 15.15) with  $d_1 = 20$  nm and  $n_1 = 1$ . Next comes the interface with a jump in the index of refraction from  $n_1 = 1$  to  $n_2 = 1.5$ . We model this by the interface matrix  $\mathbf{M}_{12}$  (eq. 15.23). The total matrix of our layered medium is thus

$$\mathbf{M}_{\text{total}} = \mathbf{M}_{12} \mathbf{M}_{\text{prop}} = \frac{1}{2\eta} \begin{pmatrix} (1 + \kappa)e^{+i k_{z,1} d_1} & (1 - \kappa)e^{-i k_{z,1} d_1} \\ (1 - \kappa)e^{+i k_{z,1} d_1} & (1 + \kappa)e^{-i k_{z,1} d_1} \end{pmatrix} \quad (19.1)$$

Remember that we describe the system from left to right, but multiply the matrices from right to left.

It is most convenient to transfer the transmission matrix  $\mathbf{M}_{\text{total}}$  into a scattering matrix (eq. 15.7) and extract the transmission  $t_{21}^{(s,p)}$  and reflection coefficients  $r_{12}^{(s,p)}$ . Using the definition of the vectorial field components (eq. 15.12), we calculate the field at the position of the molecule<sup>1</sup>. When a wave is incident from the air side with amplitudes  $E^{(s,p)}$  of the s and p-component, we get<sup>2</sup> with the length of the wave vector in medium one  $k_1 = n_1 k_0$

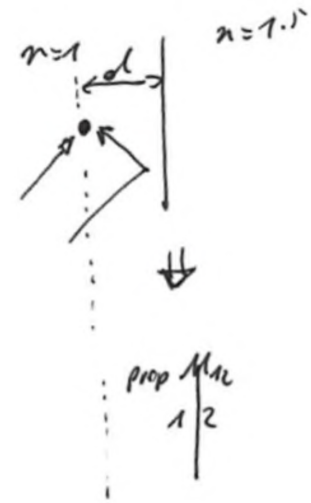


Figure 19.1: A dipole is situated at a distance  $d$  in front of a air-glass-interface. This needs two matrices  $\mathbf{M}_{\text{prop}}$  and  $\mathbf{M}_{12}$ .

<sup>1</sup> see also eq. 2.01 in Novotny and Hecht, 2012

<sup>2</sup> These fields agree with the potentials  $\Phi$  of Novotny and Hecht, 2012 eq. 10.33–38 when taking the corresponding projections  $\sin \theta$ ,  $\cos \theta$  into account, plus an additional phase flip of 180 degrees for the glass side.

$$\mathbf{E}_{\text{air}} = \begin{pmatrix} (1 - r_{12}^{(p)}) \frac{k_{z,1}}{k_1} \\ 0 \\ (1 + r_{12}^{(p)}) \frac{k_x}{k_1} \end{pmatrix} E^{(p)} + \begin{pmatrix} 0 \\ 1 + r_{12}^{(s)} \\ 0 \end{pmatrix} E^{(s)} . \quad (19.2)$$

For incidence from the glass side, we find

$$\mathbf{E}_{\text{glass}} = \begin{pmatrix} -t_{21}^{(p)} \frac{k_{z,1}}{k_1} \\ 0 \\ t_{21}^{(p)} \frac{k_x}{k_1} \end{pmatrix} E^{(p)} + \begin{pmatrix} 0 \\ t_{21}^{(s)} \\ 0 \end{pmatrix} E^{(s)} . \quad (19.3)$$

Note that the  $z$  components changes sign together with the  $k_x$ . Going away from perpendicular incidence in direction of  $+\theta$  gives therefore a different  $E_z$  than for  $-\theta$ .

The direction of a light beam can be reversed. This also holds for switching from absorption to emission of a dipole. To calculate the angular emission pattern of a dipole, it is thus convenient to calculate how well such a dipole could be excited from the direction given by the polar angle  $\theta$  and azimuthal angle  $\phi$ . We calculate the field at the position of the molecule for plane waves coming under an angle  $\theta = \arcsin k_x / (n_j k_0)$ . Following Novotny and Hecht, 2012 chapter 10, we call angles  $\theta = -90^\circ \dots 90^\circ$  coming from the air half space, and angles  $\theta = 90^\circ \dots 270^\circ$  coming from the glass half-space. It is sufficient to calculate 0 to  $180^\circ$  and apply the sign flip of the last paragraph for the second half circle. For the azimuthal angle  $\phi$ , only the relative angle between dipole and field matters, so that we can also rotate the dipole and keep the simple form of the fields. For convenience, we combine the field  $\mathbf{E}_{\text{air}}$  and  $\mathbf{E}_{\text{glass}}$  from above to a single field  $\mathbf{E}(\theta)$

$$\mathbf{E}(\theta) = \mathbf{E}_{\text{air}} f(\theta) + \mathbf{E}_{\text{glass}} (1 - f(\theta)) \quad (19.4)$$

with a suitable switching function  $f(\theta)$ . The components of this field are  $E_{x,y,z}$ , and we set  $E^{(s)} = E^{(p)} = \sqrt{1/2}$ . We construct an angle-dependent index of refraction in the same way

$$n(\theta) = n_1 f(\theta) + n_2 (1 - f(\theta)) . \quad (19.5)$$

The absorption rate of a field  $\mathbf{E}$  into a dipole  $\mu$  is proportional to  $|\mu \cdot \mathbf{E}|^2$ . As orthogonally polarized fields do not interfere, we have to sum the two polarization directions  $|\mu \cdot \mathbf{E}^{(s)}|^2 + |\mu \cdot \mathbf{E}^{(p)}|^2$ . The normalized power emitted into the direction  $(\theta, \phi)$  is thus<sup>3</sup>

$$\frac{P(\theta, \phi)}{P_0} = \frac{3}{8\pi} \frac{n(\theta)}{n_1} \frac{1}{|\mu|^2} \left[ |\mu \cdot \mathbf{E}^{(s)}|^2 + |\mu \cdot \mathbf{E}^{(p)}|^2 \right] \quad (19.6)$$

or<sup>4</sup>

$$\begin{aligned} \frac{P(\theta, \phi)}{P_0} = \frac{3}{8\pi} \frac{n(\theta)}{n_1} \frac{1}{|\mu|^2} & \left[ \mu_z^2 |E_z|^2 \right. \\ & + (\mu_x \cos \phi + \mu_y \sin \phi)^2 |E_x|^2 \\ & + (\mu_x \sin \phi - \mu_y \cos \phi)^2 |E_y|^2 \\ & \left. - \mu_z (\mu_x \cos \phi + \mu_y \sin \phi) (E_z^* E_x + E_x^* E_z) \right] \end{aligned} \quad (19.7)$$

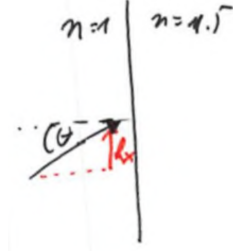


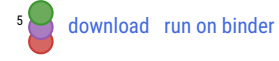
Figure 19.2: Definition of  $\theta$ .

<sup>3</sup> This reproduces Fig. 10.9 in the first edition of Novotny and Hecht, 2012.

<sup>4</sup> See also eq. 10.43 of Novotny and Hecht, 2012

The interference of the x and z-component of the field in  $\mathbf{E}^{(p)}$  leading to the last line of eq. 19.7 removes the rotational symmetry of the emission pattern. To plot a 3D polar emission pattern, one thus needs to cover  $\theta = 0 \dots 2\pi$  and  $\phi = 0 \dots \pi$  and not the other way round. When integrating the power into a cone around the z-axis, for example into a microscope objective, this last term averages out and could be neglected.

The Pluto script `dipole_at_interface`<sup>5</sup> plots the 3D angular emission pattern of a dipole in front of a glass surface, using a scheme that is also able to calculate the more complicated layer structures discussed below.



## A dipole between two metal layers

In the last section, the dipole has been on one side of a layered medium. Now we put it in one layer that is embedded from both sides in layered media. We describe both sides by transmission matrices  $\mathbf{M}_{\text{left}}$  and  $\mathbf{M}_{\text{right}}$  that can be generated by multiplying a sequence of interface and propagation matrices. We label the left-most medium 1, the right-most 3 and the medium that surround the dipole 2. This surrounding layer has a total thickness  $L$ . The dipole has a distance  $l_L$  from the left interface and  $l_R$  from the right interface, so that  $L = l_L + l_R$ . The product leading to the transmission matrix  $\mathbf{M}_{\text{left}}$  ends thus with a propagation matrix of thickness  $l_L$ , while that for  $\mathbf{M}_{\text{right}}$  starts with propagation matrix of thickness  $l_R$ .

We want to calculate the fields in layer 2 when light comes in either from left or right. Let us discuss the case that light is coming from right. The amplitudes of the waves outside the layered medium are given by

$$\begin{pmatrix} U_3^+ \\ U_3^- \end{pmatrix} = \mathbf{M}_{\text{right}} \cdot \mathbf{M}_{\text{left}} \begin{pmatrix} 0 \\ U_1^- \end{pmatrix} \quad \text{and} \quad \begin{pmatrix} U_2^+ \\ U_2^- \end{pmatrix} = \mathbf{M}_{\text{left}} \begin{pmatrix} 0 \\ U_1^- \end{pmatrix} \quad (19.8)$$

We shine in a wave of amplitude  $U_3^-$ , of which the amplitude  $U_3^+$  is reflected and  $U_1^-$  is transmitted. Nothing enters the structure from left. In the calculation, we have free choice of the amplitude  $U_1^-$  which we set for convenience to one. The overall reflection and transmission of the layered medium for illumination from right is then

$$r_{31} = \frac{U_3^+}{U_3^-} \quad \text{and} \quad t_{31} = \frac{1}{U_3^-} \quad (19.9)$$

The relative amplitudes of the fields in the layer of the dipole are for illumination from the right side

$$E_2^+ = \frac{U_2^+}{U_3^-} \quad \text{and} \quad E_2^- = \frac{U_2^-}{U_3^-} \quad (19.10)$$

The case of illumination from the left is inconvenient in this transmission matrix formalism.<sup>6</sup> However, we can switch to the scattering matrix and recover results of a Fabry-Perot interferometer. We see the left and right stack of layered media as left and right mirror in a Fabry-Perot interferometer. The separation is zero, as all phase factors are included in the reflectivity of the mirrors. We get

$$\begin{pmatrix} U_2^+ \\ U_2^- \end{pmatrix} = \frac{1}{t_{21}} \begin{pmatrix} t_{12}t_{21} - r_{12}r_{21} & r_{21} \\ -r_{12} & 1 \end{pmatrix} \cdot \begin{pmatrix} 0 \\ 1 \end{pmatrix} = \frac{1}{t_{21}} \begin{pmatrix} r_{21} \\ 1 \end{pmatrix} \quad (19.11)$$

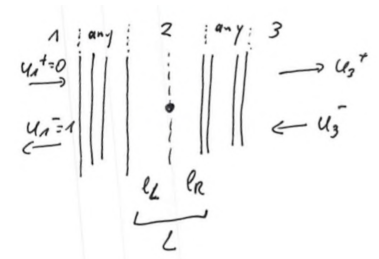


Figure 19.3: A dipole is situated inside a stack of planar media. The outermost are labelled 1 and 3, the medium around the dipole is labelled 2. The other layers are summed up in the respective matrices.

<sup>6</sup> Most easy is probably to flip the layers and calculate again for illumination from right

and

$$\begin{pmatrix} U_3^+ \\ U_3^- \end{pmatrix} = \frac{1}{t_{32}t_{21}} \begin{pmatrix} t_{21}t_{32} - r_{21}r_{32} & r_{32} \\ -r_{32} & 1 \end{pmatrix} \cdot \begin{pmatrix} r_{21} \\ 1 \end{pmatrix} \quad (19.12)$$

$$= \frac{1}{t_{32}t_{21}} \begin{pmatrix} (t_{21}t_{32} - r_{21}r_{32})r_{21} + r_{32} \\ -r_{32}r_{21} + 1 \end{pmatrix} \quad (19.13)$$

The overall reflection is thus<sup>7</sup>

$$r_{31} = \frac{U_3^+}{U_3^-} = \frac{(t_{21}t_{32} - r_{21}r_{32})r_{21} + r_{32}}{1 - r_{32}r_{21}} \quad (19.14)$$

and overall transmission

$$t_{31} = \frac{1}{U_3^-} = \frac{t_{32}t_{21}}{1 - r_{32}r_{21}} \quad (19.15)$$

The fields at the dipole for illumination from the right, i.e. medium 3, are

$$E_2^+ = \frac{U_2^+}{U_3^-} = \frac{r_{21}t_{32}}{1 - r_{32}r_{21}} \quad \text{and} \quad E_2^- = \frac{U_2^-}{U_3^-} = \frac{t_{32}}{1 - r_{32}r_{21}} \quad (19.16)$$

With this it is easy to get the field for illumination from the left, i.e. medium 1, by swapping the indices 1 and 3 and the direction of travel

$$E_2^- = \frac{r_{23}t_{12}}{1 - r_{12}r_{23}} \quad \text{and} \quad E_2^+ = \frac{t_{12}}{1 - r_{12}r_{23}} \quad (19.17)$$

Note that the denominator is the same in all four cases, as  $r_{ij} = -r_{ji}$ . It is the field-enhancement factor inside a Fabry-Perot cavity  $\mathcal{F}$

$$\mathcal{F}^{(s,p)} = \frac{1}{1 - r_{12}^{(s,p)} r_{23}^{(s,p)}} \quad (19.18)$$

The vectorial field components are

$$\mathbf{E} = E_0 \cdot \begin{pmatrix} \pm \mathcal{F}^{(p)} t_{i2}^{(p)} \left(1 - r_{2j}^{(p)}\right) \frac{k_{z,2}}{k_2} \\ \mathcal{F}^{(s)} t_{i2}^{(s)} \left(1 + r_{2j}^{(s)}\right) \\ \mathcal{F}^{(p)} t_{i2}^{(p)} \left(1 + r_{2j}^{(p)}\right) \frac{k_x}{k_2} \end{pmatrix} \quad (19.19)$$

with  $(ij) = (13)$  or  $(31)$ . The  $\pm$  decides on the direction of travel of the incident beam. When setting  $t_{12} = 1$  and  $r_{21} = 0$  we recover the result for a dipole on one side of a layered medium.

These field components can be put into eq. 19.6 to obtain the angular emission pattern of a dipole inside a layered medium. The results agree<sup>8</sup> with the approach of Polerecky, Hamrle, and MacCraith, 2000.

<sup>7</sup> Take care.  $r_{21}$  and  $r_{12}$  might be mixed up. See Christoph's thesis.

<sup>8</sup> implemented by Klas Lindfors as 'angulardistribution.m' in Matlab

## Decay rate in a layered medium

Up to now we assumed that the dipole emission is only altered in its propagation direction in the far-field, which changes the angular emission pattern. However, the local environment acts back on the dipole, changing its emission rate and oscillation frequency. This is called *Purcell effect* and is subject of chapter 9. We repeat here the essential steps and then proceed to layered media.

In a classical description, an electric dipole is following a damped harmonic oscillation. We do not care how this oscillation has started, but just follow its evolution afterwards. The dipole emits radiation that is reflected back by the environment and then acts as 'driving' term on the dipole<sup>9</sup>

$$\ddot{\mu} + \gamma_0 \dot{\mu} + \omega_0^2 \mu = \frac{q^2}{m} E_s(t) \quad (19.20)$$

Let us first discuss the dipole alone, without back-scattered field. It will oscillate with a frequency

$$\omega = \sqrt{\omega_0^2 - \frac{1}{4}\gamma_0^2} \quad (19.21)$$

and its oscillation amplitude will decay proportional to  $\exp(-\gamma_0 t/2)$  (the stored energy drops as  $\exp(-\gamma_0 t)$ ). We now require that all energy removed from the oscillator is converted into radiated power and no other sources of damping are present. This fixes the damping rate<sup>10</sup>

$$\gamma_0 = \frac{1}{4\pi\epsilon_0} \frac{2q^2\omega_0^2}{3mc^3} \quad (19.22)$$

When we now include the back-scattered field, we find<sup>11</sup> that both the damping rate and the oscillation frequency change. Not even the emission frequency is the property of an emitter alone, but also it is influenced by the environment.

$$\frac{\gamma}{\gamma_0} = 1 + q_e \frac{6\pi\epsilon_0}{|\mu_0|^2} \frac{1}{k^3} \Im(\mu_0^* \cdot E_s(r_0)) \quad (19.23)$$

$$\frac{P}{P_0} = \left. \frac{\gamma}{\gamma_0} \right|_{q_e=1} \quad (19.24)$$

$$\frac{\Delta\omega}{\gamma_0} = q_e \frac{3\pi\epsilon_0}{|\mu_0|^2} \frac{1}{k^3} \Re(\mu_0^* \cdot E_s(r_0)) \quad (19.25)$$

where  $q_e$  is the quantum efficiency of the emitter. As the amplitude of  $E_s(r_0)$  at the position of the dipole depends on the dipole's oscillation amplitude  $|\mu_0|$ , the latter cancels out, as expected.

One way to calculate  $E_s(r_0)$ , the field of the source at the source, is to use the dyadic Green's function as shown in Novotny and Hecht, 2012 and Hohenester, 2020. The idea is to write the field emitted by the dipole in k-space, including all near- and far-field components. This is the *angular spectrum representation* of chapter 18, leading to an 2D integral over all directions in k-space. The field scattered back to the dipole are these fields multiplied by the corresponding Fresnel reflection coefficients and taking the travelling phase into account.<sup>12</sup> One integrates over  $\phi$  analytically, and remains with an 1D integral over  $q = k_{\parallel}/k_0$  or equivalently over

$$s = \frac{k_{\parallel}}{k_{\text{medium}}} = \frac{q}{\sqrt{\epsilon_{\text{medium}}}} \quad \text{and} \quad s_z = \sqrt{1 - s^2} \quad , \quad (19.26)$$

where  $k_0$  is here the length of the wave vector in vacuum. We do not discuss the details of the calculations but only give the results.

Let us first look at the case of a dipole on one side of a layered medium, i.e. the example of the dipole in front of dielectric half-space discussed above. We assume again that the phase-lag of the travel to the interface is included in the reflection coefficient and get for the decay rate<sup>13</sup>

<sup>9</sup> Novotny and Hecht, 2012, chapter 8.5.2.

<sup>10</sup> Novotny and Hecht, 2012.

<sup>11</sup> Novotny and Hecht, 2012, chapter 8.5.2.

<sup>12</sup> These are plane waves, not beams, so reflections come back.

<sup>13</sup> Novotny and Hecht, 2012, eq. 10.26, and Ford and Weber, 1984, eq. 3.31

$$\begin{aligned} \frac{\gamma}{\gamma_0} = & 1 + q_e \frac{|\mu_{\parallel}|^2}{|\mu|^2} \frac{3}{4} \int_0^{\infty} \Re \left( \frac{s}{s_z} r_{12}^{(s)} - s s_z r_{12}^{(p)} \right) ds \\ & + q_e \frac{|\mu_{\perp}|^2}{|\mu|^2} \frac{3}{2} \int_0^{\infty} \Re \left( \frac{s^3}{s_z} r_{12}^{(p)} \right) ds. \end{aligned} \quad (19.27)$$

When the dipole is situated inside a layered medium, we again get Fabry-Perot like multiple reflections. These can be summed up and result in<sup>14</sup>

<sup>14</sup> Ford and Weber, 1984, eq. 3.38.

$$\begin{aligned} \frac{\gamma}{\gamma_0} = & 1 - q_e + q_e \frac{|\mu_{\parallel}|^2}{|\mu|^2} \frac{3}{4} \int_0^{\infty} \Re \left( \frac{s}{s_z} \frac{(1 + r_{23}^{(s)})(1 + r_{21}^{(s)})}{1 - r_{21}^{(s)} r_{23}^{(s)}} \right) ds \\ & + q_e \frac{|\mu_{\parallel}|^2}{|\mu|^2} \frac{3}{4} \int_0^{\infty} \Re \left( s s_z \frac{(1 - r_{23}^{(p)})(1 - r_{21}^{(p)})}{1 - r_{21}^{(p)} r_{23}^{(p)}} \right) ds \\ & + q_e \frac{|\mu_{\perp}|^2}{|\mu|^2} \frac{3}{2} \int_0^{\infty} \Re \left( \frac{s^3}{s_z} \frac{(1 + r_{23}^{(p)})(1 + r_{21}^{(p)})}{1 - r_{21}^{(p)} r_{23}^{(p)}} \right) ds \end{aligned} \quad (19.28)$$

The term  $-q_e$  corrects what would remain if all reflection coefficients  $r_{ij}$  would be set to zero. A similar form exists also for the single-sided variant above (Ford and Weber, 1984, eq. 3.30). Note that the denominator differs in the 'direction' of the reflection coefficient  $r_{21}$  from the Fabry-Perot field-enhancement factor  $\mathcal{F}$  defined above. When applied to our example of two metal layers, this equation reproduces results obtained by the Matlab implementation of Ford and Weber, 1984, eq. 3.38., given by Jun, 2010.

It is interesting to look at the integrand in these equations. The interval  $s = 0 \dots 1$  corresponds to plane waves that can propagate into the far-field, although some might undergo total internal reflection. The remaining make up the power that is detectable in the emission pattern discussed above.<sup>15</sup> The remaining part of  $s = 1 \dots \infty$  corresponds to evanescent waves. Their exponential decay is contained in the phase factor of the reflection coefficients, as here  $k_{2,z}$  become imaginary. However, in the near-field they play a role. Reflecting surfaces in the near-field of the dipole modify its emission pattern. The power associated with these values of  $q$  is either dissipated in the environment, or travels as bound modes with  $k_{\parallel} > k_2$ , for example as surface plasmon. This allows to estimate the excitation efficiency of surface plasmons by integrating eq. 19.28 over a suitable interval of  $s$ . Typically, one uses  $s = 1 \dots (2s_{\text{plasmon}} - 1)$ , which is centered on  $s_{\text{plasmon}}$  and starts at  $s = 1$ .

<sup>15</sup> When embedded in air, this corresponds to  $q = 0 \dots 1$ , but using  $q$ , not  $s$ !

### Side remark: Lossy modes are required

We found above bound modes of the multilayer system by searching for zeros the matrix element  $D$  of the transmission matrix  $\mathbf{M}$ . In the example of a single interface (or a very thick slab), we found with eq. 15.30 a relation between the dielectric functions  $\epsilon_i$  and the parallel component  $k_{z,\text{plasmon}}$  of the wave vector. For this value, the matrix element  $D$  vanishes. However, in eq. 15.7 we required that  $D$  would be different from zero, and we used this equation to calculate the decay rates (eq. 19.27 and 19.28). How does this fit?

One way out is the complex dielectric function  $\epsilon_i$ . With this, also  $k_{z,\text{plasmon}}$  in eq. 15.30 becomes complex. The zero of  $D$  does thus not occur along the real axis, which is the axis along which we integrate the decay

rates eq. 19.27 and 19.28. The problem only occurs when looking at purely dielectric systems, using purely real dielectric functions. But purely real dielectric functions violate anyway the Kramers-Kronig relation and thus causality. These should be avoided.

It is interesting to note in the complex 2D plane around  $k_{z,\text{plasmon}}$  the absolute value of the reflection coefficient  $r_{21}^{(p)}$  approaches zero, which is reached at the complex  $k_{z,\text{plasmon}}$  of eq. 15.30. However,  $r_{21}^{(p)}$  is not continuous when approaching the real axis. Along the real axis of  $k_z$ ,  $r_{21}^{(p)}$  shows a maximum very close to  $\Re(k_{z,\text{plasmon}})$ . This maximum is for a metal-dielectric interface much larger than one and leads to the peak in the decay rate.<sup>16</sup>

<sup>16</sup> Some analytic equations would be nice ...

## References

- Ford, G.W. and W.H. Weber (1984). "Electromagnetic interactions of molecules with metal surfaces". In: *Physics Reports* 113.4, pp. 195–287. [↗](#).
- Hohenester, Ulrich (2020). *Nano and Quantum Optics. An Introduction to Basic Principles and Theory*. Springer. [↗](#).
- Huang, Huiying et al. (2021). "Bright Single Photon Emission from Quantum Dots Embedded in a Broadband Planar Optical Antenna". In: *Advanced Optical Materials*, p. 2001490. [↗](#).
- Jun, Young Chul (2010). "Plasmonic Control Of Light Emission: Tailoring Light Emission Properties With Metal Nanostructures". PhD thesis. Stanford University. [↗](#).
- Novotny, Lukas and Bert Hecht (2012). *Principles of nano-optics*. 2. ed. Cambridge Univ. Press. [↗](#).
- Polerecky, Lubos, Jaroslav Hamrle, and Brian D MacCraith (2000). "Theory of the radiation of dipoles placed within a multilayer system". In: *Applied Optics* 39.22, pp. 3968–3977. [↗](#).



## **Appendices**



# Appendix A

## Julia and Pluto

Markus Lippitz  
September 24, 2021

We use the programming language *Julia*<sup>1</sup> for graphical illustrations and numerical 'experiments' in this course. I am convinced that only when you can persuade a computer to do something, to display a model, to calculate a value, only then you have really understood it. Before that, you just haven't seen all the problems.

<sup>1</sup> <https://julialang.org>

You can use Julia with different user interfaces. We use *Pluto*.<sup>2</sup>

<sup>2</sup> <https://github.com/fonsp/Pluto.jl>

### Julia

Julia is a programming language designed for numerics and scientific computing. It is a middle ground between Matlab, Python, and R. In my view, it takes the best of each of these worlds, making it especially suitable for beginners. We will discuss several example scripts together during the semester, and there will also be numerical practice problems.

### An example

First, let's look at a simple example.

```
using Plots
x = range(0, 2 * pi; length=100)
plot(x, sin.(x); label="ein Sinus")
```

For some things you need libraries which you can load with `using`. When choosing libraries, first stick to the examples I show.

Then we define a variable `x` (simply by using it) as an equidistant 'number string' between 0 and  $2\pi$  with 100 values. Functions like `range` always have required parameters defined by their position in the parameter list (here: start and end value), plus other optional ones. These follow after a semicolon in the form `<parameter>=<value>`.

Finally, we draw the sine function over this range of values. Notice the dot in `sin.(x)`. It means 'apply `sin` to all elements of `x`'. This is very convenient.



This work is licensed under a [Creative Commons "Attribution-ShareAlike 4.0 International"](https://creativecommons.org/licenses/by-sa/4.0/) license.

## Sources of information

The current version of Julia is 1.6.2. Some things have changed with version 1.0. Ignore websites that are older than 2 years or that refer to a version before 1.0.

*official documentation* on the website<sup>3</sup>. Or ask google with 'Julia' as keyword or with the library / function and appended extension '.jl'.

*examples* Julia by example<sup>4</sup>, Think julia<sup>5</sup>, Introduction to Computational Thinking<sup>6</sup>

*differences* comparison<sup>7</sup> with Matlab, Python, and other languages, and similarly as an overview table<sup>8</sup>

*Cheat Sheets* general<sup>9</sup> and for plots<sup>10</sup>

## User interfaces

There are several ways to write shorter or longer programs in Julia. Here is a selection

*command line and editor* One can use Julia interactively at the command line (REPL, read-eval-print loop). In an external editor one could write repeating commands in script files.

*IDE* This is more comfortable with an integrated environment, for example Juno<sup>11</sup>, or a Julia extension<sup>12</sup> for Visual Studio Code. This is certainly the approach for larger projects.

*Jupyter notebook* Jupyter<sup>13</sup> is composed of Julia, Python and R. These three languages can be used in a notebook format. Program code is in cells, the output and also descriptive text and graphics in between. This is particularly suitable if calculations are to be accompanied by descriptions or equations, for example in lab protocols or exercises.

Mathematica has a similar cell concept. One drawback is that cells affect the state of the kernel in the order in which they are executed. However, the order need not be the same as in the file; in particular, deleting cells does not change the kernel. This can be very confusing, or you may have to restart the kernel often.

*Pluto* One can also mix program code, text and graphics in Pluto<sup>14</sup>. The cell concept of Pluto is that of Excel, however, limited to one Excel column. The arrangement of equations in the cells does not matter. Everything is re-evaluated after each input. A logic in the background ensures that only absolutely necessary calculations are re-executed. From my point of view, this should be intuitive to use for beginners and should be quite sufficient for smaller projects. *We use Pluto as the user interface in this course.*

## Installation

*Server of EP III* To simplify your first steps you can use the Jupyter & Pluto server<sup>15</sup> of EP III. For this you have to be inside the university or con-

<sup>3</sup> <https://docs.julialang.org/en/v1/>

<sup>4</sup> <https://juliabyexample.helpmanual.io/>

<sup>5</sup> <https://benlauwens.github.io/ThinkJulia.jl/latest/book.html>

<sup>6</sup> <https://computationalthinking.mit.edu/Spring21/>

<sup>7</sup> <https://docs.julialang.org/en/v1/manual/noteworthy-differences/>

<sup>8</sup> <https://cheatsheets.quantecon.org/>

<sup>9</sup> <https://juliadocs.github.io/Julia-Cheat-Sheet/>

<sup>10</sup> <https://github.com/sswatson/cheatsheets/>

<sup>11</sup> <https://junolab.org/>

<sup>12</sup> <https://www.julia-vscode.org/>

<sup>13</sup> <https://jupyter.org/>

<sup>14</sup> <https://github.com/fonsp/Pluto.jl>

<sup>15</sup> <http://jupyter.ep3.uni-bayreuth.de>

nected via VPN. You will receive access data during the first week of the semester. Log in to the server with these. You will get to a Jupyter interface where you can manage files on the server. Click on the Pluto icon to start a Pluto interface in the web browser.

Please be considerate with this server. Its resources are rather limited.

*Local installation* Especially if you find the EP III server too slow you should install Julia and Pluto locally. A good guide is at MIT<sup>16</sup>. Short version: install Julia from the website, then install once the Pluto package in Julia locally (`import Pkg; Pkg.add("Pluto")`). To use it, call it from the Julia command line via `using Pluto; Pluto.run()`. This could go into the Julia startup file or could be passed via the (system) command line.

<sup>16</sup> <https://computationalthinking.mit.edu/Spring21/installation/>

## Using Pluto

For a nice introduction to Pluto (and Julia), see the Pluto homepage<sup>17</sup>, at MIT (here<sup>18</sup> or actually the whole site) and at WIAS.<sup>19</sup>

<sup>17</sup> <https://github.com/fonsp/Pluto.jl/wiki>

<sup>18</sup> [https://computationalthinking.mit.edu/Spring21/basic\\_syntax/](https://computationalthinking.mit.edu/Spring21/basic_syntax/)

<sup>19</sup> <https://www.wias-berlin.de/people/fuhrmann/SciComp-WS2021/assets/nb01-first-contact-pluto.html>

- Shift-Enter executes a cell
- The execution optimizer requires that each cell forms a closed block. So there must be only one command, or several need to be encapsulated by `begin ... end`.
- Each cell has only one output, that of the last line. The output is above the cell itself.
- Pluto manages libraries automatically, just use `using`. You do not need to download anything.
- Pluto automatically saves everything, but you can rename / move the file.



# Appendix B

## Fourier transformation

Markus Lippitz  
May 20, 2020

### Overview

It is useful and helpful to have an intuitive approach to the Fourier transform. The bottom line is that in experimental physics one rarely has to actually calculate a Fourier transform. Very often it is enough to know a few frequently occurring Fourier pairs and to combine them with simple rules. I would like to present this here briefly. A very nice and much more detailed presentation can be found in Butz, 2015. I follow his notation here.

Before we come to the Fourier pairs, however, some basics have to be laid first.

### Fourier series: a periodic function and its Fourier coefficients

We first consider everything here in one dimension in time or frequency space with the variables  $t$  and  $\omega = 2\pi\nu$ . Let the function  $f(t)$  be periodic in time with period  $T$ , i.e.

$$f(t) = f(t + T) \quad (\text{B.1})$$

Then this can be written as a Fourier series

$$f(t) = \sum_{k=-\infty}^{\infty} C_k e^{i\omega_k t} \quad \text{with} \quad \omega_k = \frac{2\pi k}{T} \quad (\text{B.2})$$

and the Fourier coefficients

$$C_k = \frac{1}{T} \int_{-T/2}^{T/2} f(t) e^{-i\omega_k t} dt \quad (\text{B.3})$$

Note the negative sign in the exponential function in contrast to the equation before. For real-valued functions  $f(t)$ , 'opposite'  $C_k$  are conjugate-complex, so  $C_k = C_{-k}^*$ . For  $k < 0$  the frequencies  $\omega_k$  are negative, but this is not a problem.<sup>1</sup> Thus, the zeroth coefficient  $C_0$  is just the time average of the function  $f(t)$ .

<sup>1</sup> One could alternatively require  $k \geq 0$  and apply a sin and cos series.



## An arbitrary function and its Fourier transform

Now we remove the restriction to periodic functions  $f(t)$  by letting the period  $T$  go to infinity. This turns the sum into an integral and the discrete  $\omega_k$  become continuous. Thus

$$F(\omega) = \int_{-\infty}^{+\infty} f(t) e^{-i\omega t} dt \quad (\text{B.4})$$

$$f(t) = \frac{1}{2\pi} \int_{-\infty}^{+\infty} F(\omega) e^{+i\omega t} d\omega \quad (\text{B.5})$$

Here, the first equation is the forward transformation (minus sign in the exponent), and the second is the reverse transformation (plus sign in the exponent). The symmetry is broken by the  $2\pi$ . But this is necessary if one wants to keep  $F(\omega = 0)$  as mean<sup>2</sup>. Alternatively, we could formulate all this with  $\nu$  instead of  $\omega$ , but then we would have a  $2\pi$  in many more places, though not before the integral.

We will continue with this form in a moment.

<sup>2</sup>  $F(0) = \int f(t) dt$  without  $1/T$  in front of it is meant here by Butz as mean!

## Discrete FT: a periodic number sequence and its Fourier transformed number sequence

First, a side note about the discrete Fourier transform. In particular, if one acquires and evaluates measured values with a computer, then one does not know the measured function  $f(t)$  on a continuous axis  $t$ , but only at discrete times  $t_k = k \delta t$ , nor does one know the function from  $t = -\infty$  to  $t = +\infty$ . Thus, as a starting point, we have only a finite-length number sequence  $f_k$ .

Because we do not know the sequence of numbers outside the measured interval we make the assumption that it is periodic. With  $N$  measured values the periodic time is  $T = N \Delta t$ . For simplicity, we also define  $f_k = f_{k+N}$  and thus  $f_{-k} = f_{N-k}$  with  $k = 0, 1, \dots, N-1$ . Thus the Fourier transform becomes

$$F_j = \frac{1}{N} \sum_{k=0}^{N-1} f_k e^{-k j 2\pi i / N} \quad (\text{B.6})$$

$$f_k = \sum_{j=0}^{N-1} F_j e^{+k j 2\pi i / N} \quad (\text{B.7})$$

The definition is again such that  $F_0$  corresponds to the mean. Because of  $f_{-k} = f_{N-k}$ , the positive frequencies are in the first half of  $F_j$  as the frequency increases. After that come the negative frequencies, starting at the 'most negative' frequency and increasing to the last frequency before zero. So the maximum frequency that can be represented is the Nyquist (angular) frequency

$$\Omega_{\text{Nyquist}} = \frac{\pi}{\delta t} \quad (\text{B.8})$$



## Sidenote: Delta Function

The delta function can be written as

$$\delta(x) = \lim_{a \rightarrow 0} f_a(x) \quad \text{with} \quad f_a(x) = \begin{cases} a & \text{if } |x| < \frac{1}{2a} \\ 0 & \text{other} \end{cases} \quad (\text{B.9})$$

or as

$$\delta(x) = \frac{1}{2\pi} \int_{-\infty}^{+\infty} e^{+ixy} dy \quad (\text{B.10})$$

An important property is that the delta function selects a value, i.e.

$$\int_{-\infty}^{+\infty} \delta(x) f(x) dx = f(0) \quad (\text{B.11})$$

## Important Fourier pairs

It is very often sufficient to know the following pairs of functions and their Fourier transforms. I write them here, following Butz, as pairs in  $t$  and  $\omega$  (not  $\nu = \omega/(2\pi)$ ). In the same way, one could have written pairs in  $x$  and  $k$ . The important question is whether a  $2\pi$  appears in the exponential function of the plane wave or not. So

$$e^{i\omega t} \quad \text{and} \quad e^{ikx}, \quad \text{but} \quad e^{i2\pi\nu t} \quad (\text{B.12})$$

Further, I follow here the convention made above about the asymmetric distribution of the  $2\pi$  between forward and reverse transformations. If you distribute them differently, then of course the prefactors change. A good overview of many more Fourier pairs in various ' $2\pi$ ' conventions can be found in the English Wikipedia under 'Fourier transform'. In their nomenclature, the convention of Butz used here is 'non-unitary, angular frequency'.

constant and delta function  $f(t) = a$  becomes  $F(\omega) = a 2\pi \delta(\omega)$  and  $f(t) = a \delta(t)$  becomes  $F(\omega) = a$ . This is again the asymmetric  $2\pi$ .

rectangle and sinc The rectangle function of width  $b$  becomes a sinc<sup>3</sup>, the sinus cardinalis. So from

$$f(t) = \text{rect}_b(t) = \begin{cases} 1 & \text{for } |t| < b/2 \\ 0 & \text{other} \end{cases} \quad (\text{B.13})$$

we get

$$F(\omega) = b \frac{\sin \omega b/2}{\omega b/2} = b \text{sinc}(\omega b/2) \quad (\text{B.14})$$

Gauss The Gaussian function is preserved under Fourier transform. Its width changes into the reciprocal value. So from a Gauss function of area one

$$f(t) = \frac{1}{\sigma\sqrt{2\pi}} e^{-\frac{1}{2}\left(\frac{t}{\sigma}\right)^2} \quad (\text{B.15})$$

we get

$$F(\omega) = e^{-\frac{1}{2}(\sigma\omega)^2} \quad (\text{B.16})$$

<sup>3</sup> sometimes  $\text{sinc}(x) = \sin(\pi x)/(\pi x)$  is defined, especially when  $\nu$  and not  $\omega$  is used as conjugate variable.

(two-sided) exponential decay and Lorentz curve    **From a curve decaying exponentially at both positive and negative times**

$$f(t) = e^{-|t|/\tau} \quad (\text{B.17})$$

we obtain the Lorentz curve

$$F(\omega) = \frac{2\tau}{1 + \omega^2 \tau^2} \quad (\text{B.18})$$

one-sided exponential decay    **As a side note, here the one-sided exponential decay**

$$f(t) = \begin{cases} e^{-\lambda t} & \text{for } t > 0 \\ 0 & \text{other} \end{cases} \quad (\text{B.19})$$

It will become

$$F(\omega) = \frac{1}{\lambda + i\omega} \quad (\text{B.20})$$

and it is therefore complex-valued. Its magnitude squared is again a Lorentz function

$$|F(\omega)|^2 = \frac{1}{\lambda^2 + \omega^2} \quad (\text{B.21})$$

and the phase is  $\phi = -\omega/\lambda$ .

One-dimensional point grid    **An equidistant chain of points or delta functions remains an equidistant chain under Fourier transform. The distances take the reciprocal value. So from**

$$f(t) = \sum_n \delta(t - \delta t n) \quad (\text{B.22})$$

we get

$$F(\omega) = \frac{2\pi}{\delta t} \sum_n \delta\left(\omega - n \frac{2\pi}{\Delta t}\right). \quad (\text{B.23})$$

Three-dimensional cubic lattice    **A three-dimensional primitive cubic lattice of side length  $a$  makes the transitions to a primitive cubic lattice of side length  $2\pi/a$ . A face-centered cubic lattice with lattice constant  $a$  of conventional unit cell is converted to a space-centered cubic lattice with lattice constant  $4\pi/a$  and vice versa.**

## Theorems and properties of the Fourier transform

In addition to the Fourier pairs, we need a few properties of the Fourier transform. In the following, let  $f(t)$  and  $F(\omega)$  be Fourier conjugates and likewise  $g$  and  $G$ .

linearity    **The Fourier transform is linear**

$$a f(t) + b g(t) \leftrightarrow a F(\omega) + b G(\omega) \quad (\text{B.24})$$

shift    **A shift in time implies a modulation in frequency and vice versa.**

$$f(t - a) \leftrightarrow F(\omega) e^{-i\omega a} \quad (\text{B.25})$$

$$f(t) e^{-i\omega_0 t} \leftrightarrow F(\omega + \omega_0) \quad (\text{B.26})$$

scaling

$$f(at) \leftrightarrow \frac{1}{|a|} F\left(\frac{\omega}{a}\right) \quad (\text{B.27})$$

convolution and multiplication    Convolution is converted into a product, and vice versa

$$f(t) \otimes g(t) = \int f(\zeta)g(t - \zeta)d\zeta \leftrightarrow F(\omega)G(\omega) \quad (\text{B.28})$$

and

$$f(t)g(t) \leftrightarrow \frac{1}{2\pi} F(\omega) \otimes G(\omega) \quad (\text{B.29})$$

Parseval's Theorem    The total power is the same in both time and frequency domain

$$\int |f(t)|^2 dt = \frac{1}{2\pi} \int |F(\omega)|^2 d\omega \quad (\text{B.30})$$

time derivatives

$$\frac{df(t)}{dt} \leftrightarrow i\omega F(\omega) \quad (\text{B.31})$$

### Example: Diffraction at a double slit

As an example, we consider the Fourier transform of a double slit, which just describes its diffraction pattern. The slits have a width  $b$  and a center distance  $d$ . Thus the slit is described by a convolution of the rectangular function with two delta functions at the distance  $d$

$$f(x) = \text{rect}_b(x) \otimes (\delta(x - d/2) + \delta(x + d/2)) \quad (\text{B.32})$$

The Fourier transform of the rectangular function is the sinc, that of the delta functions a constant. However, the shift in position causes a modulation in  $k$ -space. Thus, the sum of the two delta functions becomes

$$\mathcal{FT}\{\delta(x - d/2) + \delta(x + d/2)\} = e^{-ikd/2} + e^{+ikd/2} = 2 \cos(kd/2) \quad (\text{B.33})$$

The convolution with the rectangular function passes into a multiplication with the sinc. Together we get

$$\mathcal{FT}\{f(x)\} = b \frac{\sin(kb/2)}{kb/2} 2 \cos(kd/2) = \frac{4}{k} \sin(kb/2) \cos(kd/2) \quad (\text{B.34})$$

The intensity in direction  $k$  is then the squared magnitude of this.

### Two-dimensional Fourier transformation

We can extend the definition of the Fourier transformation to two and more dimensions. The conjugated variables are  $(x, y)$  and  $(k_x, k_y)$ , instead of  $t$  and  $\omega$ . The wave vector  $k_i = 2\pi/\lambda_i$  contains the factor of  $2\pi$  as in the angular frequency  $\omega$ . We define

$$F(k_x, k_y) = \iint_{-\infty}^{+\infty} f(x, y) e^{-i(k_x x + k_y y)} dx dy \quad (\text{B.35})$$

$$f(x, y) = \frac{1}{(2\pi)^2} \iint_{-\infty}^{+\infty} F(k_x, k_y) e^{+i(k_x x + k_y y)} dk_x dk_y \quad (\text{B.36})$$

When we can separate the function  $f(x, y)$  into a product of one-dimensional functions, then the Fourier transformation is simply the product of the individual Fourier transforms

$$f(x, y) = g(x) \cdot h(y) \quad \leftrightarrow \quad F(k_x, k_y) = G(k_x) \cdot H(k_y) \quad . \quad (\text{B.37})$$

A rectangle of size  $a \times b$  is transformed into a product of sinc functions

$$(x, y) = \text{rect}_a(x) \cdot \text{rect}_b(y) \quad (\text{B.38})$$

$$\leftrightarrow \quad F(k_x, k_y) = ab \text{ sinc}(k_x a/2) \text{ sinc}(k_y b/2) \quad . \quad (\text{B.39})$$

A special case of this is the rotational symmetric two-dimensional Gaussian function

$$f(x, y) = \frac{1}{2\pi\sigma^2} e^{-\frac{x^2+y^2}{2\sigma^2}} \quad \leftrightarrow \quad F(k_x, k_y) = e^{-\frac{\sigma^2}{2}(k_x^2+k_y^2)} \quad . \quad (\text{B.40})$$

One important function can not be separated into a product of one-dimensional functions: a disc of radius  $a$

$$f(x, y) = \begin{cases} 1 & \text{for } x^2 + y^2 < a \\ 0 & \text{other} \end{cases} \quad (\text{B.41})$$

is transformed into

$$F(k_x, k_y) = a \frac{J_1(\pi a \rho)}{\rho} \quad \text{width} \quad \rho = \sqrt{k_x^2 + k_y^2} \quad (\text{B.42})$$

and the (cylindrical) Bessel function of the first kind  $J_1(x)$

$$J_1(x) = \frac{1}{\pi} \int_0^\pi \cos(\tau - x \sin \tau) d\tau \quad , \quad (\text{B.43})$$

which is the cylindrical analogue of a sinc function.

## References

Butz, Tilman (2015). *Fourier Transformation for Pedestrians*. 2. ed. Springer.



# Bibliography

- Aizpurua, Javier and Rainer Hillenbrand (2012). "Localized Surface Plasmons: Basics and Applications in Field-Enhanced Spectroscopy". In: *Plasmonics*. Ed. by Stefan Enoch and Nicolas Bonod. Vol. 167. Springer series in optical sciences. [↗](#).
- Albota, M., D. Beljonne, J.-L. Brédas, et al. (1998). "Design of Organic Molecules with Large Two-Photon Absorption Cross Section". In: *Science* 281, pp. 1653–1656. [↗](#).
- Birge, R. R. (1986). "Two-Photon Spectroscopy of Protein-Bound Chromophores". In: *Acc. Chem. Res.* 19, pp. 138–146. [↗](#).
- Block, A et al. (2019). "Tracking ultrafast hot-electron diffusion in space and time by ultrafast thermomodulation microscopy". In: *Science Advances* 5.5, eaav8965. [↗](#).
- Bohren, Craig F. and Donald R. Huffman (2007). *Absorption and Scattering of Light by Small Particles*. John Wiley & Sons, Ltd. [↗](#).
- Born, Max and Emil Wolf (2002). *Principles of optics*. 7. (expanded) ed., reprinted with corr. Cambridge [u.a.]: Cambridge Univ. Press.
- Borri, Paola et al. (2002). "Rabi oscillations in the excitonic ground-state transition of InGaAs quantum dots". In: *Physical Review B* 66.8, p. 81306. [↗](#).
- Boyd, Robert W. (2008). *Nonlinear Optics*. 3. ed. Amsterdam [u.a.]: Elsevier, Acad. Press.
- Brańczyk, Agata M, Daniel B Turner, and Gregory D Scholes (2013). "Crossing disciplines – A view on two-dimensional optical spectroscopy". In: *Annalen der Physik* 526.1-2, pp. 31–49. [↗](#).
- Bransden, B. H. and C. J. Joachain (1996). *Physics of atoms and molecules*. Longman.
- Butz, Tilman (2015). *Fourier Transformation for Pedestrians*. 2. ed. Springer. [↗](#).
- Cohen-Tannoudji, Claude, Bernard Diu, and Franck Laloë (1977). *Quantum Mechanics*. Wiley.
- Cohen-Tannoudji, Claude, Jacques Dupont-Roc, and Gilbert Grynberg (2004). *Atom photon interactions*. Weinheim: Wiley-VCH. [↗](#).
- Crut, Aurélien et al. (2017). "Linear and ultrafast nonlinear plasmonics of single nano-objects". In: *Journal of Physics: Condensed Matter* 29.12, pp. 123002–123023. [↗](#).
- Demtröder, Wolfgang (2014). *Laser spectroscopy 1*. Berlin [u.a.]: Springer. [↗](#).
- Denk, W., J. H. Strickler, and W. W. Webb (1990). "Two-Photon Laser Scanning Fluorescence Microscopy". In: *Science* 248, pp. 73–76. [↗](#).



- Diels, Jean-Claude and Wolfgang Rudolph (1996). *Ultrashort laser pulse phenomena. fundamentals, techniques, and applications on a femtosecond time scale*. San Diego [u.a.]: Academic Press. [↗](#).
- Doicu, Adrian, Thomas Wriedt, and Yuri Eremin (2006). *Light Scattering by Systems of Particles-Null-Field Method with Discrete Sources-Theory and Programs*. Vol. 124. Springer series in optical sciences. Springer. [↗](#).
- Dorfmueller, Jens (2010). "Optical Wire Antennas: Near-Field Imaging, Modeling and Emission Patterns". PhD thesis. École Polytechnique Fédérale de Lausanne. [↗](#).
- Dorfmueller, Jens et al. (2010). "Plasmonic nanowire antennas: experiment, simulation, and theory". In: *Nano Letters* 10.9, pp. 3506–3603. [↗](#).
- Draine, B T (1988). "The discrete-dipole approximation and its application to interstellar graphite grains". In: *The Astrophysical Journal* 333, p. 848. [↗](#).
- Drexhage, Karl H. (1974). "Interaction of Light with Monomolecular Dye Layers". In: *Progress in Optics*. Ed. by E. Wolf. Vol. 12. Elsevier, pp. 163–232. [↗](#).
- Ford, G.W. and W.H. Weber (1984). "Electromagnetic interactions of molecules with metal surfaces". In: *Physics Reports* 113.4, pp. 195–287. [↗](#).
- Fox, Mark (2007). *Quantum optics*. Oxford University Press.
- Fuller, Franklin D and Jennifer P Ogilvie (2015). "Experimental Implementations of Two-Dimensional Fourier Transform Electronic Spectroscopy". In: *Annual Review of Physical Chemistry* 66.1, pp. 667–690. [↗](#).
- Gerry, Christopher C. and Peter L. Knight (2005). *Introductory quantum optics*. Cambridge Univ. Press. [↗](#).
- Goodman, Joseph W. (2005). *Introduction to Fourier optics*. 3. ed. Roberts.
- Göppert-Mayer, M. (1931). "Über Elementarakte mit zwei Quantensprüngen". In: *Ann. Phys.* 9, pp. 273–295. [↗](#).
- Haken, H. and H.C. Wolf (2004). *Molecular Physics and Elements of Quantum Chemistry*. Springer.
- Hamm, Peter (2005). *Principles of Nonlinear Optical Spectroscopy: A Practical Approach or: Mukamel for Dummies*. [↗](#).
- Hamm, Peter and Martin T. Zanni (2011). *Concepts and methods of 2D infrared spectroscopy*. Cambridge University Press.
- Haroche, Serge (2006). *Exploring the quantum. atoms, cavities and photons*. Oxford Univ. Press. [↗](#).
- Hens, Z. (2008). "Can the oscillator strength of the quantum dot bandgap transition exceed unity?" In: *Chemical Physics Letters* 463.4-6, pp. 391–395. [↗](#).
- Hilborn, Robert C. (2002). *Einstein coefficients, cross sections, f values, dipole moments, and all that*. arXiv: [physics/0202029](#).
- Hohenester, Ulrich (2020). *Nano and Quantum Optics. An Introduction to Basic Principles and Theory*. Springer. [↗](#).
- Hopf, Frederic A. and George I. Stegeman (1986). *Applied classical electrodynamics: Nonlinear optics*. New York: Wiley.
- Huang, Huiying et al. (2021). "Bright Single Photon Emission from Quantum Dots Embedded in a Broadband Planar Optical Antenna". In: *Advanced Optical Materials*, p. 2001490. [↗](#).

- Jackson, John David (1999). *Classical electrodynamics*. 3. ed. New York [u.a.]: Wiley.
- Jasieniak, Jacek et al. (2009). "Re-examination of the Size-Dependent Absorption Properties of CdSe Quantum Dots". In: *The Journal of Physical Chemistry C* 113.45, pp. 19468–19474. [↗](#)
- Johnson, Peter B and R.W. Christy (1972). "Optical constants of the noble metals". In: *Physical review B* 6.12, p. 4370. [↗](#)
- Jun, Young Chul (2010). "Plasmonic Control Of Light Emission: Tailoring Light Emission Properties With Metal Nanostructures". PhD thesis. Stanford University. [↗](#)
- Kaiser, W. and C. G. B. Garrett (1961). "Two-Photon excitation in  $\text{CaF}_2:\text{Eu}^{2+}$ ". In: *Phys. Rev. Lett.* 7.6, pp. 229–231. [↗](#)
- Kastrup, Lars and Stefan W Hell (2004). "Absolute Optical Cross Section of Individual Fluorescent Molecules". In: *Angewandte Chemie International Edition* 43.48, pp. 6646–6649. [↗](#)
- Khitrova, G et al. (2006). "Vacuum Rabi splitting in semiconductors". In: *Nature Physics* 2.2, pp. 81–90. [↗](#)
- Klein, Matthias W et al. (2006). "Second-harmonic generation from magnetic metamaterials". In: *Science* 313.5786, pp. 502–504. [↗](#)
- Knapp, E.W. (1984). "Lineshapes of molecular aggregates, exchange narrowing and intersite correlation". In: *Chemical Physics* 85.1, pp. 73–82. [↗](#)
- Knoester, J. (2002). "Optical properties of molecular aggregates". In: *Proceedings of the International School of Physics 'Enrico Fermi'*. Volume 149: Organic Nanostructures: Science and Applications. IOS Press, pp. 149–186. [↗](#)
- Köhler, Anna and Heinz Bässler (2015). *Electronic processes in organic semiconductors*. Weinheim: Wiley-VCH. [↗](#)
- Kreibig, Uwe and Michael Vollmer (1995). *Optical properties of metal clusters*. Berlin u.a.: Springer.
- Kuzmany, Hans (2009). *Solid-state spectroscopy. An introduction*. Second edition. Heidelberg: Springer.
- Lakowicz, Joseph R. (2010). *Principles of fluorescence spectroscopy*. New York, NY: Springer. [↗](#)
- Langguth, Lutz et al. (2016). "Drexhage's Experiment for Sound". In: *Physical Review Letters* 116.22, pp. 224301–224306. [↗](#)
- Loudon, Rodney (2001). *The quantum theory of light*. Oxford University Press.
- Macleod, H. Angus (2001). *Thin film optical filters*. 3. ed. Bristol [u.a.]: Inst. of Physics Publ. [↗](#)
- Maier, Stefan A. (2007). *Plasmonics*. Norwell: Springer Science+Business Media, LLC. [↗](#)
- Maiman, T. H. (1960). "Stimulated Optical Radiation in Ruby". In: *Nature* 187.4736, pp. 493–494. [↗](#)
- Mäkitalo, J, S Suuriniemi, and M Kauranen (2011). "Boundary element method for surface nonlinear optics of nanoparticles". In: *Optics Express* 19.23, p. 23386. [↗](#)
- Meschede, Dieter (2017). *Optics, light, and lasers*. Weinheim, Germany: Wiley-VCH. [↗](#)

- Meystre, Pierre and Murray Sargent (2007). *Elements of quantum optics*. 4. ed. Berlin [u.a.]: Springer, XII, 507 S. [↗](#).
- Meystre, Pierre and Murray Sargent III (2007). *Elements of Quantum Optics*. 4. Springer. [↗](#).
- Miller, Robert C. (1964). "Optical second harmonic generation in piezoelectric crystals". In: *Applied Physics Letters* 5.1, pp. 17–19. [↗](#).
- Milonni, Peter W. and Joseph H. Eberly (1988). *Lasers*. New York [u.a.]: Wiley.
- Mukamel, Shaul (1995). *Principles of nonlinear optical spectroscopy*. Oxford University Press.
- Myroshnychenko, V et al. (2008). "Modelling the Optical Response of Gold Nanoparticles". In: *Chem. Soc. Rev.* 39.49. [↗](#).
- Newton, Roger G (1976). "Optical theorem and beyond". In: *American Journal of Physics* 44.7, p. 639. [↗](#).
- Nolting, Wolfgang (2016). *Theoretical Physics 3 Electrodynamics*. Springer. [↗](#).
- Novotny, Lukas (2007). "Effective Wavelength Scaling for Optical Antennas". In: *Physical Review Letters* 98.26, p. 266802. [↗](#).
- Novotny, Lukas and Bert Hecht (2012). *Principles of nano-optics*. 2. ed. Cambridge Univ. Press. [↗](#).
- Obermeier, Julian, Thorsten Schumacher, and Markus Lippitz (2018). "Nonlinear spectroscopy of plasmonic nanoparticles". In: *Advances in Physics: X* 3.1, p. 1454341. [↗](#).
- Otto, Andreas (1968). "Excitation of nonradiative surface plasma waves in silver by the method of frustrated total reflection". In: *Zeitschrift für Physik A* 216.4, pp. 398–410. [↗](#).
- Parson, William W. (2015). *Modern optical spectroscopy*. Springer. [↗](#).
- Pedrotti, Frank L. et al. (2008). *Optik für Ingenieure*. 4., bearb. Aufl. Berlin [u.a.]: Springer. [↗](#).
- Pelton, Matthew, S David Storm, and Haixu Leng (2019). "Strong coupling of emitters to single plasmonic nanoparticles: exciton-induced transparency and Rabi splitting". In: *Nanoscale* 11.31, pp. 14540–14552. [↗](#).
- Peticolas, W. L., J. P. Goldsborough, and K. E. Rieckhoff (1963). "Double photon excitation in organic crystals". In: *Phys. Rev. Lett.* 10.2, pp. 43–45. [↗](#).
- Pettit, RB, J Silcox, and R Vincent (1975). "Measurement of surface-plasmon dispersion in oxidized aluminum films". In: *Physical Review B* 11.8, p. 3116. [↗](#).
- Polarecky, Lubos, Jaroslav Hamrle, and Brian D MacCraith (2000). "Theory of the radiation of dipoles placed within a multilayer system". In: *Applied Optics* 39.22, pp. 3968–3977. [↗](#).
- Prodan, E et al. (2003). "A hybridization model for the plasmon response of complex nanostructures". In: *Science* 302.5644, p. 419. [↗](#).
- Rand, Stephen C. (2016). *Lectures on light. nonlinear and quantum optics using the density matrix*. Second edition. Oxford University Press. [↗](#).
- Reithmaier, JP et al. (2004). "Strong coupling in a single quantum dot-semiconductor microcavity system". In: *Nature* 432.7014, pp. 197–200.
- Rullière, Claude, ed. (2005). *Femtosecond laser pulses. principles and experiments*. 2. ed. New York, NY: Springer, XVI, 426 S. [↗](#).



- Saleh, Bahaa E. A. and Malvin C. Teich (1991). *Fundamentals of photonics*. New York, NY [u.a.]: Wiley. [↗](#)
- Schumacher, Thorsten, Matthias Brandstetter, et al. (2016). "The optimal antenna for nonlinear spectroscopy of weakly and strongly scattering nanoobjects". In: *Applied Physics B* 122, p. 91. [↗](#)
- Schumacher, Thorsten, Kai Kratzer, et al. (2011). "Nanoantenna-enhanced ultrafast nonlinear spectroscopy of a single gold nanoparticle". In: *Nature Communications* 2.1, p. 333. [↗](#)
- Schwabl, Franz (2002). *Quantenmechanik*. 6. Auflage. Springer. [↗](#)
- Shen, Yuen R. (2003). *The principles of nonlinear optics*. Wiley.
- Strickler, S J and Robert A Berg (1962). "Relationship between Absorption Intensity and Fluorescence Lifetime of Molecules". In: *The Journal of Chemical Physics* 37.4, p. 814. [↗](#)
- Takahara, Junichi et al. (1997). "Guiding of a one-dimensional optical beam with nanometer diameter". In: *Optics Letters* 22.7, p. 475. [↗](#)
- Thomas, Philip A et al. (2020). "A New Signature for Strong Light-Matter Coupling Using Spectroscopic Ellipsometry". In: *Nano letters* 20.9, pp. 6412–6419. [↗](#)
- Tokmakoff, Andrei (2009). "10.2 Diagrammatic Perturbation Theory". In: 5.74 *Introductory Quantum Mechanics II*. MIT OpenCourseWare. [↗](#)
- Vigoureux, J.M. and D. Courjon (1992). "Detection of nonradiative fields in light of the Heisenberg uncertainty principle and the Rayleigh criterion". In: *Applied Optics* 31.16, pp. 3170–3177. [↗](#)
- Wang, Fu Xiang et al. (2009). "Surface and bulk contributions to the second-order nonlinear optical response of a gold film". In: *Physical Review B* 80.23, pp. 233402–233404. [↗](#)
- Winterhalder, M J et al. (2011). "Toward Far-field Vibrational Spectroscopy of Single Molecules at Room Temperature". In: *The Journal of Physical Chemistry B* 115.18, pp. 5425–5430. [↗](#)
- Wolpert, Christian et al. (2012). "Transient Reflection: A Versatile Technique for Ultrafast Spectroscopy of a Single Quantum Dot in Complex Environments". In: *Nano Letters* 12.1, pp. 453–457. [↗](#)
- Xu, C. and W. W. Webb (1996). "Measurement of two-photon excitation cross sections of molecular fluorophores with data from 690 to 1050 nm". In: *J. Opt. Soc. Am. B* 13.3, pp. 481–491. [↗](#)
- (1997). "Multiphoton Excitation of Molecular Fluorophores and Nonlinear Laser Microscopy". In: *Topics in Fluorescence Spectroscopy, Vol. 5: nonlinear and two-photon induced fluorescence*. Ed. by J. R. Lakowicz. Plenum Press, New York, pp. 471–540.
- Yariv, Amnon (1989). *Quantum electronics*. 3. ed. New York: Wiley.
- Yeh, Pochi (2005). *Optical waves in layered media*. Hoboken, NJ: Wiley-Interscience.
- Yurkin, Maxim A and Alfons G Hoekstra (2007). "The discrete dipole approximation: an overview and recent developments". In: *Journal Of Quantitative Spectroscopy & Radiative Transfer* 106.1-3, pp. 558–589. [↗](#)